Università degli Studi di Napoli Federico II

Università degli Studi di Napoli Federico II
Ph.D. Program in
Transportation Engineering
XXXVI Cycle

SUBMITTED IN FULFILLMENT OF THE REQUIREMENTS FOR THE DEGREE OF DOCTOR OF PHILOSOPHY

Macroscopic Modeling and Control of Mixed Traffic

by

WAHEED IMRAN

Advisor: Prof. Dr. Luigi Pariota

DIPARTIMENTO DI INGEGNERIA CIVILE EDILE E AMBIENTALE

To my loving parents and siblings.

Waheed Imran

Macroscopic Modeling and Control of Mixed Traffic

Ph.D. dissertation presented
for the fulfillment of the Degree of Doctor of Philosophy
in Transportation Engineering
by

Waheed Imran

October 2023

Approved as to style and content by

Prof. Dr. Luigi Pariota, Advisor

Università degli Studi di Napoli Federico II
Ph.D. Program in Transportation Engineering,
Department of Civil, Architectural and Environmental Engineering
XXXVI cycle

https://www.dicea.unina.it/home-2/

Candidate's declaration

I hereby declare that this dissertation submitted to obtain the academic degree of Philosophiæ Doctor (Ph.D.) in Transportation Engineering at the Department of Civil, Architectural and Environmental Engineering, is my own unaided work, that I have not used other than the sources indicated, and that all direct and indirect sources are acknowledged as references. Parts of this dissertation have been published in international journals and/or conference articles (see list of the author's publications at the end of the dissertation).

Naples, December 12, 2023

____

Waheed Imran

Summary

Highway traffic congestion, a persistent issue driven by the ongoing increase in motorization, leads to major concerns for researchers, including travel delays, traffic pollution, and road traffic safety. To diligently address the problem of traffic congestion, the dynamics of traffic flow on highways are vital to understanding for effective planning and management. Effective traffic control strategies can be designed only if accurate traffic states are known. Thus, mathematical models of traffic are harnessed to predict the future states of traffic flow on highways. In this dissertation, the principal considerations center on the macroscopic continuum second-order traffic flow models. That being the case, these macroscopic models are employed in traffic control such as Model Predictive Control (MPC). Apart from traffic control, models of traffic are employed to describe the complex dynamics of evolving traffic and for various other purposes, including, but not limited to emissions estimations, incident impact assessments and traffic enroutement based on future dynamics of traffic flow.

Lately, the Macroscopic Continuum Traffic Flow Models (MCTFMs) are extensively refined for the characteristics of Human-Driven Vehicles (HDVs), yielding positive findings, however, their practical utility is yet not fully exercised. Additionally, with the advent of Connected and Autonomous Vehicles (CAVs), certain dynamics of traffic flow such as their impact on the capacity of highways would be immense, and in particular, intrinsic characteristics such as driver behavior would significantly alter. Thus, it necessitates the need to revise the second-order traffic flow models for CAVs, and subsequently for CAVs and HDVs mixed traffic. In view of this rationale, the motivation of this dissertation is to evaluate the existing second-order traffic flow models, extend these models to mixed traffic, and later, investigate and harness them in traffic control, particularly, in MPC-based traffic flow control.

To attain the goals of this dissertation, at the outset, a comprehensive review of the literature is conducted. Aiming to expand knowledge and understanding of the second-order continuum macroscopic models. These models are presented in distinct groups, which are categorically presented and discussed from a practical standpoint. A research gap in the current literature is identified considering the CAVs, which is addressed later in this dissertation. Subsequently, a detailed appraisal of the continuum second-order traffic flow models based on sensitivity analysis and numerical simulation is presented. The models are briefly studied and investigated to reproduce various traffic conditions. The second-order continuum models are examined considering their practical significance while analyzing the functional importance of the different parameters of the models. The sensitivity of the models' parameters is analyzed using statistical methods, signifying the understanding of revising them for mixed traffic.

Further, a revamped model of mixed traffic is proposed. This model incorporates the distinct headway distance among vehicles (CAVs and HDVs) in mixed traffic. The proposed model is calibrated and validated on M50 Dublin motorway data reproduced in Simulation of Urban MObility (SUMO). The proposed model is harnessed to investigate the impacts of CAVs on conventional traffic flow. The additional practical significance of the proposed model is demonstrated by employing it in computing Level of Service (LOS) of the Dublin motorway segments with different Penetration Rate (PR) of CAVs.

Next, we proposed a novel continuum model for traffic mixture considering three classes of vehicles. To commence, the Fundamental Diagram (FD) is vital to understand, it is viewed as the basis of traffic flow theory in view of traffic mixture is not well studied. We delve deeper into the insights of the FD of traffic mixture and derive the FD of traffic mixture driven on class-specific varying headway distances of the vehicles. Subsequently, we propose a continuum second-order traffic flow model, aiming to effectively capture and analyze the traffic dynamics arising from the traffic mixture. Furthermore, the proposed model integrates the macroscopic emissions and fuel consumption model to quantify the exhaust emissions and fuel consumption resulting from the traffic mixture. Three traffic mixtures are considered (i) a mixture of CAVs and HDVs (ii) a mixture of CAVs, HDVs, and Heavy Vehicles (HVs), and (iii) a mixture of CAVs, HDVs, and Connected Heavy Vehicles (CHVs). This model is based on a theoretical framework.

Besides, a novel simulation-based approach is presented to evaluate traffic flow in the presence of CAVs. In this work, the anticipative behavior of CAVs is modeled based on the change occurrence time in traffic. Various dynamics of the macroscopic traffic flow are investigated providing the anticipative response of CAVs based on distance headway and density-dependent change occurrence time, prioritizing traffic safety with real-time applications.

Conclusively, an MPC-based Variable Speed Limit (VSL) control of motorway traffic is implemented by harnessing a continuum second-order traffic flow model for HDVs as a prediction model. Within this framework, congestion has been alleviated in some segments of the Dublin motorway, while on the other side, the congestion occurrence time is significantly minimized. Subsequently, we have used the same MPC-based framework to control traffic flow with CAVs, and we have explored alternative control variables instead of VSL in the case of CAVs. We use the time headway of CAVs as a control variable, and it yields sufficiently good results. In all, by integrating together the approach of modeling and control presented in this dissertation, can help both the industry and academia in understanding modeling and controlling of traffic flow in mixed traffic conditions.

Keywords: Anticipative Response; Continuum Second-Order Traffic Flow Models, Connected and Autonomous Vehicles; Change Occurrence Time; Driver Response; Distance Headway; Human-Driven Vehicles; Macroscopic

Models; Model Predictive Control; Mixed-Traffic Flow; Traffic Congestion; Traffic Planning and Management; Traffic Control; Time Headway

Contents

Acknowledgements

I would like to express my heartfelt gratitude to the following individuals and groups for their invaluable support and guidance throughout the journey of completing this dissertation:

1. I am sincerely thankful to my advisor, Prof. Dr. Luigi Pariota, whose determined support and guidance have been instrumental in making this research possible. Without his assistance, this endeavor would have been far more challenging.

2. I extend my gratitude to Prof. Dr. Gennaro Nicola Bifulco for their humble mentorship and caring guidance, which served as a constant source of motivation. I also appreciate their generous funding that supported my period abroad.

3. I am sincerely thankful to Prof. Dr. Tamas Tettamanti for affording me the opportunity to visit Budapest University of Economics and Technology, Budapest, BME, Hungary, as a visiting research scholar for four enriching months.

4. I thank Prof. Dr. Zawar H. Khan of the University of Victoria, Canada, for generously sharing their valuable time and engaging in discussions whenever needed. Their guidance has been indispensable.

5. I would like to acknowledge and thank Prof. Dr. Eddie Wilson, Faculty of Engineering, University of Bristol for their time and discussion, which helped me to mould my research.

6. I would like to acknowledge the valuable insights and discussions provided by Dr. Balasz Varga at BME Budapest, which significantly contributed to the development of my research.

7. My heartfelt gratitude goes to my colleague, Alessio Tesone, whose readiness to address both minor and major queries was indispensable throughout this research endeavor.

8. I am indebted to Dr. Angelo Coppola for their unfailing assistance and guidance, which played a pivotal role in the successful completion of this dissertation.

9. I would also like to extend my thanks to my lab colleagues, Luca, Nicola, Andrea, Maria, Alessandra, and Valeria, for their constant availability and support, which greatly facilitated my research.

10. Lastly, I would like to express my deep appreciation to my parents and siblings for their resolute emotional support, which provided the foundation for my academic achievements.

Each of you has played a significant role in this journey, and your contributions have not gone unnoticed. Thank you for being a crucial part of my academic and personal growth.

Naples, Italy
October 10, 2023.

Waheed Imran

List of Acronyms

ATIS Advanced Traveller Information System

ADAS Advanced Driver Assistance System

AHVs Automated Heavy Vehicles

AVs Automated Vehicles

ACC Adaptive Cruise Control

CACC Cooperative Adaptive Cruise Control

CAVs Connected and Autonomous Vehicles

CAV Connected and Autonomous Vehicle

CFL Courant-Friedrichs-Lewy

CHVs Connected Heavy Vehicles

CCAM Connected, Coordinated and Automated Mobility

CDFs Cumulative Distribution Functions

C-ITS Cooperative Intelligent Transportation Systems

CTM Cell Transmission Model

DGM	Density Gradient Model
DGMs	Density Gradient Models
EEA	European Environment Agency
FORCE	First Order Centered
FOTFMs	First Order Traffic Flow Models
FOTFM	First Order Traffic Flow Model
FD	Fundamental Diagram
GEVM	Greenshields Equilibrium Velocity Model
GHG	Green House Gasses
GKT	Gas Kinetic Traffic
GSA	Global Sensitivity Analysis
HDVs	Human-Driven Vehicles
HCM	Highway Capacity Manual
HVs	Heavy Vehicles
HPDEs	Hyperbolic Partial Differential Equations
IDM	Intelligent Driver Model
IK	Imran and Khan
IoT	Internet of Things
IBVP	Initial Boundary Value Problem
ITS	Intelligent Transportation System

ICAM	Inter-Connected and Automated Mobility
JQZ	Jiang, Qing and Zhu
KG	Khan and Gulliver
KS	Kolmogorov-Smirnov
LoDA	Level of Driving Automation
LHS	Latin Hypercubic Sampling
LOS	Level of Service
LWR	Lighthill, Whitham and Richards
MoE	Measures of Effectiveness
MCTFM	Macroscopic Continuum Traffic Flow Model
MCTFMs	Macroscopic Continuum Traffic Flow Models
MFD	Macroscopic Fundamental Diagram
MPC	Model Predictive Control
ODEs	Ordinary Differential Equations
PI	Performance Index
PW	Payne and Whitham
PDEs	Partial Differential Equations
PDE	Partial Differential Equation
PR	Penetration Rate
PRs	Penetration Rates

RMSE	Root Mean Square Error
RMSPE	Root Mean Square Percentage Error
SAE	Society for Automotive Engineers
SUMO	Simulation of Urban MObility
SOTFM	Second Order Traffic Flow Model
SOTFMs	Second Order Traffic Flow Models
SGM	Speed Gradient Model
SGMs	Speed Gradient Models
SK	Song and Karni
TTT	Total Travel Time
VSL	Variable Speed Limit
V2I	Vehicle to Infrastructure
V2V	Vehicle to Vehicle

List of Figures

List of Tables

Notations

The following notations are used within the thesis

α	Penetration Rate (PR) of Human-Driven Vehicles (HDVs)
β	PR of Connected and Autonomous Vehicles (CAVs)
Δt	Time step
Δx	Road step
Δ_{MPC}	Controller sample time
η	PR of HVs
η^*	PR of CHVs
Γ	Relaxation time
ω	Vector of traffic flow variables
$\tau(\rho)$	Density-dependent transitions occurrence time
τ_d	Time headway
τ_h	Time headway
τ_r	Reaction time

τ_{ah} Transition occurance time of HDVs

τ_{bh} Transition occurance time of CAVs

τ_{ch} Transition occurance time of HVs

τ_{hh} Harmonization time of HDVs

$\tau_{r(min)}$ Minimum reaction time

τ_{rc} Reaction time of CAVs

τ_{rh} Reaction time of HDVs

τ_{rt} Reaction time of HVs

Ξ, j Vector of the parameters of the models

$A(\omega)$ Jacobian matrix for the gradients of the functions of variables

b Lateral distance between vehicles

C Clearance gap between vehicles

c Shape factor

c_0 Backward perturbation speed

D_g Dynamic gap

d_m Maximum deceleration

dtr Transition distance

e_q Egress flow

$f(\omega)$ Function of the data variables

$g(\rho)$ Minimum safe distance as a function of density

g_p Perceived distance

g_s Safe gap

G_{ttc} Traffic transition gap of CAVs

G_{tth} Traffic transition gap of HDVs

G_{ttt} Traffic transition gap of HVs

G_{tt} Traffic transition gap

H Distance headway

H_b Headway distance for CAVs

H_h, H_a Distance headway of HDVs

i Space index

i_q Ingress flow

L Length of a vehicle

L_c Length of a connected vehicle

l_g minimum lengthways gap

L_h Length of a human-driven vehicle

$l_s(v)$ Lengthways gap as a function of velocity

L_t Length of a heavy vehicle

$l_{\Xi,j}$ lower bound of the vector of the parameters of the models

M Equidistant segment

N Number of time steps

n Time index

N_c Control horizon

N_p Prediction horizon

n_{MPC} Control time step

$S(\rho)$ relation between spacing and density

S_{min} Minimum safe distance

t_a Transition time for change occurrence for HDVs

t_b Transition time for change occurrence for CAVs

u^* Optimal control trajectory

$u_{\Xi,j}$ Upper bound of the vector of the parameters of the models

v_r Reaction velocity

ρ_{cr} Critical density

ρ_m Maximum density

ρ Density

q_m Maximum flow

q Flow

$v(\rho)$ Equilibrium velocity distribution / velocity-density relationship

v_m, v_{max}, v_f Maximum velocity

v Velocity

Chapter 1

Introduction

1.1 Background and Motivation

Highways are essential pillars of transportation systems, which are under stress due to traffic congestion, resulting from rapid urban development. Traffic congestion implies various externalities, including, but not limited to an increase in the number of traffic accidents (compromising traffic safety), Green House Gasses (GHG) emissions, noise pollution, and travel delays. It is a major economic and societal problem [2, 3, 4]. The exhaust emissions from vehicles are widely spread, and are a leading problem globally. Particularly in Europe, traffic congestion has been a source of environmental pollution in the last decade. It is estimated that over 100 million people are affected by harmful levels of exhaust emissions in the European Environment Agency (EEA)-33[1],[2] member countries. Alleviation of traffic congestion has been a challenge for researchers, traffic engineers, and planners and has been a major concern for policymakers and governments across the globe.

To alleviate traffic congestion, and for effective management of highways, understanding the dynamics of traffic flow on highways are vital. Thus, it necessitates accurate descriptions of traffic flow over time and

[1] https://www.eea.europa.eu/data-and-maps/indicators/exceedances-of-air-quality-objectives-7/assessment

[2] https://www.eea.europa.eu/data-and-maps/indicators/exposure-to-and-annoyance-by-2/assessment-1

space horizons [5]. Further, with developing Intelligent Transportation System (ITS), certain tools and methods hold immense importance. That being the case, traffic flow models are harnessed to predict traffic flow allowing us to understand various traffic dynamics such as congestion formation and dissipation, travel time estimation, exhaust emissions, and other non-equilibrium traffic phenomena [6]. Macroscopic traffic flow models are specifically harnessed on highways to predict traffic flows. The information collected with macroscopic traffic flow models is processed in many practical applications such as Model Predictive Control (MPC)-based traffic control and Advanced Traveller Information System (ATIS), allowing to alleviate traffic congestion [7].

Furthermore, with the contemporary advancements in Internet of Things (IoT) and advanced communication technologies, diverse technologies of Connected and Autonomous Vehicles (CAVs) are proposed in traffic systems to enhance traffic network performance, road safety, transport mobility, and urban accessibility [8, 9]. With these technologies environmental and noise pollution can be significantly reduced. While, with the help of ITS, proper use of ATIS and Advanced Driver Assistance System (ADAS), the dynamics of traffic alter significantly. Lately, with the advent of CAVs, research on understanding the dynamics of mixed traffic CAVs and Human-Driven Vehicles (HDVs) has been revolutionized. Recent studies suggest that traffic dynamics will alter significantly, and so will control methods. Additionally, the existing MCTFMs are not able to accurately predict the traffic flow of mixed traffic. This is because they do not take into account the distinct behavior of CAVs and HDVs such as interactions between them.

Conclusively, the penetration of CAVs in conventional traffic flow presents a paradigm shift in urban traffic dynamics. While admittedly, the current MCTFMs have been proven effective in analyzing traffic flow, their applicability to mixed traffic is impeded by the unique complexities behavior of CAVs. These models, rooted in assumptions of homogeneous behavior and lacking provisions for real-time communication and adaptive decision-making, fail to capture the interactions between CAVs and HDVs. Consequently, a critical research gap emerges, necessitating the revision of MCTFMs to accurately predict and understand mixed traffic phenomena. By refining macroscopic models to incorporate the distinct behavioral patterns, communication dynamics, and decision-making processes of CAVs, researchers can bridge this gap and provide more reliable insights into traffic flow, congestion patterns, and road network optimization. This enhancement holds immense practical significance as it enables urban planners, transportation authorities, and policymakers to formulate informed strategies for traffic management, infrastructure development, and mobility enhancement. Ultimately, revised MCTFMs tailored for mixed traffic conditions hold the potential to revolutionize urban traffic by fostering safer, more efficient, and sustainable mobility solutions in the era of Inter-Connected and Automated Mobility (ICAM) and Connected, Coordinated and Automated Mobility (CCAM).

1.2 Research Objectives

This dissertation is centered on macroscopic continuum second-order traffic flow models, and their practical applications in traffic control. The objective of this dissertation is to evaluate existing models from a practical perspective. While additionally, to propose revamped continuum macroscopic second-order traffic flow models for mixed traffic to more accurately describe the complex dynamics of mixed traffic, with the specific goals being to:

- Evaluate the existing continuum second-order traffic flow models to reproduce various traffic conditions. Identifying the most sensitive parameters for the output of the model, and presenting physical meaning and understanding of the parameters of the existing models.

- Evaluate macroscopic traffic flow in the presence of CAVs and HDVs in a connected environment. To quantify the impacts of CAVs on conventional flow, and to investigate Macroscopic Fundamental Diagram (MFD) of mixed traffic.

- Be harnessed in the computation of exhaust emissions and fuel consumption in the mixed traffic environment.

- Be harnessed in conventional traffic control. To evaluate the use of second-order continuum traffic models in conventional control such as MPC-based Variable Speed Limit (VSL) control of traffic, without CAVs.

- Propose novel control strategies with CAVs in mixed traffic by harnessing the new Macroscopic Continuum Traffic Flow Model (MCTFM) for mixed traffic.

1.3 Scientific Contribution

This dissertation integrates the state-of-the-art knowledge of the recent advancement concerning CAVs. The scientific contributions of this dissertation are as follows:

- A comprehensive and detailed understanding of the parameters of the MCTFMs is presented. The parameters of a set of MCTFMs are examined from a physical perspective and their significance is thoroughly investigated by employing sensitivity analysis and numerical simulation, contributing to the existing scientific understanding of the macroscopic models.
- A revamped MCTFM for mixed traffic flow based on a pragmatic approach employing microscopic simulations. Detailed theoretical and practical concepts are presented.
- A framework for the evaluation of the macroscopic road characteristics in the presence of CAVs, employing a simulation-based approach, contributes to road traffic safety science.
- An integrated framework for traffic flow and emission modeling in the presence of CAVs, HDVs, HVs and Automated Heavy Vehicles (AHVs) from a methodological perspective.
- Insights on the control of motorway traffic based on MPC, employing an efficient existing MCTFM as a prediction model in the process.
- A novel traffic flow control methodology with CAVs in the mixed traffic environment, insights, understanding, and contemporary projections.

1.4 Practical Utility and Applications

This dissertation holds immense significance in terms of the practical utility and applications of the MCTFMs. Further, this dissertation is centered on the modeling of the traffic flow in mixed traffic environment. As a consequence, three different new MCTFMs are formulated with distinct practical utility and real-world applications as shown in Figure. 1.1. In addition, a complete understanding of the parameters of the MCTFMs is presented to enhance their practical importance and use in real-world applications. The proposed models and evaluation methodology serve to improve the efficiency of highways. The proposed MCTFMs are robust and computationally fast, thus traffic flow analysis such as in the presence of CAVs, HDVs, HVs and AHVs would be performed more efficiently. These models can be employed in a number of practical applications, including, but not limited to:

- Real-time traffic flow predictions
- Evaluating the impacts of CAVs
- Understanding of the formation and dissipation of congestion on highways
- Estimation of GHG and fuel consumption
- Design of novel traffic control strategies
- Traffic impact assessment
- Traffic planning and management
- Dynamic and static traffic assignment
- Novel control of traffic with CAVs in mixed traffic
- Analysis of LOS of highways

Moreover, the utility and practical applications of the MCTFMs are further detailed in the main chapters of this dissertation and are outlined in the next Section of this chapter.

1.5 Dissertation Outline

The content of this dissertation is shown in Figure. 1.1, highlighting the step-wise goals achieved in this dissertation from its commencement to its conclusion. The outlines of this dissertation are as follows:

- **Chapter 2: Preliminaries and State-of-the-Art**
  This dissertation exhibits two-directional attributes that are modeling and control. First, the macroscopic modeling of traffic flow is explored and next the models are implemented in traffic control. This chapter presents preliminary definitions of the terminologies used in this dissertation and a state-of-the-art review of the macroscopic model since their inception. Chapter 2 concludes the research gaps in the existing literature which are responded to in the next chapters.

- **Chapter 3: Appraisal of the Second-Order Continuum Traffic Flow Model Employing Sensitivity Analysis and Numerical Simulation**
  In this chapter, the assessment of existing MCTFMs is conducted, involving detailed analysis based on categorical distinctions and accurate reproduction of traffic phenomena. Further, the parameters of MCTFMs are examined, grounded in their physical underpinnings. These examinations lead to the plausible ranges within which these parameters operate. Subsequently, the significance of all the parameters of MCTFMs is highlighted by employing sensitivity analysis for their impact on the output of the models and numerical simulations for qualitative comparative analysis. This chapter concludes with a major contribution to the practical implementation of MCTFMs. Additionally, it paves the way for further research.

  - Waheed Imran, Gennaro Nicola Bifulco, Angelo Coppola and Luigi Pariota. Appraisal of the Continuous Second Order Traffic Systems employing Sensitivity Analysis and Numerical Simulation. Under Review

- **Chapter 4: Macroscopic Modeling of Connected, Autonomous, and Human-Driven Vehicles: A Pragmatic Perspective**

This chapter proposes a new MCTFM for mixed traffic (CAVs and HDVs). It discusses the theoretical development of the new model. Additionally, this model is briefly assessed in this chapter. Details on the calibration and validation are documented. Further, the practical applications of the new proposed model in this chapter are briefly presented. Conclusively, this chapter paves way for the implementation of this model in traffic control, presented in chapter 8.

  – Waheed Imran, Tamás Tettamanti, Balázs Varga, Gennaro Nicola Bifulco and Luigi Pariota. Macroscopic Modeling of Connected, Autonomous and Human-Driven Vehicles: A Pragmatic Perspective. Under Review

- **Chapter 5: Characterization of Traffic Flow and Emissions Driven on the Fundamental Diagram of Traffic Mixture**
  In this chapter, various aspects of flow operations are investigated in the presence of CAVs, HDVs, HVs, and AHVs as they will have to coexist in traffic, forming a complex traffic mixture with distinct driver behaviors. Apart from traffic characteristics, characterization of exhaust emissions, and fuel consumption is vital in this complex traffic mixture, for understanding the positive outcomes of the evolving CAVs. The macroscopic emissions and fuel consumption model to quantify the exhaust emissions and fuel consumption is integrated with a new MCTFM model proposed in this chapter. This chapter aims to propose an integrated methodology for the modeling of traffic mixture through MFD of traffic contemplated with emissions model. Detailed insights regarding the complex phenomena of traffic mixture, and consequently their impacts on traffic emissions and fuel consumption are presented.

  – Waheed Imran and Luigi Pariota. Characterization of Traffic Flow and Emissions Driven on the Fundamental Diagram of Traffic Mixture. Under Review

- **Chapter 6: Macroscopic Evaluation of Traffic Flow in View of Connected and Autonomous Vehicles: A Simulation-Based Approach**

The operational performance of CAVs is vital to understand. Operating with significantly small lengthways between the vehicles, CAVs could compromise the safety of road traffic. Thus, this chapter proposes a density-dependent time for change occurrence in the framework of MCTFM. The behavior of CAVs is specifically modeled to improve road traffic safety. Finally, simulations are performed to investigate traffic patterns subject to various CAVs differentiated by their intrinsic properties such as lengthways gap and density-dependent time headway.

  – Waheed Imran and Luigi Pariota. Macroscopic Evaluation of Traffic Flow in View of Connected and Autonomous Vehicles: A Simulation-based Approach. *Alexandria Engineering Journal*, 79:581–590, 2023.

- **Chapter 7: An MPC-based VSL Control of Motorway Traffic**
  In this chapter, an existing MCTFM is employed in the MPC framework as a prediction model to control traffic flow on the Dublin motorway M50. This chapter aims to develop a framework that can be employed later to control traffic with CAVs. In the current traffic, only HDVs are considered. Various insights regarding congestion formation and its mitigation are briefly presented. This chapter concludes with plausible directions for the next major part of this dissertation, dicussed in chapter 8.

  – Waheed Imran, Alessio Tesone, Balázs Varga, Gennaro Nicola Bifulco and Luigi Pariota. An MPC-based VSL Control of Motorway Traffic by employing a Continuum Second-Order Traffic Model. Under preparation

- **Chapter 8: A Novel MPC-Driven Regulation of Traffic Flow with Connected and Autonomous Vehicles**
  This chapter proposes a novel control strategy for the control of traffic with CAVs in the mixed traffic environment. The MCTFM proposed in chapter 4 is employed in the MPC framework as a prediction model. In this chapter, conventional traffic control such as VSL is replaced with control of traffic only with CAVs by controlling

their time headway. The PRs of CAVs are used to quantify the effective PR of CAVs for effective control. Moreover, this novel control strategy is compared with conventional traffic control under various circumstances, far-reaching insights from the findings of this study are briefly discussed in this chapter.

  – Waheed Imran, Alessio Tesone and Luigi Pariota. A Novel MPC-Driven Regulation of Motorway Traffic with Connected and Autonomous Vehicles. Under preparation

- **Chapter 9: Conclusions and Future Directions**
  Finally, this chapter discusses and concludes the findings of this dissertation, suggesting future directions for research.

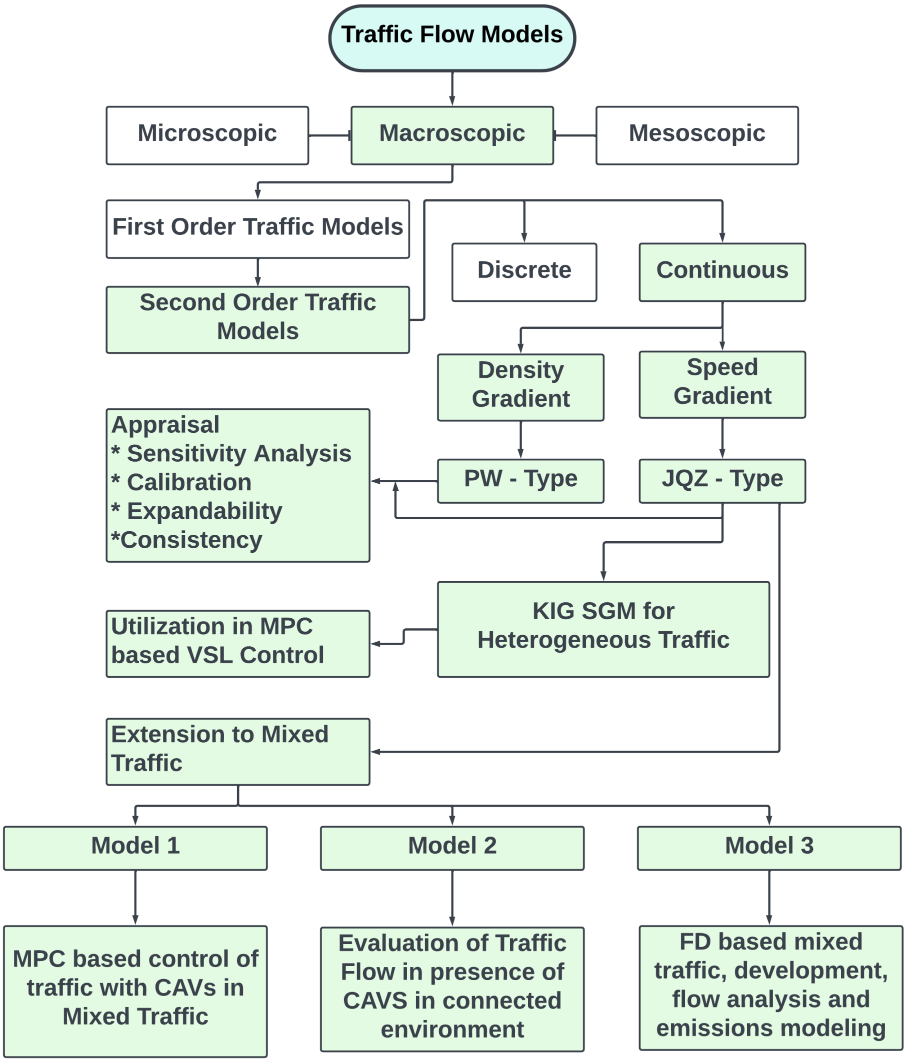

Figure 1.1. Flow chart of the contents of this Ph.D. dissertation

Chapter 2

Preliminaries and State-of-the-Art

This chapter presents the preliminary theoretical background and state-of-the-art literature review of the related research carried out in this dissertation.

2.1 Definitions

2.1.1 Traffic Flow Models

Traffic flow models are simplistic representations of real-world traffic scenarios by defining mathematical descriptions of traffic flow [5]. The dynamics of traffic flow can be predicted and possibly controlled using traffic flow models. These models can serve as the foundation for decision-making on how to improve the flow of traffic such as by analyzing the pattern of congestion formation in time and space horizon and reproducing the traffic phenomena [10]. Moreover, contemporary advancements, including the CAVs, will necessitate new policy choices aimed at understanding the dynamics of mixed traffic, and safeguarding drivers from collisions while increasing road capacity [11]. Traffic flow models are categorized based on the mathematical descriptions, and three different categories of traffic flow models are presented in the literature, that are microscopic, macroscopic, and mesoscopic.

2.1.1.1 Microscopic Traffic Models

Microscopic models consider spatiotemporal characteristics. Vehicles on the microscopic level are viewed as individual particles interacting with each other. Mostly, the time and distance headways are taken into account, and the essential component of the model is the mathematical formulation of the interaction laws between the vehicles that control the acceleration and deceleration of a single vehicle [12]. The dynamics of traffic flow based on mathematical descriptions are assessed based on the system of Ordinary Differential Equations (ODEs). These models are the most detailed with the lowest aggregation level. However, the microscopic models are computationally complex and expensive. This dissertation is solely centered on macroscopic models.

2.1.1.2 Macroscopic Traffic Models

Macroscopic models consider traffic variables such as velocity, density and flow, following the continuum mechanics. Vehicles are considered as a flow of fluid for which suitable conservation law is applicable. For this reason, macroscopic models are often called in the present context hydrodynamic models [13]. These models examine the aggregated evolution of traffic flow based on a Partial Differential Equations (PDEs) for the evolution of the relevant quantities (velocity, density, and flow) that are typically included in macroscopic models. They necessitate equilibrium speed-density relationships to substitute the interaction rules established in microscopic models, consequently, they are computationally significantly faster than microscopic models.

2.1.1.3 Mesoscopic Traffic Models

The mesoscopic models combine characteristics from macroscopic and microscopic descriptions coupled with probability distributions. They involve a high level of aggregation, but a low level of details as they typically adopt gas-kinetic analogies. Thus, these models bridge microscopic and macroscopic models [14, 15]. A distribution function that consists of a statistic of all the vehicles starting with the design and principles of a microscopic model. This distribution function is developed over time using methods from mathematical physics, and its moments, or average values, give the overall characteristics of macroscopic models and their evolution. In this way, velocity-density relations for macroscopic models are obtained, and these relations are strongly connected to the underlying microscopic models.

2.1.2 Macroscopic Fundamental Diagram

In traffic theory, velocity, density, and flow are referred to as macroscopic fundamental variables or traffic stream variables. There exists a vital relationship between these variables, represented by Fundamental Diagram (FD)s since these relationships involve macroscopic variables, so are represented by MFDs. The MFDs play a pivotal role in traffic science [16]. Different information related to traffic can be illustrated with MFDs, allowing traffic engineers and researchers to study complex insights of traffic flow, including, but not limited to congestion dynamics, free flow dynamics, and hysteresis. The basic relationship between flow(q), density (ρ), and velocity (v) is given as

$$q(x,t) = \rho(x,t) \cdot v(x,t), \tag{2.1}$$

where t and x are time and space indices. By employing this relationship $q(x,t)$ can be computed. However, in so doing, real-time information of $\rho(x,t)$ and $v(x,t)$, are needed. Thus, $v(x,t)$ can be considered as a function of density in equilibrium conditions, and the relationship between $v(x,t)$ and $\rho(x,t)$ in equilibrium conditions is given by equilibrium velocity distribution ($V(\rho(x,t))$). When changes in flow occur, traffic moves towards this distribution [17].

Greenshields [18] proposed a distribution with an inverse linear relationship between $v(x,t)$ and $\rho(x,t)$ and is given by

$$V(\rho(x,t)) = v_m\big(1 - \frac{\rho(x,t)}{\rho_m}\big), \tag{2.2}$$

where ρ_m and v_m represent maximum density and velocity, respectively. In Eq. (2.2), as $\rho(x,t)$ increases, $\frac{\rho(x,t)}{\rho_m}$ increases as well. Thus, this increase leads to a decrease in $\big(1 - \frac{\rho(x,t)}{\rho_m}\big)$, resulting in a decrease in $V(\rho(x,t))$. So, $V(\rho(x,t))$ is zero when $\rho(x,t)$ approaches ρ_m. Recalling Eq. (2.1), and replacing $v(x,t)$ with $v(\rho(x,t))$ results in

$$q(\rho(x,t)) = \rho(x,t) \cdot V(\rho(x,t)), \tag{2.3}$$

where $q(\rho(x,t))$ represents flow as a function of density. Using Eq. (2.3), the relationship between $\rho(x,t)$ and $q(\rho(x,t))$ can be established. Figure. 2.1 is the flow-density relationship obtained using speculative synthetic data employing the Greenshields model (Eq. (2.2)).

In Figure. 2.1, free flow, congested flow, capacity (maximum flow (q_m)), critical density (ρ_{cr}) and ρ_m can be observed. The shape of FD depends on the choice of $V(\rho(x,t))$. The Greenshields model results in an overestimation of the traffic quantities, and this model is only feasible for homogeneous traffic conditions. In non-homogeneous traffic, the Papageorgiou model [19] can be employed, which is given as

$$V(\rho(x,t)) = v_m \cdot \exp\Big[\frac{-1}{c}\Big(\frac{\rho(x,t)}{\rho_{cr}}\Big)^c\Big], \tag{2.4}$$

where c corresponds to a shape factor. The velocity-density relationships with the Greenshields model and the Papageorgiou model are illustrated in Figure. 2.2. Furthermore, it is to be noted that the Greenshields model presents a simplified representation of traffic flow. In reality, traffic flow in congestion is impacted by different factors, including, but not limited to driver heterogeneity, the geometry of the highway, etc. While the Greenshields equation provides a basic framework for understanding the relationship between density and velocity, other contemporary models exhibit close behavior with heterogeneous traffic.

2.1.3 Intelligent Transportation System

Lately, technological advancements have led to the development of an integrated system aimed to reduce environmental pollution, and congestion, increasing traffic safety, and controlling inefficient use of resources. This advanced framework is now widely known as ITS integrates information and communication advancements to improve the safety and efficiency of transportation networks. It combines data collection in real-time, processing, and communication to improve the operations and management of transportation systems [20]. The components and features of ITS in-

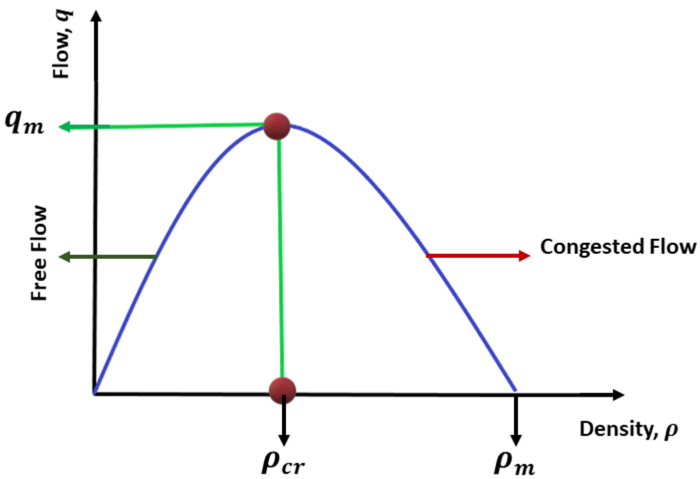

Figure 2.1. Flow-Density relationship according to the Greenshields model. Note that this figure is generated by using speculative synthetic data for the purpose of understanding.

clude, ATIS, providing real-time information regarding traffic conditions to travelers, leading to informed decisions by travelers[21]. The MCTFMs can play a pivotal role in ATIS by providing travelers with information about the future states of traffic.

The features of ITS are not limited to ATIS, but beyond. One significant feature is traffic management and control [22]. Traffic flow can be optimized by leveraging using real-time data from sensors, cameras, and detectors to monitor congestion. This information can be processed to optimize the signals timings, lane usage and benefit the users with dynamics routing information. Moreover, potential collisions and hazards can be avoided with advanced technologies such as Vehicle to Infrastructure (V2I) and Vehicle to Vehicle (V2V) communication [23]. Further features include but are not limited to, smart electronic toll collection, intelligent parking systems, environmental monitoring and management, emergency management, transportation demand management, fleet management, and traffic data collection and analysis (big data) [24, 25, 26].

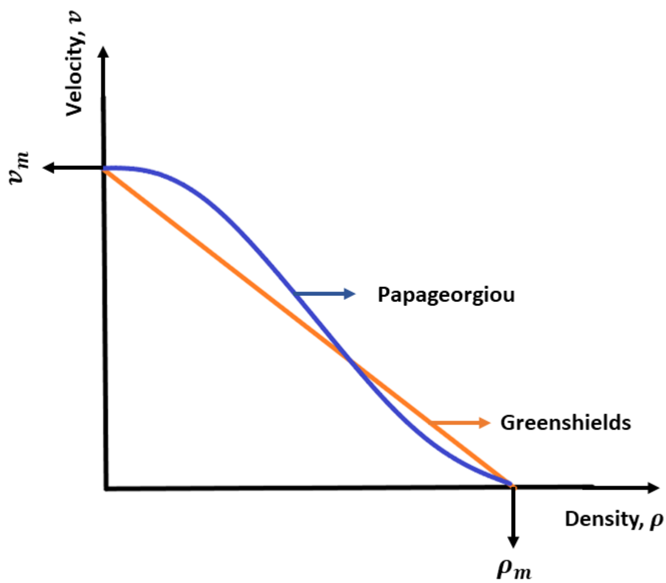

Figure 2.2. Velocity-Density relationship according to the Greenshields and Papageorgiou models. Note that this figure is generated by using speculative synthetic data for the purpose of understanding.

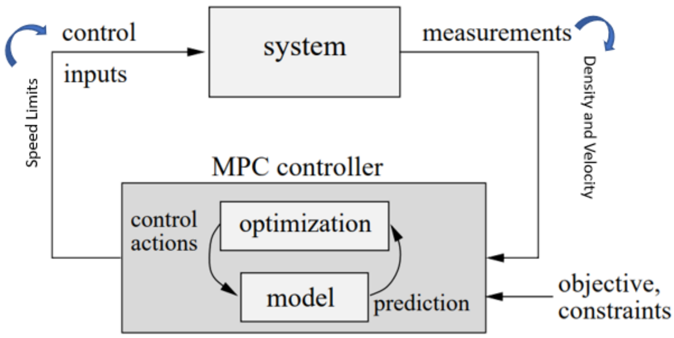

Figure 2.3. Block diagram of the MPC-based control loop.

2.1.4 Model Predictive Control

The MCTFMs predict the future states of traffic. They perform accurate short-term predictions. While the MPC considers a set of control rules by taking into the future states of traffic, thus MCTFMs can be employed in MPC-based control for robust solutions. MPC solves a constrained optimization problem and determines an optimal control variable [27, 28]. Thus, it is one of the control techniques that explicitly considers constraints. An objective function is often designed to optimize the problem by prioritizing certain traffic characteristics, the most common of which is to minimize total travel time. Certainly, the MPC tracks a reference trajectory, and a control action is determined accordingly. The predictions and optimization are repeated for the given time instances, thus, it is also called receding horizon control [29]. The prediction time and control time, known as the prediction horizon and the control horizon are vital for the output of the control. An optimal solution is achieved over short-term optimization since the error of a proximal forecast is considered to be small compared to a distant prediction [30]. The general principle of MPC is illustrated in Figure. 2.3.

2.2 State of the Art on Second-Order Traffic Flow Models

The MCTFMs assume aggregated traffic variables. These models are categorically presented as first-order and second-order traffic models [31, 32]. The first-order models comprise commonly a single-state equation and are based on velocity. While the second-order models are two-state coupled equations and are based on acceleration [33]. At the outset, Lighthill, Whitham and Richards (LWR) initiated studies on the MCTFMs between $1950's$ and $1960's$ by proposing a single-state equation model famously known as the LWR model [34, 35], which is given as

$$\frac{\partial \rho(x,t)}{\partial t} + \frac{\partial(\rho(x,t) \cdot v(x,t))}{\partial x} = i_q(x,t) - e_q(x,t), \tag{2.5}$$

where $\rho(x,t)$ is traffic density, and $v(x,t)$ is the velocity considered as a function of density such as $V(\rho(x,t))$. It represents the relationship between density and velocity in equilibrium flow conditions. Whereas, i_q and e_q are the exogenous source terms for off-ramp and on-ramp flows. While the t and x represent time and space, respectively. The first-order models are subject to assumption that the speed of vehicles is adjusted instantaneously to the value given by the velocity-density relationship based on actual density [36]. Thus, abrupt changes in flow occur which is an unrealistic traffic behavior [37]. Further, the LWR model characterizes only small changes in flow that occur instantaneously [38, 39, 40, 41]. This model is not capable to reproduce non-equilibrium traffic phenomena [42].

Soon as the shortcoming of the LWR model was noticed, an improved momentum equation to the existing first-order model was added, enabling a new model, and resolving the shortcoming of the LWR model [43]. The momentum equation primarily comprises the convection, acceleration, anticipation, and relaxation terms [44]. It is given as

$$\frac{\partial v(x,t)}{\partial t} + v(x,t)\frac{\partial v(x,t)}{\partial x} + \frac{c_0^2}{\rho(x,t)}\frac{\partial \rho(x,t)}{\partial x} = \frac{1}{\Gamma}(V(\rho(x,t)) - v(x,t)), \tag{2.6}$$

where the acceleration term is

$$\frac{\partial v(x,t)}{\partial t},$$

the convection term is

$$v(x,t)\frac{\partial v(x,t)}{\partial \rho}.$$

Whereas

$$\frac{c_0^2}{\rho(x,t)}\frac{\partial \rho(x,t)}{\partial x},$$

is the anticipation term, and

$$\frac{1}{\Gamma}(V(\rho(x,t)) - v(x,t)),$$

is the relaxation term. The acceleration and convection terms characterize the acceleration of vehicles and the effect of a vehicle on other vehicles in the vicinity with its egress and ingress in a road section. The relaxation term defines the tendency of each vehicle to travel at the desired speed depending on the congestion level of the link. $\Gamma > 0$ is the relaxation time for vehicles to adjust their velocity according to the equilibrium conditions. The reaction of drivers to the variations in traffic conditions ahead of them is characterized by the anticipation term. In other words, this term accounts for the tendency of vehicles to accelerate or decelerate [31]. c_0^2 in the anticipation term is the backward propagation speed of the perturbation or a rearward velocity constant. It corresponds to a driver's response to changes in traffic conditions. Thus, all the changes in upstream traffic propagate with a constant velocity in all traffic conditions. In other words, perturbation in traffic flow is instigated according to it. Combining Eq. (2.5) and Eq. (2.6) forms a second-order model with two-state-equations. It is widely known as the Payne and Whitham (PW) model [45, 46] which is given as

$$\begin{aligned}\frac{\partial\rho(x,t)}{\partial t}+\frac{\partial\rho(x,t)\cdot v(x,t)}{\partial x}&=i_q(x,t)-e_q(x,t),\\ \frac{\partial v(x,t)}{\partial t}+v(x,t)\frac{\partial v(x,t)}{\partial x}+\frac{c_0^2}{\rho(x,t)}\frac{\partial\rho(x,t)}{\partial x}&=\frac{1}{\Gamma}(V(\rho(x,t))-v(x,t)).\end{aligned} \tag{2.7}$$

Based on the constant anticipation rate, this model assumes that all the vehicles have uniform behavior [46].

The second-order PW model was criticized by [39] by highlighting the imperfections of the PW model that include the violation of anisotropic traffic property, and the onset of vehicles' negative speeds. Commonly, frontal traffic dynamics influence vehicles while being practically insensitive to what happens behind them. It was noted that some information generated by the motion of the vehicles travels faster than the vehicles themselves (faster-than-traffic waves). Hence it affects the frontal traffic dynamics. However, in the literature, a notion has been created that the information from the characteristic speed from behind cannot reach vehicles from behind thus affecting their dynamics.

[47] noted a while after Daganzo's criticism that in multi-lane traffic flow, lane speeds differ which allows some vehicles to travel faster than the average speed. Later, the PW model was improved by [48] distinguishing the density such that changes in traffic occur below or at the average speed. However, this can only result in realistic acceleration when the density is low [49], and otherwise, the acceleration is unrealistic. [50] argued that the faster-than-traffic waves do not necessarily violate the anisotropic property. Typical velocity faster than the average vehicle velocity could be shown to exist, with followers accelerating (or decelerating) before their leaders. This does not entail a violation of anisotropy, and it cannot be regarded as a theoretical inconsistency. Through theoretical analyses and numerical tests, they showed that these faster-than-traffic waves (characteristic velocity) could not be artifacts of the derivation of continuum models from microscopic relationships because they are also observable in the underlying car following relationships.

[51] criticized the numerical example given by [50], concluded that it could be unrealistic in real-world traffic. It has been suggested that a line of vehicles can be triggered to accelerate beginning from back to front.

Furthermore, it is shown that the faster-than-traffic waves could result in convexities in the flow-density diagram. It means the information carried by faster-than-traffic characteristics could reach vehicles from behind and affect their dynamics. Practically, the driver's presumption of frontal conditions in the PW model and its extensions are based on spatial changes in density. However, [52] successfully solved this problem by proposing an anisotropic second-order model, which is called on as JQZ in what follows on. It looks at how drivers predict what will happen ahead of them by considering how closely packed the vehicles are and how the speed changes as they move. It is given as

$$\begin{aligned} &\frac{\partial \rho(x,t)}{\partial t} + \frac{\partial \rho(x,t) \cdot v(x,t)}{\partial x} = i_q(x,t) - e_q(x,t), \\ &\frac{\partial v(x,t)}{\partial t} + (v(x,t) - c_0)\frac{\partial v(x,t)}{\partial x} = \frac{1}{\Gamma}(V(\rho(x,t)) - v(x,t)). \end{aligned} \tag{2.8}$$

This model successfully addressed the issue of anisotropy in the second-order models. However, it relies on drivers making predictions using a fixed value, which isn't very practical in real-world situations.

The adverse impacts of faster-than-traffic waves were also discussed by [53]. The performance of MCTFMs (second-order) may not be overall significant both from a theoretical and practical perspective. However, the shortcomings are comprehended in the recent extensions of the second-order models. Recently, a second-order model based on variable rearward velocity was proposed by [5]. It is the extension of [52], meaning that the model is anisotropic as well as driver presumptions are not constant as in earlier models. The second-order models are classified further into two distinct groups. Discrete traffic models consider space and time as discrete variables. They are obtained by discretizing in space and time the continuous macroscopic traffic models. Whereas continuous models assume continuous variables in space and time, and the system dynamics are represented by partial differential equations [54].

Furthermore, the second-order continuous models are revised by incorporating traffic physics, road and environment, and explicit driver behavior. These advancements offer the opportunity to delve into unexplored insights concerning traffic dynamics and to enact novel control strategies within the era of ITS. Adverse weather effects are modeled by [55]. They have employed weather-based FD by incorporating weather information, however, this model is a discrete model with global non-physical parameters. Considering driving behavior in mountainous regions, [56] proposed a continuum model that considers the tail light effect of the frontal vehicle to minimize the driving challenge. Lately, the PW model is improved by [17] by incorporating driver behavior over transitions in traffic. This model is the most recent extension of the continuum models.

Besides, some developments are [57, 58, 59], however, all of these models are based on HDVs, and do not account for the properties of CAVs. Presently, technologies such as automated driving and wireless communication are vital for the development and deployment of CAVs. They are aimed to improve traffic efficiency and safety [60, 61]. Thus, the second-order models can be revised by incorporating the properties of CAVs for a more realistic characterization of mixed traffic.

2.2.1 Refinements concerning CAVs in the framework of second-order traffic models

Lately, there have been a few advancements that consider V2V communication, Adaptive Cruise Control (ACC), and Cooperative Adaptive Cruise Control (CACC) [62, 63, 64, 65]. Concerning CACC, it has been investigated that at 100% PR, CACC reduced traffic congestion by improving highway capacity and throughput, and controlled traffic flow instabilities to a significant extent as compared to ACC. However, the literature following this approach is focused on homogeneous traffic, assuming a 100% PR, while there are some attempts that consider varying PR of ACC and CACC systems [65, 66]. With respect to the stabilization of traffic flow, results confirm that if only around 30%–40% vehicles are equipped with CACC, they enhanced the stabilization of traffic flow. These investigations laid the foundation for conducting research on the characteristics of mixed traffic flow and examining how they influence conventional traffic flow.

Based on Gas Kinetic Traffic (GKT) model, [67] proposed a second-order traffic flow model, which incorporates the ACC/CACC approach with a twofold aim. First, developing a numerical simulation tool based on a multi-lane GKT model, and second, testing its behavior under realistic traffic conditions. But, since the drawbacks of the GKT model are known, this model is only applicable to regions with low density. Its applicability in high-density regions can result in unrealistic traffic flow behavior [68]. There is a scarcity of existing literature concerning the adaptation of this model for CAVs. Besides, some studies are carried out to revise the first-order models by considering the lane-changing behavior in the presence of Automated Vehicles (AVs). One extension of the first-order model which incorporates the lane-changing behavior was proposed by [69]. This model differs from the state-of-the-art first-order LWR model with the addition of a source term that defines the rate of a lane change in flow. However, this model is only applicable to homogeneous flow as the driver behavior and transition dynamics are ignored.

Further, [70] proposed a macroscopic model for mixed traffic. A FD based on hysteresis phenomena is proposed to improve the well-known Cell Transmission Model (CTM) which is modified to capture the impacts of mixed traffic. However, this model is of first-order which is not the scope of this dissertation, further, this model does not explicitly consider the driver/vehicles interactions. The spatio-temporal characteristics of the mixed traffic are ignored which is the shortcoming of this model. Besides, considering other frameworks, the spatial characteristics of mixed traffic such as headway are studied by [71]. They have modeled the headway of vehicles in mixed traffic subjected to PR of CAVs. It is explicitly concluded that with the deployment of CAVs headway changes, this study is supported by microscopic simulations. A study on the impacts of CAVs and other AVs on mixed flow characteristics and emissions subjected to microscopic simulations in VISSIM is conducted by [72]. It has been concluded that 100% of CAVs greatly improve the freeway capacity as compared to other AVs.

The existing literature has successfully laid the foundation for investigating and comprehending the interactions among vehicles within heterogeneous traffic conditions. Nevertheless, there exist areas of research that require attention from a broader perspective. Specifically, the interactions between vehicles in mixed traffic scenarios and their consequential effects on traffic flow throughput, road capacity, and freeway performance are subjects that demand consideration. It is imperative to develop accurate models that can effectively capture the dynamics of mixed traffic. To address these issues, this dissertation introduces novel second-order traffic models. These models offer a valuable tool for characterizing mixed traffic flow, enhancing our comprehension of the aforementioned research gaps.

2.2.2 Practical applications of the second-order traffic flow models in control

In the MPC framework, as explained in Section 2.1.4, the prediction model plays a pivotal role. The second-order models are substantially efficient in reproducing real-world traffic phenomena and are computationally fast. In this dissertation, we focus on the practical applications of second-order continuous traffic flow models in control in the MPC framework with application to motorway traffic.

The design of motorways should be convenient for the users and should be comfortable and safe while ensuring the efficient movement of vehicles [73]. Traffic congestion is a challenging problem, and it is observed more often on motorways during peak hours. To tackle traffic congestion, various effective control techniques are proposed. One of the conventional control techniques is the implementation of VSL. It helps in the dissolution and reduction of traffic congestion. The second-order continuous models are rarely used in control in the MPC framework, while the discrete models are employed more often.

The control strategies are broadly classified as system and vehicle level control. The former regards traffic control on a macroscopic level since the traffic is regulated by treating all the vehicles together. The system level control is further classified as ramp and mainstream control. In ramp control the flow is intelligently managed by controlling ingress vehicles to the mainstream [74]. In mainstream control, there have been reported a number of methods such as implementing traffic diversions, it is also called routing of the traffic Routing. Another method is VSL where different road segments are controlled by implementing restrictions on posted speed [73], this approach is justified mainly for motorways. While at the vehicle level, V2V and V2I technologies for control purposes are employed. It is generally done on a microscopic level [75, 76].

In challenging scenarios characterized by heavy traffic congestion and bottlenecked road segments, the implementation of VSL control aims to preserve the reliability of speed regulations. This objective is pursued to ensure that speed limits continue to serve their primary purpose of up-holding road safety while optimizing traffic flow to its maximum capacity. The VSL system adapts the designated speed limits in response to real-time traffic conditions [77]. Categorically, two overarching methodologies for VSL implementation can be identified: the reactive and proactive approaches. The reactive approach involves the application of straightforward speed regulations in response to the detection of abnormal traffic conditions in real time. Conversely, the proactive VSL approach represents a more advanced strategy compared to its reactive counterpart. This approach leverages optimization techniques and computations that are founded on anticipated traffic states, thereby enabling a more sophisticated and pre-emptive adjustment of speed limits. The predicted states are calculated by a prediction model that looks into the future states of the traffic, preventing an abnormal traffic behavior such as severe traffic breakdown from happening [78, 79].

The VSL has been implemented in many studies [80, 81]. A VSL traffic control strategy was proposed by [82] employing kinematic wave theory. This scheme is aimed to enhance the throughput of traffic bottlenecks by proposing simple regulations, this scheme is designed only for solving moving jams [83]. A new model was proposed by [84] for VSL control of traffic. This study explicitly considers FD of traffic influenced by variable speed limit for a particular road segment. Macroscopic modeling of VSL on freeways is presented by [85]. This study employs the METANET model, however, METANET is a discrete model, and this model is not based on traffic physics. Conversely, literature reports various studies employing discrete models in implementing VSL, but the continuous models which are based on traffic physics, and are more efficient than discrete models are not employed in the design of VSL.

Furthermore, in the MPC framework, a few studies employing the discrete macroscopic models are presented [86]. An integrated approach to freeway traffic network control is presented by [87]. Based on optimal control variables they propose the MPC method. The control variables are obtained from numerical optimization. The findings suggest a significant reduction in traffic congestion, but this study is related to a discrete second-order traffic model. The MPC approach has proved significant in many studies and can bring a plausible reduction in congestion. [88] investigated the optimal perimeter control for two-region urban cities. The comparative analysis demonstrates that MPC is a better control approach in available approaches in the literature. However, this study considers homogeneous regions, thus, it can be extended to investigate heterogeneous regions. The MPC approach can be extended to freeways. Alternatively, models incorporating traffic physics should be employed in the MPC framework, exercising continuous models brings the opportunity to employ a number of control inputs, thus replacing the conventional VSL method.

Furthermore, with the advent of CAVs, the dynamics of traffic will alter, and so will the control approaches. To completely enhance the motorway performance such as to mitigate traffic congestion, a more complex control algorithm between the two, that includes optimized VSL decision-making is needed. At the system level, the accuracy of the macroscopic prediction model is significant because it describes the evolution of traffic flow [89]. The second-order continuous models incorporating traffic physics provide opportunity to control traffic by choosing alternative control inputs to VSL such as reaction time, time headway, and distance headway in the case of CAVs. The macroscopic state prediction is useful for real-time predictions and control applications.

2.3 Concluding Remarks and Direction for the Next Chapter

The fundamental concepts of traffic flow, the state of the art and basic definitions of the terminologies used in this dissertation have been reviewed in this chapter. A multifaceted compilation of the literature, one of which includes a thorough explanation of traffic models while simultaneously pointing out research gaps in the era of CAVs. The other facet is focused on the control of traffic in the MPC framework. This aspect also reveals persistent gaps in the range of applications for CAVs.

In this dissertation, the second-order continuous models and their use in control are methodically and thoroughly explored. Our strategy involves a methodical process that analyzes the details of the topic. However, the validity of second-order continuous models is still widely debated, as shown by a detailed review of the literature. As a primary concern, it becomes necessary to carefully examine the accuracy of these models. This examination is of utmost importance in order to enable the wide scope of this dissertation, the improvement of second-order continuous models to fit the context of CAVs, and their eventual incorporation into the traffic management framework.

Thus, next, we present an appraisal of the second-order continuous models. We delve deeper into the insights and properties of these models. We investigate the role of the parameters of the second-order continuous models and identify how they can be improved to incorporate CAVs. The importance of the models' parameters on the output has been analyzed by employing sensitivity analysis and the validity of these models is investigated with numerical simulation compared with microscopic simulation.

Chapter 3

Appraisal of the Second-Order Continuum Traffic Flow Model Employing Sensitivity Analysis and Numerical Simulation

3.1 Abstract

The Macroscopic Continuum Traffic Models (MCTFMs), explicitly the Second Order Traffic Flow Models (SOTFMs) are substantially known for traffic flow characterization because of their plausible simplicity, low computational efficiency, and explicit replication of non-equilibrium traffic phenomena. Categorically, the SOTFMs are presented in two distinct groups namely Density Gradient Models (DGMs), and Speed Gradient Models (SGMs) also known as anisotropic traffic flow models. Their mathematical properties are extensively studied, but investigations into their practicality are limited. Thus, in this chapter, the performance of a set of SOTFMs is qualitatively and quantitatively evaluated against reference data (ground-truth) collected in a microscopic simulator representing non-identical traffic conditions.

The evaluation is complemented with a sensitivity analysis of these systems which is employed to highlight the versatility of model parameters qualitatively and quantitatively. Results show that the SOTFMs are powerful tools to reproduce real-world traffic phenomena. As evident from the results, these systems have a lower average error when compared with the ground-truth, and the spatiotemporal pattern formation and evolution conform to that of the ground-truth. Furthermore, it is noted that the average system output is dominated by the relaxation term, but the stability of the system around the average output is affirmed by the anticipation term. A far-reaching analysis on the versatility, consistency, expandability and accuracy of a set of SOTFMs are presented distinctively.

3.2 Introduction

Traffic flow forecasting is a crucial process for effective planning, management and control of traffic movement along highway corridors. It enables transportation agencies to proactively plan and implement strategies to alleviate congestion, improve traffic flow, and reduce fuel/energy consumption. Moreover, real-time traffic flow forecasting enables travellers to make informed decisions about their travel plans, such as choosing alternate routes or modes of transportation, and can help emergency responders to plan for and respond to incidents more quickly and effectively. Therefore, gaining a comprehensive understanding and accurate description of traffic flow dynamics holds immense importance [90].

Several MCTFMs are proposed in the literature for traffic flow forecasting, among those, Second Order Traffic Systems (SOTFMs) are considered the most prominent since they can capture more complex traffic behaviors compared to First Order Traffic Flow Models (FOTFMs) [31, 91], such as traffic jams and shockwaves. These models take into account not only the current traffic volume and speed but also the rate of change of these variables over time. They are based on the assumption that drivers adjust their speed based on the traffic flow around them and the road conditions, leading to a nonlinear relationship between traffic density and traffic speed. They are particularly useful for predicting traffic conditions on highway corridors. Moreover, they offer the advantage of requiring fewer calibration efforts in comparison to other traffic systems, such as microscopic systems, which are computationally complex and possess calibration issues. It should be noted that SOTFMs are computationally faster than microscopic models [47, 92]. Conversely, it is noteworthy that the majority of SOTFMs lack a robust theoretical foundation, and due to the infrequent validation against real data, their practical utility, consistency and expandability remains less understood. Moreover, the literature pertaining to the assessment of SOTFMs is notably limited.

Lately, [53] presented a comprehensive survey covering broad aspects of most of the traffic systems already proposed in the literature. Among those, the SOTFMs are represented by the [52] (JQZ model). This model assumes that drivers adjust their speed based on the traffic flow and the road conditions and, due to its mathematical structure, can replicate complex traffic phenomena (e.g., traffic bottlenecks and speed drop) while preserving the anisotropic property of traffic. Furthermore, the model has less calibration error and the overall performance of the model is better than other models presented [5].

Notwithstanding, the assessment of the SOTFMs based on a solitary model is insufficient. Indeed, the JQZ model has been subject to criticism in the literature for its backward propagation speed of perturbation, which is based on a constant value [93, 5]. Additionally, the acceleration equation of the JQZ model can become decoupled from the continuity equation when relaxation times are larger, further diminishing its reliability. Further, the macroscopic models are extremely sensitive to initial conditions in saturated traffic conditions [94], thus it is vital to asses various traffic scenarios for to evaluate their consistency to reproduce traffic phenomena effectively, flexibility to accept heterogeneity (driver behavior), and expandability to different traffic conditions [95].

In light of the preceding rationale, this paper presents an extended evaluative study on SOTFMs, with particular emphasis on a distinctive ensemble of continuous SOTFMs renowned for their simplicity, rapid computational efficiency, ability to address negative-way travel, capacity to replicate traffic phenomena, and incorporation of traffic physics. Specifically, the paper undertakes a qualitative and quantitative analysis of the performance of SOTFMs, with the main objectives being to:

1. define the overarching characteristics of SOTFM, to elucidate the spatiotemporal evolution of traffic flow under distinct traffic con-

ditions. Specifically, the performance of the SOTFM is evaluated through a comparative analysis with external reference scenarios. The study is conducted on two non-identical traffic scenarios. It is noteworthy that the reference scenarios are designed to simulate sufficiently complex traffic conditions, without imposing excessive effects on the simulation, thereby avoiding oversimplification.

2. enhance understanding of model parameters and aiming to reducing further the computational complexity. This is obtained by performing a sensitivity analysis, which has revealed how the parameters of the different models most significantly affect their outputs. Sensitivity analysis has consequently allowed us to reduce the number of model parameters subjected to calibration.

3. improve comprehension of model parameters and related effects. To achieve this aim, a sensitivity analysis is conducted. The sensitivity analysis enables the identification of the model parameters that exert the most significant influence on the outputs of the various considered SOTFMs. As a result, the number of model parameters requiring calibration is reduced.

4. augment the comparative analysis standpoint, given the prevailing belief that SOTFMs are promising models for forecasting traffic state, it is crucial to quantify the extent to which they can accurately replicate observed traffic in a reference scenario.

3.3 Background and State of the art: Overview of the Second Order Traffic Flow Models

Macroscopic models describe traffic flow at an aggregate level by leveraging flow, density, and speed as variables to represent the behavior of groups of vehicles. These models are equated with the flow of fluid particles, for which suitable equilibrium or conservation laws can be written. For this reason, macroscopic models are often called hydrodynamic models [49, 47, 96].

Macroscopic models are computationally less demanding than mesoscopic and microscopic models, and the computational effort does not increase with increasing traffic densities (does not depend on the number of vehicles in the network). For these reasons, they are suitable for short-term forecasting in the context of network-wide coordinated traffic management. For example, they can be used in the development of dynamic traffic management and control systems or to estimate and predict average traffic flow operations.

Macroscopic models are classified on the basis of state equations as FOTFMs (or velocity-based, with one state equation) and SOTFM (or acceleration-based, with two state equations) [31, 32]. The first effort in macroscopic modeling of traffic was taken by Lighthill and Whitham in 1955 and, a year later, by Richards (1956) with the so-called LWR model [34, 35]. It describes the relationship between traffic density and speed and is based on the principle of conservation of vehicles. The model is a first order Partial Differential Equation (PDE) consisting of a continuity equation that relates the rate of change of traffic density to the difference between the inflow and outflow rates, and a velocity-density relationship that describes the relationship between traffic velocity and density. The model is mathematically expressed as follows:

$$\rho_t + \rho\big(v_e(\rho)\big)_x = 0, \tag{3.1}$$

where subscripts t and x indicate temporal and spatial partial derivatives; ρ is traffic density; and $v_e(\rho)$ is the closure relation (i.e. the speed-density relationship in equilibrium conditions). This latter is the relation between velocity and density at the equilibrium and is given by

$$v_e(\rho) = v_f \times \Big(1 - \frac{\rho}{\rho_m}\Big), \tag{3.2}$$

where v_f is the free-flow speed and ρ_m is the jam density.

First Order Traffic Flow Model (FOTFM) such as the LWR (see Eq. 3.1) are appreciated for their simplicity, but can be suitable only if one contemplate about the size and the end of a queue, i.e. the time-space trajectory of a shock [97]. Indeed, they are based on the restrictive assumption that vehicles adjust their speeds instantaneously to the value given by the closure relation based on actual density. This leads to the following issues: *i*) the speed reacts instantaneously to any variation of traffic density without any delay [37]; *ii*) start & stop and hysteresis phenomena are not captured; *iii*) is unable to describe non-equilibrium traffic phenomena [42]. For all these reasons, the LWR model is only capable of characterizing small changes in a traffic flow that occur instantaneously such that conditions on an idealized long road section [39, 40, 41, 37].

To overcome the shortcomings of the LWR model, Payne and Whitham added a momentum equation to the existing FOTFMs. This newly proposed equation is composed of the acceleration, convection, anticipation, and relaxation terms [44, 43], and is given as

$$v_t + v v_x + \frac{c_0^2}{\rho}\rho_x = \frac{1}{\tau}\big(v_e(\rho) - v\big), \tag{3.3}$$

where v_t is the acceleration term, vv_x is the convection term, $\frac{c_0^2}{\rho}\rho_x$ is the anticipation term, and $\frac{1}{\tau}(v_e(\rho) - v)$ is the relaxation term. The convection term depicts changes in the traffic speed due to the inflow and outflow of vehicles with different speeds. The relaxation term defines the tendency of each vehicle to travel at the density-dependent equilibrium speed of the link. Herein, $v_e(\rho)$ is the closure relation between velocity and density, v is the average velocity, and $\tau > 0$ is the relaxation time for vehicles to adjust their velocity according to the equilibrium velocity. Finally, the anticipation term describes the reaction of drivers to downstream traffic conditions; in other words, this term accounts for the tendency of vehicles to accelerate or decelerate [31]. Herein, c_0 represents the backward propagation speed of a perturbation, that can be assumed as constant.

Combining Eq. 3.1 and Eq. 3.3, the Payne [45] and Whitham [46] (PW) SOTFM model is be obtained:

$$\begin{aligned} &\rho_t + \rho\big(v_e(\rho)\big)_x = 0, \\ &v_t + v v_x + \frac{c_0^2}{\rho}\rho_x = \frac{1}{\tau}\big(v_e(\rho) - v\big). \end{aligned} \tag{3.4}$$

Based on the constant anticipation rate, this model assumes that all the vehicles have uniform behavior [46]. The structure of the PW model is elaborated in Table 1, and the developments till the PW model are given in Figure 3.1.

Later, Daganzo [39] highlighted some shortcomings of the PW model which include the possible onset of negative speeds of the vehicles as well

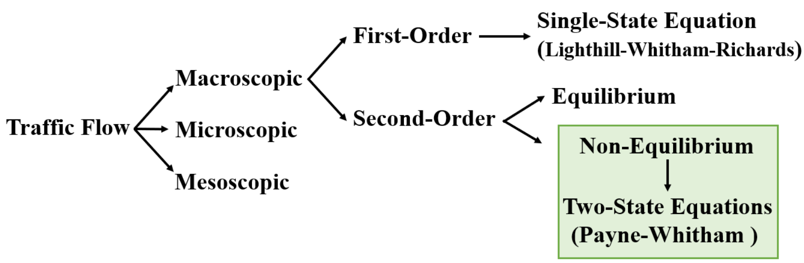

Figure 3.1. Schematic representation of the evolution of various traffic systems till the development of PW model.

as the violation of the so-called anisotropy principle. That is, a vehicle should be influenced only by the traffic dynamics ahead of it, being practically insensitive to what happens behind. Indeed, they stated that some information generated by the motion of the vehicles travels faster than the vehicles themselves (faster-than-traffic waves), hence affecting the forward traffic dynamics. However, in the literature, a notion has been created that the information from the characteristic speed from behind cannot reach vehicles from behind thus affecting their dynamics.

Since Daganzo's severe criticism, the SOTFM started to expand. For instance, Aw and Rascle [48] improved the PW model by characterizing density such that changes occur at or below the average speed. However, this can result in unrealistic acceleration when the density is high [35]. [50] argued that the faster-than-traffic waves do not necessarily violate the anisotropic property. Thus, they associated the waves with the group velocity such that the velocity at which the overall shape of the traffic waves travels. Through theoretical analysis and numerical tests, they showed that these waves could not be artifacts of the derivation of continuum models from microscopic relationships because they are also observable in the underlying car-following relationships. [51] countered that the numerical example given by Helbing and Johansson could be unrealistic in real-world traffic because it suggests that a line of vehicles can be triggered to accelerate from back to front. Furthermore, the authors showed that faster than traffic waves could result in convexities in the flow density diagram, meaning information carried by faster than traffic characteristics could reach vehicles from behind and affect their dynamics. Again, [53] suggested that the adverse effects of faster-than-traffic waves on the performance of continuum models may not be generally significant from both a theoretical and a practical perspective. However, the shortcomings are comprehended in the recent extensions of the SOTFMs which are elaborated on next.

3.4 Contemporary Argumentation

This paper aims to consider models from different classes of SOTFMs, and to evaluate their properties for different traffic mechanisms such as spatiotemporal pattern formation. To avoid too complex mathematical formulations and extensive calibration difficulties, the simplest SOTFMs are selected among the available ones presented in the literature. This selection has been done through an extensive review of the traffic systems, and considering the best output of the traffic systems available in the literature. A criterion for the selection of SOTFMs is to cover the depth of information provided by the model along with the breadth of theoretical knowledge related to the systems, which is also the uniqueness of this study.

To begin with, it is worth noting that SOTFMs can be divided into Density Gradient Model (DGM) and Speed Gradient Model (SGM) to tackle faster-than-traffic wave problems. Note that the original PW model is a DGM that considers the driver presumption of forward conditions based on density and spatial changes in density, while the SGM considers the driver presumption of forward conditions based on density and spatial changes in velocity [5]. A schematic representation of traffic systems is presented in Figure 3.2.

The PW model is based on the assumption that c_0 is a constant, which produces unrealistic behaviors since the driver presumption to forward conditions is always non-uniform. This unrealistic behavior is related to the anticipation term of the model, which is improved in the recently developed extension proposed by [98] and [99]. In literature, developments in DGM are also known as PW-type or extended PW-type models. [98] proposed a new anticipation term that characterizes traffic flow based on the lateral distance b and time headway τ_h. This model, called in what follows IK model, can characterize homogeneous and non-homogeneous flows, and is

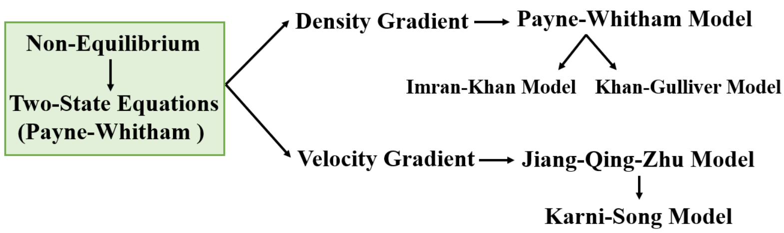

Figure 3.2. Schematic diagram of the second order traffic models as expended from PW model.

given as

$$\begin{aligned} &\rho_t + \rho\big(v_e(\rho)\big)_x = 0, \\ &v_t + v v_x + \tau_h b \rho_x = \frac{1}{\tau}\big(v_e(\rho) - v\big). \end{aligned} \tag{3.5}$$

The second extension of the PW model that has been considered is the model proposed by [99]. In this study, a new anticipation term is proposed based on alignment with the conditions ahead as a function of the difference in velocity and characterizes the changes in flow smoothly with the traffic conditions ahead. The model, called Khan and Gulliver (KG), is given as

$$\begin{aligned} &\rho_t + \rho\big(v_e(\rho)\big)_x = 0, \\ &v_t + v v_x + \frac{v_m^2 - v^2}{2dt_r}\rho_x = \frac{1}{\tau}\big(v_e(\rho) - v\big), \end{aligned} \tag{3.6}$$

where dt_r is the transition distance [99] and v_f is the maximum legal speed allowable on the road stretch.

Regarding SGM, linked to the Jiang, Qing and Zhu (JQZ) model developed by Jiang [52], which addressed the problem of traffic flow anisotropy. This approach is well aligned with the criticism of Daganzo on the isotropic behavior of the PW model. Other recent advances in this class were proposed by [5, 93]. The SOTFM proposed by [52] is given as

$$\begin{aligned} &\rho_t + \rho\big(v_e(\rho)\big)_x = 0, \\ &v_t + (v - c_0) v_x = \frac{1}{\tau}\big(v_e(\rho) - v\big). \end{aligned} \tag{3.7}$$

In Eq.3.7 the anticipation term $(c_0 v_x)$ is different from that in Eq.3.5 and

Eq.3.6 since the presumptions to forward conditions are based on spatial changes in velocity; in doing so, this model successfully responded to the criticism of Daganzo and satisfies the anisotropy property of the traffic flow. However, this model has been criticized for the constant rearward velocity propagation and has been extended by [93]. The Song and Karni (SK) model is based on a variable relation for rearward velocity propagation, which is given as

$$\begin{aligned} &\rho_t + \rho\big(v_e(\rho)\big)_x = 0, \\ &v_t + \Big(v - \frac{s(\rho)}{\tau}\Big)v_x = \frac{1}{\tau}\big(v_e(\rho) - v\big), \end{aligned} \tag{3.8}$$

where $s(\rho)$ is the macroscopic relation between spacing and density, defined as

$$s(\rho) = g(\rho) + L_c, \tag{3.9}$$

where $g(\rho)$ is the minimal safe distance as a function of density ρ and L_c is the average length of vehicles. The former term is defined as $g(\rho) = \frac{s_{min}}{\frac{\rho}{\rho_{max}}}$, where ρ_{max} is the maximum density when the traffic comes to a standstill, and s_{min} is the minimal safe distance between vehicles. The structure of all the above systems is given in Table 3.2.

The SOTFMs and their related terms are summarized in Table 3.2. The latter highlights that the only difference between all models is the anticipation term. Indeed, since the anticipation term characterizes the rearward traffic velocity as this is the response of a driver to conditions ahead, it can be devised in a number of ways. It is worth noting that the focus of this work is not the development of a new model, but the development of an evaluation process for SOTFMs such that those discussed above, and their practical utility. Traffic systems discussed in this section are the simplest representations of SOTFMs with maximum output capabilities and are seldom validated. Considering the most recent developments and analyzing these developments for most common traffic phenomena such as rarefaction and shock wave propagation, this could be a potential benchmarking study for field applications of these traffic systems.

3.5 Evaluation Methodology

This section introduces the framework for evaluating the SOTFMs, which resemble the benchmarking analysis procedure proposed in [53].

First, a set of benchmarking criteria is designed with the aim to examine the capability of the models to reflect real-world traffic phenomena and analyze their operational performance. Then, ground-truth data and simulation scenarios are selected to ensure that the benchmarking analysis outcomes are reliable. Finally, the computational framework is introduced, including the numerical schemes for the solution of the models and the optimization algorithms for calibrating the models.

The evaluation framework employed in this paper is schematized in Figure 3.3.

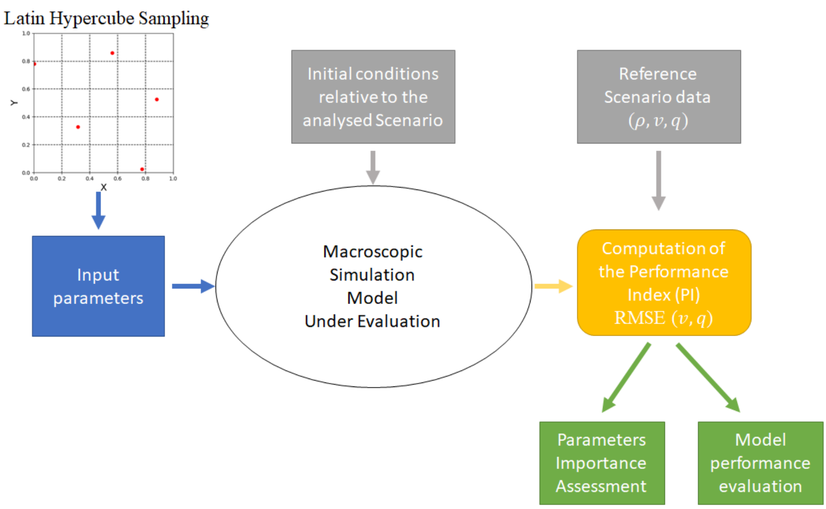

Figure 3.3. The evaluation process for SOTFMs as in the integrated framework.

3.5.1 Benchmarking criteria

The benchmarking criteria employed in this study is based on some essential aspects of traffic flow behavior that an ideal model should reflect.

More specifically, we consider two different aspects, i.e., the complex empirical phenomena and implementation considerations. The former benchmarking criterion concerns the capability of SOTFMs to describe complex phenomena, thus we examine how well each model can reproduce the flow behavior in the presence of significant and abrupt perturbations (generation and propagation of traffic oscillation). To exhaustively investigate this questions, the underlying mechanism used by each model to replicate these phenomena is considered. The latter benchmarking criterion, instead, concerns implementation considerations of the models. For instance, the robustness of each model under different traffic conditions and the parsimony of models in terms of the number of parameters.

3.5.2 ground-truth Data

A macroscopic traffic model is an abstraction of real traffic conditions, so it is necessary to verify that the model correctly reflects real traffic conditions to obtain accurate predictions. This step involves the exploitation of ground-truth traffic data, which can be derived from real (for instance through the use of traffic sensors) or synthetic data. In this work, to assess both the qualitative and quantitative performance of SOTFMs reported in Table 3.2, we exploit synthetic ground-truth data in SUMO.

3.5.2.1 Study Area

The study area is a single-lane circular road corridor with a length of 20,000 m and a maximum speed of 30 m/s. The longitudinal slopes are assumed to be negligible, meaning that the traffic conditions are not affected by changes in the elevation. Furthermore, no on/off-ramps are taken into account in this analysis. As a result, the study area can be regarded as a homogeneous section. It is worth noting that the circular layout of the corridor is particularly well suited for assessing the behavior of traffic flow in the presence of significant and abrupt perturbations [49].

Within SUMO, the study area is modeled as composed of 31 edges with different lengths to avoid any kind of speed breakdown due to sharp variations in the geometry of the road. Traffic state is recorded every 120 seconds from 31 loop detectors inside the area, one on each segment that makes up the network. The cross-sectional observations are used to reconstruct spatiotemporal traffic states.

3.5.2.2 Traffic Scenarios

To evaluate the performance of the SOTFMs two traffic scenarios are designed. More in detail, in order to achieve the benchmarking criteria introduced in 3.5.1, it is essential to cover a wide range of traffic conditions, including phenomena such as shock waves and traffic oscillations. For this reason, we have considered two non-identical traffic conditions, as shown in Figure 3.4. These conditions are the initial density conditions across the whole circular road network, i.e. the conditions at the starting point $t = 0$ of the simulation. Given the initial traffic conditions, SUMO is then used to model the evolution of traffic patterns over time and space horizon. The total simulation time is 1800 s (30 minutes) to keep the uniqueness in all kinds of traffic simulations performed in the study.

The first traffic scenario (scenario I) is depicted in Figure 3.4 (a). The initial density distribution defines a traffic condition where light traffic from behind approaches a relatively denser region. The initial density distribution for the second scenario (scenario II) is shown in Figure 3.4 (b). These initial conditions present dense traffic conditions in the downstream sections, in which light traffic is approaching a denser region between $12,000$ m to $14,000$ m and $14,000$ m to $16,000$ m. This case presents more variations in the traffic conditions compared to scenario I, sharp variations of traffic conditions are useful to analyze the ability of SOTFMs to reproduce non-equilibrium traffic phenomena.

Regarding the traffic flow composition, here we assume that it is homogeneous. To be precise, the vehicle fleet consists of road vehicles with a length of 7 m, a maximum speed of 30 m/s a maximum acceleration of 3.5 m/s^2, and a maximum deceleration of 2.2 m/s^2. The longitudinal motion of the vehicles is guided by the Krauss car-following model [100, 101], whose parameters are: the driver's desired minimum time headway $\tau_h = 1$ s, the minimum gap $g = 2.5$ m and the driver imperfection $\eta = 0.5$. All the microscopic parameters are summarised in Table 3.3. Moreover, to avoid the vehicles all assuming the same behavior, the desired speed is assumed to follow a truncated normal distribution with mean 1 (i.e., the maximum between the speed limit and the maximum speed of the vehicle), standard deviation 0.1, lower cut-off 0.2 and upper cut-off 2. This implies that ∼95% of the vehicles drive between 80% and 120% of the legal speed limit.

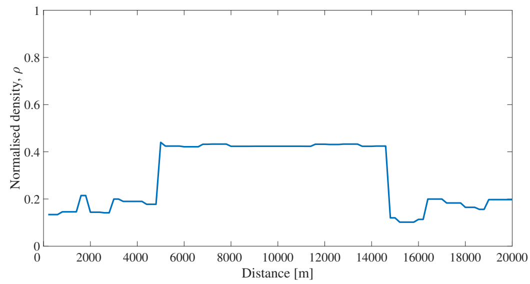

(a) Scenario I

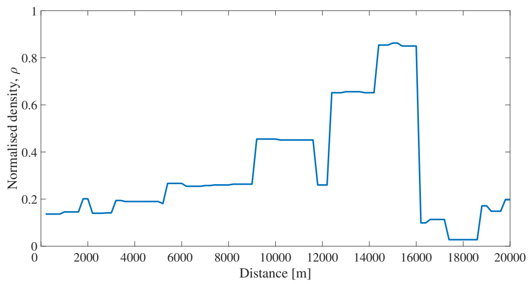

(b) Scenario II

Figure 3.4. Initial density distributions over the 20, 000 m circular road network: (a) Scenario I; (b) Scenario II.

3.5.3 Numerical Methods

The SOTFMs are sets of PDEs, demanding the numerical solution of these systems for the purpose of conducting simulations. In the literature, various numerical methods are proposed to numerically solve SOTFMs [102]. The performance of these systems are dependent enough on the choice of the numerical method used for the discretization [53]. However, the selection of the proper numerical method depends also upon the type of mathematical structure of a model. It is evident from the literature that different classes of the SOTFMs would perform differently while employing different numerical methods [103]. In this study, careful consideration has been given to the selection of the numerical decomposition method for the SOTFMs.

The conservative form of a traffic flow model is essential to obtain the solution and other important properties such as hyperbolicity and anisotropy. A generic traffic system can be represented in the conservative form as

$$\omega_t + f(\omega)_x = S(\omega), \tag{3.10}$$

where ω represents the vector of traffic flow variables (ρ and v), $f(\omega)$ denotes the functions of the data variables, and $S(\omega)$ is the source terms' vector [104, 102, 105]. The quasilinear form of the system in Eq. 3.10 is

$$\omega_t + A(\omega)\omega_x = 0, \tag{3.11}$$

where $A(\omega)$ is the Jacobian matrix for the gradients of the functions of variables.

To explain the functions of the data variable on a solution spatial and temporal grid, M equidistant segments for a total length of x_M are considered. Consequently, the length of a segment is $\Delta x = x_m/M$, which is the road spatial step. The time step is $\Delta t = t_N/N$, being t_N the total time duration and N is the number of time steps. The terms ω and $f(\omega)$ are approximated for the road segments $\left(x_i - \frac{\Delta x}{2}, x_i + \frac{\Delta x}{2}\right)$, and the data variables are obtained for each of the M segments for the time period (t_n, t_{n+1}).

The PW, IK, and KG models are solved using the First Order Centered (FORCE) scheme [14, 5] since they are DGM. The updated data variables for PW, IK, and KG models using the FORCE scheme are obtained as

$$\omega_i^{n+1} = \omega_i^n - \frac{\Delta t}{\Delta x}\left(f_{i+\frac{1}{2}}^n - f_{i-\frac{1}{2}}^n\right) + \Delta t S(\omega_i^n). \tag{3.12}$$

Instead, the models belonging to SGM family are solved using the upwind scheme [52, 93, 106]. The exact solutions cannot be guaranteed to the Riemann problem as these traffic systems are solved as a Riemann problem [107]. This problem arises because the continuity and acceleration equations are linked through the relaxation term, and the characteristic speed is not dependent on density as reported by [53]. For this reason, the speed gradient models are simulated using the scheme proposed by

[52, 106, 58]:

$$\begin{cases} \rho_i^{n+1} = \rho_i^n + \frac{\Delta t}{\Delta x}\big(\rho_i^n(v_i^n - v_{i+1}^n)\big) + \frac{\Delta t}{\Delta x}v_i^n(\rho_{i-1}^n - \rho_i^n), \\ \begin{cases} v_i^{n+1} = v_i^n + \frac{\Delta t}{\Delta x}(c_0 - v_i^n)(v_{i+1}^n - v_i^n) + \frac{\Delta t}{T}\big(v(\rho) - v_i^n\big), & \text{if} v_i^n \leq 0 \\ v_i^{n+1} = v_i^n + \frac{\Delta t}{\Delta x}(c_0 - v_i^n)(v_i^n - v_{i-1}^n) + \frac{\Delta t}{T}\big(v(\rho) - v_i^n\big). & \text{if} v_i^n \geq 0 \end{cases} \end{cases} \tag{3.13}$$

Apart from the numerical discretization, two significant aspects of SOTFMs are hyperbolicity and anisotropy. A model is hyperbolic when a perturbation (change in flow) propagates with a finite velocity, and the effect of a perturbation decreases over time. A traffic model is said to be strictly hyperbolic if the eigenvalues are real and distinct [98, 102]. Regarding the anisotropy, it requires that velocity changes are not greater than the average [105, 108]. To determine if a model is hyperbolic and anisotropic, the eigenvalues must be derived from the Jacobian matrix. To construct the Jacobian matrix, the density and SGMs are considered in the conservation form (details are given in Table 3.4). For illustration purposes, the following is presented the conservation form of the JQZ model:

$$\omega = \begin{pmatrix} \rho \\ v \end{pmatrix}_t, f(\omega) = \begin{pmatrix} \rho v \\ (\frac{1}{2}v^2 - c_0 v) \end{pmatrix}_x, S(\omega) = \begin{pmatrix} 0 \\ \left(\frac{v(\rho)-v}{\tau}\right) \end{pmatrix}. \tag{3.14}$$

Table 3.4 shows that the data variables of DGMs (PW, IK, and KG) are the same. The functions of such variables change since the driver anticipation term differs for all the models. However, the vector of the source term remains unchanged for all models because the relaxation term is the same as shown in Table 3.2. This vector is also responsible for the linkage between continuity and acceleration equations, thus it plays a crucial role in the qualitative analysis of these systems.

Table 3.1. Payne Whitham (PW) model structural terms

Term	**Mathematical Representation**	**Description**
Convection	vv_x	Characterizes the impacts of vehicles on ingress and egress
Anticipation	$\frac{c_0^2}{\rho}\rho_x$	Characterizes the driver response to forward conditions
Speed Constant	c_0	Backward speed of wave propagation
Relaxation	$\frac{1}{\tau}\left(v_e(\rho) - v\right)$	Tendency of vehicle to achieve desired velocity
Relaxation Time	τ	Time for the adjustment of velocity
Closure relation	$v_e(\rho)$	Equilibrium velocity distribution

Table 3.2. The SOTFM and their structural terms forming a system of Partial Differential Equations (PDEs).

Term	IK	KG	JQZ	SK
Gradient	Density	Density	Velocity	Velocity
Convection	vv_x	vv_x	vv_x	vv_x
Anticipation	$\tau_h b \rho_x$	$\frac{v_m^2 - v^2}{2dt_r}\rho_x$	$c_0 v_x$	$\frac{s(\rho)}{\tau} v_x$
Relaxation	$\frac{1}{\tau}(v_e(\rho) - v)$	$\frac{1}{\tau}\left(v_e(\rho) - v\right)$	$\frac{1}{\tau}\left(v_e(\rho) - v\right)$	$\frac{1}{\tau}\left(v_e(\rho) - v\right)$

Table 3.3. SUMO network characteristics and parameters.

Description	Value	Unit
Vehicle length	7	m
Maximum speed	30	m/s
Maximum acceleration	3.5	m/s^2
Maximum deceleration	2.2	m/s^2
Minimum safe gap $s_{\min}$	2.5	m
Desired minimum time headway	1	s
Driver imperfection η	0.5	[]
Number of Detectors	31	[]
Aggregation time of traffic data	120	s

Table 3.4. Conservation form of the Second Order Traffic Systems

Model	ω	f (ω)	S (ω)
PW	$\begin{pmatrix} \rho \\ \rho v \end{pmatrix}_t$	$\begin{pmatrix} \rho v \\ (\frac{(\rho v)^2}{\rho} + c_0^2 \rho) \end{pmatrix}_x$	$\begin{pmatrix} 0 \\ \rho \left(\frac{v_e(\rho)-v}{\tau} \right) \end{pmatrix}$
IK	$\begin{pmatrix} \rho \\ \rho v \end{pmatrix}_t$	$\begin{pmatrix} \rho v \\ (\frac{(\rho v)^2}{\rho} + \tau b \rho) \end{pmatrix}_x$	$\begin{pmatrix} 0 \\ \rho \left(\frac{v_e(\rho)-v}{\tau} \right) \end{pmatrix}$
KG	$\begin{pmatrix} \rho \\ \rho v \end{pmatrix}_t$	$\begin{pmatrix} \rho v \\ (\frac{1}{2} v^2 + (\frac{v_m^2 - v^2}{2 d t_r}) \rho) \end{pmatrix}_x$	$\begin{pmatrix} 0 \\ \rho \left(\frac{v_e(\rho)-v}{\tau} \right) \end{pmatrix}$
JQZ	$\begin{pmatrix} \rho \\ v \end{pmatrix}_t$	$\begin{pmatrix} \rho v \\ (\frac{1}{2} v^2 - c_0 v) \end{pmatrix}_x$	$\begin{pmatrix} 0 \\ \rho \left(\frac{v_e(\rho)-v}{\tau} \right) \end{pmatrix}$
SK	$\begin{pmatrix} \rho \\ v \end{pmatrix}_t$	$\begin{pmatrix} \rho v \\ (\frac{1}{2} v^2 - \frac{h(\rho)}{\tau} v) \end{pmatrix}_x$	$\begin{pmatrix} 0 \\ \rho \left(\frac{v_e(\rho)-v}{\tau} \right) \end{pmatrix}$

The eigenvalues are derived from the Jacobian matrix of the systems, which for the specific case of the JQZ model is

$$A(\omega) = \begin{pmatrix} v & \rho \\ 0 & v - c_0 \end{pmatrix}, \tag{3.15}$$

hence the corresponding eigenvalues are

$$\lambda_1 = v - c_0, \lambda_2 = v. \tag{3.16}$$

The Jacobian and corresponding eigenvalues of all the models (including JQZ) are listed in Table 3.5. The Jacobian matrix differs for all the models, resulting in different eigenvalues. If the eigenvalues are real and distinct, the model is hyperbolic. The eigenvalues of all the traffic systems are real and distinct, so they are hyperbolic. This is an important check for SOTFMs as it is a mandatory property. Anisotropy is not always mandatory. If one of the eigenvalues is less than the average velocity while the second eigenvalue is equal to the average velocity, the model exhibits anisotropic behavior: alterations in traffic conditions occur at or below the average velocity and are influenced by the rearward velocity. Traffic state variations with the JQZ and SK models occur at or below the average velocity, so the anisotropic property is satisfied. Note that in free flow conditions, traffic perturbations evolve according to λ_2 in the forward direction while during congestion they evolve according to λ_1 in the rearward direction in the speed gradient model and vice versa for the density gradient models.

Table 3.5. Jacobian matrix, eigenvalues, hyperbolicity, and anisotropy of the SOTFM.

Model	Jacobian A(ω)	Eigen Values	Hyperbolic	Anisotropic
IK	$\begin{pmatrix} 0 & 1 \\ -v^2+\tau b & 2v \end{pmatrix}$	$\lambda_1 = v + \sqrt{\tau b}, \lambda_2 = v - \sqrt{\tau b}$	✓	-
KG	$\begin{pmatrix} 0 & 1 \\ -v^2+(\frac{v_m^2-v^2}{2dt_r}) & 2v \end{pmatrix}$	$\lambda_1 = v + \sqrt{(\frac{v_m^2-v^2}{2dt_r})}, \lambda_2 = v - \sqrt{(\frac{v_m^2-v^2}{2dt_r})}$	✓	-
JQZ	$\begin{pmatrix} v & \rho \\ 0 & v-c_0 \end{pmatrix}$	$\lambda_1 = v - C_0, \lambda_2 = v$	✓	✓
SK	$\begin{pmatrix} v & \rho \\ 0 & v-\frac{h(\rho)}{\tau} \end{pmatrix}$	$\lambda_1 = v - \frac{h(\rho)}{\tau}, \lambda_2 = v$	✓	✓

3.5.4 Setup for the Computational Procedure

The road network is introduced in Section 3.5.2.1, while the initial traffic conditions are the illustrated in Figure 3.4. To compare the results with the ground-truth data (SUMO), the traffic variables are recorded each 120 s, and detectors are assumed to be located in the same positions as the ones in SUMO. The maximum density is set equal to 1, which is the normalized relative maximum density of the road. As a reference curve in the macroscopic traffic environment, the Greenshields equilibrium velocity distribution is employed.

A crucial step for resolution consistency is to define the grid size and the boundary conditions. We set the road spatial step as $\Delta x = 200$ m and the temporal step $\Delta t = 1$ s. To account for the circular road conditions, periodic boundary conditions such as

$$\begin{aligned} \rho(L,t) &= \rho(0,t), \\ v(L,t) &= v(0,t), \end{aligned} \tag{3.17}$$

are employed. That is, traffic states at the first and last segments are the same. The dominance of exercising circular road conditions is that the perturbations remain in the road section and travel with traffic waves that describe the model property to successfully absorb perturbations with time. It is worth noting that before the start of experiments for all traffic scenarios, the initial density distributions have been verified, and are well aligned with the those observed in SUMO. All the parameters used for the setup of a generic considered SOTFM are listed in Table 3.6.

3.5.5 Framework for Model Calibration

This section discusses the framework employed for calibrating the SOTFMs on the ground-truth data. Calibration is a crucial task that allows a model to fit a real system. From a practical point of view, this task consists in finding the optimal set of values of the parameters that allow the model itself to reproduce, in the best possible way, the behavior of a real system. It is worth noting that the structural terms of the different SOTFMs are listed in Table 3.1, while the set of parametric variables along with their range of variation for each SOTFMs is reported in Table 3.7. It is worth

Table 3.6. Initial parameters settings for the macroscopic simulations.

Description	**Value**	**Unit**
Maximum Speed	30	m/s
Maximum Normalized Density	1	[ ]
Closure Relation	Greenshields	m/s
Time Step Δt	1	s
Aggregation time of traffic data	120	s
Road step Δx	200	m

noting that all the parameters are assumed to be uniformly distributed in their specific range of variation.

The optimal set of values is the solution of a constrained minimization problem in which the objective function expresses the deviation of the simulated measurements from those observed:

$$\min_{\Xi} f(\xi_{data}, \xi_{model}), \tag{3.18}$$

subject to the following constraints

$$l_{\Xi,j} \leq \Xi_j \leq u_{\Xi,j} \; j = 1, ..., 5 \tag{3.19}$$

where $f(\xi_{data}, \xi_{model})$ is the objective function to be minimised used, being ξ_{data} and ξ_{model} the simulated and observed traffic data; Ξ_j is the vector of the model parameters for the generic considered SOTFMs j ($j = 1, ..., 5$); $l_{\Xi,j}$ and $u_{\Xi,j}$ are model parameters upper and lower bounds, respectively.

In this case, the defining state variable used for the calibration is the flow q, hence the objective function is

$$f(\xi_{data}, \xi_{model}) = [q_d(t) - q_{d,m}(t)]^2, \tag{3.20}$$

where $q_d(t)$ is the flow estimated by the SOTFMs and $q_{d,m}(t)$ is the ground-truth flow.

The problem in Eq. (3.18) cannot be solved analytically, since it is a simulation model. In this study, for the full-scale calibrate model, we follow the approach proposed by [109] and [110], varying all the parameters simultaneously to investigate the impact of variation in parameters on the average output of the models. The different combinations of the SOTFMs parameter are sampled via the Latin Hypercubic Sampling (LHS) [111], and for each input combination, a simulation run is performed. In order to cover as much as possible the entire possible space of values, 4000 samples are generated, which means 4000 combinations of the parameters for each considered SOTFMs. For each combination of the parameters of the generic SOTFMs j, we run the SOTFMs and then calculate a PI for comparison purposes. To evaluate the global performance of the SOTFMs for each set of values of the parameters, we compute as PI the Root Mean Square Error (RMSE) of the flow q over the whole time series:

$$PI = \sqrt{\frac{\sum_{i=1}^{M}\sum_{t=1}^{N}[q_d(t) - q_{d,m}(t)]^2}{N \cdot M}}, \tag{3.21}$$

Then, we chose as solution of the problem the set of values of the parameters that return the lowest PI.

Table 3.7. SOTFMs parameters, their admissible range of variations and calibrated values for Scenario I and Scenario II.

Model	PI (I/II)	Parameter	Admissible Range	Calibrated Value (I/II)	Unit
IK	0.078 / 0.10	b	0.1 – 1	0.75 / 0.95	[]
		v_f	28 - 32	30.72 / 30.78	m/s
		τ	5 – 20	5.28 / 19.62	s
		τ_h	1 – 20	17.23 / 13.87	s
KG	0.083 / 0.10	τ_r	0.7 – 1.7	0.78 / 0.73	s
		v_f	28 - 32	30.70 / 30.68	m/s
		τ	5 – 20	5.12 / 19.42	s
		s_{st}	1 – 5	3.15 / 4.42	m
JQZ	0.091 / 0.125	c_0	5 - 25	24.81 / 15.56	m/s
		v_f	28 – 32	30.09 / 30.21	m/s
		τ	5 – 20	19.65 / 19.95	s
SK	0.089 / 0.12	s_{min}	1 – 6	5.51 / 4.51	m
		v_f	28 – 32	30.09 / 30.27	m/s
		τ	5 – 20	19.66 /19.48	s
		τ_r	0.7 – 1.7	0.78/0.99	s
		L_c	7 – 10	9.18 / 7.40	m

3.5.6 Framework for Sensitivity Analysis

This section discusses the methodological framework employed for sensitivity analysis, which aims to identify and analyze trends, patterns, and insights of the considered SOTFMs. That is, to obtain a comprehensive knowledge of the parameters of each model and their contribution to the performance of each model. This is a crucial step for understanding the behavior of any model's output related to any change in parametric variables.

In order to perform a comprehensive and systematic investigation, the SOTFMs are analyzed both qualitative and quantitative. The qualitative analysis is assessed through scatter plots, which provide straightforward and intuitive evidence of the relationship between the input factors (in this case the parameters of SOTFMs) and the output (the PI in Eq. (3.21)). The quantitative analysis involves two different tests to assess the impact of SOTFMs parameters on the performance of the model itself. The first one employ the Pearson correlation coefficient R to spot the (linear) correlation between the parameters of SOTFMs and the output of the simulation (in this case the PI). The second approach consists of a Global Sensitivity Analysis (GSA).

3.5.7 Linear Correlation Analysis

The linear analysis investigates the linear dependence between two random variables. As a measure of linear dependence between two random variables, in this study we employ the Pearson correlation coefficient R [112]: it is the ratio between the covariance of two variables and the product of their standard deviations; thus, it is a normalized measurement assuming always a value between -1 and 1. To evaluate the significance of the results, i.e. for testing the hypothesis that there is no relationship between the observed phenomena (null hypothesis), the p-values are calculated: if p is smaller than the significance level (0.05), then the corresponding correlation in R is considered significant. Moreover, the lower bound (R_l) and upper bound (R_u) for a 95% confidence interval for each coefficient are used to analyze the limits of the values of the parameters within the given dataset.

The linear analysis is widely employed because of its simplicity, ease of implementation and ease of interpretation of the results. Hence, it is here used to have a first insight into the relationships between the parameters and the output variable (PI). However, this approach does have some limitations: it is too simplistic to capture real-world complexity; linear regression makes strong assumptions that independent and dependent variables are linearly related, which may not be the case; outliers can have a large effect on the output; inability to determine parameter importance.

3.5.8 The PAWN Global Sensitivity Analysis

An efficient way to study the influence of SOTFMs parameters on the PI is to perform a GSA: it considers the variation of each input factor (the parameter of the SOTFMs in this case) within its space of variability to identify the interaction with the output (PI). To determine the relative impact of each input factor on the output variability, the sensitivity indexes are computed. These indexes range from 0 to 1, with higher values indicating greater influence and a value of zero indicating non-influence. The identification of influential and non-influential parameters could enhance and simplify the calibration process of SOTFMs since the inputs that do not affect the model performance could be considered as fixed [113].

Different GSA methods exist in the technical literature [114]. Here we employ the PAWN distribution-based sensitivity analysis method proposed by [115]; the method has been widely applied in climate or atmospheric sciences for assessing complex environmental models [116, 117], but recently it has been employed also in the transportation filed for the safety assessment of Automated Driving Systems [118]. The choice of this specific sensitivity method lies in its easy applicability to nonlinear models, its independence from the type of output distributions (e.g. symmetric, multimodal, or highly skewed) and the ability to provide robust results even for relatively low sample size.

To commence, consider the generic input-output relationship $Y = f(X)$, where $X = [x_1, x_2, ..., x_p, ..., x_m] \in \mathscr{H} \subseteq \mathscr{R}^M$ the input vector of M factors and $Y \in \mathscr{R}$ the scalar output variable. The PAWN measures the sensitivity of the output y of the model (the RMSE, in our case) to variations of an input x_p (the value of a parameter of SOTFMs) by the distance between the unconditional distribution of y (obtained by varying all the inputs) and the conditional distribution obtained when all the inputs change but x_p. It is worth noting that the conditional and unconditional distributions are characterized by their Cumulative Distribution Functions (CDFs). Since we are interested in employing datasets generated via a generic sampling strategy (the LHS in this case), the computation of PAWN indexes needs to be approximated numerically. The approximation procedure, proposed by [119], consists of dividing the range of variation of each input factor x_p into n equally spaced intervals, each of which is denoted as $\mathscr{I}_k(k = 1, ..., n)$ and adopted to define the conditional sample $YU_{pk}(\forall p \in M)$. The unconditional sample YU corresponds with the entire sample Y. The distance between distributions is measured by the Kolmogorov-Smirnov (KS) statistics:

$$KS(\mathscr{I}_k) = \max_y |\hat{F}_y(y) - \hat{F}_{y|x_p}(y|x_p) \in \mathscr{I})|, \tag{3.22}$$

being $\hat{F}_y(y)$ the empirical distribution of the unconditional sample YU; $\hat{F}_{y|x_p}(y|x_p) \in \mathscr{I}$ the observed distribution of a conditional sample YU_{pk} obtained by varying all factors but $x_p(\forall p \in M)$, which is set to the k-th conditioning value $\bar{x}_p^{(k)}$. The PAWN index $\hat{S}_p$ considers a statistic (maximum, median or mean) over all possible values that x_p can assume:

$$\hat{S}_p = stat_{k=1,...,n} KS(\mathscr{I}_k). \tag{3.23}$$

Due to approximation errors, the sensitivity indexes of non-influential parameters could have a non-zero values. To recognize influential and non-influential input factors, an artificial input factor (dummy parameter) that does not affect the output distribution is introduced. That is, $F_{y|x_p}(y|x_{m+1})$ for all conditioning points in Eq. (3.22). If the sensitivity index value of an input factor is larger than the one of the dummy $\hat{S}_{dummy}$, it is considered influential.

In this study, we run $\Gamma = 4000$ simulations (the same used for the calibration) to estimate the unconditional distribution of the output (PI). Starting from this generic input–output dataset $< x, y >$, the PAWN indexes are computed following the approximation procedure described above. We split the range of variation of each input factor xp into $n = 20$ equally spaced intervals and define the conditional sample YU_{pk} $(\forall p \in M)$ accordingly. The PAWN analysis is implemented using the MATLAB adaptation of the latest version of the SAFE toolbox developed by [120].

3.6 Results

This Section presents and discusses the results of the evaluation analysis for each considered SOTFMs, under traffic scenarios I and II shown in Figure 3.4. For the purpose of calibration, once the traffic data from SUMO is obtained, the calibration procedure, as described in Section 3.5.5, is performed to identify optimal parameters of the SOTFMs. Given the optimal set of variables, spatio-temporal pattern formation on the corridor based on the fundamental traffic variable "q" is observed which is again compared with results from SUMO. The admissible ranges of the parametric variables are tabulated in Table 3.7.

It is worth noting that the recent work of [94] proved that traffic flow models are sensitive to initial conditions, then the sensitivity of their parameters might become tricky. The models are all the more sensitive the more congested the traffic conditions are. On the other side, macroscopic traffic flow models exhibit self-affinity fractals, displaying similar behavior at different scales or levels of magnification for which the basic relation is the fundamental diagram (speed-density relationship in particular). The relaxation and the anticipation terms play a pivotal role in this case: the former dominates the overall performance as it depends on the fundamental diagram, while the latter guarantees the stability of SOTFMs when non-equilibrium traffic phenomena occur. Thus, some parameters of the SOTFMs could be of second importance for calibration and statistical significance, but they assume a crucial role in the stability and intrinsic properties of the SOTFMs as demonstrated by [42]. Moreover, the results depend on the objective and on the indices used to evaluate the sensitivity, hence the influence of a parameter on a model should be studied in a broader sense. To systematically analyze the overall behavior of any model (and the impact of its parameters) it would therefore be correct to consider different aspects.

According to the above discussion, we consider two different scenarios, namely Scenario I and Scenario II, characterized by different prevailing traffic conditions in Figure 3.4. For both of them, we calibrated the SOTFMs considering the whole set of parameters and evaluated qualitatively and quantitatively their performance. The calibrated values for the parameters of SOTFMs for all the three considered conditions are given in Table 3.7.

3.6.1 Scenario I

3.6.1.1 Results of Full Calibrated Models

The spatiotemporal pattern formation and evolution based on traffic flow for all the traffic models are shown in Figure 3.5. Qualitative results demonstrate that the SOTFM replicates the reference traffic scenario without violating the basic assumptions and fundamentals. This scenario is analyzed for 1800 s (30 minutes), and a very engaging and close interplay is observed between all systems. The spatiotemporal pattern formation and evolution of SUMO is shown in Figure 3.5 (a). For the initial 900 s, there are large variations in flow, and the flow in denser regions evolves slowly forming fairly two different traffic flow conditions. While this pattern formation eventually reaches a uniform flow rate over time, albeit, another considerable fact with SUMO is analyzed, which is clear from the flow formation pattern that is randomness in the values of flow and is distinctly reflected in the color banding. Note that this randomness can result in higher PI, however, it is important to assess the performance of SOTFM against such complex scenarios so that they are investigated in their true essence.

The spatiotemporal pattern formation and evolution based on the flow of the IK model for 1800 s (30 minutes) is illustrated in Figure 3.5 (b). It is worth noticing that the spatiotemporal pattern formation and evolution of the IK model is similar to the SUMO. The spatio-temporal evolution pattern of the IK model is sufficiently accurate. Initially, the denser traffic evolves and eventually reaches an almost uniform flow level after 1080 s, very persistent with the reference SUMO. The interplay of SUMO and IK in following the mechanism of spatiotemporal pattern formation and evolution is sound and validates the capabilities of the model to depict real-world traffic. The PI of the IK model is 0.078.

Figure 3.5 (c) illustrates the spatiotemporal pattern formation and evolution of flow of the KG model over $20,000$ m circular road for 1800 s (30 minutes). Yet again, the traffic dynamics between KG and SUMO are the same as for the DGM such as IK model. The PI of the KG model is 0.083, there are differences between instantaneous flow rates as for the other models of the group, but the pattern formation and evolution are consistent. On the other hand, the KG model replicates precisely the IK model which verifies the consistency of these systems with each other.

The spatiotemporal pattern formation and evolution of the JQZ model are shown in Figure 3.5 (d). Like the DGM, the SGM has the same trends in pattern formations as SUMO. The PI of this model is 0.091, and the spatiotemporal pattern formation and evolution are plausible. The SK model Follows the same trends in pattern formation and flow evolution as shown in Figure 3.5 (e), and the PI is 0.088. Such consistent agreement of SOTFMs with SUMO is vital to understanding the interplay between microscopic and macroscopic traffic systems. Eventually, the SOTFMs produced equally the same results and there is no significant difference in PI values. Since all the SOTFMs can reproduce the first scenario, we now move to a more complex scenario with large variations in traffic states to calibrate and evaluate the performance of SOTFMs.

3.6.1.2 Results of the Sensitivity Analysis for Scenario I

Here we analyze the relationship between the input parameters of each SOTFMs (3.7) and the output (PI) both qualitatively and quantitatively.

3.6.1.2.1 IK Model Analysis of the IK model involves four parameters listed in 3.7, namely v_f, τ, τ_h and b.

Figure. 3.6 illustrates the scatter plots of these variables, which refer to the analysis of all the simulation runs and the same number of points (4000, one for each run) compose each plot. The y-axis of each subplot corresponds to the output variable y (PI), whereas the x-axis refers to a different SOTFMs parameter. The results clearly show the different degrees of correlation between PI and the considered variables of the model, as well as the output dispersion w.r.t. the mean. More specifically, Figure 3.6 (c) highlights shows a significant nonlinear correlation between PI and v_f, while a minor relation exists with τ (Figure 3.6 (d)). The remaining parameters τ_h and b do not seem to have a significant effect on the output.

The results of the linear analysis confirm that the most statistically

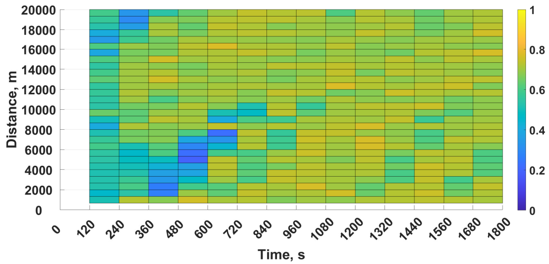

(a) Flow evolution in SUMO.

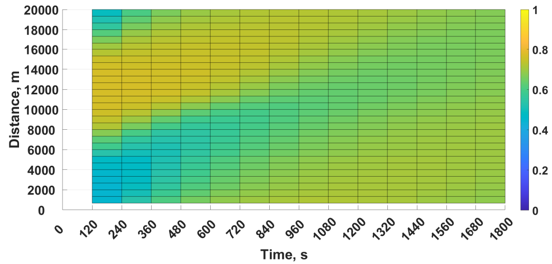

(b) Flow evolution of IK model.

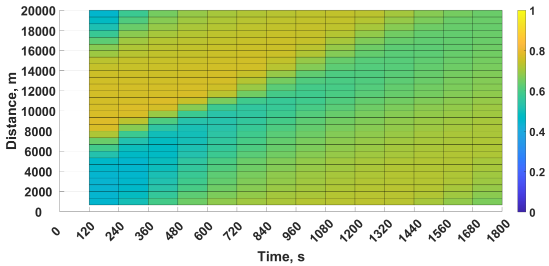

(c) Flow evolution of KG model.

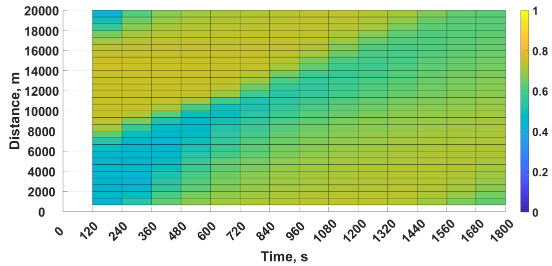

(d) Flow evolution of JQZ model.

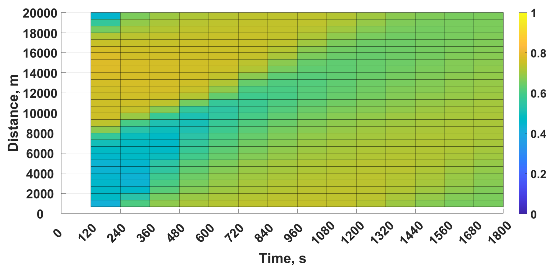

(e) Flow evolution of SK model.

Figure 3.5. Flow evolution over time (1800 s - x-axis) and space (20,000 m road section y-axis) given the initial conditions as defined by scenario I: a) SUMO, used as ground-truth; b) PW model; c) IK model; d) KG model; e) JQZ model; f) SK model.

significant parameter is v_f with $R = -0.80$ (high negative degree of correlation) and a p-value approximately equal to 0. The R_l and R_u for R are -0.81 and -0.79, indicating a small range of dispersion for v_f. The R of τ is 0.09 with a p-value approximately equal to 0, indicating a very weak correlation with PI. The R of τ_h and b are approximately equal to 0 with a p-value approximately higher than the threshold (0.05), indicating that the result is not statistically significant. These parameters can be fixed to any value from their feasible range, although the role of these parameters is tricky in congested situations. It is worth noting that the significance of the parameters also depends on the situation in which they are used, for instance, b characterizes the sideways distances between the vehicles, but in this study, it appears irrelevant also because the simulations are performed on a single lane, thus the impact of sideways distance on traffic flow is trivial.

Finally, the results of GSA in 3.10(a) highlight that the most influential input factor is v_f, while τ has a relatively low effect. The median sensitivity value of b is slightly above the threshold line, indicating a minor effect on the model performance. Regarding the last parameter τ_h, its sensitivity index is slightly below the threshold line, hence it does not affect significantly the performance of the model. The distribution boxes indicate that v_f is more dispersed than the other parameters followed.

3.6.1.2.2 KG Model The analysis of the KG model involves four parameters listed in Table 3.7, τ_r, v_f, τ and s_{st}.

Figure 3.7 illustrates the scatter plots of these variables, which refer to the analysis of all the simulation runs. The results clearly show the different degrees of correlation between PI and the variables of the model, as well as the output dispersion w.r.t. the mean. More specifically, Figure 3.7 (c) highlights shows a significant nonlinear correlation between PI and v_f, while a very weak correlation emerges with τ (Figure 3.6 (d)). The remaining parameters τ_h and s_{st} do not seem to have a significant effect on the output.

The results of the linear analysis confirm that most statistically significant parameter is v_f with $R = -0.79$ (high negative degree of correlation) and a p-value approximately equal to 0. The R_l and R_u for R are -0.81 and -0.79, indicating a small range of dispersion for v_f. The R of τ is 0.09

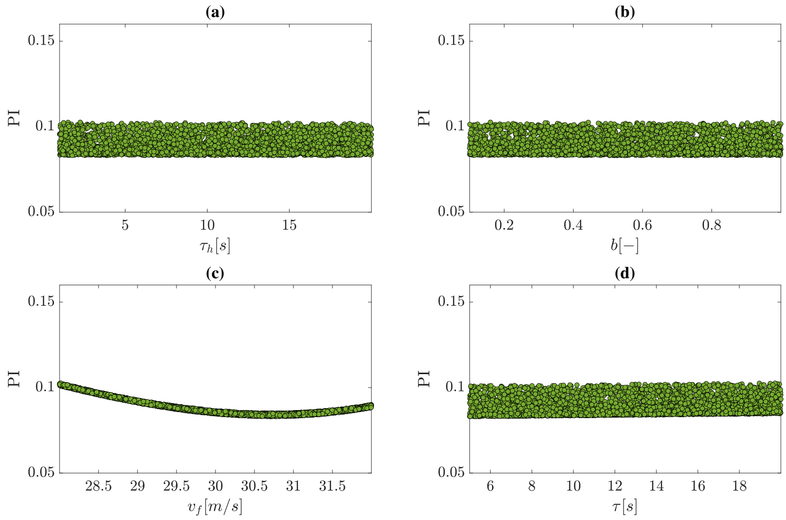

Figure 3.6. Scatter plots of each input parameter of IK model against the PI output for scenario I: a) time headway τ_h; b) lateral distance ration b; c) free-flow speed v_f; d) relaxation-time τ.

with a p-value approximately equal to 0, indicating a very weak correlation with PI. The R of τ_r and s_{st} are approximately equal to 0 with p-value approximately higher than the threshold (0.05), meaning that the results are not statistically significant.

Finally, the results of GSA in 3.10(b) confirm that the most influential input factor is v_f, while τ is a second-importance parameter. The median sensitivity value of s_{st} and τ_r are slightly below the threshold line, thus these parameters can be considered as non influential. The distribution boxes indicate that v_f is more dispersed than the other parameters followed.

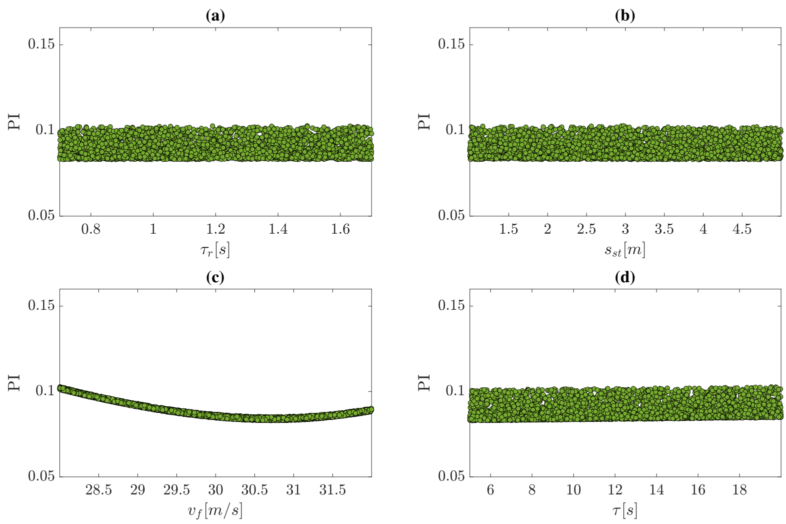

Figure 3.7. Scatter plots of each input parameter of KG model against the PI output for scenario I: a) reaction time τ_r; b) standstill distance s_{st}; c) free-flow speed v_f; d) relaxation-time τ.

3.6.1.2.3 JQZ Model Three parameters are considered for the JQZ model, namely c_o, v_f and τ.

Figure 3.8 illustrates the scatter plots of these variables, which refer to the analysis of all the simulation runs. The results demonstrate clearly show the different degree of correlation between PI and the considered variables of the model, as well as the output dispersion w.r.t. the mean. The scatter plot results in Figure 3.8(a) clearly show the nonlinear correlation between v_f and PI. A moderate correlation emerges from Figure 3.8(b) with c_o, while a weak correlation exists with τ as in Figure 3.8(c).

The linear analysis results in Table 3.8 confirm the outcome of the visual analysis. The outcome confirm that the most statistically significant parameter is v_f with $R = -0.55$ (moderate negative degree of correlation) and a p-value approximately equal to 0. The R_l and R_u are -0.58 and -0.53, indicating a limited range of dispersion for v_f. The R of c_0 is -0.44 with a p-value approximately equal to 0, indicating a negative moderate degree of correlation between c_0 and PI. The R_l and R_u are -0.42 and -0.47 indicating the range of variation is limited. In the ens, the R of τ is -0.19 with a p-value approximately equal to 0, hence a weak correlation exists.

Finally, the results of GSA in 3.10 are in line with the previous results. Indeed, the most influential input factor is v_f, followed by c_o. Regarding then τ, its sensitivity value is slightly above the threshold line, thus the parameter has a minor (but still significant) effect on the performance of the model.

3.6.1.2.4 SK Model Five parameters are considered for the SK model, namely v_f, τ, τ_r, s_{min} and L_c

Figure 3.9 illustrates the scatter plots of these variables, which refer to the analysis of all the simulation runs. The results demonstrate clearly show the different degree of correlation between PI and the considered variables of the model, as well as the output dispersion w.r.t. the mean. The scatter plot results in Figure 3.9(d) clearly show the nonlinear correlation between v_f and PI. Moreover, a weak correlation emerges from scatter plots in Figure 3.9(a), Figure 3.9(c) and Figure 3.9(e) with s_{min}, τ_r and τ respectively. No correlation trend can be appreciated with L_c (Figure 3.9(b)).

The linear analysis results in Table 3.8 confirm the outcome of the visual analysis. The outcome confirm that the most statistically significant parameter is v_f with $R = -0.56$ (moderate negative degree of correlation) and a p-value approximately equal to 0. The R_l and R_u are -0.60 and -0.54, indicating a limited range of dispersion for v_f. The R of τ is -0.23

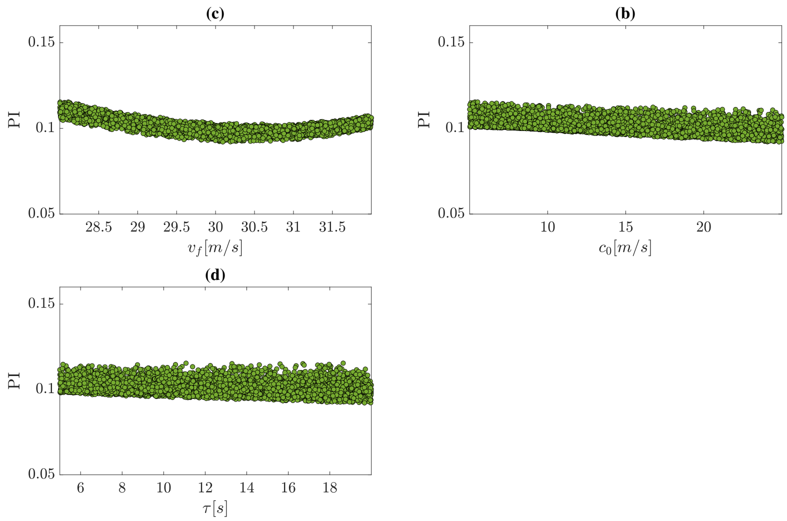

Figure 3.8. Scatter plots of each input parameter of the JQZ model against the PI output for scenario I: a)free-flow speed v_f; b) backward speed c_0 d) relaxation-time τ.

with a p-value approximately equal to 0, indicating a negative moderate degree of correlation between τ and PI. The R_l and R_u are -0.26 and -0.20 indicating the range of variation is limited. The R of τ_r is 0.31 with a p-value approximately equal to 0, indicating a positive moderate degree of correlation between τ_r and PI. The R_l and R_u are 0.29 and 0.34 indicating the range of variation is limited. The R of τ_r is -0.26 with a p-value approximately equal to 0, indicating a positive moderate degree of correlation with PI. The R_l and R_u are -0.30 and -0.23 indicating the range of variation is limited. Finally, the R of L_c is -0.05 with a p-value almost equal to 0, indicating a very weak degree of correlation with PI.

The results of GSA in 3.10(d) confirm that the most influential input factor is v_f. Three parameters s_{min}, τ and τ_r are second-importance parameters, while L_c resulted to be non important since its sensitivity value is slightly above the threshold line.

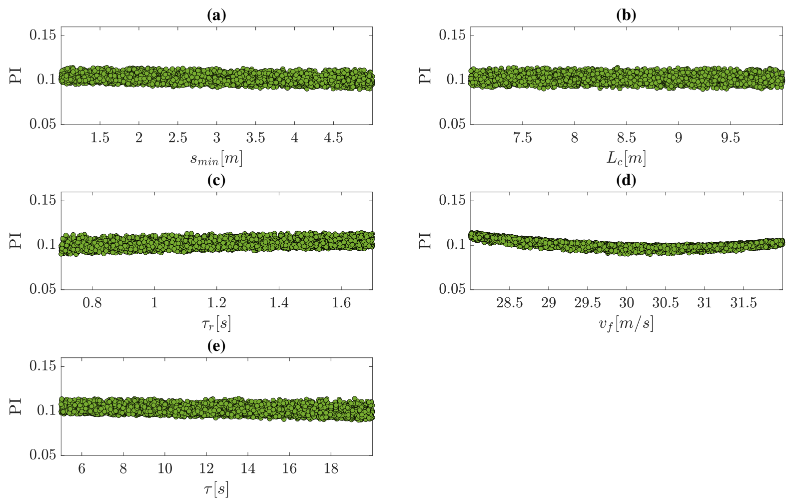

Figure 3.9. Scatter plots of each input parameter of the SK model against the PI output for scenario I: a) minimum safe distance s_{min}; b) vehicle length L_c; c) reaction-time τ_r; d) free-flow speed v_f; e) relaxation-time τ.

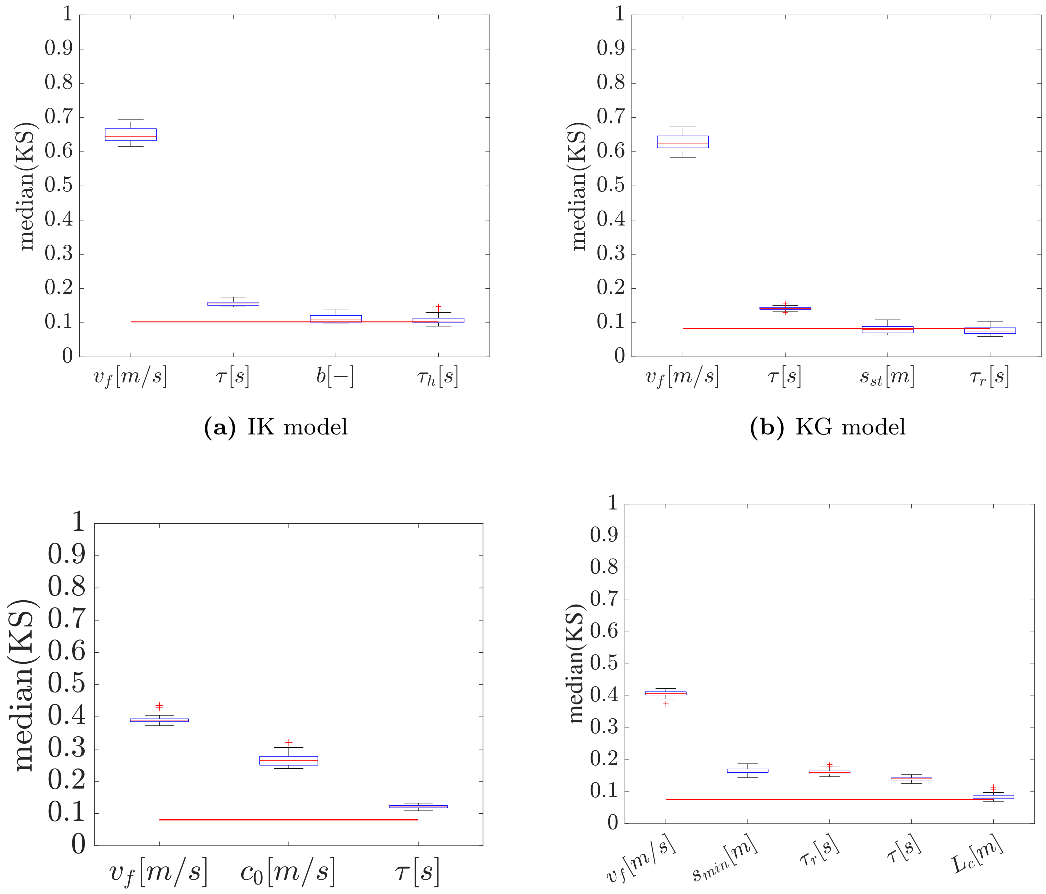

(a) IK model

(b) KG model

(c) JQZ model

(d) SK model

Figure 3.10. PAWN sensitivity indexes for each input factor of the SOTFMs for the scenario I. Bootstrapping estimates the distribution of each PAWN index. Boxplots are employed to display variation in the sample: the bottom and top edges of a box indicate the 25th and 75th percentiles, while the red line inside the box the median value. The horizontal red line represents the KS of the dummy parameter. Input parameters are sorted according to their PAWN index values. Results for: a) IK model; b) KG model; c) JQZ model; d) SK model

3.6.2 Scenario II

3.6.2.1 Results of Full Calibrated Models

The calibrated values for parametric variables of SOTFMs for scenario II (a) are listed in Table 3.7. The models with the lowest value of PI are KG and IK, followed by SK and JQZ.

The initial density distribution corresponds to a traffic condition where light traffic conditions such that relative density between 0.15 and 0.45 approaches a denser traffic condition downstream. This dense region represents congestion due to an inactive bottleneck and sharp changes in traffic. Such conditions create non-equilibrium traffic phenomena and the role of the anticipation term of the SOTFMs becomes vital. As with large changes in traffic, the stability of the models can be compromised. In Figure 3.11 (a), a visible shockwave is generated when upstream traffic approaches the denser traffic downstream at $14,000$ m which propagates backward until 720 s (12 minutes), to $10,800$ m. Beyond this point in time and space, the traffic stabilizes and the shockwave dissipates, moving in the downstream traffic direction. Until 1200 s (20 minutes), the rear end of this traffic is approached by traffic from upstream creating uniform flow traffic conditions in the corridor as a result of circular geometry. This traffic scenario depicts a realistic traffic condition in which a shockwave is formed and dissipated with time. The same behavior is replicated by the SOTFMs as shown in Figure 3.11 (c)-(e).

The spatiotemporal pattern formation of the IK model as shown in Figure 3.11 (b), this model obeys the trends in pattern formation as in 3.11 (a). The pattern formation (which represents a shock and rarefaction wave) is observed, and smooth traffic flow is observed over time. The PI for this model is 0.10, replicating the scenario II (a) with the KG model as shown in Figure 3.11 (c), it follows the same trends as by the IK model, and the PI is 0.10. Thus, both of these models (IK and KG) can be employed in congested traffic situations, however, the use is subject to the sensitivity and efforts in the calibration of the parameters of the models, which is investigated later in this paper.

The spatiotemporal pattern formation of the SGM such as the JQZ and SK is shown in Figure 3.11 (d) and 3.11 (e), respectively. The early behavior of both models is close to that of the SUMO. An almost similar flow pattern is followed by both models. There are variations in the predicted flow values after 14 minutes but this behavior is common because changes in these systems occur over the velocity gradient, which is faster than the DGTS. The PI of the JQZ model is 0.125 while for the SK model, it is 0.12. The flow behavior of each kind of SOTFMs stabilizes with time, so it is important to rely on the early behavior of the models. If the initial behavior of any model is satisfied it is more likely that it will result in a consistent outcome. It is important to note that larger PI values can also be attributed to the simulation prediction time. In general, the DGTS outperforms the SGM in both traffic scenarios.

3.6.2.2 Results of Senstivity Analysis

Here we analyse the relationship between the input parameters of each SOTFMs (3.7) and the output (PI) both qualitatively and quantitatively.

3.6.2.2.1 IK Model Analysis of the IK model involves four parameters listed in 3.7, namely v_f, τ, τ_h and b.

Figure 3.12 illustrates the scatter plots of these variables, which refer to the analysis of all the simulation runs and the same number of points (4000, one for each run) compose each plot. The y-axis of each subplot corresponds to the output variable y (PI), whereas the x-axis refers to a different SOTFMs parameter. The results demonstrate clearly show the different degree of correlation between PI and the considered variables of the model, as well as the output dispersion w.r.t. the mean. More specifically, Figure 3.6(c) highlights shows a significant nonlinear correlation between PI and v_f, while the remaining parameters τ_h, b and τ do not exhibit a trend (seem to have a significant effect on the output).

The results of the linear analysis confirm that most statistically significant parameter is v_f with $R = -0.77$ (high negative degree of correlation) and a p-value approximately equal to 0. The R_l and R_u for R are -0.78 and -0.75, indicating a small range of dispersion for v_f. The value of R for τ_h, b and τ is close to zero, indicating a weak or null association. Moreover, the p-value for τ_h and b is higher than the threshold value (0.05), hence the results related to these variable are no statistically significant.

The results of GSA in 3.16(a) confirm that the most influential input factor is v_f, while τ has a minor influence on the performance of the model.

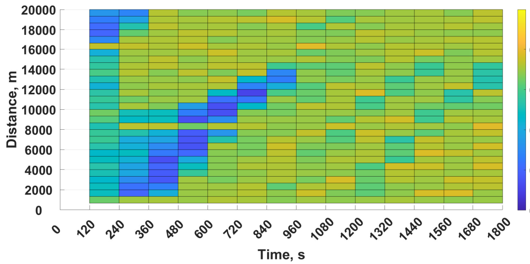

(a) Flow evolution in SUMO.

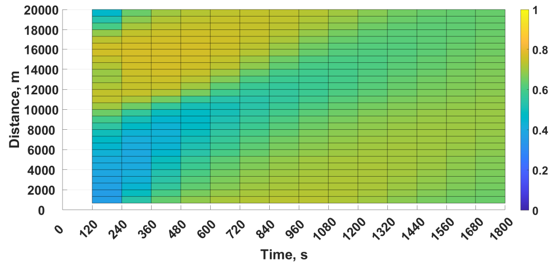

(b) Flow evolution of IK model.

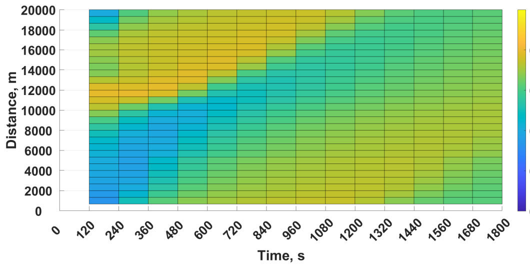

(c) Flow evolution of KG model.

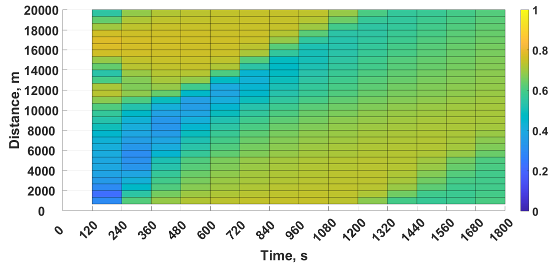

(d) Flow evolution of JQZ model.

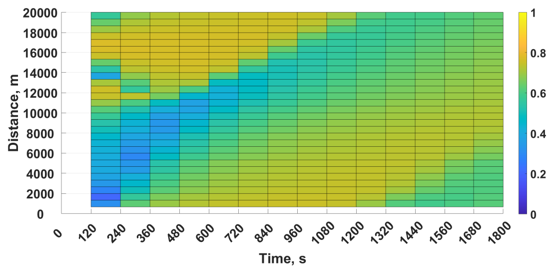

(e) Flow evolution of SK model.

Figure 3.11. Flow evolution over time (1800 s - x-axis) and space (20,000 m road section y-axis) given the initial conditions as defined by scenario II: a) SUMO, used as ground-truth; b) IK model; c) KG model; d) JQZ model; e) SK model.

The median sensitivity value of b and τ_h are slightly below the threshold line, indicating a negligible influence of these parameter on PI.

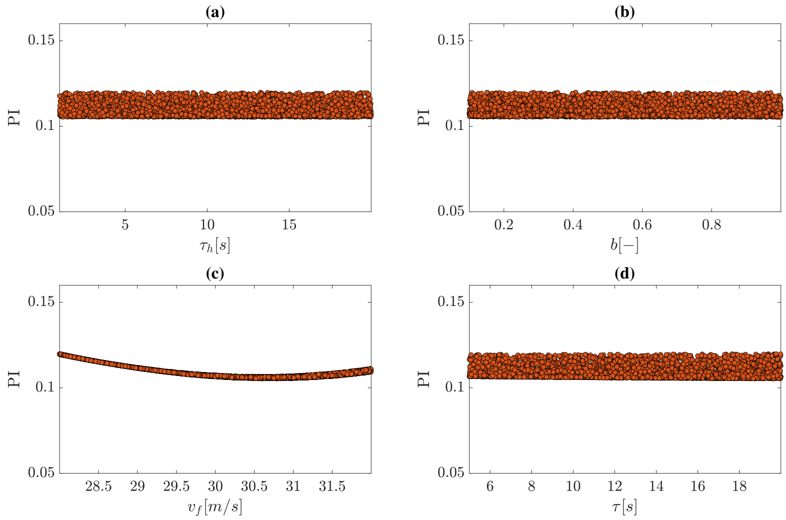

Figure 3.12. Scatter plots of each input parameter of IK model against the PI output for scenario II: a) time headway τ_h; b) lateral distance ration b; c) free-flow speed v_f; d) relaxation-time τ.

3.6.2.2.2 KG Model The analysis of the KG model involves four parameters listed in Table 3.7, τ_r, v_f, τ and s_{st}.

Figure 3.13 illustrates the scatter plots of these variables, which refer to the analysis of all the simulation runs. The results demonstrate clearly show the different degree of correlation between PI and the considered variables of the model, as well as the output dispersion w.r.t. the mean. More specifically, Figure 3.7(c) highlights shows a significant nonlinear correlation between PI and v_f, while the remaining parameters τ_r, τ and s_{st} do not seem to have a significant effect on the output.

The results of the linear analysis confirm that most statistically significant parameter is v_f with $R = -0.76$ (high negative degree of correlation) and a p-value approximately equal to 0. The R_l and R_u for R are -0.77 and -0.74, indicating a small range of dispersion for v_f. The value of R for

τ_r, τ and s_{st} is close to zero, indicating a weak or null association. Moreover, the p-value for τ_r and s_{st} is higher than the threshold value (0.05), hence the results related to these variable are no statistically significant.

Finally, the results of GSA in 3.16(b) confirm that the most influential input factor is v_f, while τ is a second-importance parameter. The median sensitivity value of s_{st} and τ_r are slightly below the threshold line, thus these parameters can be considered as non influential.

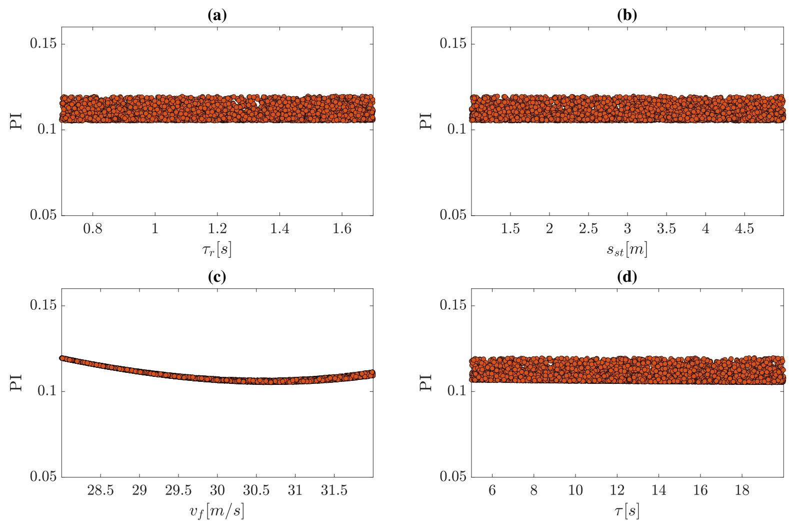

Figure 3.13. Scatter plots of each input parameter of KG model against the PI output for scenario II: a) reaction time τ_r; b) standstill distance s_{st}; c) free-flow speed v_f; d) relaxation-time τ.

3.6.2.2.3 JQZ Model Three parameters are considered for the JQZ model, namely c_o, v_f and τ. The scatter plot results in Figure 3.14(a) clearly show the nonlinear correlation between v_f and PI, while the ones in Figure 3.14(b) and in Figure 3.14(c) depict a weak correlation with c_o and τ.

The linear analysis results in Table 3.8 confirm the outcome of the visual analysis. The outcome confirm that the most statistically significant parameter is v_f with $R = -0.41$ (moderate negative degree of correlation) and a p-value approximately equal to 0. The R_l and R_u for R are -0.44 and -0.38, indicating a limited range of dispersion for v_f. The R of c_0 is -0.15 with a p-value almost equal to 0, indicating a negative weak degree of correlation between c_0 and PI. The R_l and R_u for R are -0.18 and -0.12 indicating the range of variation is limited. Similarly, the R of τ is -0.14 with a p-value almost equal to 0, hence a low degree of correlation exists. Whereas, the R_l and R_u for R are -0.17 and -0.11.

The results of GSA in 3.16 confirm that the most influential input factor is v_f. Regarding τ and c_o, they resulted to be second-importance parameters, i.e. they have a minor but still significant effect on the performance of the model.

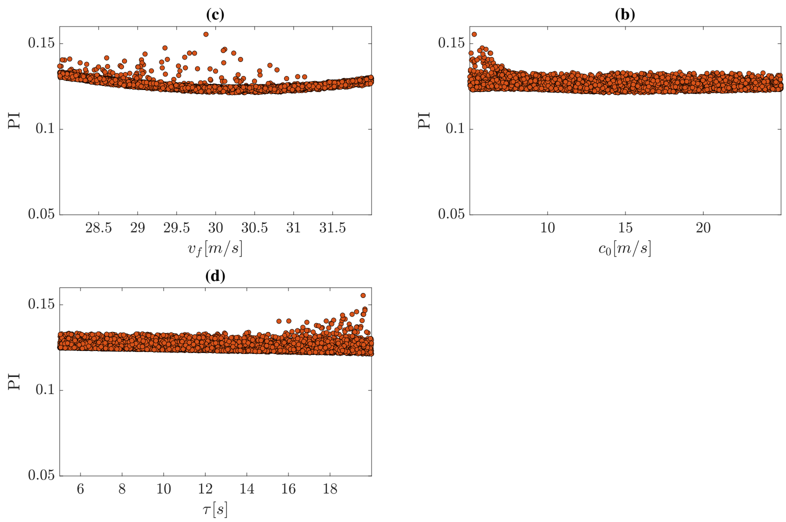

Figure 3.14. Scatter plots of each input parameter of the JQZ model against the PI output for scenario II: a)free-flow speed v_f; b) backward speed c_0 d) relaxation-time τ.

3.6.2.2.4 SK Model Five parameters are considered for the SK model, namely v_f, τ, τ_r, s_{min} and L_c

Figure 3.15 illustrates the scatter plots of these variables, which refer to the analysis of all the simulation runs. The results demonstrate clearly show the different degree of correlation between PI and the considered variables of the model, as well as the output dispersion w.r.t. the mean. The scatter plot results in Figure 3.15(d) clearly show the nonlinear correlation between v_f and PI. Moreover, a weak correlation emerges from scatter plots in Figure 3.15(a), Figure 3.15(c) and Figure 3.15(e) with s_{min}, τ_r and τ respectively. No correlation trend can be appreciated with L_c (Figure 3.15(b)).

The linear analysis results in Table 3.8 confirm the outcome of the visual analysis. The outcome confirm that the most statistically significant parameter is v_f with $R = -0.43$ (moderate negative degree of correlation) and a p-value approximately equal to 0. The R_l and R_u are -0.45 and -0.40, indicating a limited range of dispersion for v_f. The R of τ is -0.12 with a p-value approximately equal to 0, indicating a negative moderate degree of correlation between τ and PI. The R_l and R_u are -0.15 and -0.08 indicating the range of variation is not small. The R of τ_r is 0.18 with a p-value approximately equal to 0, indicating a positive moderate degree of correlation between τ_r and PI. The R_l and R_u are 0.15 and 0.21 indicating the range of variation is limited. The R of τ_r is -0.16 with a p-value approximately equal to 0, indicating a positive moderate degree of correlation with PI. The R_l and R_u are -0.19 and -0.13 indicating the range of variation is limited. Finally, the R of L_c is -0.02 with a p-value almost equal to 0, indicating a very weak degree of correlation with PI.

The results of GSA in 3.16(d) confirm that the most influential input factor is v_f. Three parameters s_{min}, τ and τ_r are second-importance parameters, but still significantly affecting the performance of the model. Finally, L_c resulted to be non important since its sensitivity value is slightly above the threshold line.

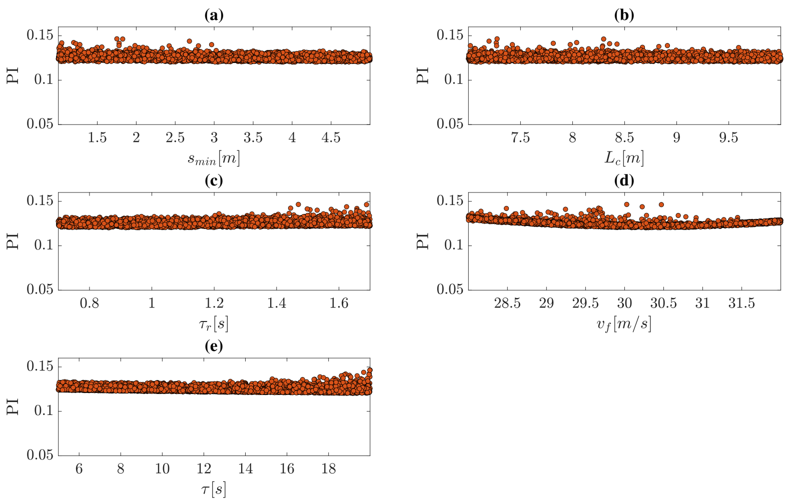

Figure 3.15. Scatter plots of each input parameter of the SK model against the PI output for scenario II: a) minimum safe distance s_{min}; b) vehicle length L_c; c) reaction-time τ_r; d) free-flow speed v_f; e) relaxation-time τ.

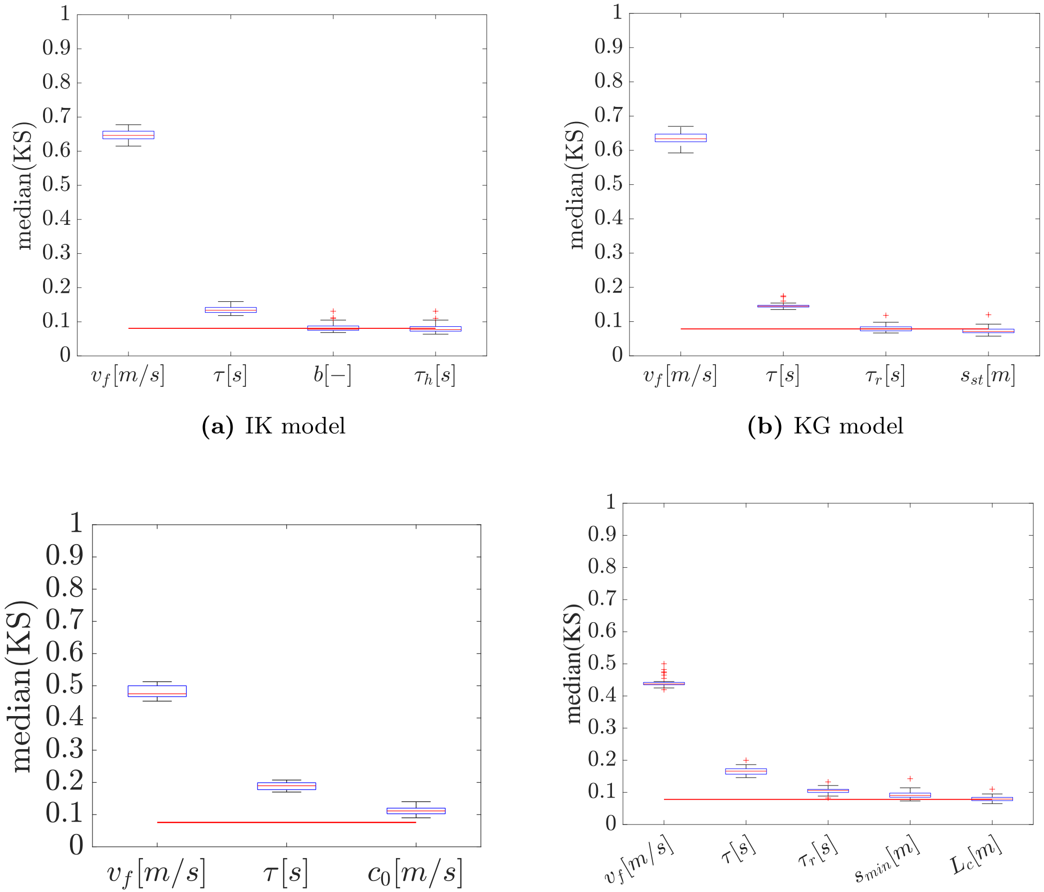

(a) IK model

(b) KG model

(c) JQZ model

(d) SK model

Figure 3.16. PAWN sensitivity indexes for each input factor of the SOTFMs for scenario II. Bootstrapping estimates the distribution of each PAWN index. Boxplots are employed to display variation in the sample: the bottom and top edges of a box indicate the 25th and 75th percentiles, while the red line inside the box the median value. The horizontal red line represents the KS of the dummy parameter. Input parameters are sorted according to their PAWN index values. Results for: a) IK model; b) KG model; c) JQZ model; d) SK model

Table 3.8. Pearson (R) with R_l and R_u and p-values of SOTFMs parameters for scenarios I and II.

Model	Parameter	c_0		v_f		τ		τ_h		b		τ_r		s_{min}		L_c		s_{st}	
		I	II	I	II	I	II	I	II	I	II	I	II	I	II	I	II		
IK	R	-		-0.80	-0.77	0.09	-0.04	0.01	-0.01	0.01	-0.02	-		-		-		-	
	p-value	-		~ 0	~ 0	~ 0	~ 0	0.48	0.30	0.50	0.16	-		-		-		-	
	R_l	-		-0.81	-0.78	0.06	-0.07	-0.01	-0.04	-0.02	-0.05	-		-		-		-	
	R_u	-		-0.79	-0.75	0.12	-0.01	0.04	0.01	0.04	0.009	-		-		-		-	
KG	R	-		-0.79	-0.76	0.09	-0.07	-		-		-0.01	0.01	-		-		-0.003	-0.01
	p-value	-		~ 0	~ 0	~ 0	~ 0	-		-		0.21	0.48	-		-		0.84	0.33
	R_l	-		-0.81	-0.77	0.06	-0.11	-		-		-0.05	-0.01	-		-		-0.03	-0.04
	R_u	-		-0.78	-0.74	0.12	-0.04	-		-		0.01	0.04	-		-		0.02	0.01
JQZ	R	-0.44	-0.15	-0.55	-0.41	-0.19	-0.14	-		-		-		-		-		-	
	p-value	~ 0	~ 0	~ 0	~ 0	~ 0	~ 0	-		-		-		-		-		-	
	R_l	-0.47	-0.18	-0.58	-0.44	-0.21	-0.17	-		-		-		-		-		-	
	R_u	-0.42	-0.12	-0.53	-0.38	-0.15	-0.11	-		-		-		-		-		-	
SK	R	-		-0.56	-0.43	-0.23	-0.12	-		-		0.32	0.18	-0.29	-0.16	-0.06	-0.02	-	
	p-value	-		~ 0	~ 0	~ 0	~ 0	-		-		~ 0	~ 0-	~ 0	~ 0	~ 0	0.11	-	
	R_l	-		-0.58	-0.45	-0.26	-0.15	-		-		0.29	0.15	-0.32	-0.19	-0.09	-0.05	-	
	R_u	-		-0.54	-0.40	-0.20	-0.08	-		-		0.35	0.21	-0.26	-0.13	-0.03	-0.005	-	

3.6.3 Computational Effort Analysis

The computational effort required to resolve numerical schemes for SOTFMs is influenced by factors such as spatial and temporal discretization, the complexity of the traffic model, and the size of the simulated domain. To obtain general indications of the computational effort required by each model, we analyzed the time required to run, on average, one simulation.

Before analyzing the results, it is worth noting that: *i*) the simulations have been carried out on a Lenovo P14, vPRO, intel core i7; *ii*) the results are related to the employed numerical schemes.

Table 3.9. Time required to run, on average, one simulation for each SOTFMs for Scenario I and Scenario II.

Model	Average Simulation Time [s] (I/II)
IK	0.4376 / 0.5773
KG	0.3998 / 0.4121
JQZ	0.0013 / 0.0013
SK	0.0014 / 0.0015

Results in Table 3.9 show that JQZ and SK models are much faster, both in Scenario I and Scenario II, than IK and KG (i.e., require less computational effort). Furthermore, the results show that the execution time does not vary or increase slightly between Scenarios I and II for all models except the IK, for which it instead increases by approximately 35 percent.

3.7 Discussion

The analysis carried out in the previous Section evaluates the performance of the SOTFMs in reproducing the ground-truth traffic conditions. Moreover, the sensitivity analysis revealed the significant parameters, for each model, for calibration purposes.

All the SOTFMs can reproduce closely the ground-truth data, hence confirming their suitability for practical applications. The results highlight how sensitive the models are to initial conditions: the values of the parameters vary depending on the initial conditions and, more generally, on the traffic conditions observed. It is important to note that the models, under congested prevailing traffic conditions, are able to replicate the mechanism of formation and dissipation of shock waves, which is crucial for understanding the evolution of traffic dynamics. The results confirmed that the relaxation term plays a vital role as it mitigates any change in traffic flow; however, the instigation of perturbation is due to anticipation, and the model stability strictly depends on this term. During transient phases, i.e. when a significant variation of traffic condition occurs, the response of SOTFMs is not always uniform but strictly depends upon the intensity of change in the specific traffic condition. The outcome shows, also, that SOTFMs can be employed based on the scenario where they are deemed fit. Some models could perform better in light traffic conditions while some of them in dense conditions. Additionally, the underlying principles of all models are different, thus, it is very important to verify them before employing them in particular traffic conditions.

Regarding the importance of SOTFMs parameters, it is evident from the results of sensitivity analysis that most of the parameters are significant, while a few are not. Qualitative and linear regression analysis proved to be useful tools to evaluate the relationship between an evaluation index and the models' parameters. However, in the case of nonlinear relationships, GSA approaches are more suitable to identify the parameters that actually affect the performance of a model. The results further confirm that these models are strongly influenced by initial conditions: some parameters may or may not be significant based on the observed prevailing traffic conditions. Thus, the calibration of such models should be done carefully, and parameters values should be updated on the basis of actual traffic conditions.

Finally, the computational analysis highlights how different models require different resolution times (the time needed to complete a simulation). In particular, JQZ and SK models have a less resolution time, on average, about 250 times shorter than that of IK and KG. The computational efficiency of SOTFMs is a key aspect for their practical applicability since:

- a less computationally demanding model allows for quicker simulation times. This is especially beneficial for scenarios where rapid decision-making or real-time analysis is crucial, as well as for exploratory analysis.

- Reduced computational demands mean that the model can run on less powerful hardware or be applied to larger and more complex traffic scenarios without requiring extensive computational resources. Lower computational demands often translate to lower costs, both in terms of hardware requirements and energy consumption.
- A less computationally intensive model is more suitable for real-time applications, such as traffic management systems and intelligent transportation systems.
- Models that are not overly computationally demanding are more scalable, meaning they can be applied to larger geographic areas or more extensive transportation networks without a significant increase in computational costs.

3.8 Conclusion

In this Chapter, we investigate the properties and performances of a set of notable representatives of Second Order Traffic Systems (SOTFMs). Specifically, four models are considered: two density gradient traffic systems (IK and KG) and two velocity gradient traffic systems (JQZ and SK). The mathematical structure of each model, as well as its features (Jacobian matrix, eigenvalues, hyperbolicity, and anisotropy), are studied.

We carried out an extensive simulation analysis to evaluate (and compare) comprehensively the performance of SOTFMs in reproducing the ground-truth traffic. Each model is implemented on two scenarios, characterized by different traffic conditions; moreover, structural parameters of the SOTFMs are considered as uniformly distributed random variables within a feasible range of variations. To accomplish this task, $\Gamma = 4000$ simulations runs, for each model under each traffic scenario, are performed.

The results demonstrate that all the SOTFMs can reproduce well the ground-truth: the speed gradient systems replicate the spatiotemporal pattern formation of SUMO, including complex traffic phenomena, in all scenarios. The IK and KG models present the best performances (lowest PI values) for both scenarios, followed by SK and JQZ. Going into detail of the first two models, the IK performs the best under light traffic conditions (PI $= 0.078$), while under congested conditions the IK and the KG have comparable performance. Generally, all the SOTFMs perform better under light traffic conditions (Scenario I). It is crucial to emphasize that, in instances of congested traffic conditions, the models exhibit the ability to replicate the mechanisms involved in the formation and dissipation of shock waves. This is crucial for comprehending the evolution of traffic dynamics. The findings affirm that the relaxation term assumes a pivotal role by mitigating alterations in traffic flow. However, it is noteworthy that the induction of perturbations is mitigated by the anticipation term, thereby rendering the stability of the model contingent upon this term. In transient phases, characterized by substantial variations in traffic conditions, the response of the SOTFMs is not uniformly consistent.

To identify and analyze trends, patterns, and insights of the considered SOTFMs, such as obtaining comprehensive knowledge about the parameters of each model and their contribution to the performance of each model, we employ different approaches. The qualitative analysis is assessed through scatter plots, which provide straightforward and intuitive evidence of the relationship between the SOTFMs input factors and the output (the PI in Eq. (3.21)). The quantitative analysis involves the Pearson correlation coefficient R to spot the (linear) correlation between and the PAWN Global Sensitivity Analysis (GSA) method. The outcome of sensitivity analysis shows that most of the parameters are significant, while a few are not. Qualitative and linear regression analysis proved to be useful tools to evaluate the relationship between an evaluation index and the models' parameters. However, to determine the relative impact of each input factor on the output variability, the GSA-based approach proved to be more effective. This is particularly true in the cases of non-linear relationships, for which the linear analysis produces biased results. It is concluded that parameter fixing can reduce the computational effort, but this operation should be performed carefully since some parameters may or may not be significant based on the observed prevailing traffic conditions. This implies that the values of such models should be updated periodically according to actual traffic conditions. It is also worth noting that the SOTFMs, for several reasons such as replication of real-world phenomena, fast computations, consistency, expandability, and simplicity, could be extremely serviceable in control applications.

Future work in the same direction could include the time-varying sensitivity analysis of the performance of SOTFMs, the employment of different laws for the fundamental diagram, different traffic conditions, the exploitation of real traffic data, and the evaluation under mixed traffic conditions.

3.9 Preview of the Next Chapter

In this Chapter, we extensively examined models known as MCTFMs, specifically focusing on SOTFMs. Using a systematic approach, which involved detailed scenarios and sensitivity analysis, we gained valuable insights into how well SOTFMs can simulate and replicate various complex traffic situations. Our findings highlight that these models are robust, not only simulating but also accurately reproducing different traffic scenarios. Each model offers a unique understanding of traffic dynamics.

In the next chapter, we will delve into a more challenging aspect, adapting and improving SOTFMs to handle mixed traffic. This involves the presence of CAVs alongside traditional HDVs on highways. This shift is crucial for our research, holding significant implications for both academics and practical applications. The main goal of the upcoming chapter is to enhance SOTFMs to effectively manage the complexities of mixed traffic scenarios. We aim to make substantial contributions to the field of traffic modeling and control, especially in incorporating CAVs into SOTFMs. Our objective is to develop advanced models for traffic management that consider the coexistence of CAVs and HDVs, ensuring efficient highway management.

Chapter 4

Macroscopic Modeling of Connected, Autonomous, and Human-Drive Vehicles: A Pragmatic Perspective

4.1 Abstract

Several interdisciplinary investigations have delved into the influence of Connected and Autonomous Vehicles (CAVs) on traffic network performance, with expectations for positive outcomes. However, a crucial factor to consider is the transitional phase during which both Human-Driven Vehicles (HDVs) and CAVs will coexist on the roadways. To gain a comprehensive understanding of the dynamics of this mixed traffic scenario, it is imperative to develop adequate models that capture the interactions between CAVs and HDVs.

In our study, we introduce a Second-Order Traffic Flow Model (SOTFM) that relies on the dynamic headway distance between vehicles in mixed traffic settings. This model serves as a valuable tool for comprehending the complex interplay between CAVs and HDVs and its implications on traffic flow. Our findings indicate that as the Penetration Rate (PR) of CAVs increases, there are notable enhancements in both the average traffic velocity and the Level of Service (LOS) of the traffic network. These

improvements are indicative of the positive influence that a higher PR of CAVs can have on overall traffic performance.

To ensure the reliability and applicability of our proposed model, we subject it to rigorous validation through microscopic simulations. These simulations replicate various traffic scenarios while considering a range of Penetration Rates (PRs) for CAVs. The consistency of our model in replicating real-world traffic dynamics under different PR conditions underscores its utility and robustness.

Importantly, the model we present has practical implications. It can be effectively utilized in traffic forecasting, offering valuable insights into how traffic conditions may evolve as Connected and Autonomous Vehicle (CAV) adoption rates change. Additionally, it holds promise for real-time traffic control applications, where optimizing traffic flow in mixed traffic environments can significantly improve overall transportation efficiency.

In all, our study contributes to the growing body of research exploring the impact of CAVs on traffic networks. By introducing a SOTFM and validating it through simulations, we provide a practical framework for understanding and harnessing the potential benefits of CAVs in mixed traffic scenarios, with direct applications in traffic forecasting and real-time traffic management.

4.2 Introduction

Traffic congestion on freeways has become a significant problem. It leads to increased socio-economic costs, as well as environmental issues caused by CO2 emissions [121]. To resolve this problem, many studies have suggested innovative and creative methodologies in the last decades. With the development of the Internet of Things (IoT) and communication technologies, diverse technologies of Connected and Autonomous Vehicles (CAVs) are proposed in traffic systems to enhance traffic network performance, road safety, transport mobility, and urban accessibility [11]. One of the ongoing major trends in the automotive sector is the development of Cooperated, Connected and Automated Mobility (CCAM). In order to ensure the optimal mobility environment for the general public, CCAM aims to support the automobile industry as it transitions to connected and automated driving. By 2040–2050, the Penetration Rate (PR) of CAVs is anticipated to surge [122]. However, due to many policy and technical obstacles, CAVs will have a marginal PR in the next few years [123]. Until a consensus is reached on their impacts on safety, operations in a mixed environment, and legislation, there will be legal barriers for CAVs to operate.

In the near future, CAVs' PR will be modest, and it is anticipated that Human-Driven Vehicles (HDVs) and CAVs will share the road for a considerable amount of time. Contrary to merely using HDVs, the combination of CAVs and HDVs may show some complex traffic flow characteristics [124, 125, 126]. There is a dire need for research on this type of mixed traffic flow up to this point [127]. At all scales (microscopic, mesoscopic, and macroscopic), appropriate models and modeling methodologies are required in order to accurately depict the changing dynamics and capacities of mixed traffic flow as they will alter significantly with CAVs [128].

So far, several benefits of CAVs have been identified. CAVs are able to run with significantly less spacing or headway [129]. As a result, it is anticipated that the traffic capacity of highways with CAVs would grow [130, 131, 132], and the Level of Service (LOS) of highways will improve. However, despite the benefits of CAVs being identified and studied on the microscopic level, a few studies involving CAVs are presented on the macroscopic level.

The macroscopic approach is used due to its capability of reliable traffic flow modeling, at the same time with moderate computational complexity (compared to microscopic modeling) [53, 133, 134]. The macroscopic approach mostly considers two kinds of models known as the first-order and second-order models. There are several derivations of second-order models in the literature, such as those that are derived from the extension of car-following models using Taylor's expansion [135]. Another strategy is to construct analogies from fluid movement in order to derive the structural terms of the second-order traffic model [136, 137, 98, 5], and the additions of viscous and diffusion terms to the existing momentum equations [138]. Nonetheless, these derived formulations are only applicable to HDVs, and not to CAVs as they are not explicitly revised for the characteristics of CAVs-HDVs mixed traffic. In this perspective, the conventional second-order macroscopic traffic model (JQZ model) [52] is revised in order to capture the impact of CAVs on conventional traffic flow. The revised second-order model is based on the dynamic headway distance of CAVs and HDVs in a mixed traffic environment.

The main contributions of this chapter can be summarized as follows:

1. A new second-order traffic model is proposed by taking into account the spatio-temporal characteristics of the HDVs and CAVs to model dynamic headway distance between vehicles.

2. Nonetheless, conventional velocity-density relationship models fail to explicitly account for the variability introduced by CAVs. The incorporation of a shape factor becomes indispensable in the modeling of traffic within a heterogeneous environment. In pursuit of this objective, an enhanced model for the velocity-density relationship is assessed, given its heightened sensitivity to the outcomes of macroscopic models

3. A verification of the effectiveness of the proposed model is carried out by performing a comparative analysis of the proposed model with microscopic simulations on the Dublin motorway. Some macroscopic aspects such as the average velocity and Level of Service (LOS) of mixed traffic are analyzed using the proposed model.

4.3 Mixed Traffic Flow Modeling

The headway distance is the distance from the front bumper of a leading vehicle to that of the following vehicle [139], it comprises the gap between two vehicles and the length of a leading vehicle. The gap between two vehicles is a driver's intrinsic property, it varies according to the traffic conditions and is a dynamic gap D_g since vehicles are in motion [140]. With the advanced capabilities of CAVs, which include the ability to maintain shorter headway distances compared to HDVs, D_g for CAVs differs from that of HDVs. This variation depends on the class-specific reaction time and velocity [141].

Vehicles maintain a minimum clearance gap to avoid collisions, which is a safe gap denoted as g_s between the vehicles. Conversely, the clearance gap increases with an increase in the velocity of a vehicle. It is not possible for vehicles to maintain a uniform g_s as in standstill conditions; thus, an additional distance is perceived, represented as g_p. This perceived distance is a function of traffic transition time (τ) and average velocity (v). Therefore, the D_g between the vehicles is the sum of g_s and g_p. Variations in traffic occur according to g_p then D_g is computed as

$$D_g = g_s + g_p, \tag{4.1}$$

and the headway distance is

$$H = L + D_g, \tag{4.2}$$

where L is a vehicle's average length.

Adjustments in headway distance are characterized by τ which vary for various classes of vehicles [142]. Thus, in non-identical traffic conditions, a driver's response to changes ahead is not unique, and the g_p is computed as

$$g_p = v \cdot \tau, \tag{4.3}$$

Traffic adjustments will occur according to Eq. (4.2), it will induce stochasticity in the traffic which is further refined hereafter.

The τ is the transition time for change occurrence. In other words, it is the time over which a change in traffic state occurs. Transition distance is the distance covered whenever a traffic state changes. For a small transition distance than a safe distance, a collision between vehicles will occur. Conversely, for a larger safe transition distance, driver reaction is safer. A safe transition distance is achieved during reaction time τ_r when perceiving a forward traffic change, and the harmonization time τ_b to take action to harmonize to changes ahead [143], thus

$$\tau = \tau_r + \tau_b. \tag{4.4}$$

The safe gap g_s to avoid accident occurrence is the stopping required in case the leading vehicle velocity reduces to zero. Thus, τ_b is the stopping time while adjusting to g_s, and during this time the vehicles apply maximum deceleration d_m. g_s can be modeled for HDVs and CAVs from the well-known law of motion [143, 144, 145], it is

$$g_s = \frac{v^2}{2d_m}, \tag{4.5}$$

The following vehicle will harmonize with the leading vehicle by covering g_p and adjusting to g_s while applying d_m.

The intrinsic vehicle characteristics, such as reaction and harmonization times, have improved with the development of CAVs, and they have been investigated in a number of studies [146, 147]. From a motion viewpoint, with improved intrinsic vehicle characteristics, the two vehicle classes, CAVs and HDVs will maintain a non-identical headway in mixed traffic conditions. Considering the characteristics of mixed traffic, the class of each vehicle will have a non-identical headway distance. For HDVs, it is represented by H_a, and is

$$H_a = L + \frac{v^2}{2d_m} + (v \cdot \tau)_{HDV}, \tag{4.6}$$

and that for CAVs is represented by H_b, and is

$$H_b = L + \frac{v^2}{2d_m} + (v \cdot \tau)_{CAV}. \tag{4.7}$$

In Eq. (4.6) and Eq. (4.7), τ and d_m are different for HDVs and CAVs.

During transitions, the response of drivers/vehicles is characterized by reaction velocity v_r [134] which is a function of the actual headway distance and the transitions occurring time, it is

$$v_r = \frac{h}{\tau}. \tag{4.8}$$

It is the change in velocity when traffic changes occur from free flow to congested flow and vice versa. In the case of free flow, reaction time increases, the D_g is relaxed and vice versa. The v_r for HDVs and CAVs will be non-identical. For HDVs, it is represented by ζ, and is

$$\zeta = \frac{H_a}{\tau_a}, \tag{4.9}$$

where τ_a is the transition time for change occurrence by HDVs. Reaction velocity for CAVs is denoted by φ , and is

$$\varphi = \frac{H_b}{\tau_b}, \tag{4.10}$$

where τ_b is the transition time of CAVs.

Furthermore, the dispersion effect of the speed of multi-class traffic is characterized by anticipation. That is, how identical driver/vehicle reacts to traffic conditions presumed. Drivers/vehicles usually reduce speed while approaching heavy traffic downstream, and vice versa for light traffic. The second-order traffic models take into account this property of flow, which in Eq. (2.8) is

$$(v(x,t) - c_0)\frac{\partial v(x,t)}{\partial x}, \tag{4.11}$$

demonstrating that traffic patterns alter spatially with gradients of velocity. In a practical sense, c_0 is the driver's response to the changes in traffic which is not always uniform. It is characterized by reaction velocity, in this study, it is given by Eq. (4.9) for HDVs, and Eq. (4.10) for CAVs. In most studies, c_0 is considered constant, implying that a driver or vehicle will always have a uniform response in non-identical conditions. However, this assumption is incorrect and lacks physical meaning. Lately, this assumption has been corrected for HDVs, however, revising this for CAVs is significant for a more accurate traffic characterization.

The response of the following vehicle is significantly influenced by the leading vehicle, and it is regarded as an anisotropy principle in traffic flow. Further, in macroscopic systems, the typical behavior of flow is regarded as a traffic wave that is traffic-traveling-wave [50]. It is not possible to study the behavior of a single car at the macroscopic level; instead, we must study typical traffic behavior as a traffic-traveling-wave. The behavior of the traffic-traveling-wave changes once the perturbation in traffic is instigated. The anticipation term is responsible for these changes [11]. In a single vehicle class, it is straightforward, but in more than one class, the anticipation impact is complex. The traffic-traveling-wave must precisely be captured for accurate characterization of traffic flow. Theoretical studies on the behavior of traffic-traveling-wave are scarce in the context of mixed traffic.

Thus, to commence, we propose a new anticipation term, which couples the behavior of CAVs and HDVs based on the PR of CAVs and HDVs. Therefore, it is essential to introduce the share of each class in traffic. This can be done by introducing the PR of CAVs in the anticipation term. To introduce PR of CAVs, let it be represented by σ, multiplying it with

Eq. (4.10), we get

$$\varphi_* = \sigma \cdot \varphi, \tag{4.12}$$

and ζ is updated as

$$\zeta_* = (1 - \sigma) \cdot \zeta, \tag{4.13}$$

where σ is between 0 and 1.

The anticipation term Eq. (4.11) can now be revised for mixed traffic by averaging the responses of CAVs and HDVs. This can be achieved by taking the weighted average of ζ_* and φ_*, thus

$$[\zeta_* + \varphi_*](\frac{\partial v}{\partial x}). \tag{4.14}$$

The backward propagation speed of disturbances in traffic is determined by $[\zeta_* + \varphi_*]$.

To this end, the anticipation term of the second-order model is revised, and from then on, another significant model input $V(\rho(x,t))$ is discussed. The choice of velocity-density relationship can greatly affect the model output. Specifically when a pragmatic approach is followed, and when traffic data is gathered from an external source. Traffic behavior is stochastic, which means traffic is not always in equilibrium. In second-order models, this property is when the average velocity of vehicles is tuned as per the density-dependent velocity, which is equilibrium velocity and given by $V(\rho(x,t))$. Such changes are modeled through the relaxation term commonly known as the speed adaptation term. It details how vehicles adapt their speed to the steady-state speed and is characterized as

$$\frac{V(\rho(x,t)) - v(x,t)}{\Gamma}, \tag{4.15}$$

where Γ is the traffic relaxation time, and $\Gamma > 0$. The average velocity of vehicles is tuned to equilibrium velocity over Γ. It has been shown that small Γ results in stable traffic [42]. The CAVs have a smaller relaxation time so they can adjust to equilibrium conditions quickly compared to HDVs [148]. This is another vital parameter for modeling the impact of CAVs on regular traffic, however, as with other parameters, the importance of Γ is also linked to the PR of CAVs.

To provide a more comprehensive explanation of Γ, we examine a flow of vehicles comprising HDVs and CAVs. When HDVs follow other HDVs, their response to changes in traffic conditions is relatively sluggish. In contrast, CAVs play a crucial role, as research has shown that they can adapt more quickly to such changes compared to other vehicle types [149, 150]. Taking into account this observed behavior, when the proportion of CAVs in the traffic, referred to as the PR, increases, the value of Γ decreases. This decrease is attributed to the faster adaptability of CAVs to traffic conditions. It's worth noting that the specific value of Γ used in our analysis has been carefully calibrated and validated through simulations. Thus, as the PR of CAVs rises, Γ experiences a reduction in its value.

In simulations, we use Γ_p, which is a calibrated value for each traffic scenario according to the PR of CAVs. The relaxation term can be written as

$$\frac{V(\rho(x,t)) - v(x,t)}{(\Gamma_p)}, \tag{4.16}$$

where Γ_p is the relaxation time of the proposed model, and is obtained as:

$$\min_{\Gamma_p} f(\xi_{data}, \xi_{model}), \tag{4.17}$$

subject to the following constraints

$$l_{\Gamma_p} \leq \Gamma_p \leq u_{\Gamma_p} \tag{4.18}$$

where $f(\xi_{data}, \xi_{model})$ is the objective function to be minimised used, being ξ_{data} and ξ_{model} the SUMO and the proposed model traffic data.

Traffic velocity is inversely proportional to traffic density, as the most simple model to describe this relationship is the Greenshields Equilibrium Velocity Model (GEVM) [151, 152]. It describes velocity as a linear monotonic decreasing function of the density and is

$$V(\rho(x,t)) = v_f \cdot \big(1 - \frac{\rho(x,t)}{\rho_m}\big), \tag{4.19}$$

where v_f is the maximum velocity, $\rho(x,t)$ and ρ_m are the average and maximum traffic density, respectively. The Papageorgiou model for velocity-density relationship [19] is supposed to capture the variation in the slope of the velocity-density relationship as an exponential function. It is given as

$$V(\rho(x,t)) = v_f \cdot \exp\big[\frac{-1}{c}\big(\frac{\rho(x,t)}{\rho_{cr}}\big)^c\big], \tag{4.20}$$

where c is the shape factor, and ρ_{cr} corresponds to critical density. In ideal situations, the Greenshields model can be used, but in case there are large variations in driver/vehicle behavior, the Greenshields model's performance can be questioned. Thus, we investigate the Papageorgiou model that could be employed in the modeling of CAVs, details of which are given in the next section.

The second-order traffic model now can be revised for CAVs and HDVs. The anticipation term of the second-order traffic model in (2.8) presented by [52] is modified, and the new proposed model is presented as

$$\begin{aligned} &\frac{\partial \rho(x,t)}{\partial t} + \frac{\partial \rho(x,t)\cdot v(x,t)}{\partial x} = i_q(x,t) - e_q(x,t), \\ &\frac{\partial v(x,t)}{\partial t} + (v(x,t) - [\zeta_* + \varphi_*])\frac{\partial v(x,t)}{\partial x} = \frac{V(\rho(x,t)) - v(x,t)}{(\Gamma_p)}. \end{aligned} \tag{4.21}$$

According to Eq. (4.21), perturbations in traffic will be captured by $[\zeta_* + \varphi_*]$. This would induce a non-uniform class-specific behavior of traffic. While the steady state will be guaranteed by relaxation term through $V(\rho)$ over Γ_p.

4.4 On the Fundamentals of Mixed Traffic Dynamics using SUMO Simulations

In this section, a thorough analysis of mixed traffic is performed in order to understand mixed traffic dynamics. First, traffic behavior is extensively studied from several microscopic experiments performed in Simulation of Urban MObility (SUMO) [100, 101]. Recently, [1] presented a study on the impacts of CAVs on conventional traffic by considering PR and Level of Driving Automation (LoDA) [153] of CAVs introduced by the Society for Automotive Engineers (Society for Automotive Engineers (SAE)[1]). They have examined the effectiveness and safety of traffic

[1] https://www.sae.org/blog/sae-j3016-update

when CAVs are introduced to the Dublin motorway[2]. The data used in their study was gathered from historical data[3] of Irish roadways. We follow the same study design for the microscopic simulations to establish homogeneity in both studies.

In [1], Level of Driving Automation (LoDA) 2 and LoDA 4 are modeled, LoDA 2 refers to Advanced Driver Assistance Systems (ADAS) which control the vehicle, but requires driver supervision at all time while LoDA 4 refers to fully automated driving. The PRs of CAVs are 0%, 7%, 20%, 40%, and 70%, the LoDA is different for each PR as shown in Table 4.2. In microscopic simulations, the motion of vehicles is a result of the combination of longitudinal and lateral models. Concerning longitudinal behavior, vehicle acceleration relies on a car-following model that can be fine-tuned to reproduce a variability of driving styles or vehicle capabilities such as cars and heavy vehicles. Lateral behavior is computed using a lane-changing model, that usually features decisions based on the surrounding lanes' perception. The parameters of these models allow fine-tuning of the driving behaviors. While these types of models have been shown suitable for reproducing traffic behavior and flow instabilities [154].

However, the literature does not converge on using a specific model per vehicle type. HDVs use the default car-following model of SUMO which represents LoDA 0. Further, LoDA 2 is assumed for CAVs, to be connected through V2V communication, and their acceleration relies on an implementation of CACC [155]. For CAVs, LoDA 4, Intelligent Driver Model (IDM) is used as it better mimics the behavior of an automated system and is more conservative since designed to be collision-free [154]. The car following models and the parameters are given in Table 4.1.

4.4.1 The Dublin Motorway Corridor

The Dublin motorway corridor, and its characteristics are presented in this section. The motorway corridor is M50 which is a 11 km, and 4 lanes (each side) stretch in Dublin city including two major interchanges with on-ramps and off-ramps to national roads N7 and N9. In order to evaluate the macroscopic variables from the motorway corridor, it is further

[2]https://github.com/maxime-gueriau/ITSC2020CAVimpact
[3]https://data.gov.ie/dataset/traffic-volumes

Table 4.1. Models and parameters used in microscopic simulations [1].

Description	HDV	LoDA 2	LoDA 4
Car-following models	Krauss	CACC	IDM
Vehicle type	Car	Car	Car
Speed deviation (%)	0.1	0.05	0.05
Time headway (s)	1.2	0.8	0.6
Minimum gap (m)	2.5	1.5	1
Max acceleration ($\frac{m}{s^2}$)	2.5	1.5	1
Deceleration ($\frac{m}{s^2}$)	7.5	7.5	7.5
Maximum deceleration ($\frac{m}{s^2}$)	9	9	9
Imperfection	0.5	0.05	0.05
Lane changing models			
Cooperation	0.5	0.5	1
Anticipation	0.5	0.5	1

Table 4.2. Total PR of CAVs and specific PR subjected to LoDA of CAVs [1].

Scenario	HDVs (%)	CAVs (LoDA 2) (%)	CAVs (LoDA 4) (%)	CAVs (%)
A	100	0	0	0
B	93	5	2	7
C	80	15	5	20
D	60	30	10	40
E	30	50	20	70

refined and divided into 7 different segments on each side. Each segment comprises different sub-segments, some of which have on and off-ramps. The corridor with details is shown in Figure 4.1. We evaluate the corridor from segment 1 to segment 7 (one side), it has 2 off-ramps and 3 on-ramps.

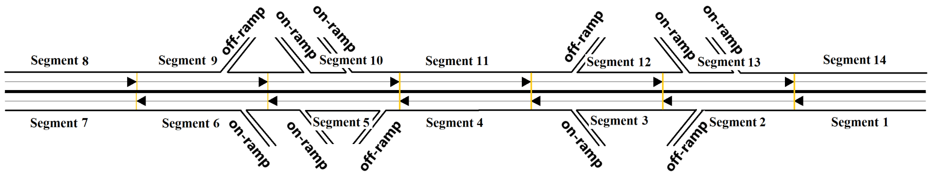

Figure 4.1. Motorway corridor representation, corridor analyzed from right to left (segment 1 to segment 7).

Table 4.3. Segments of the Dublin motorway and the segment lengths (Δx).

Description							
Segments	1 and 14	2 and 13	3 and 12	4 and 11	5 and 10	6 and 9	7 and 8
Δx (Km)	2	0.972	1	2.16	2.357	1.81	0.701

4.4.2 Analysis of the Macroscopic Traffic Variables using Microscopic Traffic Simulations

4.4.2.1 The Velocity-Density Relationship

The velocity-density relationship is the most vital input for second-order models. It is directly linked to the relaxation term, and the traffic is adjusted to steady-state speed according to this term. Thus, the choice of a velocity-density model as input for second-order models guarantees accurate model output. There are a number of models available in the literature for the velocity-density relationship. However, to the best of our knowledge, there is no specific model that directly takes into account CAVs. Thus, we employ the Papageorgiou model (see Eq. (4.20)) by calibrating it according to the traffic data from SUMO. The calibrated parameters are given in Table 4.4.

In Figure 4.2, the velocity-density relationships are given with assorted PRs of CAVs. It is demonstrated that with the increase in PR of CAVs there is a decrease in the slope between velocity-density relationship. The scatter plot represents the velocity-density relationships computed directly from SUMO, and the lines show the least-square fittings of the Papageorgiou model. The Papageorgiou model results in similar outcomes to that of SUMO with the calibrated values.

In Figure 4.3, a more detailed quantification of the improvement in velocity is demonstrated. When density is 20 veh/km/lane, the velocity is 60 km/hour with 0% CAVs. For the same density when CAVs' PR is increased to 7%, the velocity is 61 km/hour. It increases to 64 km/hour with 20% CAVs. The velocity is 70 km/hour and 72 km/hour with 40% and 70% CAVs. Similarly, there is always an increase in velocity with varying PR considering a reference value of density. This trend is almost similar for reference density of 40, 60, and 80 veh/km/lane.

For reference density 40 veh/km/lane, the velocity with 0% CAVs is 28 km/hour. It is 33 km/hour with 7% CAVs, while the velocity 38 km/hour. For 40% and 70% CAVs, it is 45 km/hour and 48 km/hour, respectively. For reference density 60 veh/km/lane, the velocity with 0% CAVs is 12 km/hour. It is 14 km/hour with 7% CAVs which increases to 16 km/hour with 20% CAVs. With 40% and 70% CAVs, the velocity is 25 km/hour and 31 km/hour, respectively. For reference density 80 veh/km/lane, the velocity with 0% CAVs is almost 0 km/hour, and it is the same for 7% CAVs. With 20% CAVs, the velocity is 4 km/hour, while it is 11 km/hour and 20 km/hour with 40% and 70% CAVs, respectively.

Whenever a change in flow occurs, the system is adjusted to the equilibrium. This change is mitigated by the relaxation term which directly considers the velocity-density relationship. A robust representation of a velocity-density relationship is responsible for the accurate output of the macroscopic models.

4.4.2.2 The Flow-Density Relationship

The relationship between flow and density is given by $q(\rho)$. Figure. 4.4 to Figure. 4.8 depicts different traffic scenarios. The scatter plots are measurements from SUMO, considered as reality. ρ and v are mea-

Table 4.4. Calibrated parameters for the Papageorgiou velocity-density model.

PR	v_f	ρ_{cr}	c	R^2
0	100	28	1.320	0.99
7	100	30	1.325	0.99
20	100	32	1.330	0.99
40	100	38	1.310	0.99
70	100	47	1.150	0.99

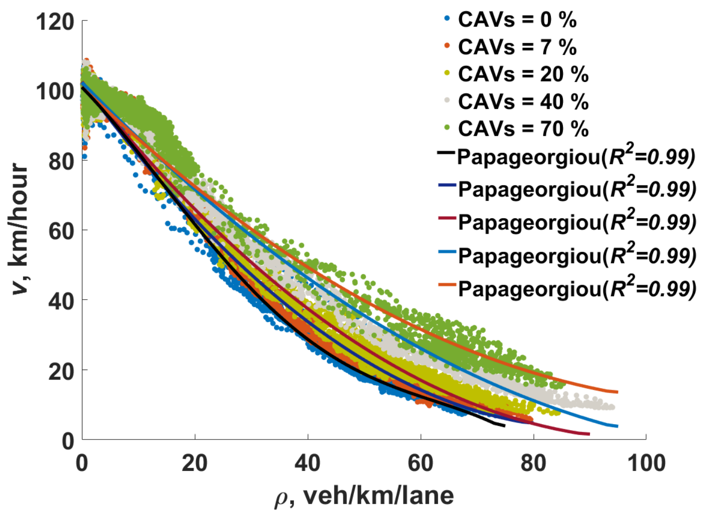

Figure 4.2. The velocity-density relationship subjected to 0%, 7%, 20%, 40% and 70% PRs of CAVs.

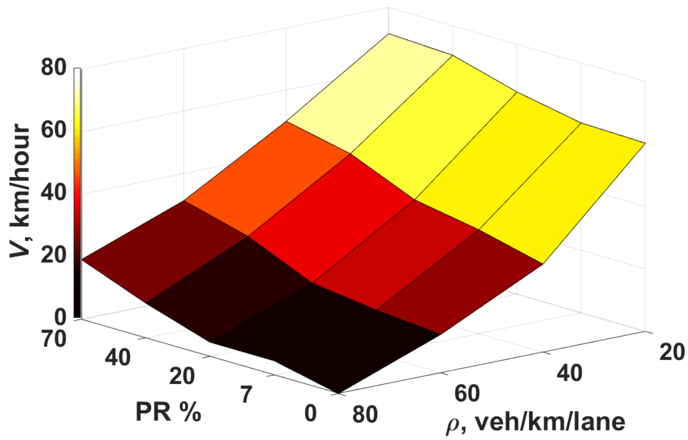

Figure 4.3. The velocity subjected to varying PR of CAVs considering a reference density.

sured directly from SUMO, and flow (q) is computed as

$$q = \rho \cdot v, \tag{4.22}$$

while the blue line is the least-square fitting of the flow-density relationship computed as

$$q(\rho) = \rho \cdot V(\rho), \tag{4.23}$$

using the Papageorgiou model (Eq. (4.20)) for $V(\rho)$. Figure 4.4 is $q(\rho)$ when the CAVs are not deployed such that CAVs are 0% and HDVs are 100%. The maximum flow (q_m) is 1308 veh/hour/lane, and the critical density (ρ_{cr}) is 28 veh/km/lane. Beyond the occurrence of ρ_{cr}, the figure represents congestion. Figure 4.5 represents $q(\rho)$ with CAVs 7%, and HDVs 93%, the changes are small. ρ_{cr} is 30 veh/km/lane, and the q_m is 1386 veh/hour/lane. Similarly, $q(\rho)$ with 20% CAVs is shown in Figure 4.6, and that for 40% and 70% CAVs is demonstrated in Figure 4.7 and Figure 4.8, respectively. With 20% CAVs, the ρ_{cr} improves which is 31 veh/km/lane, and the q_m is 1493 veh/hour/lane.

When CAVs are 40%, the ρ_{cr} is 39 veh/km/lane, and the q_m improves significantly to 1775 veh/hour/lane. With 70% CAVs, the relationship further improves. ρ_{cr} is 47 veh/km/lane, and the q_m is 1973 veh/hour/lane.

It is evident from the results that the ρ_{cr} improves greatly, and the q_m increases with the increase in PR of CAVs. The improvements are due to the enhanced intrinsic and extrinsic characteristics of CAVs such as small reaction times. Furthermore, with 0% CAVs in Figure 4.4, the capacity drop is evident, but as the PR of CAVs increases from 0% to 70%, the capacity drop vanishes. Capacity drop is caused by the delayed response over the transitions, but since the CAVs have smaller reaction times, the delay is eliminated resulting in enhanced flow over transitions.

The improvement in macroscopic variables is subjected to enhanced microscopic characteristics of the mixed traffic. The CAVs are believed to maintain smaller headways as compared with HDVs. In these experiments we clearly see when CAVs with smaller headways are penetrated in the traffic, there is an increase in the capacity which can be gauged with ρ_{cr}, v_m, q_m and the shape of the velocity-density and flow-density relationships. Next, the revised macroscopic second-order model is evaluated.

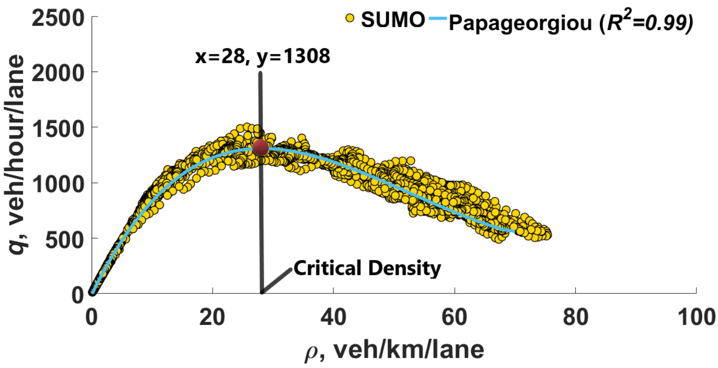

Figure 4.4. The flow-density relationship based on PR, HDVs =100% and CAVs = 0%.

4.5 Performance Evaluation of the Proposed Model

The performance of the proposed second-order is evaluated in this section. Since the proposed second-order model is a system of Hyperbolic

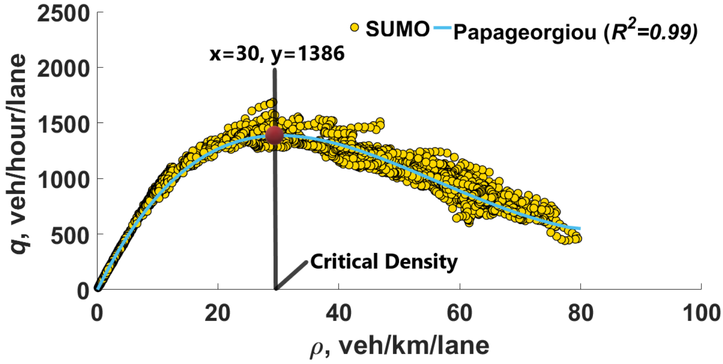

Figure 4.5. The flow-density relationship based on PR, HDVs =93% and CAVs = 7%.

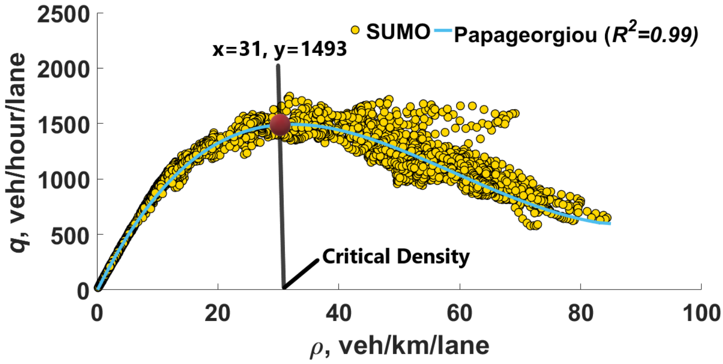

Figure 4.6. The flow-density relationship based on PR, HDVs =80% and CAVs = 20%.

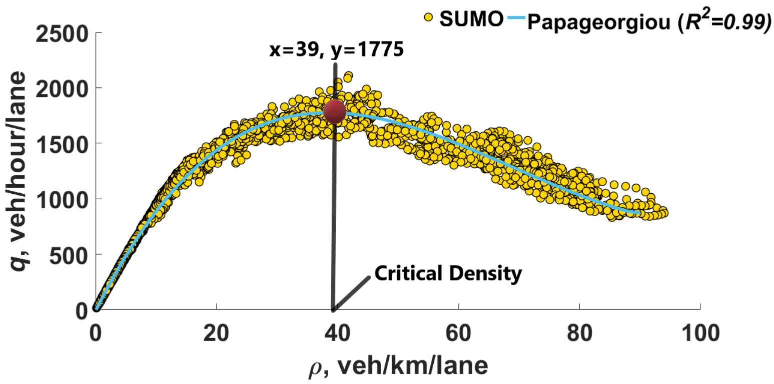

Figure 4.7. The flow-density relationship based on PR, HDVs =60% and CAVs =40%.

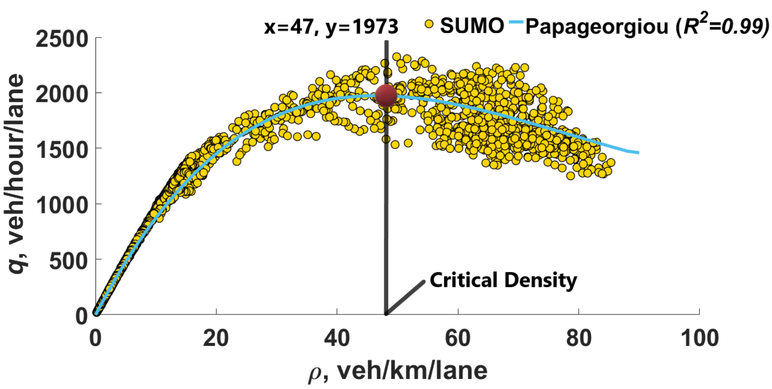

Figure 4.8. The flow-density relationship based on PR, HDVs =30% and CAVs =70%.

Partial Differential Equations (HPDEs), it is numerically solved by employing a conservative scheme proposed by [52]. The density dynamics are computed as

$$\rho_i^{n+1} = \rho_i^n + \frac{\Delta t}{\Delta x}(\rho_i^n(v_i^n - v_{i+1}^n)) + \frac{\Delta t}{\Delta x}v_i^n(\rho_{i-1}^n - \rho_i^n) + i_{q_i}^{\ n} - e_{q_i}^{\ n}, \quad (4.24)$$

where the subscripts i and n are space and time indices. The velocity dynamics is computed according to Eq. (4.21) which if $v_i^n \leq (\max(\zeta_*, \varphi_*))$ is

$$v_i^{n+1} = v_i^n + \frac{\Delta t}{\Delta x}([\zeta_* + \varphi_*] - v_i^n)(v_{i+1}^n - v_i^n) + \frac{\Delta t}{\Gamma}(V(\rho_i^n) - v_i^n), \quad (4.25)$$

and otherwise, it is

$$v_i^{n+1} = v_i^n + \frac{\Delta t}{\Delta x}([\zeta_* + \varphi_*] - v_i^n)(v_i^n - v_{i-1}^n) + \frac{\Delta t}{\Gamma}(V(\rho_i^n) - v_i^n). \quad (4.26)$$

In (4.24), (4.25) and (4.26), Δx and Δt are the road and time steps. Furthermore, this scheme is only stable if the Courant-Friedrichs-Lewy (CFL) condition [156] is satisfied, that is

$$v_m \frac{\Delta t}{\Delta x} \leq 1. \quad (4.27)$$

The proposed model is validated on data from SUMO. Δx is the length of each segment which is in accordance with SUMO. The time step Δt is 0.5 s for SUMO, and 1 s for the proposed macroscopic model. The total simulation time is 24 hours (86400 s). It is worth mentioning that as the proposed second-order model is Initial Boundary Value Problem (IBVP). Thus, the data from the $1st$ segment and the $7th$ segment are used as initial conditions for the proposed second-order model. The results are shown from the $2nd$ segment to the $6th$ segment of the Dublin motorway corridor.

Five different traffic scenarios which are differentiated by the PR of the CAVs are reproduced with the proposed second-order model. The velocity-density relationship $V(\rho)$ is calibrated for each scenario, and the Papageorgiou model [19] is used for this relationship as elaborated in the previous section. Errors arising from fixed parameters such as segment lengths are structured errors that are carefully handled. The error of the prediction model is an unstructured error that is reduced to minimal value by calibrating the parameters of the proposed and JQZ model by employing the as discussed in Section 3.5.5. The proposed and JQZ model parameters are given in Table 4.5. The prediction error is quantified based on Root Mean Square Percentage Error (RMSPE). The proposed second-order model is validated on the simulated data from SUMO. A comparative analysis of the results of the proposed, JQZ models and SUMO is presented.

Table 4.5. Simulation parameters for the traffic models.

Description	Value
Simulation time	24 hours
Length of the motorway corridor	11 km ($11,000$ m)
Maximum velocity	100 km/hour (28 m/s)
Time step, Δt for the proposed model	1 s
Simulation time step, Δt for SUMO	0.5 s
Estimation time step for SUMO	20 s
Reaction time (HDVs)	1.2 s
Reaction time (CAVs)	0.4 s
Harmonization time (HDVs)	$\tau_b = 0.5$ s
Harmonization time (CAVs)	$\tau_b = 0.5$ s
Average length of a vehicle, L	4 m
Minimum gap	1.5 m
Maximum deceleration , d_m (CAVs)	7 ms^{-2}

Table 4.6. Calibrated parameters for the proposed and JQZ models.

Parameter	Range	Unit	Scenarios				
			1	2	3	4	5
c_0	5 - 30	ms^{-1}	11.31	11.33	12.02	15.42	19.10
Γ_{jqz}	1 - 35	s	24.97	24.03	22.02	19.61	13.53
Γ_p	1 - 35	s	21.71	21.01	18.70	14.20	11.63

4.6 Validation of the Proposed Model against Simulated Data

The average density and velocity behavior of the proposed and JQZ models is evaluated and compared with SUMO for validation. The proposed model replicates the SUMO's density and velocity behavior with a smaller prediction error compared to the JQZ model. The prediction error on density and velocity is given in Table 4.7. The density and velocity behavior with CAVs = 0% is shown in Figure 4.9a and Figure 4.9b, respectively. The density behavior of the proposed model is alike SUMO, and the prediction error is as low as 1.24%. While the prediction error on velocity is 1.80%. The density and velocity behavior with CAVs = 7% is shown in Figure 4.10a and Figure 4.10b, respectively. The density and velocity dynamics are replicated accurately, while the prediction error on density and velocity is 1.22% and 1.59%, respectively.

The density and velocity behavior with CAVs = 20% is shown in Figure 4.11a and Figure 4.11b, respectively. The density prediction error is 1.23%, and that for the velocity is 1.59%. With CAVs = 40% CAVs, the density and velocity behavior are illustrated in Figure 4.12a and Figure 4.12b, respectively. The prediction error is 1.12 % on density and 1.35 % on velocity. Similarly, it is 0.91 % and 1.27 % on density and velocity, respectively with CAVs = 70% which is shown in Figure 4.13a and Figure 4.13b for density and velocity respectively.

The JQZ model [52] results are also shown in Figures 4.9-4.13, and the prediction error is tabulated in Table 4.7. As compared to the proposed model, the JQZ model has a large prediction error. As the PR of CAVs in SUMO increases the JQZ model prediction error decreases. The reason for this is “uniformity" in driving behaviors, the changes in traffic occur with a uniform value that is given by c_0 in the model. This is because of the similar characteristics of CAVs. Interestingly, the second-order JQZ model can have large prediction errors in more heterogeneous traffic conditions such as when the PR of CAVs is 0%, and the vehicles are not operating with the same driving characteristics. But while the PR of CAVs increases the average behavior becomes more uniform.

The reason JQZ model's prediction error is the uniform value of c_0. As disturbances in traffic are instigated according to c_0, this model always presumes similar behavior to any traffic condition, which can further deteriorate the model performance in more chaotic traffic conditions. The JQZ model with higher PR of CAVs can be used for the prediction of traffic states, but not for evaluative properties such as impacts of CAVs on shockwave dissipation time and distance because driving/vehicle characteristics are not considered in this model. Conversely, the proposed model closely replicated the density and velocity of SUMO. It is evident that the proposed model is well capable of reproducing the traffic dynamics. The parameters of the proposed model, and the choice of velocity-density relationship results in a plausible output of the model.

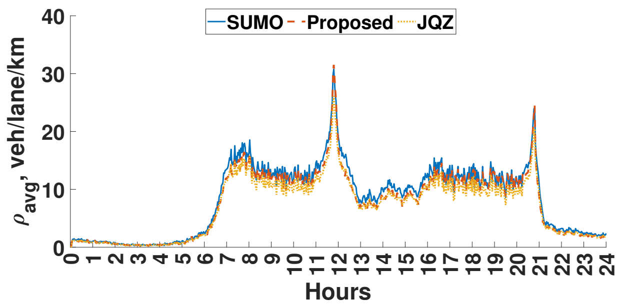

(a) The average density behavior of the proposed, JQZ model and SUMO, HDVs =100 % and CAVs = 0 %.

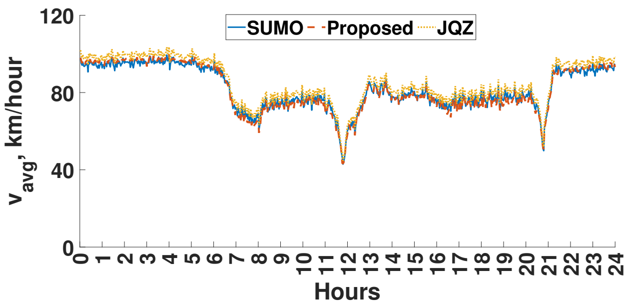

(b) The average velocity behavior of the proposed, JQZ model and SUMO, HDVs =100 % and CAVs = 0 %.

Figure 4.9. The average velocity and density behavior of the proposed, JQZ model and SUMO with HDVs =100 % and CAVs = 0 % aggregated on the whole motorway corridor.

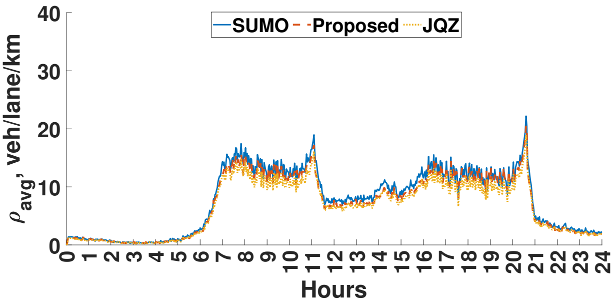

(a) The average density behavior of the proposed, JQZ model and SUMO, HDVs =93 % and CAVs = 7 %.

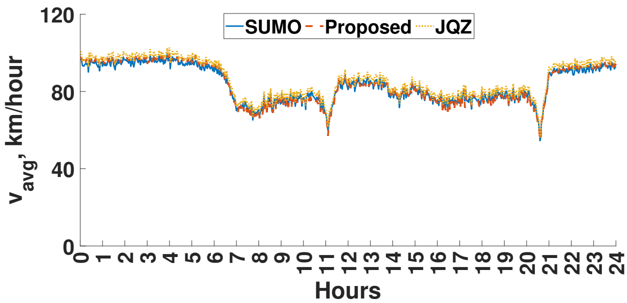

(b) The average velocity behavior of the proposed, JQZ model and SUMO, HDVs =93 % and CAVs = 7 %.

Figure 4.10. The average velocity and density behavior of the proposed, JQZ model and SUMO with HDVs =93 % and CAVs = 7 % aggregated on the whole motorway corridor.

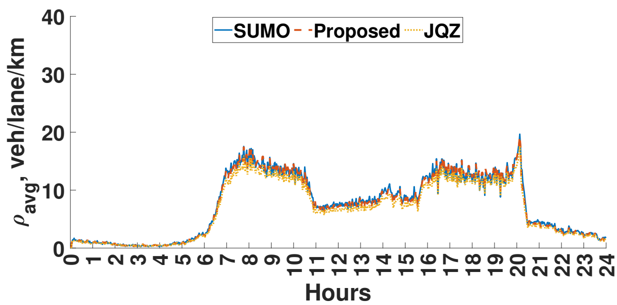

(a) The average density behavior of the proposed model, JQZ and SUMO, HDVs =80 % and CAVs = 20 %.

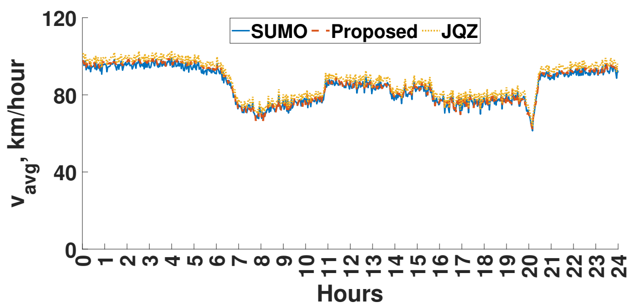

(b) The average velocity behavior of the proposed model, JQZ and SUMO, HDVs =80 % and CAVs = 20 %.

Figure 4.11. The average velocity and density behavior of the proposed, JQZ model and SUMO with HDVs =80 % and CAVs = 20 % aggregated on the whole motorway corridor.

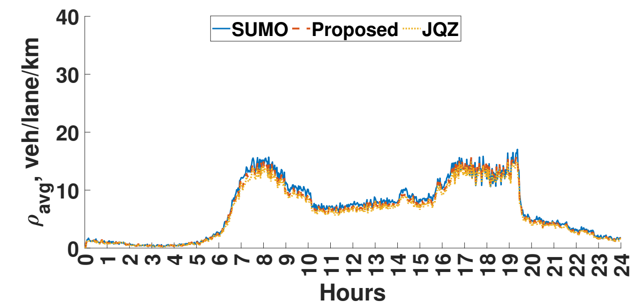

(a) The average density behavior of the proposed model, JQZ and SUMO, HDVs =60 % and CAVs = 40 %.

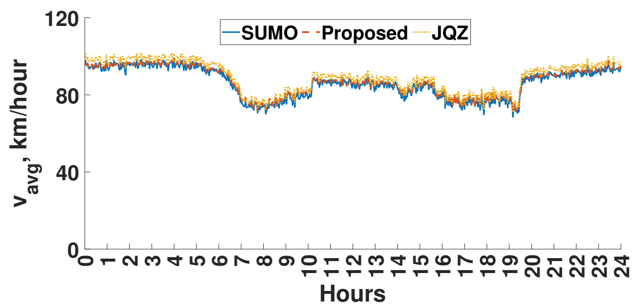

(b) The average velocity behavior of the proposed model, JQZ and SUMO, HDVs =60 % and CAVs = 40 %.

Figure 4.12. The average velocity and density behavior of the proposed, JQZ model and SUMO with HDVs =60 % and CAVs = 40 % aggregated on the whole motorway corridor.

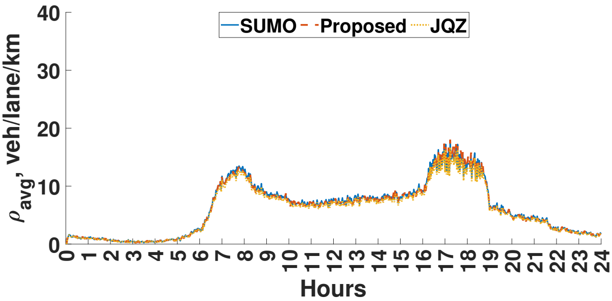

(a) The average density behavior of the proposed, JQZ model and SUMO, HDVs =30 % and CAVs = 70 %.

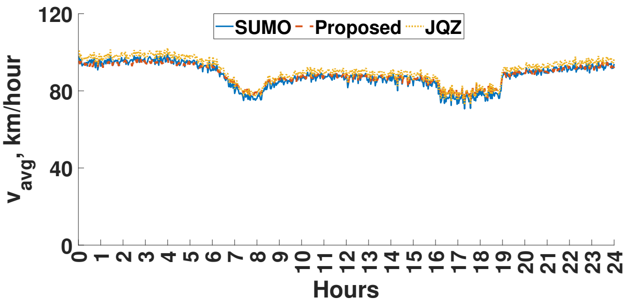

(b) The average velocity behavior of the proposed, JQZ model and SUMO, HDVs =30 % and CAVs = 70 %.

Figure 4.13. The average velocity and density behavior of the proposed, JQZ model and SUMO with HDVs =30 % and CAVs = 70 % aggregated on the whole motorway corridor.

Table 4.7. The RMSPE (%) on density and velocity of the proposed model and the JQZ model as compared with SUMO subjected to varying PR of CAVs.

	RMSPE (%) of the proposed model		RMSPE (%) of the JQZ model	
PR (%) of CAVs	Density	Velocity	Density	Velocity
0	1.24	1.80	3.11	4.92
7	1.22	1.59	3.53	5.03
20	1.23	1.60	3.76	5.21
40	1.12	1.35	3.93	5.95
70	0.91	1.27	1.90	3.12

4.7 Applications of the Proposed Model

In this section, the efficacy of the proposed model is exemplified in relation to the fundamental attributes of the Dublin motorway. The rapid computational efficiency of the proposed model enables a more efficient assessment of the LOS. Moreover, the proposed model facilitates the examination of spatio-temporal evolution of traffic variables, specifically velocity in this study. Additionally, it provides a means to analyze pertinent insights pertaining to the propagation and dissipation of a shockwave.

4.7.1 The LOS Analysis

The LOS is a quality measure of the highways introduced by the Highway Capacity Manual (HCM) [157]. LOS is a metric (defined by letters from A to F) that designates a variety of operational circumstances for a specific kind of facility. HCM defines six LOS letters, A through F, where A stands for the highest level of service and F for the lowest. These definitions are based on the facility's Measures of Effectiveness (MoE). Effectiveness is typically measured in terms of speed, travel time, density and delay. The proposed model is used in the same experimental setup to asses the LOS of the Dublin motorway. It is done to quantify the effectiveness of CAVs on the LOS of the motorway.

The LOS of the segments of the Dublin motorway is evaluated using the traffic conditions over the motorway between `22:00` and `21:00`. We only evaluate the evening peak hour. The LOS of each segment of the motorway is shown in Figure 4.14. To understand the Figure, we recall Figure 4.1. It is important to note that there are off-ramps in segments 2 and 5, while there are on-ramps in segments 3, 5, and 6. For segment 2 when the CAVs' PR is 0%, the LOS is C, and with 7% it is again C. The LOS of segment 2 improves with 20% CAVs, it is B, and further improves to A with 40% and 70%, respectively. Segment 3, when the PR of CAVs is 0% and 7%, the LOS is C. While with 20% CAVs it is B. It improves to A with 40% and 70% CAVs.

The LOS of segment 4 with 0% and 7% CAVs is D, and it is C with 20% CAVs. The LOS improves to A with 40% and 70% CAVs. The LOS is D with with 0% and 7% CAVs. The LOS of which is C with 20%, while it improves to A with 40% and 70% CAVs. Similarly, in segment 6, the LOS is B with 0% and 7% CAVs whereas it is A for 20%, 40% and 70% CAVs. Thus, from the result, it is concluded that CAVs significantly contribute to the improvement of the LOS of the motorway. The analysis of the LOS is vital for many reasons such as traffic control purposes and asset management domains. The proposed model can be employed to effectively analyze the LOS with less complex computational efforts as compared to manual procedures and microscopic simulations.

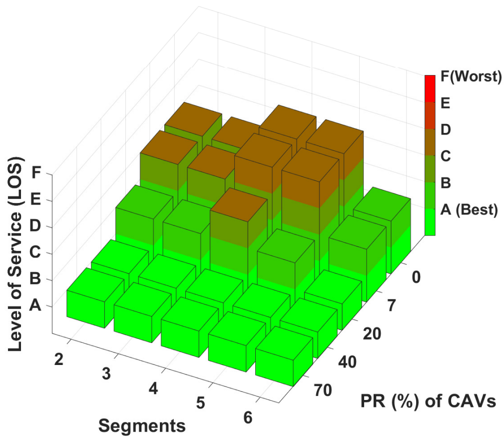

Figure 4.14. The LOS of the Dublin motorway for segment 2 to segment 6 subjected to CAVs' PR = 0%, 7%, 20%, 40% and 70%.

4.7.2 Macroscopic Spatio-Temporal Analysis of the Velocity

The velocity evolution with the proposed model over 24 hours with varying PRs of CAVs on the motorway corridor is shown in Figure 4.15. It is evident that the velocity evolution improves with the increase in the PR of CAVs. From the analysis of the motorway corridor, we observed that major velocity breakdowns occur in segments 2, 3, 4 and 5. The velocity breakdowns occur due to vehicular interactions at the off-ramp in segment 2, at the on-ramp in segment 3, and at the off-ramp in segment 4. The velocity during these breakdowns is as low as 16.91 km/hour when the

PR of CAVs is 0%. With CAVs = 0%, the velocity evolution is shown in Figure 4.15a. A very clear pattern of velocity breakdowns is observed. It is observable that the minimum velocity 16.91 km/hour between `11:00` and `13:00` in the first half of the day. In the second half of the day between `20:30` and `21:30`, again the velocity is minimum, and major breakdown occurs in segment 3 and segment 4.

The velocity evolution of mixed traffic with CAVs = 7% is shown in Figure 4.15b. The velocity breakdowns are visible, major velocity breakdowns occur in segment 2, segment 3, and segment 4, and the minimum velocity is 19.60 km/hour. A little enhancement is noticed in the frequency of velocity breakdowns. The velocity evolution of mixed traffic with CAVs = 20% is shown in Figure 4.15c. The velocity breakdowns improved significantly, major velocity breakdown occurred in segment 4, and the minimum velocity is 25.43 km/hour. The velocity evolution of mixed traffic with CAVs = 40% is shown in Figure 4.15d. The velocity breakdowns are further smoothed out. Segment 3 and segment 4 has no velocity breakdowns. The minimum velocity is recorded in segment 2, and it is 26.44 km/hour. This behavior is enhanced when the CAVs = 70%, the variations in velocity are almost smoothed out, velocity behavior is consistent as depicted in Figure 4.15e, and the minimum velocity 31 km/hour is in segment 2. With the increase in the PR of CAVs, the velocity breakdowns are smoothed out, and the overall corridor performance improves. The harmonization of vehicles is rapid due to the improved response of CAVs resulting in a smooth flow.

However, in the current experimental setup, the impacts of the parameters of the proposed model on traffic flow cannot be explicitly determined. There is no impedance on the off-ramps and on-ramps due to which the traffic perturbation once generated dissipates abruptly with a change in the vehicles' characteristics. In other words, the shockwaves are not sustained for longer times due to which their formation and dissipation times cannot be analyzed. Moreover, the JQZ model cannot be employed to investigate the impacts of the microscopic characteristics on the evolution of traffic explicitly. Thus, we showcase the capability of the proposed model to investigate the impacts of the microscopic such as the reaction time of the CAVs on the evolution of traffic. This being the case, we employ circular boundary conditions. In this case, the perturbation in traffic is sustained, and the CAV characteristics defined by the proposed model parameters can be explicitly investigated. For this purpose, the results of this study are further extended on a circular road in section 4.7.3.

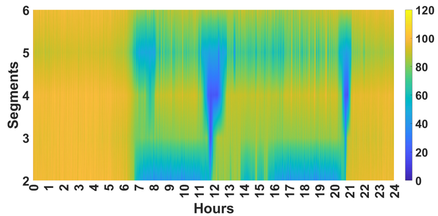

(a) Velocity evolution on the motorway corridor, HDVs =100% and CAVs = 0%.

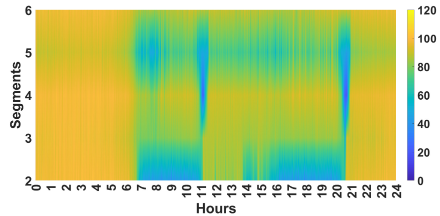

(b) Velocity evolution on the motorway corridor, HDVs =93% and CAVs = 7%.

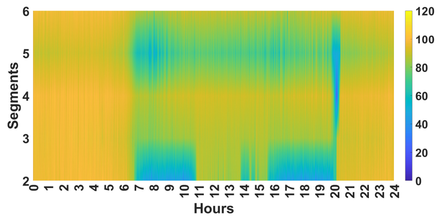

(c) Velocity evolution on the motorway corridor, HDVs =80% and CAVs = 20%.

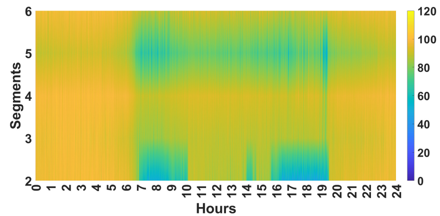

(d) Velocity evolution on the motorway corridor, HDVs =60% and CAVs = 40%.

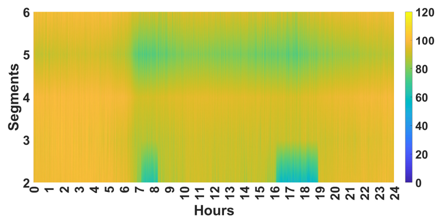

(e) Velocity evolution on the motorway corridor, HDVs =30% and CAVs =70%.

Figure 4.15. Velocity evolution on the motorway corridor with assorted PRs of CAVs.

4.7.3 Spatio-Temporal Analysis of a Shockwave in the presence of CAVs

The proposed model is based on dynamic headway with characteristics of CAVs defined by traffic physics. Previously, the proposed model was validated by generating ground truth in SUMO, and the prediction accuracy of the proposed model was evaluated. But, for the impacts of the parameters of the proposed model, a perturbed traffic condition with an inactive bottleneck is needed. The proposed model's parameters can be analyzed accurately if there is a continuous flow with no off-ramps and on-ramps. The perturbation in traffic will travel along the traffic, and the impact of the parameters on the traffic can be better evaluated. For this reason, we have designed a 20 km long circular road with periodic boundary conditions;

$$\rho(L,t) = \rho(0,t),\ v(L,t) = v(0,t). \tag{4.28}$$

The simulations are performed for 1800 s (30 minutes). The CAVs' PR is set to a reference 40%, and only τ_r is varied. Five different τ_r are considered that are 0.5 s, 1.0 s, 1.5 s, 2.0 s and 2.5 s. A shockwave resulting from an inactive bottleneck is analyzed subject to these τ_r. The shockwave distance and time of occurrence are compared. The shockwave subjected to different τ_r with CAVs= 40% is shown in Figure. 4.16 to Figure. 4.20. The shockwave distance and time for different τ_r are given in Table 4.8. We have considered τ_r for the evaluation due to its sensitivity on the model output with respect to other parameters of the proposed model as we analyzed from our experiments.

The shockwave dynamics with $\tau_r = 0.5$ s is shown in Figure 4.16, and the propagation distance and time are given in Table 4.8. The tail of the bottleneck is at $14,400$ m, the shockwave propagates from this point to $12,400$ m. The propagation distance of the shockwave is 2000 m, and it takes 158 s for it to start dissipating. The shockwave dynamics with $\tau_r = 1.0$ s is shown in Figure 4.17. The tail of the bottleneck is at $1,4400$ m, and the shockwave resulting from this bottleneck is propagated backward till $12,200$ m. The shockwave propagation distance is 2200 m, and it takes 226 s to start dissipating. The difference between the propagation time with $\tau_r = 0.5$ s is 68 s.

The shockwave dynamics with $\tau_r = 1.5$ s is shown in Figure 4.18. The

Table 4.8. The shockwave distance and time subjected to τ_r = 0.5 s, 1.0 s, 1.5 s, 2.0 s and 2.5 s with PR of CAVs = 40%.

τ_r (s)	Propagation distance (m)	Propagation time (s)
0.5	2000	158
1.0	2200	226
1.5	2310	251
2.0	2400	268
2.5	2800	319

tail of the bottleneck is at $14,400$ m, and the shockwave propagates backward till $12,090$ m. The shockwave propagation distance is 2310 m, and it takes 251 s to start dissipating. With $\tau_r = 2.0$ s, the shockwave dynamics are illustrated in Figure 4.19. The tail of the bottleneck is at $14,400$ m, and the shockwave propagates backward till $12,000$ m. The shockwave propagation distance is 2400 m, and it takes 268 s to start dissipating. Similarly, the shockwave dynamics with $\tau_r = 2.5$ s is shown in Figure 4.20. The tail of the bottleneck is at $14,400$ m, and the shockwave propagates backward till $11,600$ m. The shockwave propagation distance is 2800 m, and it takes 319 s to start dissipating. The insights from these simulations are plausible for many reasons. The impact of τ_r is explicitly analyzed. It is evident from the results that τ_r of CAVs can significantly improve the traffic flow operations when CAVs are 40%. Results could be different for various PRs of CAVs. The proposed model could be employed in traffic control applications in the presence of CAVs to develop new control strategies.

4.8 Conclusion

A new macroscopic Second-Order Traffic Flow Model (SOTFM) incorporating the characteristics of Connected and Autonomous Vehicles (CAVs) was proposed. It is based on class-specific reaction velocity considering dynamic headway distance. The proposed model has been investigated and validated with a high-fidelity traffic simulator (SUMO). It is evident from the results that the proposed model can replicate differ-

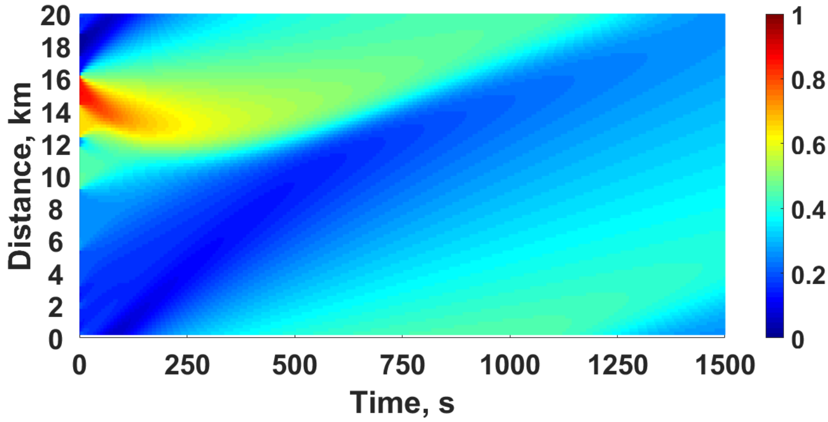

Figure 4.16. Shockwave formation and dissipation with $\tau_r = 0.5$ s in presence of CAVs = 40%.

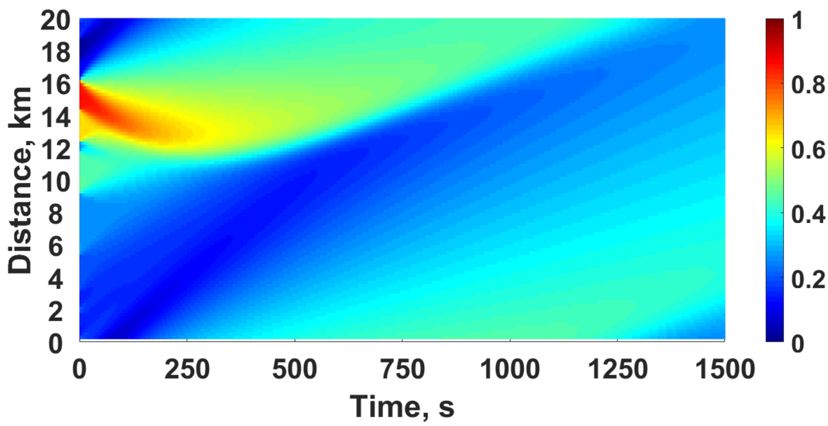

Figure 4.17. Shockwave formation and dissipation with $\tau_r = 1.0$ s in presence of CAVs = 40%.

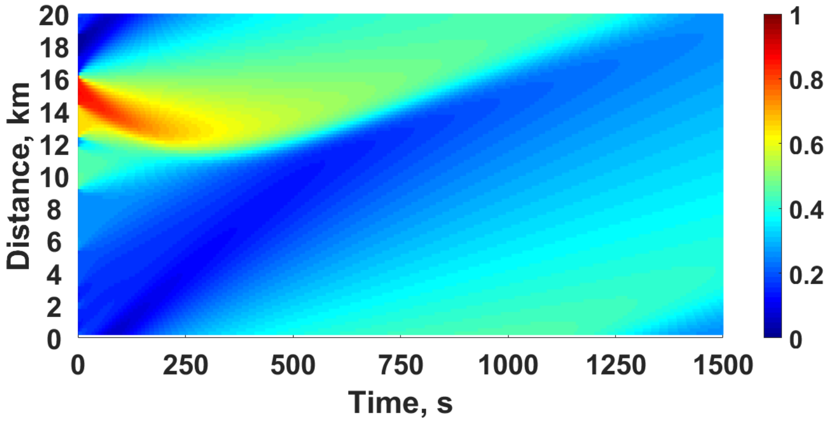

Figure 4.18. Shockwave formation and dissipation with $\tau_r = 1.5$ s in presence of CAVs = 40%.

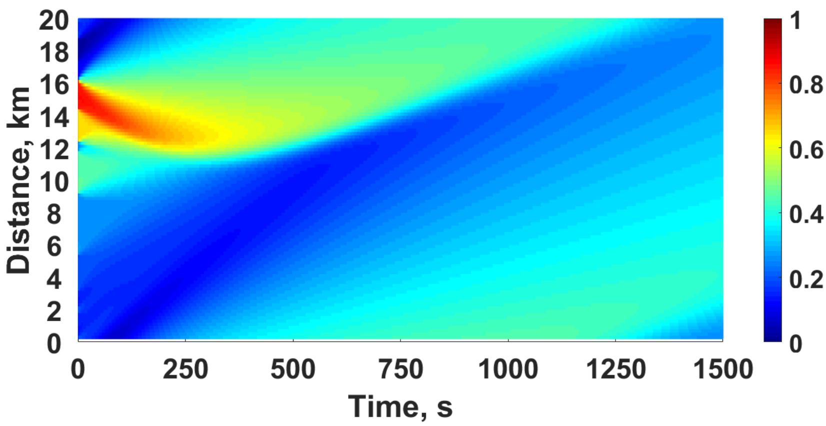

Figure 4.19. Shockwave formation and dissipation with $\tau_r = 2.0$ s in presence of CAVs = 40%.

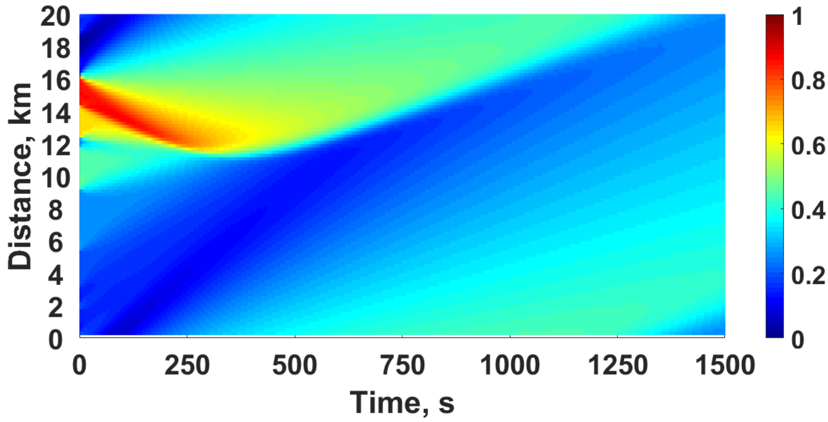

Figure 4.20. Shockwave formation and dissipation with $\tau_r = 2.5$ s in presence of CAVs = 40%.

ent traffic conditions subjected to assorted Penetration Rates (PRs) of CAVs. Macroscopic analysis of corridor velocity was carried out. It is concluded that the average velocity of the motorway corridor improves by 20 km/hour with the increase in PR of CAVs from 0% to 70%. Furthermore, CAVs maintain small headway, thus with the increase in the PR of CAVs, the capacity of the road increases which helps in the mitigation of congestion.

CAVs also have a smaller reaction and harmonization times due to which changes in traffic occur faster compared to Human-Driven Vehicles (HDVs). The investigations showed that the Level of Service (LOS) of the Dublin motorway enhances with the increase in PR of CAVs. It is evident from the results that CAVs can improve LOS D to LOS A. Furthermore, shockwave analyses were performed in order to check the effectiveness of the parameters of the proposed model. Particularly, the impact of the reaction time of CAVs ($\tau_{r(CAVs)}$) on a shockwave dissipation time has been evaluated. It is observable that CAVs with smaller $\tau_{r(CAVs)}$ can reduce the shockwave occurrence time and distance.

In all, the proposed model provides a more realistic characterization of mixed traffic. All the model parameters are traffic physics-based which reduces the calibration efforts. Thus, the proposed model can be employed for the characterization of mixed traffic, and control of traffic flow. The more, it can also be extended to investigate exhaust emissions resulting from a traffic flow.

Further application of the proposed model includes its use in traffic control as a prediction model. With the proposed model, traffic dynamics can be studied based on microscopic characteristics such as reaction time and headway distance. Thus, allowing to replace conventional traffic control such as Variable Speed Limit (VSL) with other control variables such as reaction time, harmonization time and deceleration of CAVs. Additionally, one vital aspect of the proposed model is that it is based on a fundamental diagram calibrated with data, for real-time applications, the model can be revised to consider the modeling of the parameters of the fundamental diagram. More, various vehicle classes can be incorporated, ranging from conventional vehicles (HDVs) to different automation levels of CAVs. Additionally, the second-order models can be revised to consider the influence of Cooperative Intelligent Transportation Systems (C-ITS) technologies, which enable communication between vehicles and infrastructure, leading to cooperative behaviors and enhanced traffic management. This comprehensive approach would account for the diverse elements present in modern traffic scenarios, allowing for a more accurate representation of traffic flow dynamics in complex mixed traffic environments.

4.9 Preview of the Next Chapter

This section has pragmatically examined mixed traffic using microscopic simulation data as a basis for our Second-Order Traffic Flow Model (SOTFM). We successfully fine-tuned the speed-density relationship through this data, revealing an interactive relationship between microscopic and macroscopic simulations. Although our proposed model has demonstrated its capabilities, there is more work to be done.

To enhance our comprehension and practical applications, further research is essential. We need to expand the model to accommodate additional vehicle types and investigate exhaust emissions and fuel consumption details within this framework. As traffic mixtures introduce more complexity, we require robust strategies, especially for the speed-density relationship, to precisely capture these dynamics.

Considering this perspective, the subsequent section introduces an integrated macroscopic model that combines traffic and emission models. This integration is crucial for conducting vital investigations, such as simultaneous predictions of traffic flow and emissions. By effectively incorporating the intricacies of traffic mixtures into the Fundamental Diagram (FD), our proposed integrated macroscopic model becomes a powerful tool for efficient traffic flow planning and management.

Chapter 5

Characterization of Traffic Flow and Emissions Driven on the Fundamental Diagram of Traffic Mixture

5.1 Abstract

The advent of Connected and Autonomous Vehicles (CAVs) and Connected Heavy Vehicles (CHVs) has transformed traffic studies. CAVs and CHVs will have to coexist in traffic alongside Human-Driven Vehicles (HDVs) and Heavy Vehicles (HVs) on the freeways forming a complex traffic mixture. This coexistence necessitates the understanding of the dynamics of traffic mixture to improve the operations of freeways. To commence, the Fundamental Diagram (FD) is vital to understand, it is viewed as the basis of traffic flow theory in view of traffic mixture is not well studied. We delve deeper into the insights of the FD of traffic mixture and derive the FD of traffic mixture driven on class-specific varying headway distances of the vehicles. Subsequently, we propose a continuum second-order traffic flow model, aiming to effectively capture and analyze the traffic dynamics arising from the traffic mixture. Furthermore, the proposed model integrates the macroscopic emissions and fuel consumption model to quantify the exhaust emissions and fuel consumption resulting

from the traffic mixture.

Two traffic mixtures are considered

- a mixture of CAVs and HDVs, and
- a mixture of CAVs, HDVs and HVs

Results manifest that the average velocity on the freeway corridor momentously improves with an increasing PR of CAVs in a traffic mixture. The average velocity of traffic mixture (HDVs-CAVs) improves by 67.65% with increasing PR of CAVs from 0% to 100%, and it improves by 63.63% when there are only 5% HVs in the traffic mixture (HDVs-CAVs-HVs). CAVs can limit traffic oscillations, consequently, improving the spatio-temporal velocity and density evolution. As a result, fuel consumption and exhaust emissions are minimized which are computed using the proposed model in conjunction with an emission model, and are verified through numerical simulations.

5.2 Introduction

Traffic congestion on freeways leads to high exhaust emissions and fuel consumption resulting in increased socio-economic costs, as well as environmental issues [121, 158, 159]. Connected and Autonomous Vehicles (CAVs) have the potential to reduce traffic congestion by enabling a smoother flow of traffic through robust communication with traffic. Consequently, exhaust emissions and fuel consumption could be reduced. CAVs could also use algorithms to optimize vehicle speeds and routes which will help prevent unnecessary stops due to heavy traffic conditions. It is expected that by 2040–2050, the Penetration Rate (PR) of CAVs will surge [122]. However, due to many policy and technical obstacles, CAVs will have a marginal PR in the next few years [123]. Typically, there will be a transition period over which Human-Driven Vehicles (HDVs), CAVs, and Heavy Vehicles (HVs) will operate simultaneously forming a traffic mixture.

This traffic mixture may show some complex traffic flow characteristics [124, 125]. Thus, it is significant to understand the dynamics of traffic mixture in order to maintain smoother flow operations. There is a dire need for research on this type of mixed traffic flow [127]. At all scales (microscopic, mesoscopic, and macroscopic), appropriate models and modeling methodologies are required in order to accurately depict the changing dynamics and capacities of mixed traffic flow as they will alter significantly [128].

To date, various benefits of CAVs have been identified that are

1. CAVs will be able to detect obstacles on a road. This will greatly reduce the number of car accidents and fatalities on the roads, thus enhancing traffic safety.

2. CAVs can help manage traffic congestion by driving at precise speeds and maintaining appropriate distances between vehicles. CAVs are able to run with significantly less spacing or headway. Due to the smaller reaction times of CAVs in traffic mixture, the interactions among vehicles at off-ramps and on-ramps occur quickly, resulting in smoother flow operations. As a result, it is anticipated that the traffic capacity of highways with CAVs would grow [130, 131, 132], and the Level of Service (LOS) of highways will improve. They could also optimize routes for faster travel times with fewer delays due to traffic jams or construction projects on highways resulting in increased efficiency.

3. Unlike HDVs, CAVs are more fuel efficient because they won't waste energy in sudden starts, stops, or unnecessary acceleration/deceleration. This would result in less environmental pollution from vehicle emissions over time if these technologies were widely adopted globally ensuring decreased pollution.

Modeling traffic flow in view of HDVs, CAVs, CHVs and HVs is important to accurately simulate and interpret how CAVs will interact with the environment. With an increase in the number of CAVs on the freeways, it is essential to understand how they will communicate with other drivers/vehicles, obey road rules, react to signs/barriers, and adjust speed when merging onto a highway or changing lanes. Apt modeling helps us create realistic simulations which can be used to identify potential hazards posed by these new technologies, and help traffic engineers determine appropriate measures for managing infrastructure efficiently. Additionally, such models can help identify areas that might require improvements in terms of infrastructure upgrades or Intelligent Transportation Systems (ITS).

Macroscopic models can be effectively used to evaluate flow of traffic mixture. Macroscopic approach is employed due to its capability of reliable traffic flow modeling, and moderate computational complexity [53, 133, 134]. One widely known group of macroscopic models is the second-order traffic flow models. However, they are not explicitly revised for the characteristics of traffic mixture (HDVs-CAVs-CHVs-HVs). In this perspective, the conventional continuum second-order macroscopic traffic model [52] is revised in order to incorporate the characteristics of traffic mixture. The revised continuum second-order model is based on the class-specific varying headway distances of HDVs, CAVs, and HVs, and explicitly uses a PR-based Fundamental Diagram (FD) of the traffic mixture.

The main contributions of this chapter can be summarized as follows:

1. A new second-order continuum traffic model is proposed by taking into account the varying headway distances of the HDVs, CAVs, CHVs, and HVs. The parameters of the FD explicitly consider the PR of HDVs, CAVs, and HVs, resulting in non-uniform shape of the FD.

2. Fuel consumption and exhaust emissions are investigated for traffic mixture by integrating a macroscopic emissions model with the proposed model.

3. The performance of the proposed model is evaluated on a 20 km circular highway. Far-reaching analysis of the characteristics of traffic mixture are presented.

5.3 Modeling of the Dynamics of Traffic Mixture

5.3.1 Modeling of the Class-Specific Headway Distance

The headway distance is the space needed between two vehicles in order to achieve a safe and comfortable driving experience. Traffic flow dynamics alter significantly with headway distance (H), headway time (τ_d), reaction time (τ_r) which consequently impact the highway capacity. Accurate characterization of traffic flow based on these parameters is vital for plausible descriptions and understanding of the evolution of traffic flow.

Moreover, the characteristics of HDVs, CAVs, and HVs could be differentiated based on headway distance, τ_d, and τ_r. We exploit the typical headway distance assuming the characteristics of traffic mixture to characterize traffic flow.

The distance from the front bumper of a leading vehicle to that of the following vehicle is defined as headway distance [139] as shown in Figure 5.1. Typically, this distance comprises of length of a vehicle (L), the clearance gap (C) between the vehicles at standstill, and the traffic transitions gap (G_{tt}) which is taken into consideration whenever there is a change in the traffic state. The G_{tt} between the vehicles is a dynamic gap, and is a vehicle or driver's intrinsic property [140]. It is different for non-identical traffic conditions subjected to different classes of the vehicles such as HDVs, CAVs, CHVs and HVs in traffic mixture. It significantly depends upon the class-specific reaction time and velocity [141].

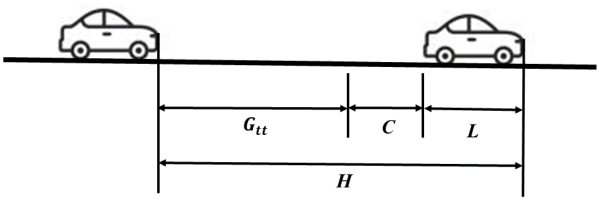

Figure 5.1. Headway distance representation considering the length of a vehicle (L), clearance gap (C), and the gap during traffic transitions (G_{tt}).

Thus, the headway distance is

$$H = G_{tt} + C + L. \tag{5.1}$$

The τ_r is the amount of time it takes for a driver to recognize and respond to a situation on the road. The greater the H between two vehicles, the more time a driver has to react. Therefore, as H increases, τ_r should also increase. Consequently, adjustments in H are characterized by τ_r, which is different for various classes of vehicles in non-identical traffic conditions [142], thus, the G_{tt} can be modeled differently. In non-identical traffic conditions, a vehicle or driver's response to changes ahead is not unique, and the G_{tt} is computed as

$$G_{tt} = v \cdot \tau_r, \tag{5.2}$$

where v is the class-specific average velocity. The H is often considered a constant which is, however, not correct. Headway distance in Eq. (5.1) will result in a non-identical value depending on the traffic state.

Investigations of the impacts of vehicle classes on the average traffic flow have always been a concern of researchers. With the emergence of CAVs, the intrinsic vehicle properties have improved, and they have been investigated in a number of studies [146, 147]. From a motion viewpoint, with improved intrinsic vehicle characteristics, the three-vehicle classes, CAVs, HVs. CHVs and HDVs will maintain a non-identical headway in mixed traffic conditions. Considering the characteristics of traffic mixture, the class of each vehicle will have a unique headway distance that is because of the difference in the τ_r of the vehicles. For HDVs, it is represented by H_h, and is

$$H_h = G_{tth} + C_h + L_h, \tag{5.3}$$

that for CAVs is represented by H_c, and is

$$H_c = G_{ttc} + C_c + L_c, \tag{5.4}$$

and for HVs is represented by H_t, and is

$$H_t = G_{ttt} + C_t + L_t. \tag{5.5}$$

For HVs, the headway distance can vary depending on the size and weight of each vehicle, as well as the speed at which they are traveling. Generally, it is recommended that there should be around four seconds of time gap between two HVs moving at normal speeds. For CAVs, the recommended headway distance may be much smaller than for traditional HDVs and HVs due to their superior sensing capabilities. The CAVs with advanced technology such as lane-keeping assistance systems can calculate more accurately how far away from other objects they need to remain in order to ensure a safe journey for all involved. This means that CAVs usually require less room between them compared with HDVs and HVs, when both are traveling along a road at similar speeds. Finally, for HVs (usually heavy commercial trucks or other large freight carriers), a larger headway distance is required due to their sheer size and weight combined with low acceleration capability. HVs often require greater distances between them in order to maintain an acceptable level of safety on public roads. From Eqs. (5.3), (5.4), and (5.5), it is clear that the class-specific headway will be non-identical. The G_{tt} for each class will be computed from the average speed and the τ_r of the HDVs, CAVs, and HVs. While the C is always different when HDV is followed by a CAV and HV, and vice versa, whereas the L is the same for CAVs and HDVs, and different for HVs.

5.3.2 Modeling of the Parameters of the Fundamental Diagram

The fundamental traffic flow variables are velocity (v), density (ρ) and flow (q). These three variables are related to each other, they all affect the capacity and Level-of-Service (LOS) for roadway segments and highways. Higher q is associated with higher v, while a small ρ can result in large headway distance. Higher v results in small headway distance and so forth. Ultimately, these factors must be considered together when exploring traffic behavior of traffic mixture. The relationship between these variables is

$$q(x,t) = \rho(x,t) \cdot v(x,t). \tag{5.6}$$

The $\rho(x,t)$ can be presumed as the reciprocal of H, when the $\rho(x,t)$ is large the H is small, and vice versa, it is computed as

$$\rho(x,t) = \frac{1}{H}. \tag{5.7}$$

Assorted classes of vehicle have different characteristics such as the clearance gap between HDV and HDV is larger than that of a CAV and CAV. Similarly, the clearance gap and average length of HVs are larger than both, CAVs and HDVs, thus the headway dynamics will be different for them. The class-specific $\rho(x,t)$ can then be computed by substituting Eqs. (5.3), (5.4), and (5.5) in Eq. (5.7),

$$\rho(x,t) = \begin{cases} \frac{1}{H_h}, & \text{HDVs} \\ \frac{1}{H_c}, & \text{CAVs} \\ \frac{1}{H_t}. & \text{HVs} \end{cases} \tag{5.8}$$

Substituting Eq. (5.7) in Eq. (5.6), it gives

$$q(x,t) = \frac{v(x,t)}{H}. \tag{5.9}$$

thus considering the class-specific characteristics, the q can be computed as

$$q(x,t) = \begin{cases} \frac{v(x,t)}{H_h}, & \text{HDVs} \\ \frac{v(x,t)}{H_c}, & \text{CAVs} \\ \frac{v(x,t)}{H_t}. & \text{HVs} \end{cases} \tag{5.10}$$

Eqs. (5.8) and (5.10) are true when a single class of vehicles is considered. For a traffic mixture, these relationships can be exploited by introducing the PR of each class. The PR of three classes of vehicles is represented as

$$\begin{cases} PR_{HDVs} = \alpha, \\ PR_{CAVs} = \beta, \\ PR_{HVs} = \eta. \end{cases} \tag{5.11}$$

Eq. (5.8) can then be exploited to take into account the class-specific PRs as

$$\rho(x,t) = \begin{cases} \frac{1}{(\alpha \times H_h)+(\beta \times H_c)}, & \text{CAVs and HDVs} \\ \frac{1}{(\alpha \times H_h)+(\beta \times H_c)+(\eta \times H_t)}. & \text{CAVs, HDVs and HVs} \end{cases} \tag{5.12}$$

Eq. (5.12) yields average density subjected to the average velocity and class-specific reaction times. If we consider free-flow traffic conditions, critical density (ρ_{cr}) can be computed by considering the free-flow velocity (v_f) instead of v. Substituting Eq. (5.1), Eq. (5.7) gives

$$\rho(x,t) = \frac{1}{G_{tt} + C + L}. \tag{5.13}$$

If class-specific characteristics are considered the ρ_{cr} can be computed as

$$\rho_{cr} = \begin{cases} \frac{1}{G_{tth}+C_h+L_h}, & \text{HDVs} \\ \frac{1}{G_{ttc}+C_c+L_c}, & \text{CAVs} \\ \frac{1}{G_{ttt}+C_t+L_t}, & \text{HVs} \end{cases} \tag{5.14}$$

where $G_{tt} = v_f \cdot \tau_r$, and τ_r is different for all the three vehicle classes. The ρ_{cr} of the mixed traffic can be as

$$\rho_{cr} = \begin{cases} \frac{1}{(\alpha\times(G_{tth}+C_h+L_h))+(\beta\times(G_{ttc}+C_c+L_c))}, & \text{CAVs and HDVs} \\ \frac{1}{(\alpha\times(G_{tth}+C_h+L_h))+(\beta\times(G_{ttc}+C_c+L_c))+(\eta\times(G_{ttt}+C_t+L_t))}. & \text{CAVs, HDVs and HVs} \end{cases} \tag{5.15}$$

Eq. (5.15) can be further exploited to determine the maximum flow (q_m) of mixed traffic as

$$q_m = \begin{cases} \frac{v_f}{(\alpha\times(G_{tth}+C_h+L_h))+(\beta\times(G_{ttc}+C_c+L_c))}, & \text{CAVs and HDVs} \\ \frac{v_f}{(\alpha\times(G_{tth}+C_h+L_h))+(\beta\times(G_{ttc}+C_c+L_c))+(\eta\times(G_{ttt}+C_t+L_t))}. & \text{CAVs, HDVs and HVs} \end{cases} \tag{5.16}$$

The maximum density (ρ_m) can be computed by setting $v = 0$ (jam traffic conditions) in Eq. (5.14), thus

$$\rho_m = \begin{cases} \frac{1}{C_h+L_h}, & \text{HDVs} \\ \frac{1}{C_c+L_c}, & \text{CAVs} \\ \frac{1}{C_t+L_t}, & \text{HVs} \end{cases} \tag{5.17}$$

ρ_m of mixed traffic can then be computed as

$$\rho_m = \begin{cases} \frac{1}{(\alpha\times(C_h+L_h))+(\beta\times(C_c+L_c))}, & \text{CAVs and HDVs} \\ \frac{1}{(\alpha\times(C_h+L_h))+(\beta\times(C_c+L_c))+(\eta\times(C_t+L_t))}. & \text{CAVs, HDVs and HVs} \end{cases} \tag{5.18}$$

Due to the assorted characteristics of all types of vehicles, the ρ_{cr}, ρ_m, and q_m will always vary subject to class-specific PRs. These parameters can be directly employed to estimate the FD of traffic. From a real-time forecasting standpoint, the continuum perspective of modeling is vital since the FD directly employs the values of ρ_{cr} and ρ_m. In continuum second-order traffic flow models, the velocity-density relation is most sensitive to model output. Thus, taking into account the class-specific PR and headway distances would allow us to capture the behavior of the traffic mixture more realistically.

5.3.3 Analysis of the Mixture Fundamental Diagram

The FD is evaluated based on the derivations in Section 5.3.2. The ρ_{cr} is computed using Eq. (5.15), ρ_m and q_m are computed using Eqs. (5.18), and (5.16), respectively. The class-specific parameters are given in Table 5.3. First, a traffic mixture of HDVs and CAVs is considered to evaluate the behavior of the FD in the presence of CAVs with assorted PRs. The mixture FD of HDVs and CAVs is shown in Figure 5.2, and the analysis is further elaborated in Table 5.1. When $\alpha = 1$ (100% HDVs), the ρ_{cr} is 17 veh/km whereas the ρ_m and q_m are 133 veh/km and 1756 veh/hour, respectively. We consider this as the base case scenario, and henceforth we introduce the PR of CAVs (β) to understand the FD of traffic mixture.

With $\beta = 0.2$ (20%) CAVs, the ρ_{cr} and ρ_m are 19 veh/km and 138 veh/km, respectively while the q_m is 2022 veh/hour. The ρ_{cr} and ρ_m are 22 veh/km and 144 veh/km, respectively with $\beta = 0.4$ (40% CAVs), and the q_m is increased to 2384 veh/hour. With $\beta = 0.6$ (60% CAVs), the ρ_{cr} is 27 veh/km, and the ρ_m is 151 veh/km, while the q_m is 2903 veh/hour. When $\beta = 0.8$ (80% CAVs), the ρ_{cr} is 34 veh/km, and ρ_m is 158 veh/km. The q_m is 3711 veh/hour. With $\beta = 1$ (100%) CAVs, the ρ_{cr} and ρ_m are 48 veh/km and 166 veh/km, respectively while the q_m is 5143 veh/hour.

The mixture FD of HDVs, CAVs and HVs is shown in Figure 5.3, and the analysis is further elaborated in Table 5.2. Now, the mixture comprises of three classes of vehicles. The PR of HVs, $\eta = 0.05$ (5% of the total traffic) which is uniform throughout the analysis. When $\alpha = 0.95$, $\beta = 0$, and $\eta = 0.05$, the ρ_{cr} is 15 veh/km, ρ_m is 122 veh/km, and q_m is 1669 veh/hour. When $\alpha = 0.75$, $\beta = 0.2$, and $\eta = 0.05$, the ρ_{cr} and ρ_m is 17 veh/km and 127 veh/km, respectively, while the q_m is 1907 veh/hour. The ρ_{cr} is 20 veh/km, ρ_m is 132 veh/km, and q_m is 2226 veh/hour with $\alpha = 0.55$, $\beta = 0.4$, and $\eta = 0.05$.

When $\alpha = 0.35$, $\beta = 0.6$, and $\eta = 0.05$, the ρ_{cr} is 24 veh/km, ρ_m is 138 veh/km, and q_m is 2672 veh/hour. When $\alpha = 0.15$, $\beta = 0.8$, and $\eta = 0.05$, the ρ_{cr} and ρ_m is 31 veh/km and 143 veh/km, respectively, while the q_m is 3341 veh/hour. The ρ_{cr} is observed to be 38 veh/km, ρ_m is 148 veh/km,

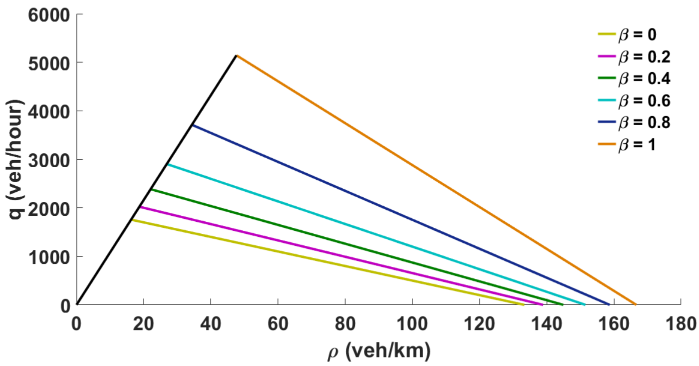

Figure 5.2. Fundamental diagram with assorted PR of CAVs (β) and HDVs (α).

and q_m is 4114 veh/hour with $\alpha = 0$, $\beta = 0.95$, and $\eta = 0.05$. The FD in both mixtures such as CAVs and HDVs and CAVs, CHVs and HVs is greatly influenced by the PR of CAVs. It is clear that the HVs reduce the efficiency of road networks. Further, the CHVs will reduce the resistance caused to traffic flow by HVs, thus, we will also investigate the impact of CHVs on the overall throughput of traffic in later sections.

Table 5.1. The ρ_{cr}, ρ_m, and q_m of FD subjected to assorted PR of HDVs (α) and CAVs (β).

α	β	η	ρ_{cr} (veh/km)	ρ_m (veh/km)	q_m (veh/hour)
1	0	0	17	133	1756
0.8	0.2	0	19	138	2022
0.6	0.4	0	22	144	2384
0.4	0.6	0	27	151	2903
0.2	0.8	0	34	158	3711
0	1	0	48	166	5143

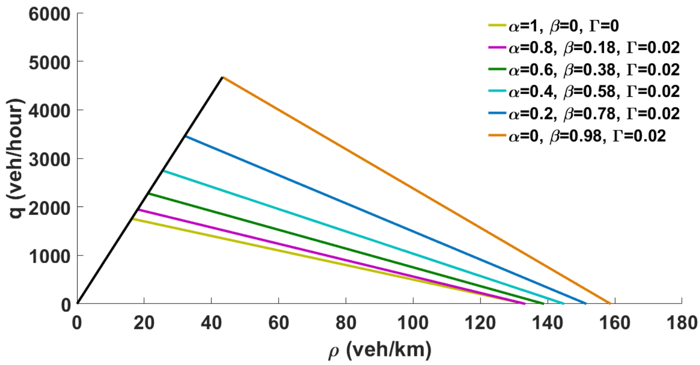

Figure 5.3. Fundamental diagram with assorted PR of HDVs (α), CAVs (β), and HVs (η).

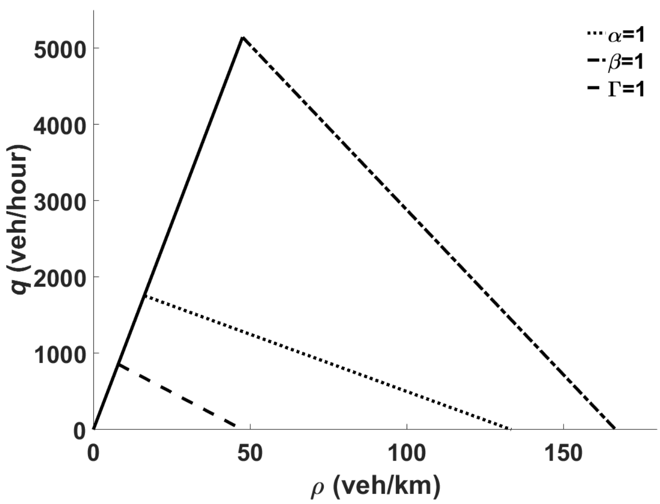

Figure 5.4. Fundamental diagram homogeneous vehicle class, HDVs (α), CAVs (β), and HVs (η).

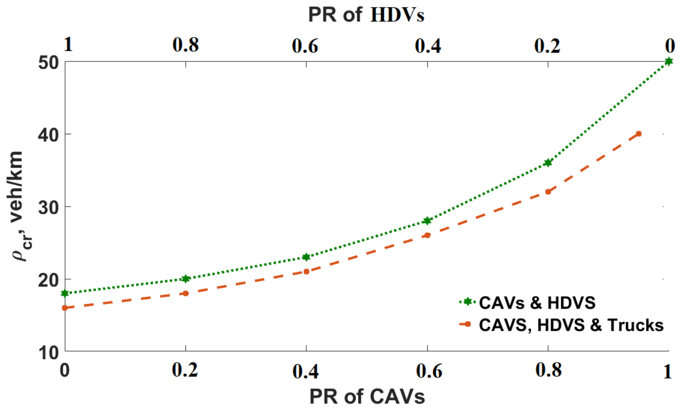

Figure 5.5. Improvement in ρ_{cr} subject to assorted PRs of CAVs in the traffic mixture (HDVs-CAVs-HVs). The PR of HVs is $\eta = 0.05$ which is unform throughout the analysis.

Table 5.2. The ρ_{cr}, ρ_m, and q_m of FD subjected to assorted PR of HDVs (α), CAVs (β), and HVs (η).

α	β	η	ρ_{cr} (veh/km)	ρ_m (veh/km)	q_m (veh/hour)
0.95	0	0.05	15	122	1669
0.75	0.2	0.05	17	127	1907
0.55	0.4	0.05	20	132	2226
0.35	0.6	0.05	24	138	2672
0.15	0.8	0.05	31	143	3341
0	0.95	0.05	38	148	4114

5.3.4 The Revamp Continuum Second-Order Traffic Model

The continuum second-order traffic models are introduced in Chapter 2 (see Section 2.2). The gaps and shortcomings of these models are also detailed, reckon with traffic mixture. In this Section, we revise the anticipation term of the continuum second-order model [52]. The driver presumption is altered from the original work to take into account the impacts of the variations in traffic and to introduce class-specific PRs. During traffic transitions, the response of drivers/vehicles is characterized by reaction velocity v_r [134] which is a function of the actual H and the transition occurring time, it is

$$v_r = \frac{H}{\tau}. \tag{5.19}$$

It is the change in velocity when traffic changes occur from free flow to congested flow and vice versa. In the case of free flow, τ_r increases, resulting in a large H and vice versa. The v_r for HDVs, CAVs, and HVs will be different. For HDVs, it is represented by ζ, and is

$$\zeta = \frac{H_a}{\tau_{ah}}, \tag{5.20}$$

where τ_{ah} is the transition time for change occurrence by HDVs, which is the sum of τ_{rh} and harmonization time τ_{hh}. Reaction velocity for CAVs is denoted by φ , and is

$$\varphi = \frac{H_b}{\tau_{bh}}, \tag{5.21}$$

where τ_{bh} is the transition time of CAVs. Reaction velocity for HVs is denoted by γ , and is

$$\gamma = \frac{H_c}{\tau_{ch}}, \tag{5.22}$$

where τ_{ch} is the transition time of HVs.

Furthermore, the dispersion effect of the speed of traffic mixture is characterized by anticipation. That is, how identical driver/vehicle reacts to traffic conditions presumed. Drivers/vehicles usually reduce speed while approaching heavy traffic downstream, and vice versa for light traffic. The second-order traffic models take into account this property of flow, which in Eq. (2.8) is

$$(v(x,t) - c_0)\frac{\partial v(x,t)}{\partial x}, \tag{5.23}$$

demonstrating that traffic patterns alter spatially with gradients of velocity. In a practical sense, c_0 is the driver response to the changes in traffic which is not always uniform. It is characterized by reaction velocity, in this study, it is given by Eq. (5.20) for HDVs, and Eq. (5.21) for CAVs. In most of the studies, c_0 is considered as constant which means a driver or vehicle will always have a uniform response in non-identical conditions which is not correct and has no physical meaning. This has been revised by many researchers and corrected for HDVs. However, revising this for the mixture of HDVs, CAVs, and HVs is significant for more accurate traffic characterization of traffic.

The response of the following vehicle is significantly influenced by the leading vehicle, and it is regarded as an anisotropy principle in traffic flow. It forms the basis of traffic hypotheses since, in mixed traffic, they will manifest according to the predominant class-specific average behavior. To be explicit, in macroscopic systems, the typical behavior is regarded as a traffic wave that is traffic-traveling-wave [50]. It is not possible to study the behavior of a single car at the macroscopic level, instead, we must study typical traffic behavior as a traffic-traveling-wave. In the case of CAVs, HDVs, and HVs this traffic-traveling-wave is modified in accordance with the dominating average behavior of either CAVs, HDVs, and HVs. Therefore, it is essential to introduce the share of each class in traffic in order to identify the prevailing behavior of traffic-traveling-wave. This can be done by introducing a class-specific PR because realistically the traffic is 100% comprised of HDVs, and to understand the impact of CAVs and HVs, the PR of CAVs and HVs must be taken into account.

To introduce PR, we multiply it with Eq. (5.21), we get

$$\varphi_* = \alpha \cdot \varphi, \tag{5.24}$$

and ζ is updated as

$$\zeta_* = \beta \cdot \zeta, \tag{5.25}$$

while η is updated as

$$\gamma_* = \eta \cdot \gamma, \tag{5.26}$$

where α, β, and η are the PR of HDVs, CAVs, and HVs, ranging between 0 and 1. The anticipation term Eq. (5.23) is now revised for traffic mixture, and is

$$[\zeta_* + \varphi_* + \gamma_*](\frac{\partial v}{\partial x}). \tag{5.27}$$

To this end, the anticipation term of the second-order model is revised, and from then on, another significant model input $V(\rho(x,t))$ is discussed. The choice of velocity-density relationship can greatly affect the model output. Traffic behavior is stochastic, it means traffic is not always in equilibrium. In second-order models, this property is when the average velocity of vehicles is tuned as per the density-dependent velocity, which is equilibrium velocity and given by $V(\rho(x,t))$. Such changes are modeled through the relaxation term commonly known as the speed adaptation term. It details how vehicles adapt their speed to the steady-state speed and is characterized as

$$\frac{V(\rho(x,t)) - v(x,t)}{T}, \tag{5.28}$$

where v is the average traffic velocity and T is the traffic relaxation time. The average velocity of vehicles is tuned to equilibrium velocity over T. It has been shown that small T results in stable traffic [42]. The CAVs have smaller relaxation time so they can adjust to equilibrium conditions quickly compared to HDVs [148]. This is another vital parameter for modeling the impact of CAVs on regular traffic, however, as other parameters, the importance of T is also linked to class-specific PR. The Papageorgiou model for velocity-density relationship [19] is supposed to capture the variation in the slope of the velocity-density relationship as an exponential function. It is given as

$$V(\rho(x,t)) = v_f \cdot \exp\big[\frac{-1}{c}(\frac{\rho(x,t)}{\rho_{cr}})^c\big], \tag{5.29}$$

where c is the shape factor of slope, and ρ_{cr} corresponds to critical density. In real-time simulations of mixture traffic, the ρ_{cr} for Eq. (5.29) can be computed directly by using Eq. (5.15) for traffic mixture.

The second-order traffic model now can be revised for HDVs, CAVs, and HVs. The anticipation of the second-order traffic model in (2.8) presented by [52] are modified, and the new proposed model is presented as

$$\begin{cases} \frac{\partial \rho(x,t)}{\partial t} + \frac{\partial \rho(x,t)\cdot v(x,t)}{\partial x} = 0, \\ \frac{\partial v(x,t)}{\partial t} + (v(x,t) - [\zeta_* + \varphi_* + \gamma_*]))\frac{\partial v(x,t)}{\partial x} = \frac{V(\rho(x,t)) - v(x,t)}{(T(\zeta_*,\varphi_*,\gamma_*))}. \end{cases} \tag{5.30}$$

According to Eq. (5.30), perturbation in traffic will be instigated according to the dominating traffic class. This would induce a non-uniform class-specific behavior of traffic. While the steady state will be guaranteed by relaxation term through $V(\rho)$ over class-specific relaxation time. If a change in flow propagates with a finite velocity, then the model is hyperbolic. Thus, the effect of a perturbation decreases over time. A traffic model is strictly hyperbolic if the eigenvalues are real and distinct. Anisotropy requires that velocity changes are not greater than the average. The eigenvalues are obtained from the Jacobian matrix to determine anisotropy and hyperbolicity. To construct the Jacobian matrix, a model is considered in conservation form.

The backward propagation velocity in the proposed continuum model is characterized by $(\zeta_* + \varphi_* + \gamma_*)$. Thus, the proposed model in conservative form is

$$\psi = \begin{pmatrix} \rho \\ v \end{pmatrix}_t, f(\psi) = \begin{pmatrix} \rho v \\ (\frac{1}{2}v^2 - (\zeta_* + \varphi_* + \gamma_*)v) \end{pmatrix}_x, S(\psi) = \left(\frac{V(\rho) - v}{T}\right), \tag{5.31}$$

where ψ represents the data variables ρ and ρv, while the vector of functions of the data variables is $f(\psi)$. The vector representing the source terms is $S(\psi)$. The proposed continuum model's Jacobian matrix $A(\psi)$ while setting $\psi = (\rho, v)$ is

$$A(\psi) = \begin{pmatrix} v & \rho \\ 0 & v - (\zeta_* + \varphi_* + \gamma_*) \end{pmatrix}, \tag{5.32}$$

and the eigenvalues of Eq. (5.32) are

$$\lambda_1 = v - (\zeta_* + \varphi_* + \gamma_*), \lambda_2 = v. \tag{5.33}$$

From Eq. (5.33) the proposed continuum traffic model traffic mixture is hyperbolic as the eigenvalues are real and distinct. Since changes in traffic travel at and below the average velocity, thus, the system is also anisotropic. Backward propagation of velocity evolves with λ_2 in the frontal direction, while during congested flow, it evolves with λ_1 in a backward direction [5].

The proposed second-order model is a system of HPDEs. It is numerically solved by employing a conservative scheme proposed by [52]. The density dynamics are computed as

$$\rho_i^{n+1} = \rho_i^n + \frac{\Delta t}{\Delta x}(\rho_i^n(v_i^n - v_{i+1}^n)) + \frac{\Delta t}{\Delta x} v_i^n(\rho_{i-1}^n - \rho_i^n), \tag{5.34}$$

where the subscripts i and n are space and time indices. The velocity dynamics is computed according to Eq. (5.30) which if

$$v_i^n \leq (\zeta_* + \varphi_* + \gamma_*)$$

is

$$v_i^{n+1} = v_i^n + \frac{\Delta t}{\Delta x}([\zeta_* + \varphi_* + \gamma_*] - v_i^n)(v_{i+1}^n - v_i^n) + \frac{\Delta t}{(\eta(\zeta_*, \varphi_*, \gamma_*))}(V(\rho_i^n) - v_i^n), \tag{5.35}$$

and otherwise it is

$$v_i^{n+1} = v_i^n + \frac{\Delta t}{\Delta x}([\zeta_* + \varphi_* + \gamma_*] - v_i^n)(v_i^n - v_{i-1}^n) + \frac{\Delta t}{(\eta(\zeta_*, \varphi_*, \gamma_*))}(V(\rho_i^n) - v_i^n). \tag{5.36}$$

where Δx and Δt are the road and time steps. Furthermore, this scheme is only stable if the Courant-Friedrichs-Lewy (CFL) condition [156] is satisfied, that is

$$v_m \frac{\Delta t}{\Delta x} \leq 1. \tag{5.37}$$

5.4 The Macroscopic Model For Fuel Consumption and Exhaust Emissions

The widely used microscopic VT Model [160] is transformed to macroscopic emissions and fuel consumption model by [161], and it is expressed as

$$\ln(MOE_e) = \sum_{r=0}^{3}\sum_{s=0}^{3}(\sigma^e_{r,s} \times v^r \times a^s), \tag{5.38}$$

where $\ln(MOE_e)$ is the consumption rate of energy or exhaust emissions. v^r represents the instantaneous velocity while a^s is instantaneous acceleration. The coefficients of the regression are $\sigma^e_{r,s}$ (see Table 1 of [161]). The acceleration a^s, is

$$\frac{\partial v(x,t)}{\partial t} + v(x,t)\frac{\partial v(x,t)}{\partial x}. \tag{5.39}$$

Using the difference scheme of [52], it is discretized as

$$\frac{v_i^{n+1} - v_i^n}{\Delta t} + v_i^n \frac{v_{i+1}^n - v_i^n}{\Delta x}. \tag{5.40}$$

Thus, Eq. (5.38) can be expressed as

$$\ln(MOE_e) = \sum_{r=0}^{3}\sum_{s=0}^{3}\big(\sigma^e_{r,s} \times (v_i^n)^r \times (\frac{v_i^{n+1} - v_i^n}{\Delta t} + v_i^n \frac{v_{i+1}^n - v_i^n}{\Delta x})^s\big), \tag{5.41}$$

and finally, Eq. (5.41) become

$$\Theta = \sum_{r=0}^{3}\sum_{s=0}^{3}\exp\big(\sigma^e_{r,s} \times (v_i^n)^r \times (\frac{v_i^{n+1} - v_i^n}{\Delta t} + v_i^n \frac{v_{i+1}^n - v_i^n}{\Delta x})^s\big), \tag{5.42}$$

where Θ represents the desired quantity to be calculated. We integrate Eq. (5.42) with Eq. (5.35) and Eq. (5.36) to calculate the fuel consumption and exhaust emissions according to the dynamics envisioned by the proposed model.

5.5 Performance Evaluation of the Proposed Continuum Second-Order Model for Traffic Mixture

The performance of the proposed continuum second-order model is evaluated on a 20 km freeway corridor. The simulation parameters are given in Table 5.3. The corridor is divided into 100 segments, and the road step (Δx) and time step (Δt) are 200 m and 1 s, respectively. The total simulation (T_s) time is 30 minutes, the relaxation time (T) is 20 s. The Papageorgiou model is employed for velocity-density relation. Moreover, typical parameter values are selected for the other parameters of the model. Circular boundary conditions such as

$$\begin{cases} \rho(X,t) = \rho(0,t), \\ v(X,t) = v(0,t), \end{cases} \tag{5.43}$$

are employed in order to evaluate the traffic perturbation over the entire corridor for 30 minutes. An inactive bottleneck (caused by a merge) is employed sidewise to create a strong congested point. The purpose of this is to observe a very strong shockwave that should remain in the corridor for the whole simulation time, thus, it could allow us to evaluate the impacts of CAVs, CHVs and HVs on conventional traffic flow.

5.5.1 Spatio-Temporal Analysis of the Velocity Subject to Assorted PRs of CAVs

The evolution of the velocity with the proposed model is analyzed. In this experiment, only CAVs and HDVs are considered in the traffic mixture. The velocity evolution is observed for 30 minutes with assorted PRs of CAVs and HDVs, and the results are given in Table 5.4. The velocity evolution over the freeway corridor with $\alpha = 1$ and $\beta = 0$ is shown in Figure 5.6. A sharp velocity breakdown occurs between segments 68 and 72. The impact of this breakdown is propagated backward, and a very timid velocity patterns are observed. The v_{min} is 7.23 km/hour while the v_{max} and v_{avg} are 100 km/hour and 46.0 km/hour, respectively.

The velocity evolution over the freeway corridor with $\alpha = 0.80$ and $\beta = 0.20$ is shown in Figure 5.7. The velocity breakdown between segments 68 and 72 improves incrementally. The v_{min} is 10.21 km/hour while the v_{max} and v_{avg} are 100 km/hour and 50.88 km/hour, respectively. The v_{avg} of the corridor improves by 10.60%. With $\alpha = 0.60$ and $\beta = 0.40$, the velocity evolution is demonstrated in Figure 5.8. The v_{min} is 14.42 km/hour while the v_{max} and v_{avg} are 100 km/hour and 57.00 km/hour, respectively. The v_{avg} of the corridor improves by 23.91%.

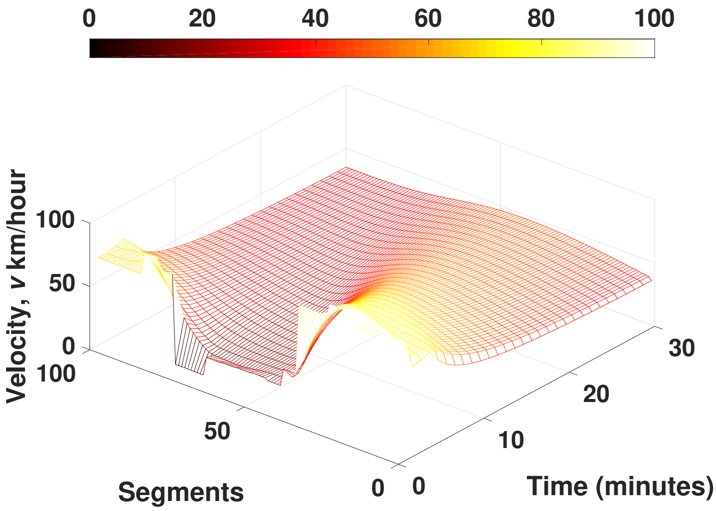

Figure 5.6. Spatio-temporal velocity evolution over the freeway corridor with $\alpha = 1$ and $\beta = 0$.

The velocity evolution over the freeway corridor with $\alpha = 0.40$ and $\beta = 0.60$ is shown in Figure 5.9. The velocity breakdown between segments 68 and 72 improves significantly. The v_{min} is 20.35 km/hour while the v_{max} and v_{avg} are 100 km/hour and 63.00 km/hour, respectively. The v_{avg} of the corridor improves by 36.95%. With $\alpha = 0.20$ and $\beta = 0.80$ as in Figure 5.10, the velocity breakdown is smoothed out efficiently. The v_{avg} of the corridor improves by 50.28%. Whereas the v_{min} is 29.00 km/hour while the v_{max} and v_{avg} are 100 km/hour and 69.13 km/hour, respectively.

The velocity evolution over the freeway corridor with $\alpha = 0$ and $\beta = 1$ is shown in Figure 5.11. The velocity adjustments are sharp, and the velocity breakdown is eliminated very soon. The velocity evolution is smoother, and a homogeneous pattern is observed. The v_{min} is observed to be 40.57 km/hour while the v_{max} is 100 km/hour. The v_{avg} of the corridor improves by 67.65%, and is observed to be 77.12 km/hour. It is demonstrated that CAVs significantly improve the efficiency of the freeway corridor. With the increase in the PR of CAVs, a more homogeneous velocity behavior is achieved.

Table 5.3. Parameters for the Simulation.

Description	Notation	Value
Average length of a vehicle (HDV)	L_h	4.5 m
Average length of a vehicle (CAV)	L_c	4.5 m
Average length of a vehicle (HV)	L_t	16.5 m
Clearance gap (HDV)	C_h	3
Clearance gap (CAV)	C_c	1.5
Clearance gap (HV)	C_t	5
Reaction time (HDV)	τ_{rh}	1.5 s
Reaction time (CAV)	τ_{rc}	0.5 s
Reaction time (HV)	τ_{rt}	2.5 s
Maximum velocity	v_f	100 km/hour
Velocity-Density relationship	V(ρ)	[19]
Length of Corridor	X	20, 000 m
Road Step	Δx	200 m
Time Step	Δt	1 s
Segments	i	100
Simulation time	T_s	30 mins (1800 s)
Relaxation time	T	20 s

Table 5.4. Analysis of the minimum velocity (v_{min}), maximum velocity (v_{max}), average velocity (v_{avg}), and the % improvement subject to assorted PRs of HDVs and CAVs.

α	β	η	v_{min}	v_{max}	v_{avg}	Improvement (%)
1	0	0	7.23	100	46.00	-
0.80	0.20	0	10.21	100	50.88	10.60
0.60	0.40	0	14.42	100	57.00	23.91
0.40	0.60	0	20.35	100	63.00	36.95
0.20	0.80	0	29.00	100	69.13	50.28
0	1	0	40.57	100	77.12	67.65

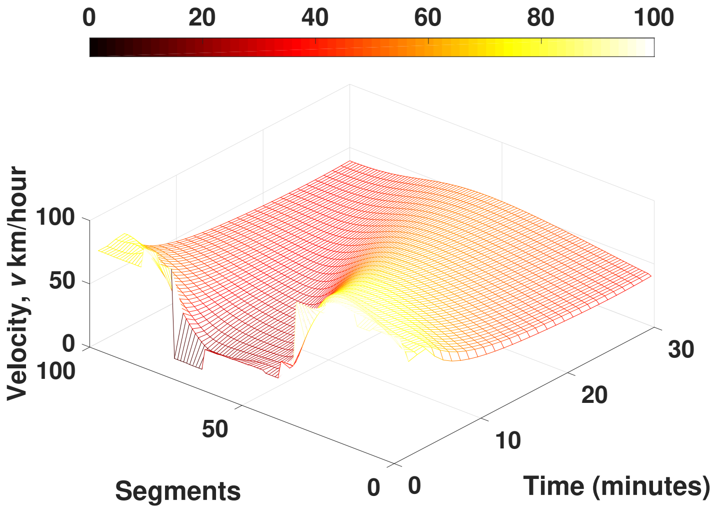

Figure 5.7. Spatio-temporal velocity evolution over the freeway corridor with $\alpha = 0.80$ and $\beta = 0.20$.

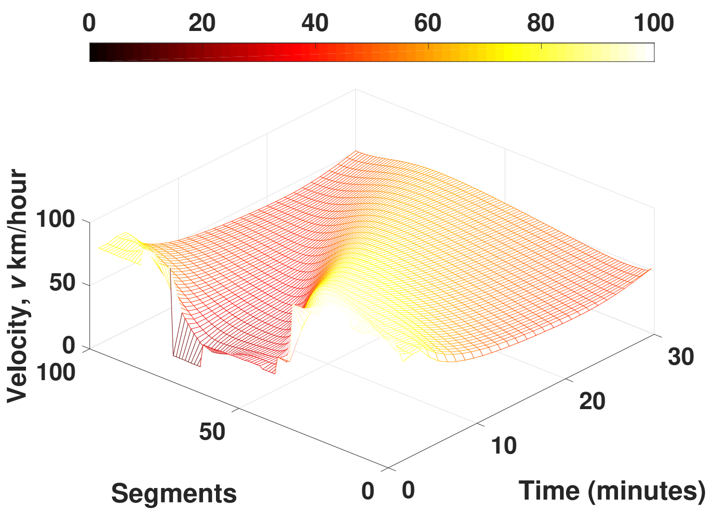

Figure 5.8. Spatio-temporal velocity evolution over the freeway corridor with $\alpha = 0.60$ and $\beta = 0.40$.

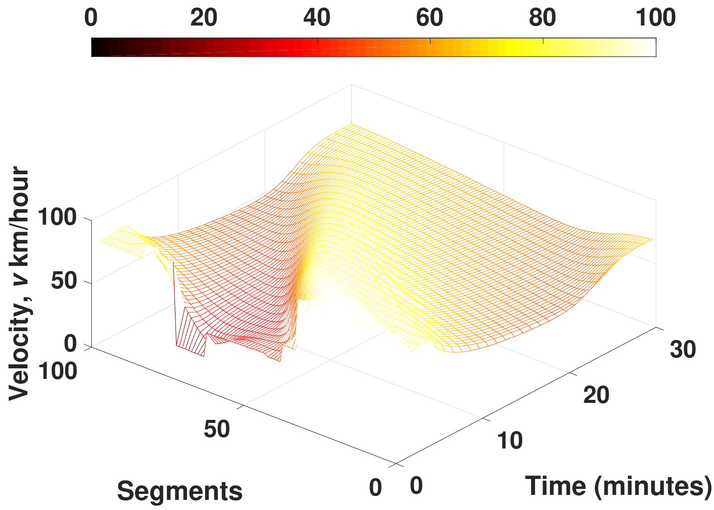

Figure 5.9. Spatio-temporal velocity evolution over the freeway corridor with $\alpha = 0.40$ and $\beta = 0.60$.

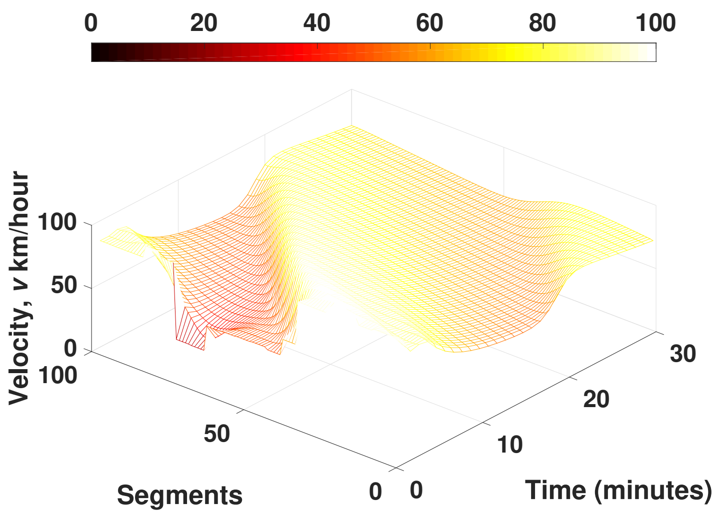

Figure 5.10. Spatio-temporal velocity evolution over the freeway corridor with $\alpha = 0.20$ and $\beta = 0.80$.

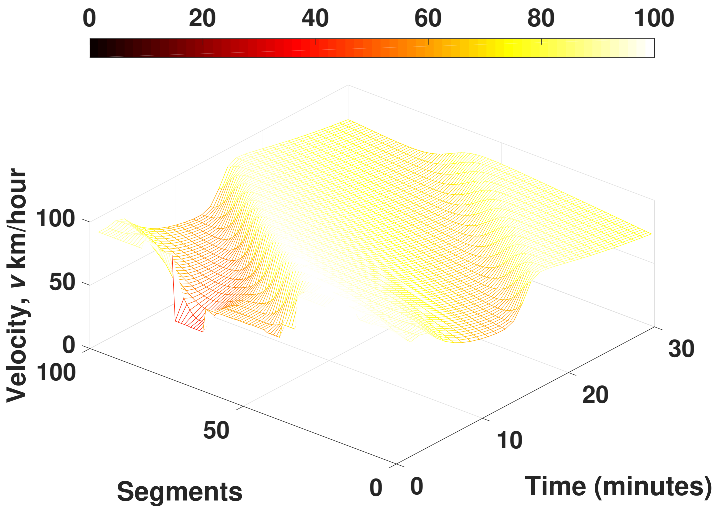

Figure 5.11. Spatio-temporal velocity evolution over the freeway corridor with $\alpha = 0$ and $\beta = 1$.

5.5.2 Spatio-Temporal Analysis of the Velocity Subject to Assorted PRs of CAVs, a traffic mixture of HDVs, CAVs and HVs

The spatio-temporal evolution of velocity of the traffic mixture comprised of HDVs, CAVs and HVs is shown in Table 5.5. The velocity evolution is observed for 30 minutes with assorted PRs of HDVs, CAVs and HVs, and the results are given in Table 5.5. With $\alpha = 0.95$, $\beta = 0$ and $\eta = 0.05$, the velocity evolution is shown in Figure 5.12. An abrupt velocity breakdown is observed between segments 68 and 72 which propagates upstream. The v_{min} is 6.30 km/hour while the v_{max} is 100 km/hour. The v_{avg} is 44.00 km/hour which is less than the v_{avg} when the mixture comprises of CAVs and HDVs only. It is observable that HVs enable resistance to the flow resulting in deteriorated traffic characteristics.

The velocity evolution of traffic mixture with $\alpha = 0.75$, $\beta = 0.20$ and $\eta = 0.05$ is shown in Figure 5.13. Refinements in the velocity breakdowns are observed, the v_{min} is 8.90 km/hour. The v_{max} is 100 km/hour and the v_{avg} is 48.50 km/hour. Further enhancements of the velocity breakdown are observed when $\alpha = 0.55$, $\beta = 0.40$ and $\eta = 0.05$ as shown in Figure 5.14. The v_{min} and v_{max} are 12.54 km/hour and 100 km/hour, respectively, while the v_{avg} is 54.17 km/hour. Similarly, when $\alpha = 0.35$, $\beta = 0.60$ and $\eta = 0.05$ as shown in Figure 5.15. The v_{min} and v_{max} are 17.60 km/hour and 100 km/hour, respectively, while the v_{avg} is 60.24 km/hour.

The velocity evolution of the traffic mixture with $\alpha = 0.15$, $\beta = 0.80$ and $\eta = 0.05$ is shown in Figure 5.16. It is smoother than before, and adjustments in velocity are quick resulting in faster propagation of velocity breakdown downstream. The v_{min} is 25.01 km/hour while the v_{max} and v_{avg} are 100 km/hour and 66.92 km/hour, respectively. With $\alpha = 0$, $\beta = 0.95$ and $\eta = 0.05$ is shown in Figure 5.17. The v_{min} is 32.40 km/hour while the v_{max} and v_{avg} are 100 km/hour and 72.23 km/hour, respectively. It is observable that the velocity breakdowns significantly improve with the increase in PR of CAVs. Nonetheless, it also observed that the HVs are enabling friction to velocity evolution over time. From these results, it will be helpful to also analyze the impact of CHVs on the velocity. Thus, next we analyze the evolution of velocity in the presence of HDVs, CAVs and CHVs.

Table 5.5. Analysis of the minimum velocity (v_{min}), maximum velocity (v_{max}), average velocity (v_{avg}), and the % improvement subject to assorted PRs of HDVs, CAVs and HVs.

α	β	η	v_{min}	v_{max}	v_{avg}	Improvement (%)
0.95	0	0.05	6.30	100	44.00	-
0.75	0.20	0.05	8.90	100	48.50	10.22
0.55	0.40	0.05	12.54	100	54.17	23.11
0.35	0.60	0.05	17.60	100	60.24	36.90
0.15	0.80	0.05	25.01	100	66.92	50.00
0	0.95	0.05	32.40	100	72.23	63.63

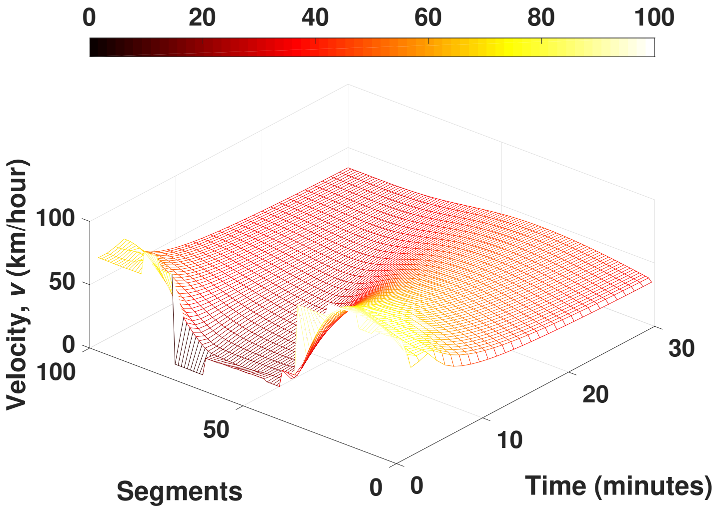

Figure 5.12. Spatio-temporal velocity evolution over the freeway corridor with $\alpha = 0.95$, $\beta = 0$ and $\eta = 0.05$.

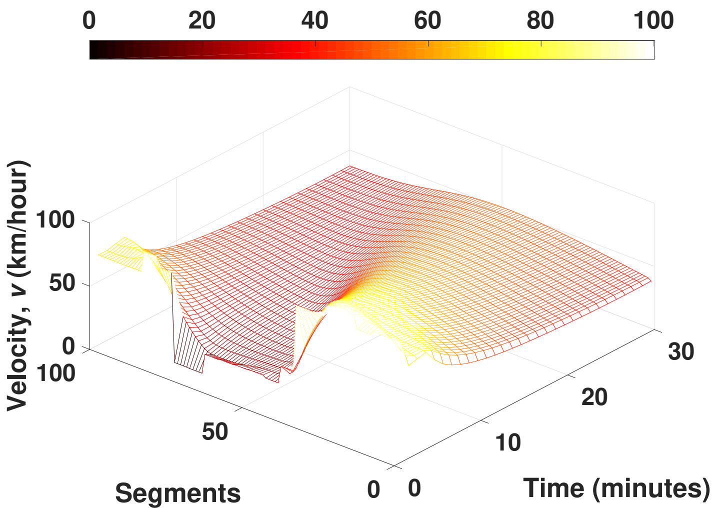

Figure 5.13. Spatio-temporal velocity evolution over the freeway corridor with $\alpha = 0.75$, $\beta = 0.20$ and $\eta = 0.05$.

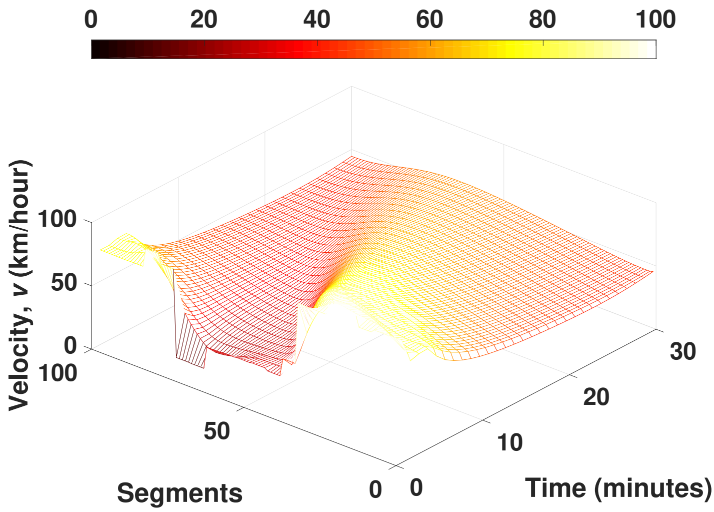

Figure 5.14. Spatio-temporal velocity evolution over the freeway corridor with $\alpha = 0.55$, $\beta = 0.40$ and $\eta = 0.05$.

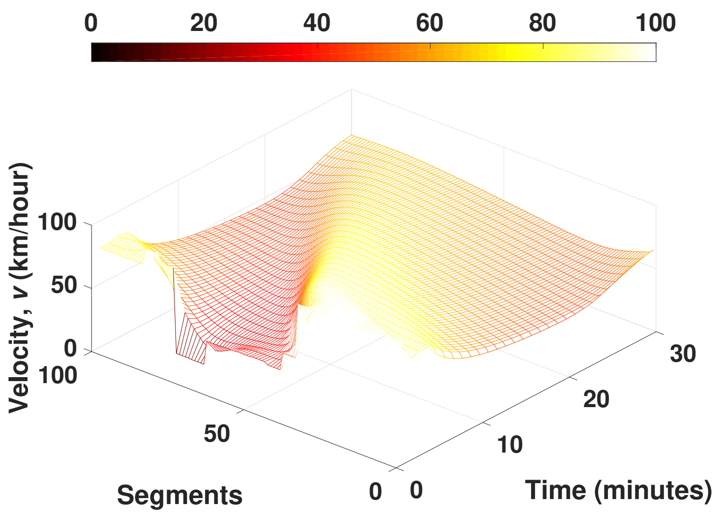

Figure 5.15. Spatio-temporal velocity evolution over the freeway corridor with $\alpha = 0.35$, $\beta = 0.60$ and $\eta = 0.05$.

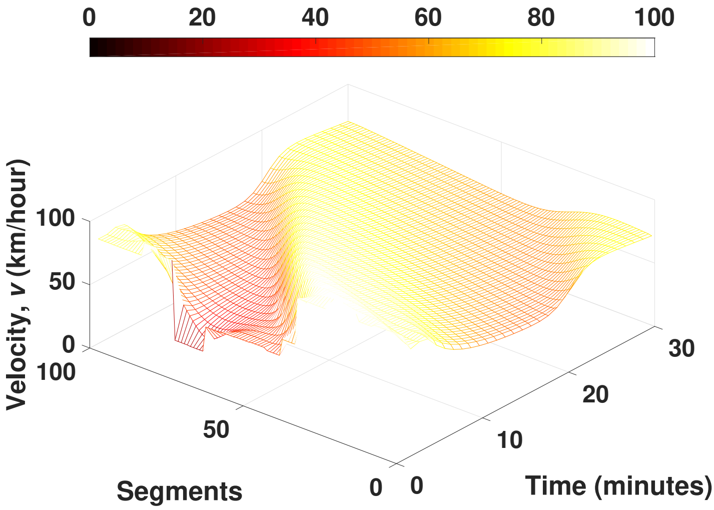

Figure 5.16. Spatio-temporal velocity evolution over the freeway corridor with $\alpha = 0.15$, $\beta = 0.80$ and $\eta = 0.05$.

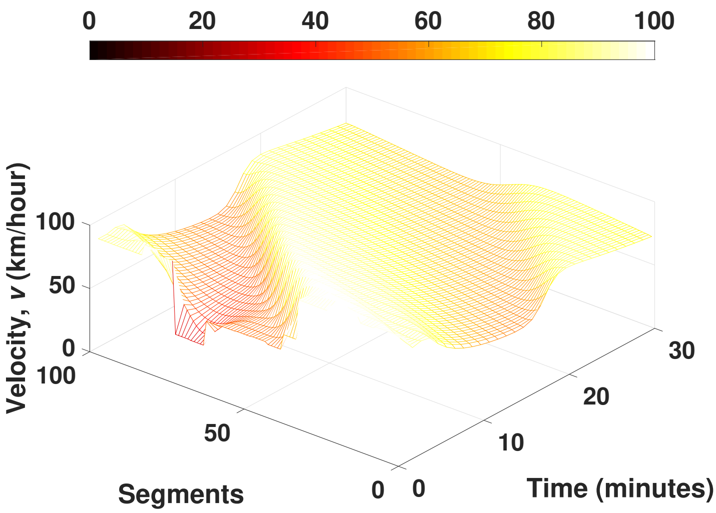

Figure 5.17. Spatio-temporal velocity evolution over the freeway corridor with $\alpha = 0$, $\beta = 0.95$ and $\eta = 0.05$.

5.5.3 Spatio-Temporal Analysis of the Velocity Subject to Assorted PRs of CAVs, a traffic mixture of HDVs, CAVs and CHVs

The velocity evolution of the traffic mixture (HDVs-CAVs-CHVs) is analyzed, and the results are summarized in Table 5.6. Since only 5% HVs are connected, there are few difference with the previously studied scenario where the HVs are conventional. The velocity breakdown occur between segments 68 and 72 which evolves upstream, the velocity breakdown dissipation is slow. The velocity evolution when the $\alpha = 0.95$, $\beta = 0$ and $\eta^* = 0.05$ is shown in Figure 5.18. Some improvements are observed, the v_{min} is 7.38 km/hour, while the v_{max} and v_{avg} are 100 km/hour and 46.11 km/hour, respectively. The velocity evolution with $\alpha = 0.75$, $\beta = 0.20$ and $\eta^* = 0.05$ is demonstrated in Figure 5.19. The v_{min} is 10.42 km/hour, and the v_{max} and v_{avg} are 100 km/hour and 51.20 km/hour, respectively.

The velocity evolution with $\alpha = 0.55$, $\beta = 0.40$ and $\eta^* = 0.05$ is shown in Figure 5.20. The velocity breakdown recovers soon as compared to the previous scenario. The v_{min} and v_{max} are 14.71 km/hour and 100 km/hour while the v_{avg} is 56.87 km/hour. The velocity evolution with $\alpha = 0.35$, $\beta = 0.60$ and $\eta^* = 0.05$ is shown in Figure 5.21. The velocity evolution is fast downstream, and the breakdown impact on upstream traffic is lower than before. The v_{min} and v_{max} are 20.77 km/hour and 100 km/hour while the v_{avg} is 63.27 km/hour.

The velocity evolution when the $\alpha = 0.15$, $\beta = 0.80$ and $\eta^* = 0.05$ is shown in Figure 5.22. The evolution of velocity is smoother and fast, the v_{min} is 29.33 km/hour, while the v_{max} and v_{avg} are 100 km/hour and 70.15 km/hour, respectively. The velocity evolution with $\alpha = 0$, $\beta = 0.95$ and $\eta^* = 0.05$ is demonstrated in Figure 5.23. The velocity evolution is almost uniform and is significantly improved. Velocity breakdown occurs at the start, but it is recovered soon. The v_{min} is 37.98 km/hour, and the v_{max} and v_{avg} are 100 km/hour and 75.66 km/hour, respectively.

A detailed comparison of the v_{avg} of the corridor between the three different scenarios such as (i) HDVs and CAVs, (ii) HDVs, CAVs and HVs, and (iii) HDVs, CAVs and CHVs is presented in Figure 5.24. The bars in the Figure represent v_{avg} of different traffic mixtures with assorted PRs. It is observable that the v_{avg} of HDVs and CAVs, and HDVs, CAVs and

CHVs is are comparable. The differences are small for all PRs. While the v_{avg} of HDVs, CAVs and HVs is smaller as compared to the other two traffic mixtures. CAVs and CHVs significantly contribute to eliminate oscillations in the velocity over the entire time horizon, while HVs add impedance to the flow resulting in deteriorated traffic conditions.

Table 5.6. Analysis of the minimum velocity (v_{min}), maximum velocity (v_{max}), average velocity (v_{avg}), and the % improvement subject to assorted PRs of HDVs, CAVs and CHVs.

α	β	η^*	v_{min}	v_{max}	v_{avg}	Improvement (%)
0.95	0	0.05	7.38	100	46.11	-
0.75	0.20	0.05	10.42	100	51.20	11.03
0.55	0.40	0.05	14.71	100	56.87	23.33
0.35	0.60	0.05	20.77	100	63.27	37.21
0.15	0.80	0.05	29.33	100	70.15	52.13
0	0.95	0.05	37.98	100	75.66	64.08

5.5.4 Spatio-temporal Analysis of Density Shockwave Subject to Assorted PRs of HDVs, CAVs, HVs and CHVs

The spatio-temporal analysis of density shockwave is shown in Figure 5.25 to Figure 5.30 for HDVs and CAVs while in Figure 5.31 to Figure 5.36 for HDVs, CAVs and HVs, and HDVs, CAVs and CHVs. In Figure 5.25, the traffic mixture is $\alpha = 1$ and $\beta = 0$, the shockwave originating between segments 68 and 72 propagates backward, resulting in a traffic jam upstream for some time. The lines in the Figure are the line of the same value (contour line) of density. It is observed that the lines are distorted due to the oscillatory behavior of traffic. With $\alpha = 0.80$ and $\beta = 0.20$, a minor improvement is observed as in Figure 5.26. The shockwave propagation is faster, and the distortion is reduced to some extent, meaning that the oscillations are reduced.

The trend in improvement of the propagation of shockwave is observable with the increase in the PR of CAVs. With $\alpha = 0.60$ and $\beta = 0.40$, the oscillations are further reduced and the propagation is significantly improved as shown in Figure 5.27. Similarly, the shockwave propagation is

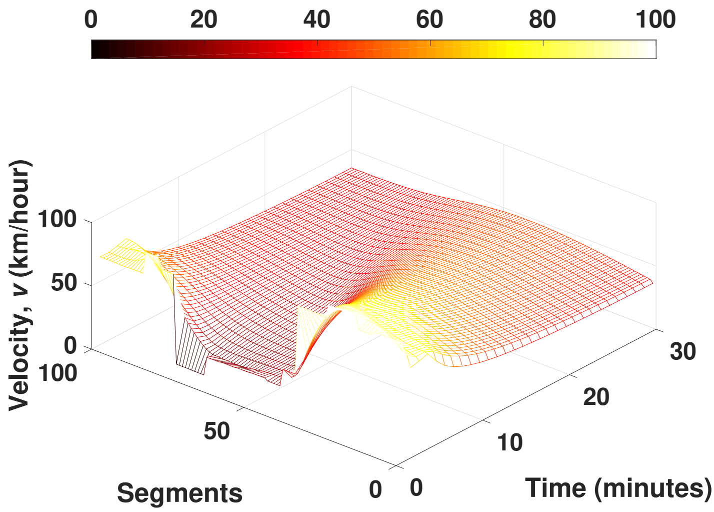

Figure 5.18. Spatio-temporal velocity evolution over the freeway corridor with $\alpha = 0.95$, $\beta = 0$ and $\eta^* = 0.05$.

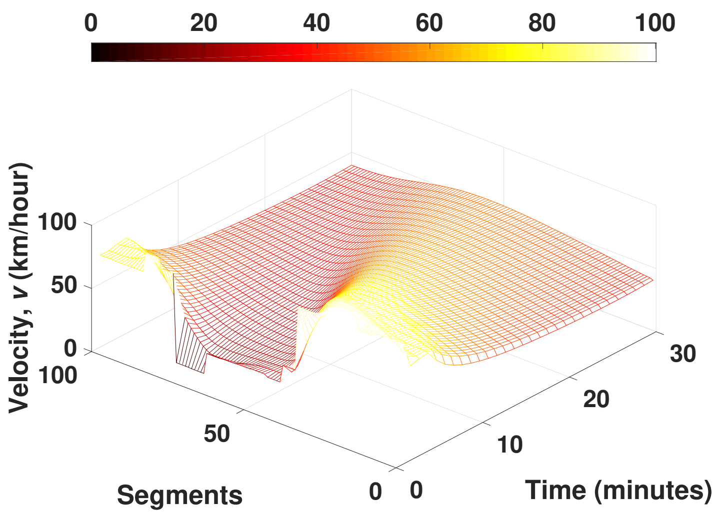

Figure 5.19. Spatio-temporal velocity evolution over the freeway corridor with $\alpha = 0.75$, $\beta = 0.20$ and $\eta^* = 0.05$.

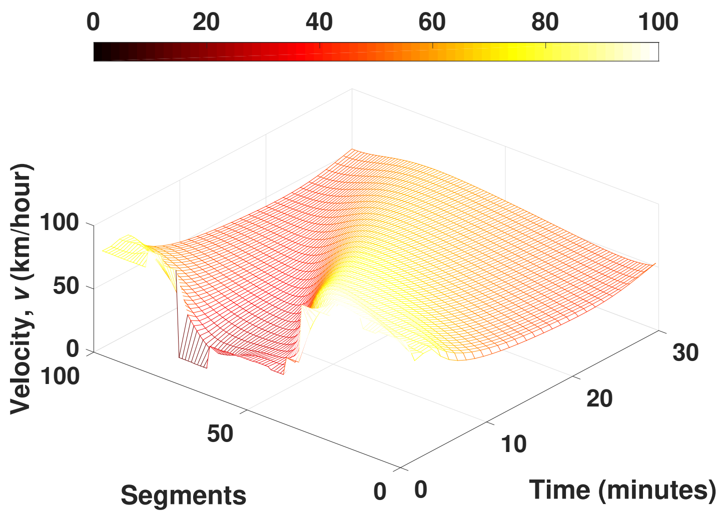

Figure 5.20. Spatio-temporal velocity evolution over the freeway corridor with $\alpha = 0.55$, $\beta = 0.40$ and $\eta^* = 0.05$.

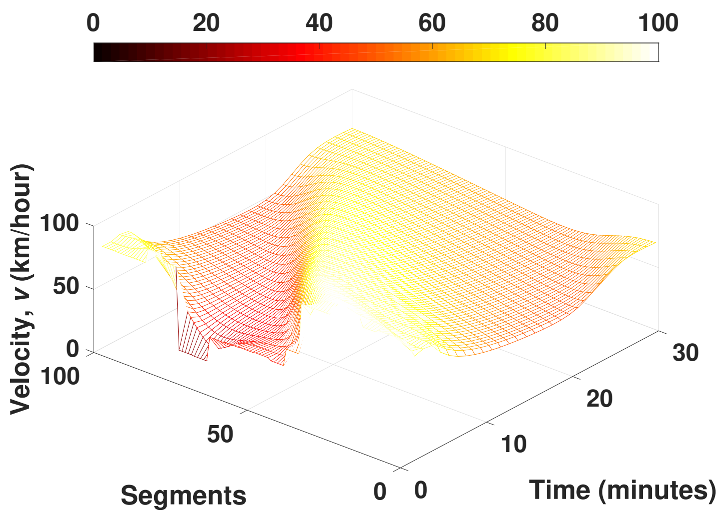

Figure 5.21. Spatio-temporal velocity evolution over the freeway corridor with $\alpha = 0.35$, $\beta = 0.60$ and $\eta^* = 0.05$.

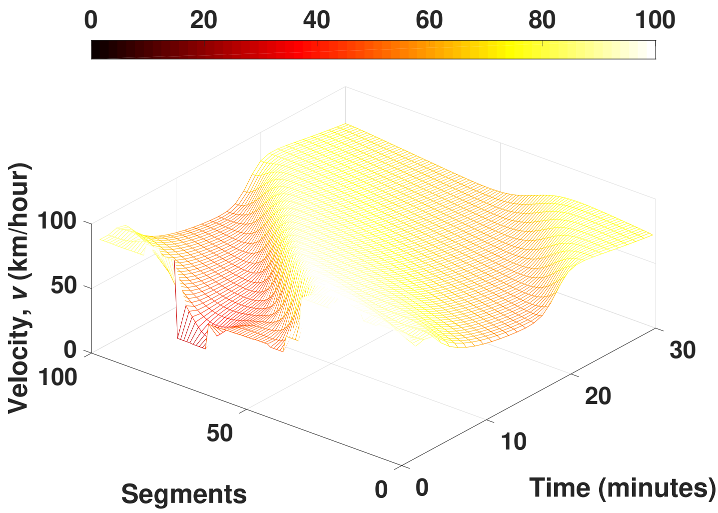

Figure 5.22. Spatio-temporal velocity evolution over the freeway corridor with $\alpha = 0.15$, $\beta = 0.80$ and $\eta^* = 0.05$.

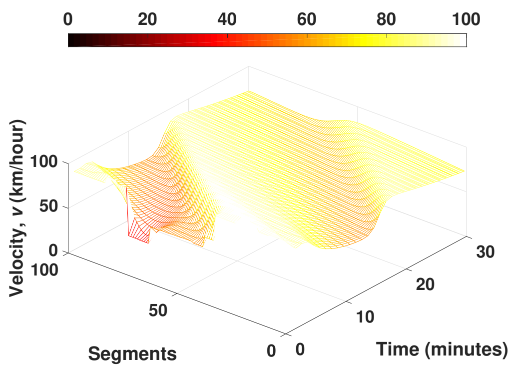

Figure 5.23. Spatio-temporal velocity evolution over the freeway corridor with $\alpha = 0$, $\beta = 0.95$ and $\eta^* = 0.05$.

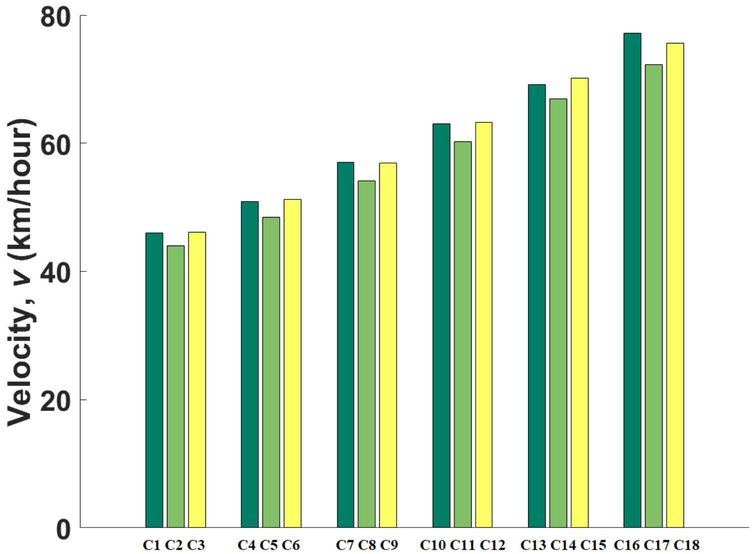

	C1	C2	C3	C4	C5	C6	C7	C8	C9	C10	C11	C12	C13	C14	C15	C16	C17	C18
α	1	0.95	0.95	0.8	0.75	0.75	0.6	0.55	0.55	0.4	0.35	0.35	0.2	0.15	0.15	0	0	0
β	0	0	0	0.2	0.2	0.2	0.4	0.4	0.4	0.6	0.6	0.6	0.8	0.8	0.8	1	0.95	0.95
Γ	0	0.05	0	0	0.05	0	0	0.05	0	0	0.05	0	0	0.05	0	0	0.05	0
Γ́	0	0	0.05	0	0	0.05	0	0	0.05	0	0	0.05	0	0	0.05	0	0	0.05

Figure 5.24. Comparison of v_{avg} of three traffic mixtures such as (i) HDVs and CAVs (ii) HDVs, CAVs and HVs (iii) HDVs, CAVs and CHVs. Single bar represent each traffic mixture with particular PR of the HDVs, CAVs, HVs and CHVs.

even with $\alpha = 0.40$ and $\beta = 0.60$ as shown in Figure 5.28, and a very sharp propagation downstream is observed with $\alpha = 0.20$ and $\beta = 0.80$, and $\alpha = 0$ and $\beta = 1$ as in Figure 5.29 and Figure 5.30 respectively. CAVs enable the traffic to move with higher velocity maintaining smaller headways during congestion which allow the shockwave to propagate downstream relatively fast compared to HDVs. CAVs significantly reduce shockwave occurrence time and backward propagation distance.

The spatio-temporal analysis of density shockwave for HDVs, CAVs, HVs and CHVs is shown in Figure 5.31 to Figure 5.36. This experiment is designed to evaluate the impact of conventional (Human-Driven) HVs and CHVs coupled with CAVs on conventional traffic flow. The PR of HVs and CHVs is unform such that it is always 5% (0.05). In Figure 5.31 to Figure 5.36, the continuous line represents the shockwave propagation in presence of HVs, while the dashed lines represent the propagation of CHVs. The HDVs and CAVs are subjected to assorted PRs.

It is observable that HVs is inducing impedance to the flow, and the shockwave propagation is slower. This impact is more frequent during the congestion occurrence, it is due to the higher τ_{rh} of HVs. The increase in PR of CAVs can help reduce the impedance caused by HVs. The difference can be observed in Figure 5.25 to Figure 5.30 and Figure 5.31 to 5.36. Conversely, the shockwave propagation in presence of CHVs is smoother. With the increase in PR of CAVs the shockwave propagation is faster, and the oscillations are eliminated, but the the presence of CHVs has still a little impact on the propagation, it is due to the length of the CHVs which affects the critical density of the road.

5.5.5 Analysis of Critical Density Subject to Assorted PRs of HDVs and CAVs

The ρ_{cr} for HDVs and CAVs is evaluated in this section. The time taken by traffic to reach $\rho(x,t)$ beneath the ρ_{cr} is demonstrated in Figure 5.37 to Figure 5.42, and the results are given in Table 5.7. The initial traffic conditions are the same throughout the analysis. There is a significant improvement in the ρ_{cr} with the increase in PR of CAVs. The $\rho(x,t)$ beyond ρ_{cr} represents traffic congestion. Thus, increase in the PR of CAVs can limit traffic congestion, and can enhance the density shockwave evolution resulting in smoother flow.

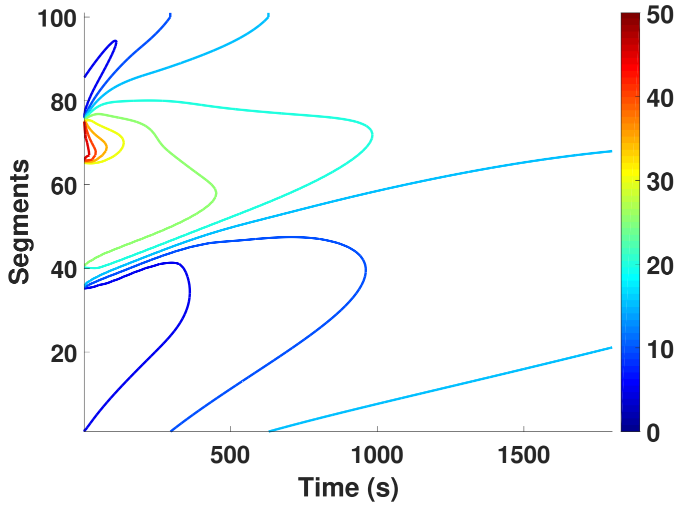

Figure 5.25. Spatio-temporal analysis of a density shockwave over the freeway corridor with $\alpha = 1$ and $\beta = 0$.

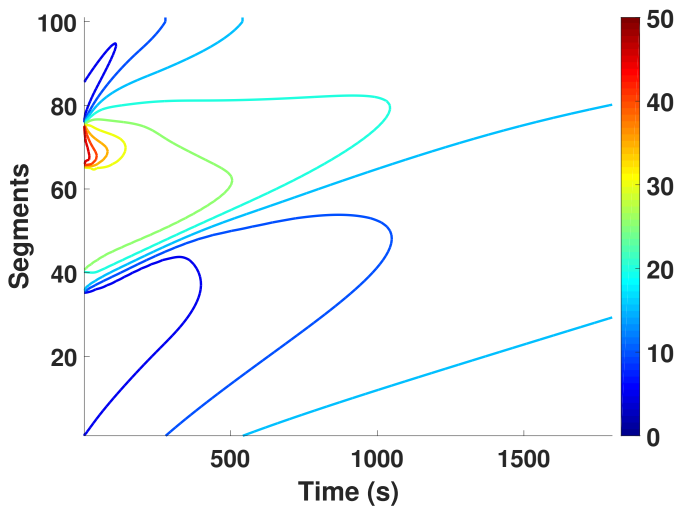

Figure 5.26. Spatio-temporal analysis of a density shockwave over the freeway corridor with $\alpha = 0.80$ and $\beta = 0.20$.

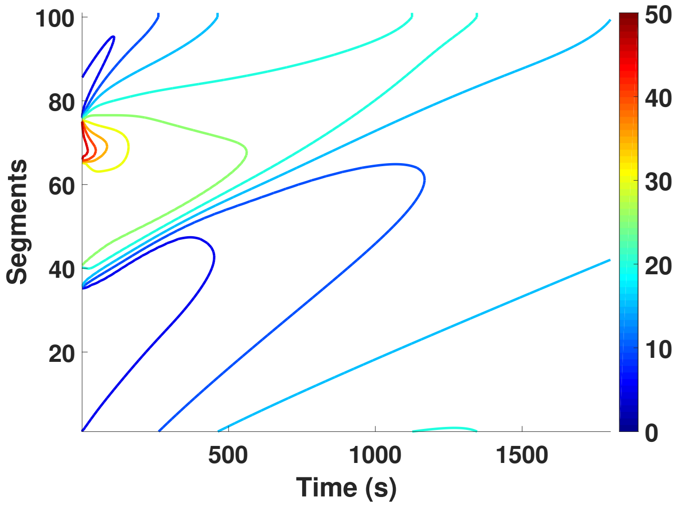

Figure 5.27. Spatio-temporal analysis of a density shockwave over the freeway corridor with $\alpha = 0.60$ and $\beta = 0.40$.

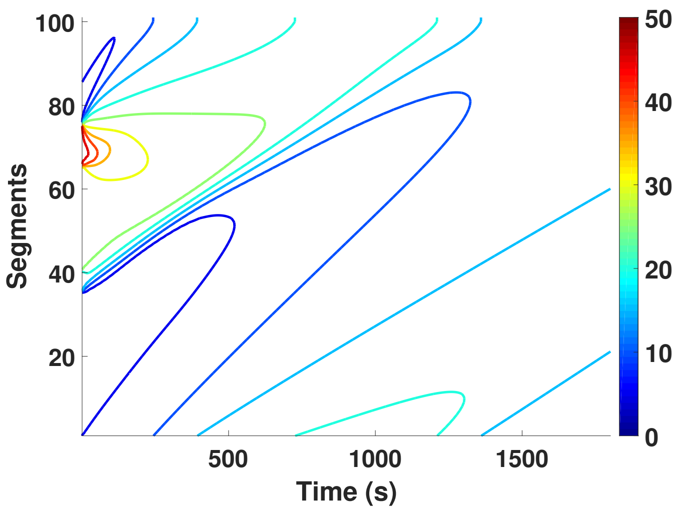

Figure 5.28. Spatio-temporal analysis of a density shockwave over the freeway corridor with $\alpha = 0.40$ and $\beta = 0.60$.

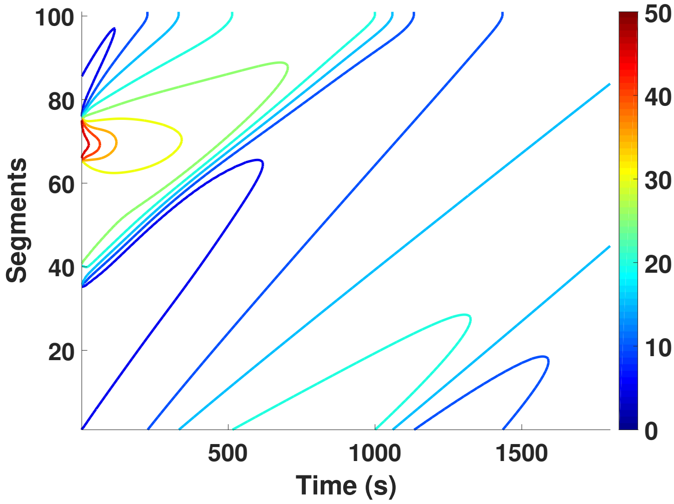

Figure 5.29. Spatio-temporal analysis of a density shockwave over the freeway corridor with $\alpha = 0.20$ and $\beta = 0.80$.

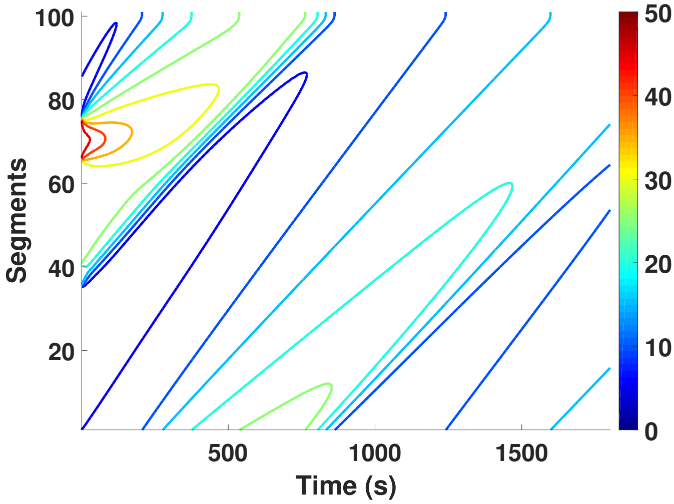

Figure 5.30. Spatio-temporal analysis of a density shockwave over the freeway corridor with $\alpha = 0$ and $\beta = 1$.

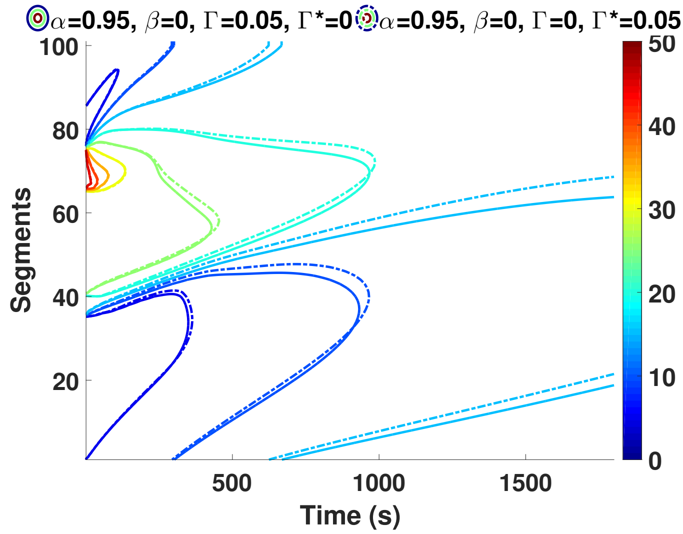

Figure 5.31. Spatio-temporal analysis of a density shockwave over the freeway corridor with assorted PRs of HDVs, CAVs, HVs and CHVs.

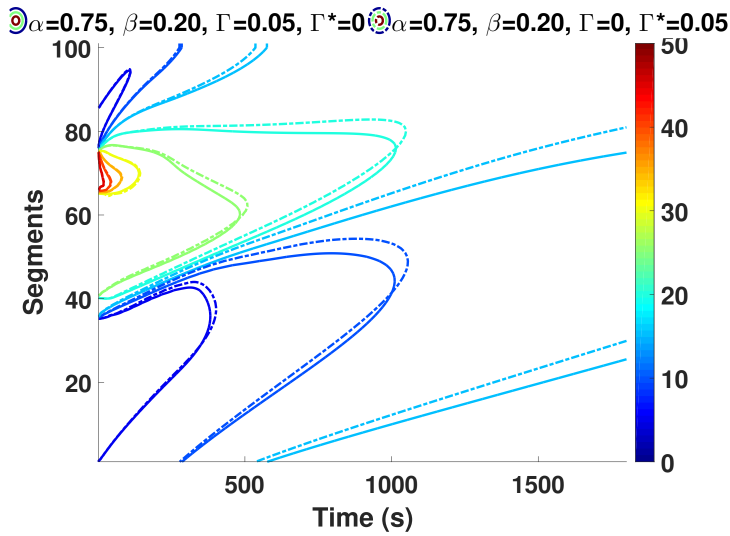

Figure 5.32. Spatio-temporal analysis of a density shockwave over the freeway corridor with assorted PRs of HDVs, CAVs, HVs and CHVs.

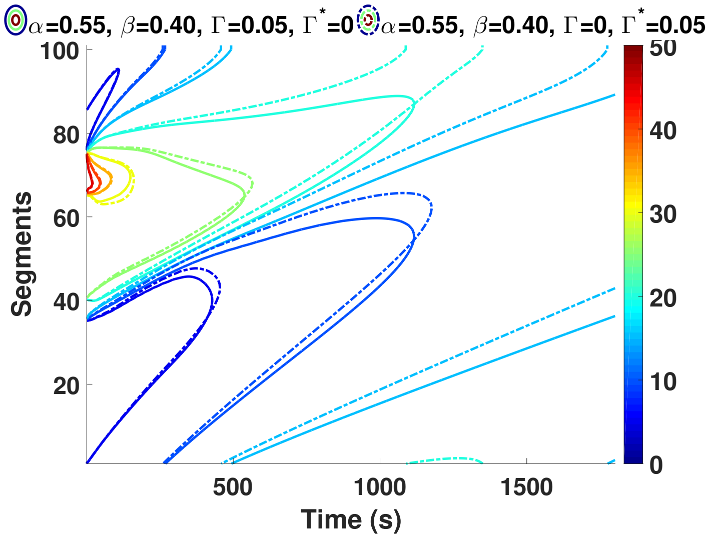

Figure 5.33. Spatio-temporal analysis of a density shockwave over the freeway corridor with assorted PRs of HDVs, CAVs, HVs and CHVs.

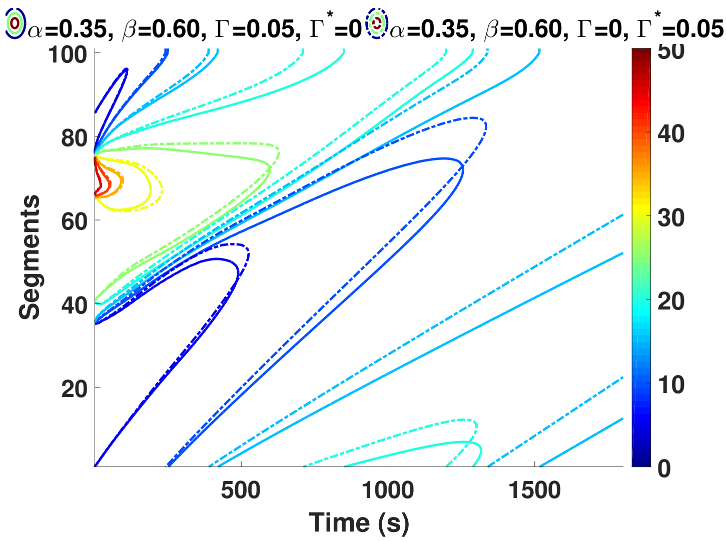

Figure 5.34. Spatio-temporal analysis of a density shockwave over the freeway corridor with assorted PRs of HDVs, CAVs, HVs and CHVs.

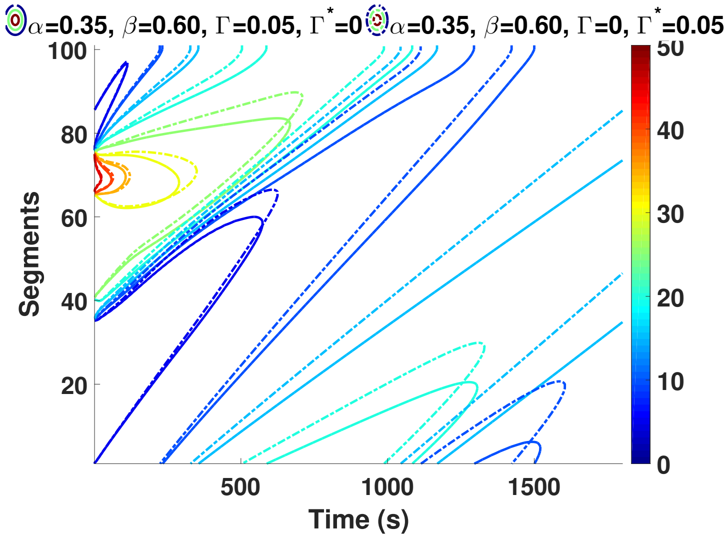

Figure 5.35. Spatio-temporal analysis of a density shockwave over the freeway corridor with assorted PRs of HDVs, CAVs, HVs and CHVs.

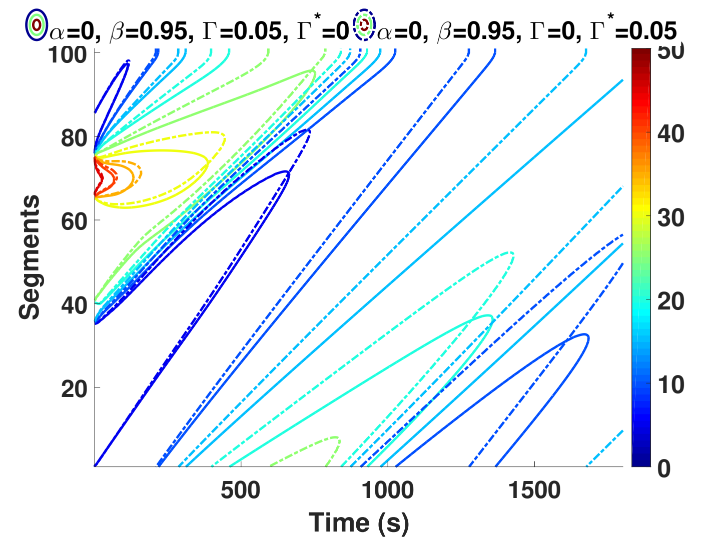

Figure 5.36. Spatio-temporal analysis of a density shockwave over the freeway corridor with assorted PRs of HDVs, CAVs, HVs and CHVs.

The time taken by $\rho(x,t)$ to normalize beneath ρ_{cr} with $\alpha = 1$ and $\beta = 0$ shown is shown in Figure 5.37. Initially, the traffic is dense, traffic congestion is observed which smooths out with time. It takes 1560 s, for $\rho(x,t)$ beyond ρ_{cr} to start normalizing beneath ρ_{cr}. It represents that the congestion duration is large. With $\alpha = 0.80$ and $\beta = 0.20$, the results are shown in Figure 5.38, the $\rho(x,t)$ tends to smooth, and the time taken by $\rho(x,t)$ to evolve beneath ρ_{cr} is 1080 s. With $\alpha = 0.60$ and $\beta = 0.40$, the results are shown in Figure 5.39, the propagation of flow further enhances, and the $\rho(x,t)$ normalizes beneath ρ_{cr} quickly. The time take by $\rho(x,t)$ to normalize beneath ρ_{cr} is 660 s.

The time taken by ρ with $\alpha = 0.40$ and $\beta = 0.60$ to normalize beneath ρ_{cr} is 360 s and the results are shown in Figure 5.40,. Similary with $\alpha = 0.20$ and $\beta = 0.80$, the results are shown in Figure 5.41, since the ρ_{cr} changes with the increase in PR of CAVs, thus the congested peaks in traffic are reduced, the time taken by $\rho(x,t)$ to normalize beneath ρ_{cr} is 60 s. With $\alpha = 0$ and $\beta = 1$ as in Figure 5.42, the traffic is not congested since the traffic demand is same for all cases, thus, if all vehicles are CAVs, with the current demand there will no congested peaks in traffic, and the evolution of traffic flow will smoother.

Table 5.7. Analysis of the normalization time of ρ beneath ρ_{cr} in traffic mixture.

α	β	time (s) taken to normalize
1	0	1560
0.80	0.20	1080
0.60	0.40	660
0.40	0.60	360
0.20	0.80	60
0	1	–

5.6 Fuel Consumption and Exhaust Emissions

The total fuel consumption and exhaust emissions are investigated subject to assorted PR of CAVs in mixed traffic (HDVs and CAVs) using

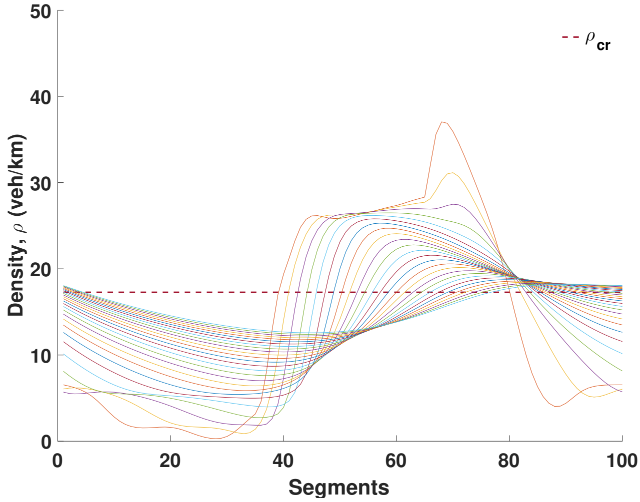

Figure 5.37. Analysis of the normalization of $\rho(x,t)$ beneath ρ_{cr} with $\alpha = 1$ and $\beta = 0$.

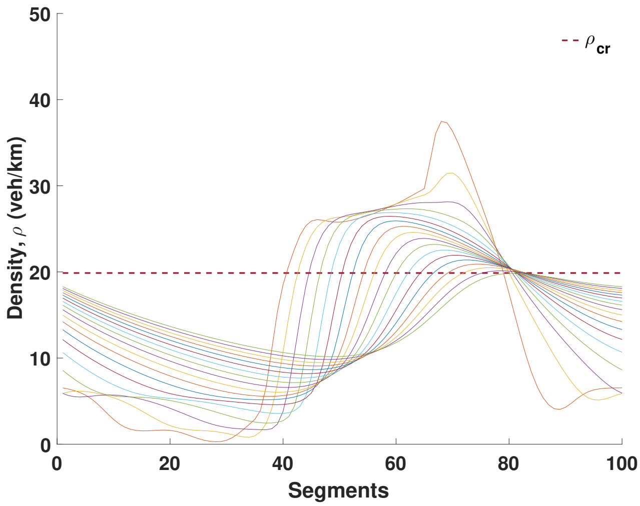

Figure 5.38. Analysis of the normalization of $\rho(x,t)$ beneath ρ_{cr} with $\alpha = 0.80$ and $\beta = 0.20$.

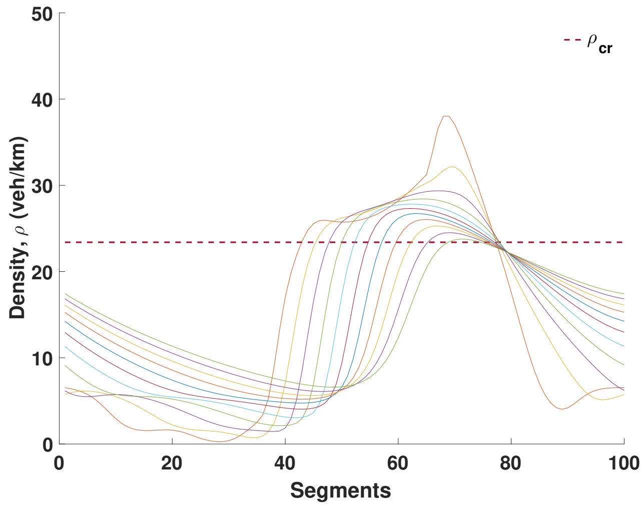

Figure 5.39. Analysis of the normalization of $\rho(x,t)$ beneath ρ_{cr} with $\alpha = 0.60$ and $\beta = 0.40$.

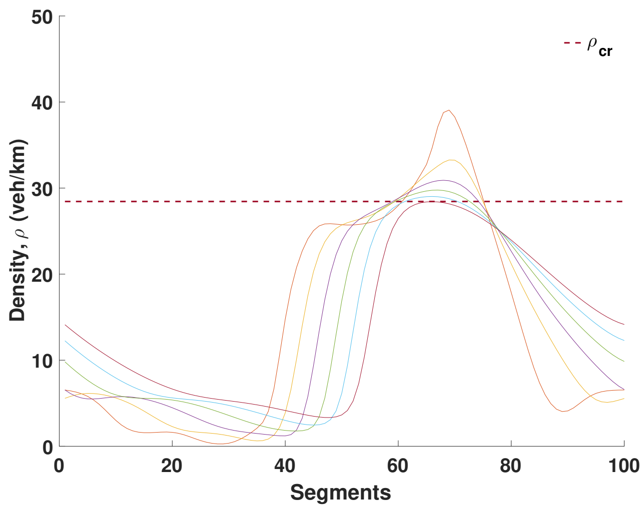

Figure 5.40. Analysis of the normalization of $\rho(x,t)$ beneath ρ_{cr} with $\alpha = 0.40$ and $\beta = 0.60$.

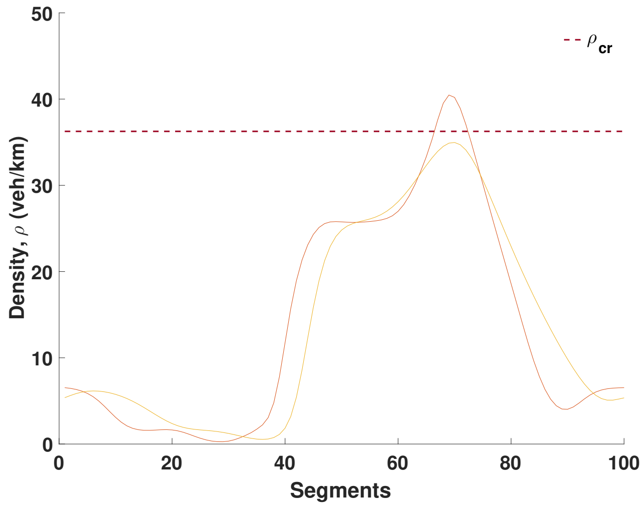

Figure 5.41. Analysis of the normalization of $\rho(x,t)$ beneath ρ_{cr} with $\alpha = 0.20$ and $\beta = 0.80$.

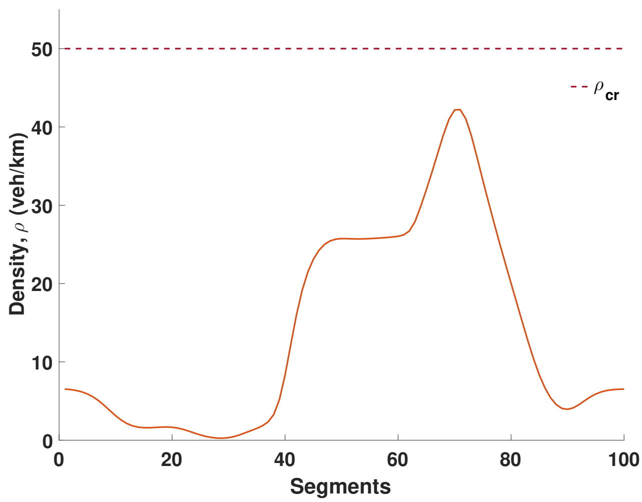

Figure 5.42. Analysis of the normalization of $\rho(x,t)$ beneath ρ_{cr} with $\alpha = 0$ and $\beta = 1$.

Eq. 5.42. The results are shown in Figure 5.43 to Figure 5.46. It is observed that with the increase in the PR of CAVs, the fuel consumption is significantly decreased. With $\alpha = 1$ and $\beta = 0$, the total fuel consumption is 1.3038×10^5 ml which significantly decreases to 5.4856×10^4 ml with $\alpha = 0$ and $\beta = 1$.

The CO emissions are also investigated, significant improvement in reduction of CO emissions is observed. Total emissions with $\alpha = 1$ and $\beta = 0$ are 2.5018×10^5 mg. While CO emissions with $\alpha = 0$ and $\beta = 1$ reduces to 2.4508×10^3 mg. Similar improvemenet is observed for other exhaust emissions such as HC and NOx. Total HC emissions with $\alpha = 1$ and $\beta = 0$ are 8.2999×10^4 mg, which reduces to 1.1723×10^4 mg with $\alpha = 0$ and $\beta = 1$.

The NOx emissions also improve with the increasing PR of CAVs. Total NOx emissions with $\alpha = 1$ and $\beta = 0$ are 1.210×10^5 mg. Later, when $\alpha = 0$ and $\beta = 1$, a significant reduction in NOx emissions is observed, total emissions are estimated to be 1.5524×10^4 mg. The proposed model can be effectively put in practice to evaluate the harmful environmental emissions caused by HDVs. The CAVs will significantly improve the environmental emissions and fuel consumption which is regarded as the most beneficial outcome of the recent technological developments.

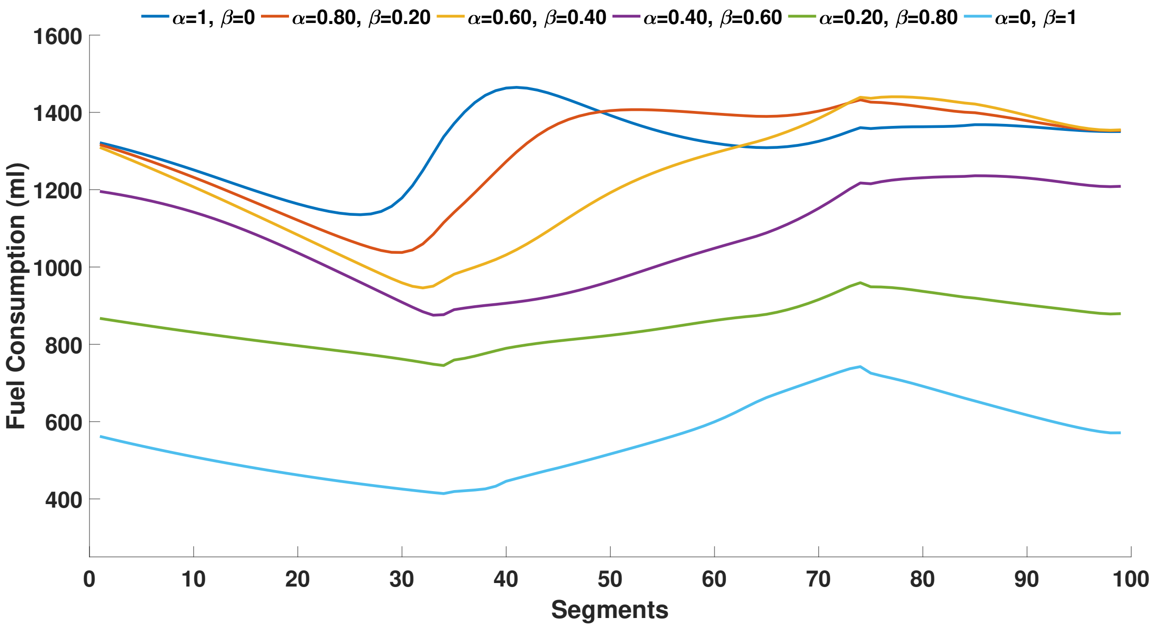

Figure 5.43. Fuel consumption subject to assorted PR of α and β.

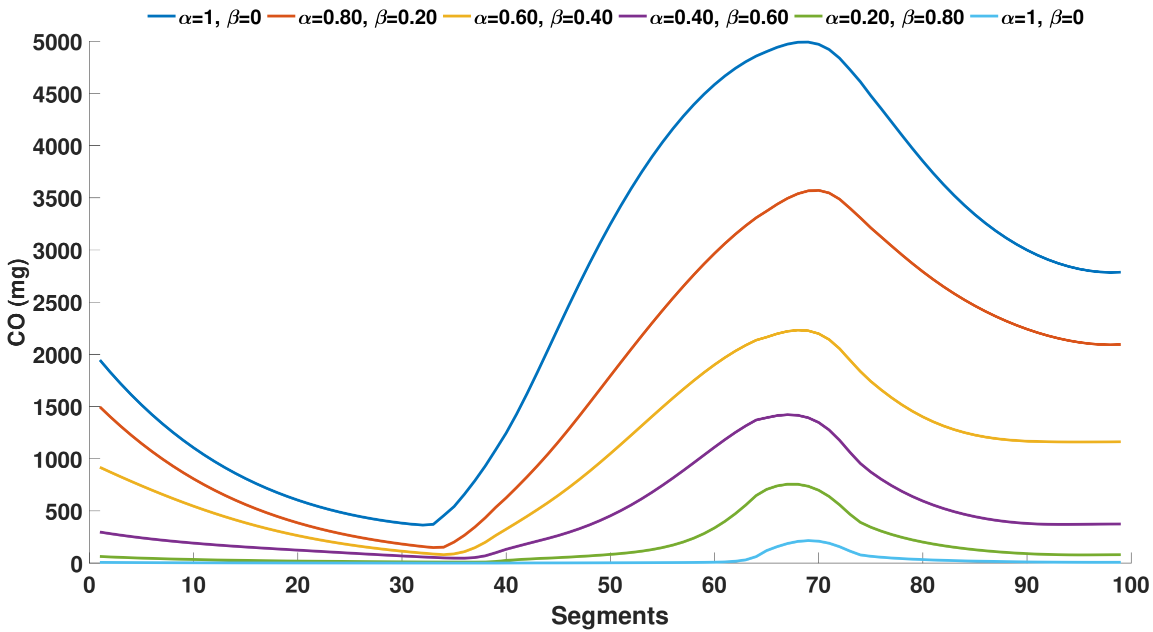

Figure 5.44. CO emissions subject to assorted PR of α and β.

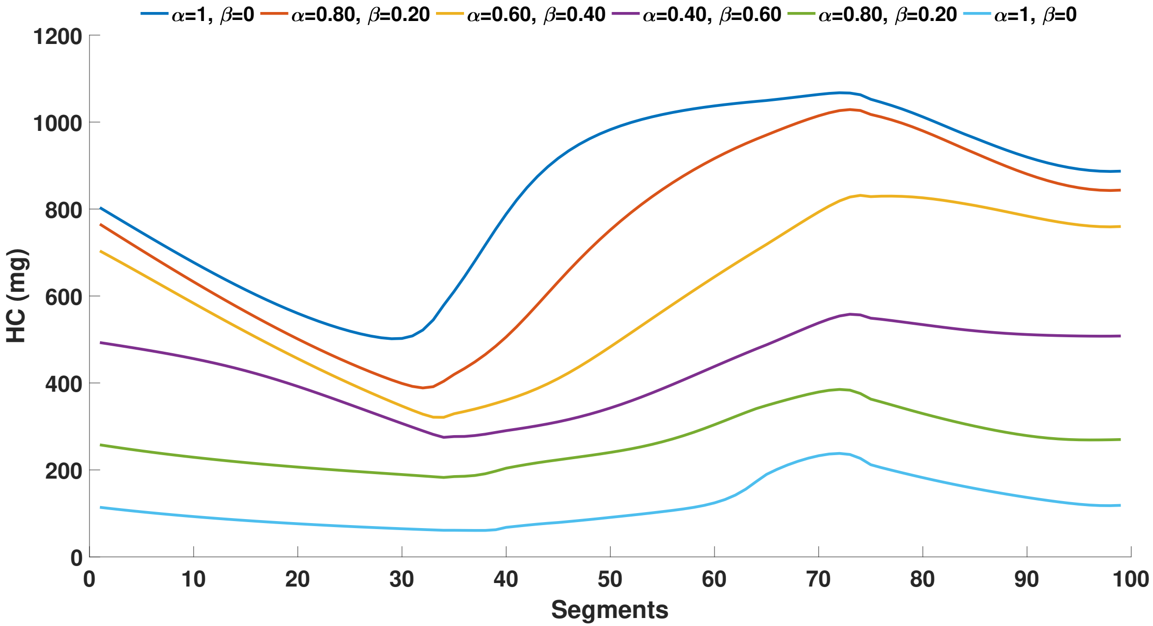

Figure 5.45. HC emissions subject to assorted PR of α and β.

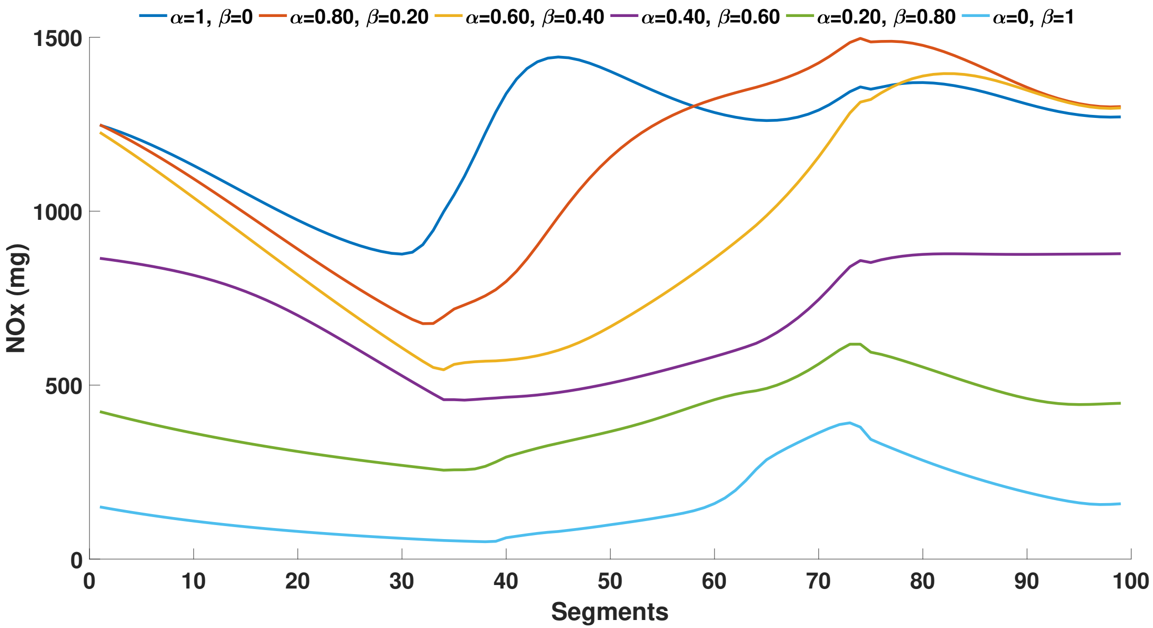

Figure 5.46. NOx emissions subject to assorted PR of α and β.

5.7 Conclusion

A revamped macroscopic traffic flow model for traffic mixture of Human-Driven Vehicles (HDVs), Connected and Autonomous Vehicles (CAVs) and Heavy Vehicles (HVs) is proposed. The proposed model explicitly reckon the dynamics of headway of a traffic mixture. The parameters of the Fundamental Diagram (FD), which are essential for the accurate characterization of flow are computed subject to the class-specific Penetration Rates (PRs). The proposed model is integrated with a macroscopic emissions and fuel consumption model to quantify the improvement resulted by CAVs. The proposed model is tested on a 20 km circular freeway with a congested point to observe the evolution of velocity and density shockwave over space and time horizon caused by the traffic congestion.

First, a traffic mixture of HDVs and CAVs is investigated with the given conditions. It is evident from the results that with the increase in the PR of CAVs in the traffic mixture, the velocity breakdowns are controlled. It is observable that the average velocity (v_{avg}) of the corridor is improved by 67.65% with $\beta = 1$ (CAVs=100%). The density shockwave is tackled soon after it is initiated when $\beta = 1$, and the propagation is smoother as compared to the base scenario where $\alpha = 1$ (HDVs=100%) and $\beta = 0$ (CAVs=0%). The spatio-temporal evolution of velocity is quicker with increasing PR of CAVs.

Conversely, when the PR of HVs is introduced (the PR of HVs is uniform throughout the numerical tests, and a mixture of HDVs, CAVs and HVs is considered), a traffic friction was observed. It is noted that compared to the traffic mixture of HDVs and CAVs, the improvement in v_{avg} is lower. From the base scenario, an improvement of 63.63% is observed. Which is lower than the first case. While this improvement is 64.08% when 5% uniform Connected Heavy Vehicles (CHVs) are considered in traffic mixture of HDVs, CAVs and CHVs.

Exhaust emissions and fuel consumption are computed for traffic mixture of HDVs and CAVs. The total fuel consumption significantly reduces from 1.3038×10^5 ml with $\alpha = 1$ and $\beta = 0$ to 5.4856×10^4 ml with $\alpha = 0$ and $\beta = 1$. The CO emissions decreases from 2.5018×10^5 mg with $\alpha = 1$ and $\beta = 0$ to 2.4508×10^3 mg with $\alpha = 0$ and $\beta = 1$. Similarly, the total HC emissions with $\alpha = 1$ and $\beta = 0$ are 8.2999×10^4 mg, which reduces to

1.1723×10^4 with $\alpha = 0$ and $\beta = 1$. Vital improvement in NOx emissions is recorded. The total NOx emission improve from 1.210×10^5 mg with $\alpha = 1$ and $\beta = 0$ to 1.5524×10^4 mg with $\alpha = 0$ and $\beta = 1$.

Overall, the revised second-order macroscopic traffic flow model account for the unique characteristics of CAVs, and accurately capture the impact of these vehicles on traffic flow. The proposed model can be employed by transportation planners and policymakers to better understand the potential benefits and challenges of CAVs and develop strategies to further maximize their benefits while minimizing their negative impacts. The more, the proposed model can be used in traffic control by designing a control strategy with CAVs.

5.8 Preview of the Next Chapter

In this Chapter, we introduced an integrated macroscopic model that links traffic flow and emissions, proving its potential for understanding mixed traffic dynamics. By integrating microscopic details into the fundamental traffic diagram, we've advanced our understanding of how different vehicle types interact on the road.

The next section presents a new macroscopic model that extends beyond conventional boundaries. This model proactively considers the density-dependent process time of Connected and Autonomous Vehicles (CAVs), emphasizing their minimal reaction time for safe maneuvers. By depicting changes in traffic conditions as a function of density, this approach promises deeper insights into mixed flow dynamics.

Our upcoming objective is to enhance our understanding of mixed traffic and improve safety by modeling optimal process times for CAVs. This will contribute to a more comprehensive and robust model, optimizing CAV operations on highways and informing traffic flow planning for safer and more efficient road networks.

Chapter 6

Macroscopic Evaluation of Traffic Flow in view of Connected and Autonomous Vehicles: A Simulation-based approach

6.1 Abstract

The macroscopic evaluation of road traffic characteristics is vital as they will alter significantly with the emergence of Connected and Autonomous Vehicles (CAVs). The macroscopic second-order traffic flow models are emerging as essential tools to observe the evolutionary dynamics of traffic flow. These models are significantly improved to describe the dynamics of traffic flow in view of Human-Driven Vehicles (HDVs). However, proficient macroscopic second-order traffic flow models are indispensable in comprehending and elucidating the descriptions of traffic flow dynamics, particularly in view of evolving CAVs. Therefore, we propose a macroscopic second-order traffic model that distinguishes CAVs from HDVs by meticulously considering their distinct driving characteristics. The proposed model incorporates lengthways between the vehicles,

and the reaction time of the CAVs, and is evaluated on a 20,000 m ring road. The findings show that with smaller lengthways and reaction times of CAVs, traffic evolves quickly during transitions. An increase in average traffic velocity is observed as the reaction time is significantly small. It has been demonstrated that CAVs can significantly limit variations in velocity resulting in smoother flow operations.

6.2 Introduction

The macroscopic traffic flow models are vital for the characterization of traffic flow because they provide a simplified, but accurate description of traffic behavior. These models rely on empirical data and mathematical principles, predicting traffic patterns, analyzing traffic congestion, and allowing users to evaluate freeways' efficiency. The macroscopic models consider aggregate traffic variables such as velocity (v), density (ρ) and flow (q), thus, providing a simplified view of traffic behavior in time and space. This simplification allows for the analysis of traffic flow at an aggregated level, making it easier to understand traffic patterns and congestion dynamics [162]. Further, macroscopic models can be employed to analyze traffic flow on various spatial and temporal scales such as from single intersections to entire transportation networks. In addition, the macroscopic models are computationally efficient, making them well-suited for real-time traffic management and control [37].

Overall, the macroscopic traffic flow models are essential for characterizing traffic flow because they provide a simplified yet accurate representation of traffic behavior on a larger scale, allowing for efficient transportation planning and management. However, they are yet to be analyzed if these models could be used for the evaluation of traffic flow with emerging Connected and Autonomous Vehicles (CAVs). In the context of traffic flow, complex driving behaviors at the microscopic level exert a profound influence on the overall dynamics of traffic [17]. The advent of CAVs holds great promise for enhancing the microscopic traffic characteristics. However, the extent of the positive impacts remains largely unexplored, requiring the development of robust and computationally efficient tools (traffic models). To the best of our knowledge, existing macroscopic traffic models have not been extended to encompass the unique attributes of CAVs adequately. Consequently, to bridge this gap, our study aims to propose a second-order macroscopic model that investigates and optimizes network efficiency in view of CAVs by refining the underlying properties of CAVs.

6.3 The Macroscopic Second-Order Traffic Flow Model for Connected and Autonomous Vehicles

The longitudinal gap between two vehicles in a traffic stream is lengthways gap. The minimum distance between two vehicles to ensure that the driver of the following vehicle has enough time to react to unforeseen changes in forward traffic is a minimum lengthways gap. The total lengthways gap is the sum of the minimum lengthways gap and the distance traveled by the vehicle during the driver's reaction time. In other words, it is the gap between two consecutive vehicles that includes both the gap between the vehicles and the distance traveled by the leading vehicle while the driver of the following vehicle reacts to any situation. The properties of traffic flow are impacted by lengthways gap. It determines the capacity of a roadway or a traffic lane. If the lengthways gap is small, more vehicles can pass through a given point in a given time, leading to higher traffic flow rates. Second, lengthways gap affects traffic safety. With small lengthways gap there is a risk of accidents. Conversely, with large lengthways gap, road capacity reduces.

The anisotropic behavior of a driver refers to the response to traffic ahead [163, 99]. During traffic alignment to conditions ahead, a driver always maintains a safe lengthways gap. Thus, the total lengthways gap as a function of velocity is

$$l_s(v(x,t)) = l_g + (\tau_r \times v(x,t)), \tag{6.1}$$

where l_g is the minimum lengthways gap between vehicles, τ_r is the reaction time, and $v(x,t)$ is the average velocity. In a similar manner, considering the safe time which is the sum of density-dependent reaction time, and the safe time over which the vehicles harmonize to a change in traffic, this time is transition occurrence time, and is

$$\tau(\rho(x,t)) = \frac{\tau_{r(min)}}{\frac{\rho(x,t)}{\rho_m}} + \tau_h, \tag{6.2}$$

where $\tau_{r(min)}$ is the minimum reaction time of CAVs, $\rho(x,t)$ is average density, ρ_m is maximum density, and τ_h is the harmonization time [40]. Practically, the harmonization time for any given traffic condition can be computed as

$$\tau_h = \frac{\tau_{r(min)} \times v_m}{v(x,t)}, \tag{6.3}$$

where v_m is maximum velocity. Thus, substituting Eq. (6.3), Eq. (6.2) gives

$$\tau(\rho(x,t)) = \frac{\tau_{r(min)}}{\frac{\rho(x,t)}{\rho_m}} + \frac{\tau_{r(min)} \times v_m}{v(x,t)}. \tag{6.4}$$

Eq. (6.4) is the density-dependent transition time over which the total lengthways gap is maintained.

Since the backward propagation speed of traffic perturbation is given by c_0 in the second-order model, it corresponds to driver behavior. It is characterized by reaction velocity [164], and this reaction velocity is based on safe lengthways gap and density-dependent transition time [5] is

$$\vartheta = \frac{l_s(v(x,t))}{\tau(\rho(x,t))}. \tag{6.5}$$

According to Eq. 6.5, the reaction velocity of the vehicles will vary according to the traffic conditions. Over traffic transitions, the $\tau(\rho(x,t))$ will be small due to the smaller $\tau_{r(min)}$ and τ_h allowing rapid change in traffic state over considerably small $l_s(v(x,t))$. This distinguishes the reaction velocity of CAVs from HDVs as the HDVs' $\tau_{r(min)}$ and l_g differ from that of the CAVs.

Thus, replacing the c_0 in Eq. (2.8) with ϑ, the proposed model is

$$\begin{aligned} &\frac{\partial \rho}{\partial x} + \frac{\partial \rho(x,t) \cdot v(x,t)}{\partial t} = 0, \\ &\frac{\partial v(x,t)}{\partial t} + (v(x,t) - \vartheta)\frac{\partial v(x,t)}{\partial x} = \frac{V(\rho(x,t)) - v(x,t)}{T}. \end{aligned} \tag{6.6}$$

The proposed second-order model is numerically solved by employing a conservative scheme proposed by [52]. The density dynamics are computed as

$$\rho_i^{n+1} = \rho_i^n + \frac{\Delta t}{\Delta x}(\rho_i^n(v_i^n - v_{i+1}^n)) + \frac{\Delta t}{\Delta x} v_i^n(\rho_{i-1}^n - \rho_i^n), \tag{6.7}$$

where the subscripts i and n are space and time indices. The velocity dynamics is computed according to Eq. (6.6) which if

$$v_i^n \leq \vartheta$$

is

$$v_i^{n+1} = v_i^n + \frac{\Delta t}{\Delta x}(\vartheta - v_i^n)(v_{i+1}^n - v_i^n) + \frac{\Delta t}{T}(V(\rho_i^n) - v_i^n), \tag{6.8}$$

and otherwise, it is

$$v_i^{n+1} = v_i^n + \frac{\Delta t}{\Delta x}(\vartheta - v_i^n)(v_i^n - v_{i-1}^n) + \frac{\Delta t}{T}(V(\rho_i^n) - v_i^n). \tag{6.9}$$

where Δx and Δt are the road and time steps. Furthermore, this scheme is only stable if the Courant-Friedrichs-Lewy (CFL) condition [156] is satisfied, that is

$$v_m \frac{\Delta t}{\Delta x} \leq 1, \tag{6.10}$$

we have ensured this necessary condition in our numerical simulations.

The speed-density relationship [19] is employed for $V(\rho)$. It is given as

$$V(\rho(x,t)) = v_m \cdot \exp\left[\frac{-1}{c}\left(\frac{\rho}{\rho_{cr}}\right)^c\right], \tag{6.11}$$

where c corresponds to shape factor, and ρ_{cr} is the critical density. It is computed as a footprint of $l_s(v(x,t))$ during free flow conditions such as $1/l_s(v(x,t))$ which ensures that ρ_{cr} will vary according to the change in $\tau_{r(min)}$. For mixed traffic, ρ_{cr} can be computed by introducing the Penetration Rate (PR) and parameters of HDVs as $1/(((\alpha) \times l_s(v(x,t)) + ((1-\alpha) \times l_s(v(x,t)))$, where α is the penetration rate of CAVs. The parameters of HDVs are given in Section 6.4.9.

6.4 Numerical Simulation of the Proposed Model in all-CAVs Environment

The proposed model in view of CAVs is evaluated in this Section. Numerical simulations are performed over a 20,000 m ring road with periodic boundary conditions such as

$$\rho(L,t) = \rho(0,t),\ v(L,t) = v(0,t). \tag{6.12}$$

The simulation parameters are given in Table 6.1. Total simulation time T_s is 1800 s. Different values for l_g and $\tau_{r(min)}$ are employed to quantify their impacts on the traffic flow.

Table 6.1. Parameters for the Simulation.

Description	Notation	Value	Unit
Lengthways gap	l_g	12, 15, 17, 20,	m
Minimum reaction time	$\tau_{r(min)}$	0.2, 0.4, 0.6, 0.8, 1	s
Maximum velocity	v_m	28	m/s
Velocity-Density relation	$V(\rho(x,t))$	[19]	m/s
Shape factor	c	1	-
Length of Corridor	X	20,000	m
Road Step	Δx	200	m
Time Step	Δt	1	s
Segments	i	100	-
Simulation time	T_s	1800	s
Relaxation time	T	15	s

6.4.1 Analysis of average velocity subject to assorted minimum reaction times of CAVs

The impact of $\tau_{r(min)}$ on the average velocity of the corridor is analyzed in this Section. Velocity evolution improves with a significantly small $\tau_{r(min)}$, results are given in Table 6.2. It is observable that average velocity increases from 16.30 m/s to 21.30 m/s when $\tau_{r(min)}$ is reduced from 1 s to 0.2 s. In Fig. 6.1, the impact of $\tau_{r(min)}$ on the average velocity of the corridor is presented. With $\tau_{r(min)}$=1 s, the velocity behavior is not smooth. Between segments 68 and 72, the average velocity is minimum. Clearly, as a result of the minimum average velocity occurrence, the velocity behavior upstream is affected. But when $\tau_{r(min)}$=0.2 s, the velocity behavior is smooth, and significant improvement is observable.

Table 6.2. Evaluation of average velocity over the entire corridor with varying $\tau_{r(min)}$.

$\tau_{r(min)}$ (s)	1	0.8	0.6	0.4	0.2
v (m/s)	16.30	17.32	18.53	19.85	21.30

6.4.2 Analysis of average velocity (v) subject to assorted minimum gap minimum gap

The impact of l_g on the average velocity of the corridor is analyzed in this Section. In all, the average velocity of the corridor improves with small l_g, results are given in Table 6.3. CAVs are able to maintain small gaps between each other. It is observable that average velocity increases from 18.03 m/s to 20.01 m/s when l_g is reduced from 20 m to 12 m. The $\tau_{r(min)}$ is uniform for all the varying values of l_g, and it is 0.5 s. In Fig. 6.2, the impact of l_g on the average velocity of the corridor is demonstrated. With l_g=20 m, the velocity behavior is not smooth. Between segments 68 and 72, the average velocity is minimum. Clearly, as a result of the minimum average velocity occurrence, the velocity behavior upstream is also affected. But when l_g=12 m, the velocity behavior is fairly smooth, and significant improvement is observable.

Table 6.3. Evaluation of average velocity over the entire corridor with varying l_g.

l_g (s)	20	17	15	12
v (m/s)	18.03	18.71	19.17	20.01

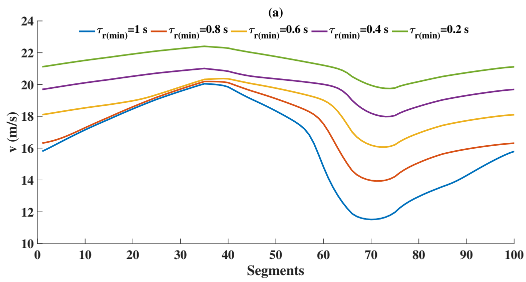

Figure 6.1. Average velocity over the corridor with varying $\tau_{r(min)}$ and fixed l_g=15 m.

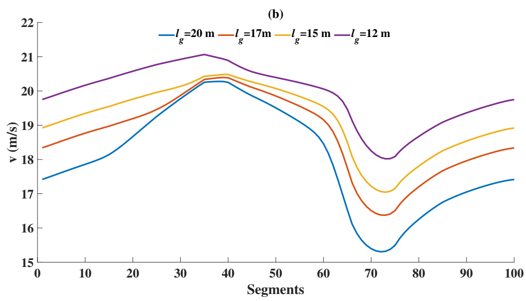

Figure 6.2. Average velocity over the corridor with varying l_g and fixed $\tau_{r(min)}$=0.5 s.

6.4.3 Analysis of critical density subject to assorted minimum reaction time and lengthways gap

The impact of $\tau_{r(min)}$ and l_g on ρ_{cr} is evaluated in this Section. There is a significant improvement in ρ_{cr} when $\tau_{r(min)}$ and l_g are small. The impact of $\tau_{r(min)}$= 1 s, 0.8 s, 0.6 s, 0.4 s and 0.2 s and l_g= 15 m and 12 m are particularly evaluated. The results are tabulated in Table 6.4. For all values of $\tau_{r(min)}$, two assorted values of l_g are considered. When $\tau_{r(min)}$=1 s and l_g=15 m, the ρ_{cr} is 0.023 veh/m which is almost similar to an all HDVs environment. When $\tau_{r(min)}$=1 s and l_g=12 m, the ρ_{cr} is 0.025 veh/m, it reflects with small gaps among the vehicles, the capacity increases. When $\tau_{r(min)}$=0.8 s and l_g=15 m, the ρ_{cr} is 0.026 veh/m, and it increases to 0.029 veh/m when $\tau_{r(min)}$=0.8 s and l_g=12 m.

Similarly, when $\tau_{r(min)}$=0.6 s and l_g=15 m, the ρ_{cr} is 0.031 veh/m which increases to 0.034 veh/m when $\tau_{r(min)}$=0.6 s and l_g=12 m. The ρ_{cr} is 0.038 when $\tau_{r(min)}$=0.4 s and l_g=15 m while it increases to 0.043 veh/m when $\tau_{r(min)}$=0.4 s and l_g=12 m. When $\tau_{r(min)}$=0.2 s and l_g=15 m, the ρ_{cr} is 0.048 veh/m which increases to 0.056 veh/m when $\tau_{r(min)}$=0.2 s and l_g=12 m. It is evident from the results that smaller $\tau_{r(min)}$ and l_g result in higher ρ_{cr}. Thus, it can be concluded that road capacity alters significantly in the presence of CAVs.

Table 6.4. Analysis of ρ_{cr} with assorted τ_r and l_g.

τ_r (s)	l_g (m)	ρ_{cr} (veh/m)
1	15	0.023
	12	0.025
0.8	15	0.026
	12	0.029
0.6	15	0.031
	12	0.034
0.4	15	0.038
	12	0.043
0.2	15	0.048
	12	0.056

6.4.4 Spatio-temporal evolution of density and velocity with minimum gap=12 m and minimum reaction time=1 s

The spatio-temporal evolution of density over the corridor for 1800 s with $\tau_{r(min)} = 1$ s and $l_g = 12$ m is shown in Figure 6.3. The main performance indicator to evaluate the density evolution with varying characteristics is the spillback distance and time of the density shockwave. Initially, a very strong traffic congestion (perturbation) point (inactive bottleneck) is created to generate the density shockwave. The tail of perturbation is segment 67, while over time, the density shockwave originates, and the spillback is observed until segment 59 for 493 s, after which shockwave is observed to dissipate. Overall, the evolution of density shockwave is slow, and the spillback impacts traffic upstream. Next, the velocity evolution is assessed, and then the $\tau_{r(min)}$ is changed to analyze its impact on the spatio-temporal evolution of density and velocity.

The spatio-temporal evolution of velocity over the corridor for 1800 s with $\tau_{r(min)} = 1$ s and $l_g = 12$ m is shown in Figure 6.4. Initially, velocity breakdown occurs, and the minimum velocity of the congestion is observed to 4.94 m/s. The velocity of the density spillback is observed to vary between 4.94 m/s and 7.97 m/s which improves with time. With the dissipation of density shockwave, the velocity evolution witnessed improvement and reached 14.50 m/s after 1800 s. For a more clear elaboration of the results, the spillback velocity represented by a line (impact line) and impact zone with a triangle is shown in Figure 6.5. For the sake of comparison, we will be referring to the impact line and impact zone from Figure 6.5.

6.4.5 Spatio-temporal evolution of density and velocity with minimum gap=12 m and minimum reaction time=0.8 s

The spatio-temporal evolution of density over the corridor for 1800 s with $\tau_{r(min)} = 0.8$ s and $l_g = 12$ m is shown in Figure 6.6. In this case, the tail of perturbation is segment 67, while over time density shockwave originates, and the spillback is observed until segment 61 for 428 s, after which shockwave is observed to dissipate. Overall, the evolution of density

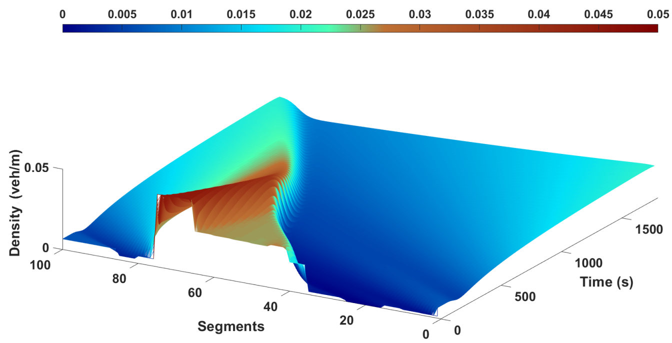

Figure 6.3. Spatio-temporal evolution of density over the corridor for 1800 s with $\tau_{r(min)}$= 1 s and l_g= 12 m.

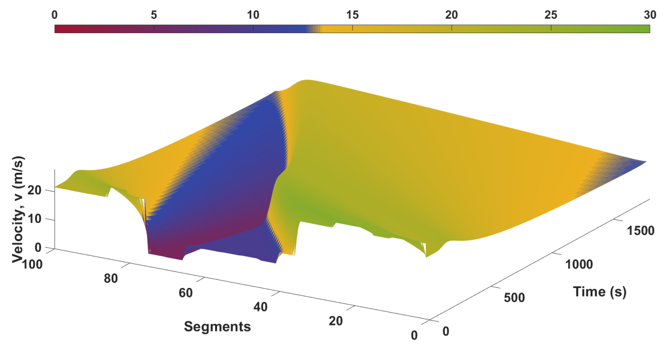

Figure 6.4. Spatio-temporal evolution of velocity over the corridor for 1800 s with $\tau_{r(min)}$= 1 s and l_g= 12 m.

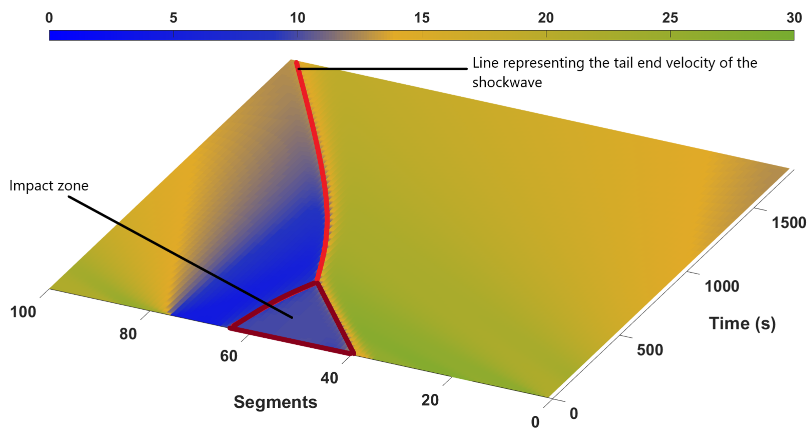

Figure 6.5. Conceptual representation of the impact line and impact zone.

shockwave slightly improves, and the spillback impacts traffic upstream. The impact zone is smaller as compared to the previous case.

The spatiotemporal evolution of velocity over the corridor for 1800 s with $\tau_{r(min)} = 0.8$ s and $l_g = 12$ m is shown in Figure 6.7. Initially, velocity breakdown occurs, and the minimum velocity of the congestion is observed to 5.90 m/s. The velocity of the density spillback is observed to vary between 5.90 m/s and 10.83 m/s which improves with time. With the dissipation of the density shockwave, the velocity evolution witnessed improvement and reached 15.11 m/s after 1452 s.

6.4.6 Spatio-temporal evolution of density and velocity with minimum gap=12 m and minimum reaction time=0.6 s

The spatio-temporal evolution of density over the corridor for 1800 s with $\tau_{r(min)} = 0.6$ s and $l_g = 12$ m is shown in Figure 6.8. The tail of perturbation is segment 67, while over time density shockwave originates, and the spillback is observed until segment 64 for 394 s, after which the shockwave is observed to dissipate. Overall, the evolution of density shockwave improves, and the spillback impacts traffic upstream. The impact zone is smaller as compared to that with $\tau_{r(min)} = 1$ s and 0.8 s.

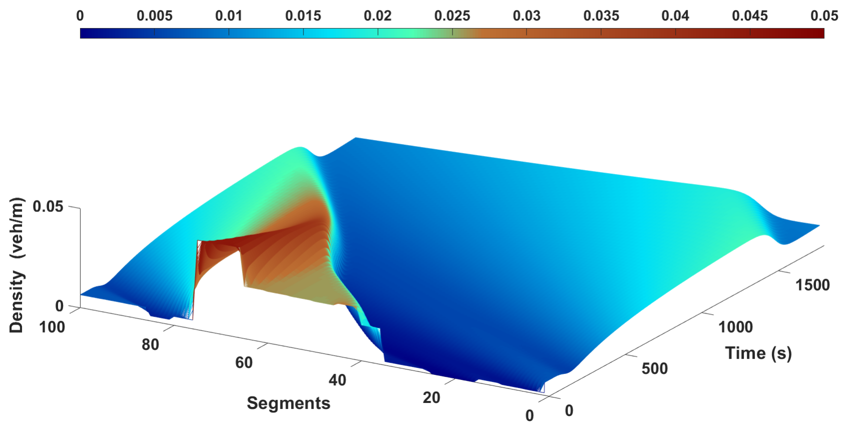

Figure 6.6. Spatio-temporal evolution of density over the corridor for 1800 s with $\tau_{r(min)}$= 0.8 s and l_g= 12 m.

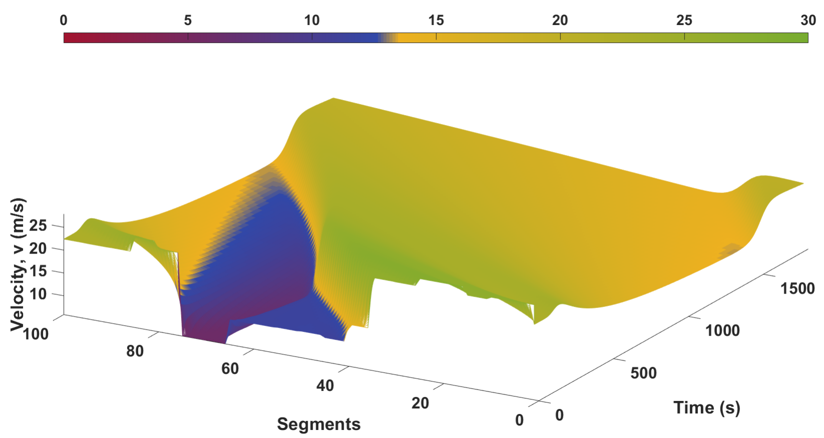

Figure 6.7. Spatio-temporal evolution of velocity over the corridor for 1800 s with $\tau_{r(min)}$= 0.8 s and l_g= 12 m.

The spatio-temporal evolution of velocity over the corridor for 1800 s with $\tau_{r(min)} = 0.6$ s and $l_g = 12$ m is shown in Figure 6.9. Velocity breakdown occurs initially, the minimum velocity of the congestion is observed to 7.70 m/s. The velocity of the density spillback is observed to vary between 7.70 m/s and 13.50 m/s which improves with time. With the dissipation of density shockwave the velocity evolution witnessed improvement and reached 18.80 m/s after 1191 s.

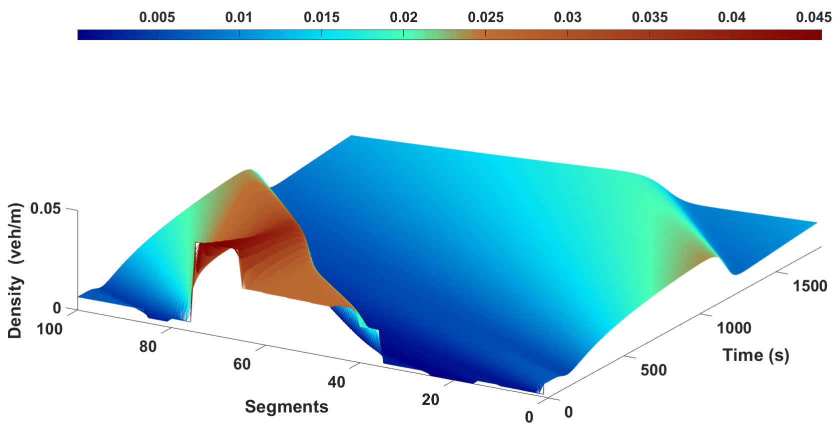

Figure 6.8. Spatio-temporal evolution of density over the corridor for 1800 s with $\tau_{r(min)}$= 0.6 s and l_g= 12 m.

6.4.7 Spatio-temporal evolution of density and velocity with minimum gap=12 m and minimum reaction time=0.4 s

The spatio-temporal evolution of density over the corridor for 1800 s with $\tau_{r(min)} = 0.4$ s and $l_g = 12$ m is shown in Figure 6.10. The tail of perturbation is segment 67, while over time density shockwave originates, and the spillback is observed until segment 66 for 204 s, after which the shockwave is observed to dissipate. Overall, the evolution of density significantly improves, and the spillback has less impact on the upstream traffic. The impact zone is considerably small as compared to that with $\tau_{r(min)} =$ 1 s, 0.8 s and 0.6 s.

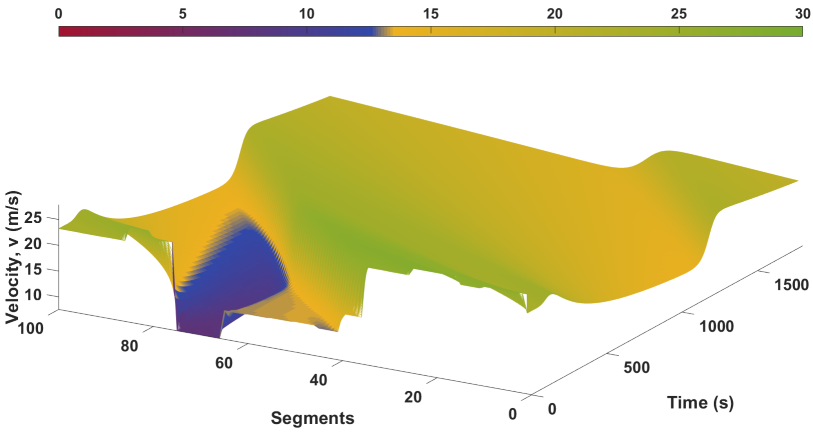

Figure 6.9. Spatio-temporal evolution of velocity over the corridor for 1800 s with $\tau_{r(min)}$= 0.6 s and l_g= 12 m.

The spatio-temporal evolution of velocity over the corridor for 1800 s with $\tau_{r(min)}$ = 0.4 s and l_g = 12 m is shown in Figure 6.11. Velocity breakdown occurs initially, the minimum velocity of the congestion is observed to 10.82 m/s. The velocity of the density spillback is observed to vary between 10.82 m/s and 15.40 m/s which further improves with time. With the dissipation of the density shockwave, the velocity evolution is smooth and reaches 21.90 m/s after 976 s.

6.4.8 Spatio-temporal evolution of density and velocity with minimum gap=12 m and minimum reaction time=0.2 s

The spatio-temporal evolution of density over the corridor for 1800 s with $\tau_{r(min)}$ = 0.2 s and l_g = 12 m is shown in Figure 6.12. The tail of perturbation is segment 67, it is observable that there is no spillback of density shockwave. The congestion dissipates soon and has almost negligible impact on upstream traffic. Moreover, the evolution of density is significantly faster without deteriorating the upstream while the impact zone is negligible.

The spatio-temporal evolution of velocity over the corridor for 1800

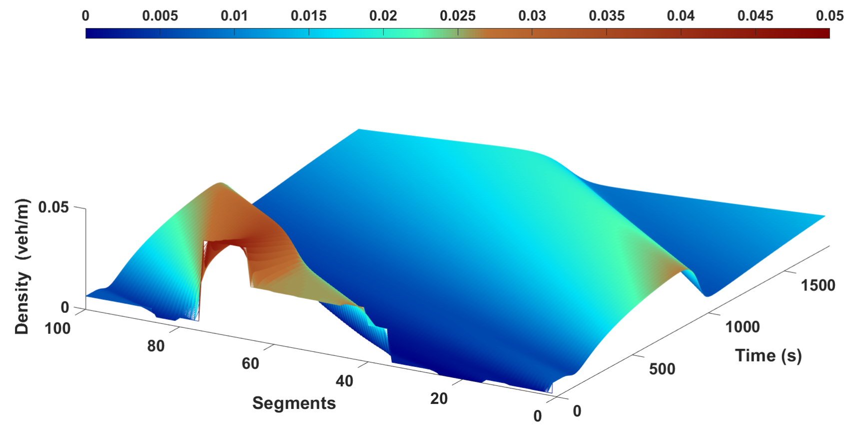

Figure 6.10. Spatio-temporal evolution of density over the corridor for 1800 s with $\tau_{r(min)}$= 0.4 s and l_g= 12 m.

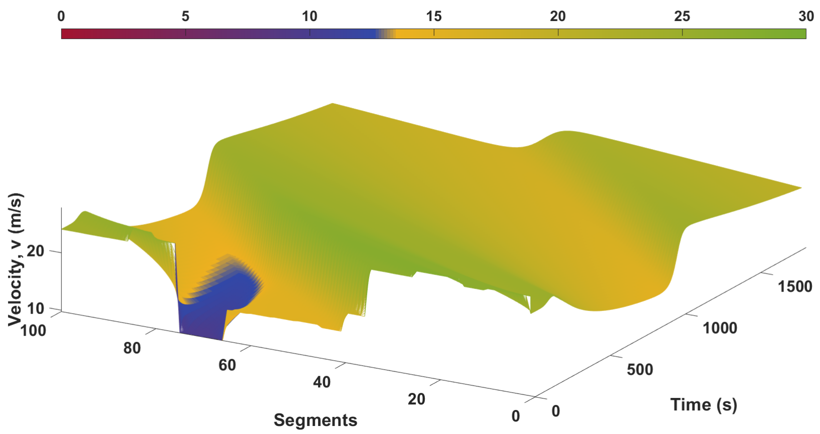

Figure 6.11. Spatio-temporal evolution of velocity over the corridor for 1800 s with $\tau_{r(min)}$= 0.4 s and l_g= 12 m.

s with $\tau_{r(min)} = 0.2$ s and $l_g = 12$ m is shown in Figure 6.13. Velocity breakdown occurs initially as a response to initial perturbation, but this breakdown is recovered as soon as it occurs. The minimum velocity of the congestion is observed to 14.20 m/s. With the dissipation of the congestion the velocity reaches 25.10 m/s after 800 s.

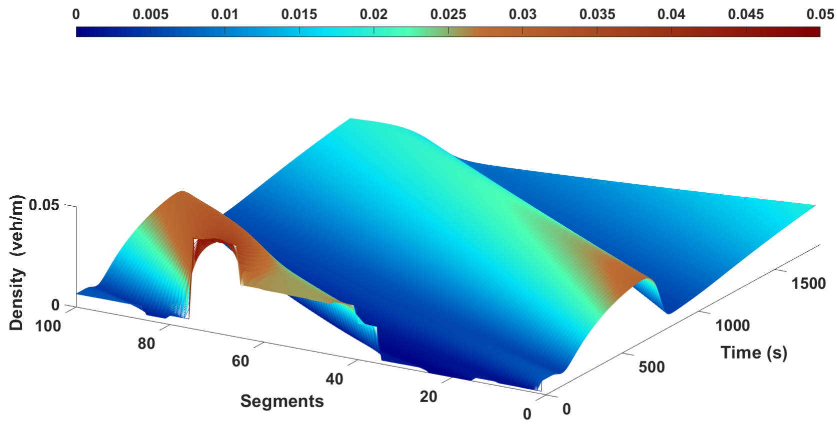

Figure 6.12. Spatio-temporal evolution of density over the corridor for 1800 s with $\tau_{r(min)}$= 0.2 s and l_g= 12 m.

6.4.9 Comparative Evaluation of the Traffic Flow Dynamics in Mixed Traffic Environment

This section unveils the outcomes of the comparative analysis performed to assess traffic flow in the coexistence of CAVs and HDVs. The analysis takes into account three different scenarios: the first, all the vehicles are HDVs, the second scenario has 100% CAVs, while the third replicates a balanced composition where 50 % of the vehicles are CAVs and the remaining are HDVs.

The spatio-temporal evolution of velocity with HDVs is shown in Figure 6.14. Overall, lower velocity trends are observable. The velocity evolution is slower, and the breakdowns are higher. The impact zone and line are greater. Furthermore, the evolution is not smooth compared to the velocity evolution of CAVs in Figure 6.15. This situation is due to the fact

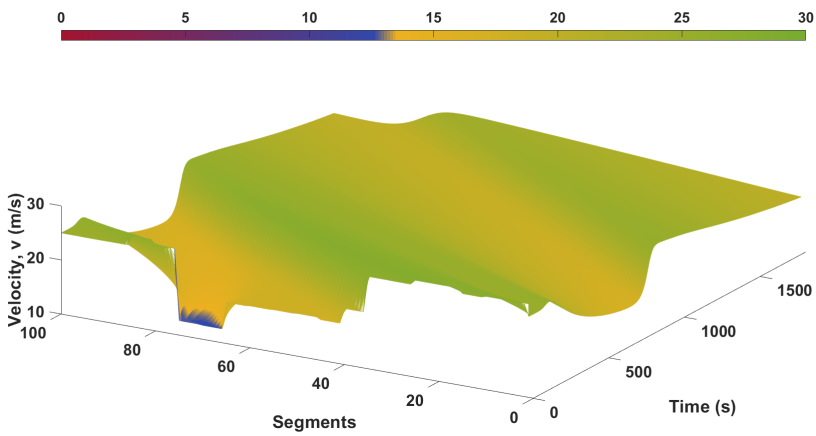

Figure 6.13. Spatio-temporal evolution of velocity over the corridor for 1800 s with $\tau_{r(min)}$= 0.2 s and l_g= 12 m.

that HDVs have larger $\tau_{r(min)}$ compared to CAVs. For HDVs, the $\tau_{r(min)}$ is 1 s, while for the CAVs it is 0.2 s. The comparative analysis is further supported by analyzing the variance of velocity in all the cases, discussed later.

Conversely, the velocity evolution in all-CAVs environment is smooth as illustrated in Figure 6.15, and the velocity breakdowns and variations are limited. The impact zone is significantly reduced while the evolution patterns are sufficiently smooth. The perturbations are recovered soon due to the small $\tau_{r(min)}$ of CAVs. Furthermore, the results are expanded in the mixed traffic environment (50% CAVs and 50% HDVs) as shown in Figure 6.16. The differences between all-CAVs and all-HDVs environments are clearly observable. Compared to all-HDVs environment, significant advancements are observed in the velocity evolution. The perturbations are recovered soon while the velocity impact zone and line sufficiently improve. This qualitative analysis of spatio-temporal evolution of velocity allows us to acknowledge significant advancement caused by the penetration of CAVs in the network.

To further enhance the outcomes of this study, we illustrate the variance of velocity in three different traffic scenarios as explained earlier in this section. The variance of velocity is shown in Figure 6.17. In all-HDVs environment the variance of velocity vary between 4.12 and 67.41 for the total simulation time. From the results, we conclude that the variations in traffic are larger as large variations are illustrated in Figure 6.14. In mixed environment, the variance of velocity varies between 2.88 and 49.01. The variance of velocity reduces significantly in this scenario due to the penetration of CAVs.

The dynamics of traffic alter significantly with CAVs in the network. In all-CAVs environment, the variance of velocity varies between 2.05 and 26.12. The variance of velocity reduces significantly in this scenario. Results justify that with the advent of CAVs, the traffic dynamics improve significantly, and the velocity evolution is smoother resulting in higher flows, improved critical density, and maximized jam density. Moreover, due to the smoother evolution of velocity, the corresponding perturbations (variations) in traffic flow are minimized.

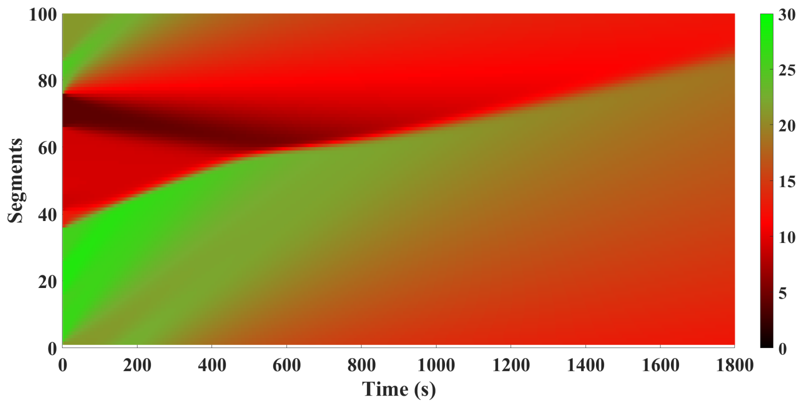

Figure 6.14. Spatio-temporal evolution of velocity over the corridor for 1800 s with $\tau_{r(min)}$= 1 s in all-HDVs environment.

6.5 Conclusion

A macroscopic second-order traffic flow model is proposed to evaluate traffic flow in view of Connected and Autonomous Vehicles (CAVs). CAVs are assumed to maintain smaller gaps (lengthways) among the vehicles

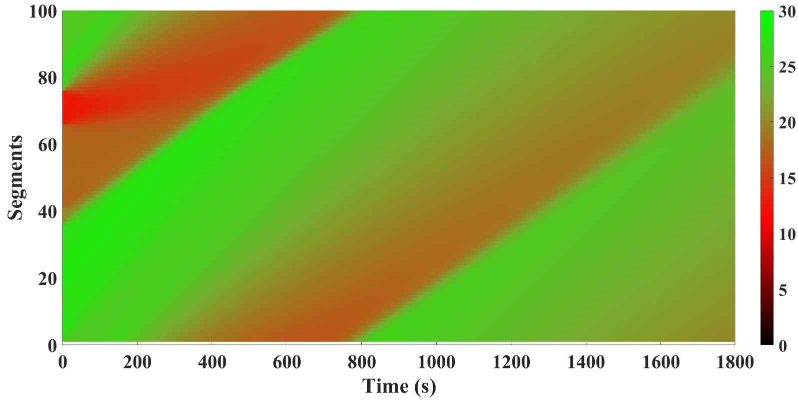

Figure 6.15. Spatio-temporal evolution of velocity over the corridor for 1800 s with $\tau_{r(min)}$= 0.2 s and l_g= 12 m in all-CAVs environment.

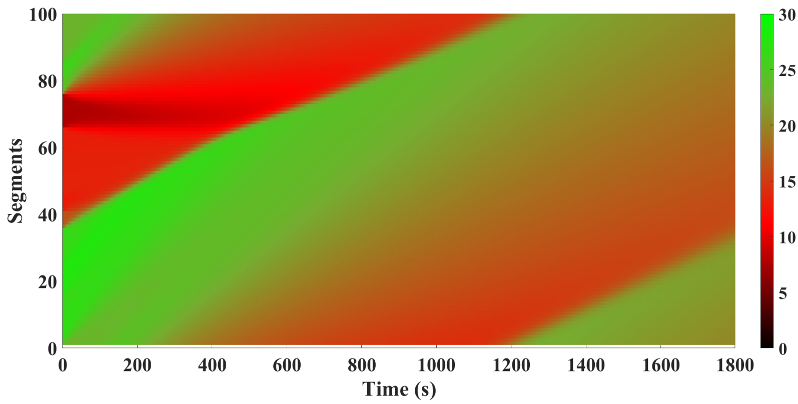

Figure 6.16. Spatio-temporal evolution of velocity over the corridor for 1800 s with $\tau_{r(min)}$= 0.2 s for CAVs and $\tau_{r(min)}$= 1 s for HDVs in mixed-environment.

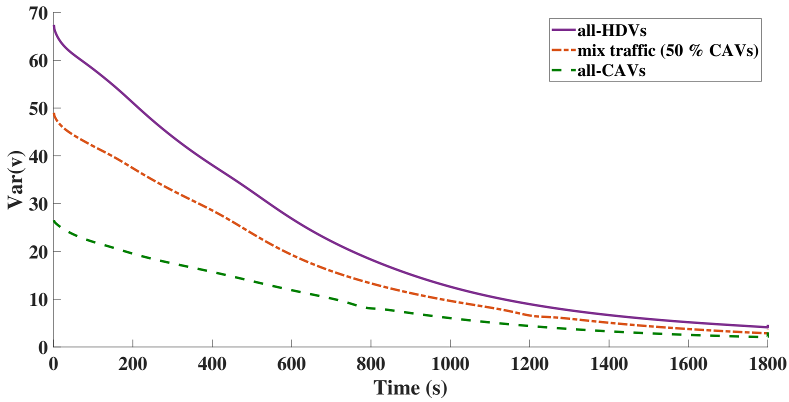

Figure 6.17. Variance of velocity over the corridor for 1800 s for **a)** all-HDVs, **b)** mixed traffic and **c)** all-CAVs.

and run with extremely small reaction times ($\tau_{r(min)}$) compared to Human-Driven Vehicles (HDVs). The macroscopic second-order traffic flow models have been extensively revised for HDVs in the past decade. But to evaluate the characteristics of traffic flow in view of CAVs, a more detailed macroscopic second-order traffic model is needed which can accurately and more realistically characterize traffic flow centered on the properties of CAVs. For this purpose, a new model is proposed which incorporates the dynamics of traffic flow more efficiently. This model considers the lengthways $l_s(v(x,t))$ among vehicles. Factors such as $\tau_{r(min)}$ and minimum lengthways gap (l_g) of CAVs are explicitly employed to describe traffic dynamics.

Numerical simulations are performed in all-CAVs, all-HDVs and a mixed environment such that 50% CAVs and the remaining are HDVs. Assorted values of $\tau_{r(min)}$ and l_g are used to quantify the impact of CAVs of the average behavior of traffic flow. First, the average velocity is analyzed, and it is observable that the average velocity of the ring road significantly improves with smaller values of $\tau_{r(min)}$. The average velocity of the ring road increases from 16.30 m/s to 21.30 m/s when $\tau_{r(min)}$ is reduced from 1 s to 0.2 s. While the average velocity increases from 18.03 m/s to 20.01 m/s varying the l_g from 20 m to 12 m. As a result of the robust communicative properties of CAVs, they can maintain smaller $\tau_{r(min)}$ and l_g which subsequently significantly alter the road capacity. The critical density (ρ_{cr}) of the ring road is thoroughly analyzed. The ρ_{cr} improves by 52% to 55% depending on the assorted values of $\tau_{r(min)}$ and l_g. It is a plausible development.

Conversely, the dynamics in all-HDVs and mixed environment are different. In all-HDVs, the velocity evolution deteriorates and larger variations in velocity are observable while in the mixed environment the penetration of CAVs contributes to improvement in the velocity evolution, and the variations are limited. The proposed model can be employed in the evaluation of the properties of CAVs in traffic flow, and in deciding the optimal parameters for their operations on highways. The proposed model can also be used in control applications to optimize the values of $\tau_{r(min)}$ and l_g, subsequently alleviating traffic congestion. As a future research direction, traffic stability associated with critically small values of $\tau_{r(min)}$ could be analyzed, and the performance of the proposed model could be compared with microscopic simulations to guarantee its use in traffic planning and management.

6.6 Preview of the Next Chapter

Up to this point in the dissertation, we have introduced several innovative macroscopic traffic models, each developed with a distinct aim: to contribute to the expansion of the scientific literature in transportation engineering. What distinguishes our proposed model is its versatility; it extends beyond the domain of traffic control involving Connected and Autonomous Vehicles (CAVs), with potential applications in Intelligent Transportation Systems (ITS), including Advanced Traveler Information Systems (ATIS) and route management. This concludes our research segment focused on model development and conceptualization.

In the next phase of our study, our focus will shift to the practical implementation and assessment of the model introduced in Chapter 4. The upcoming chapter will explore the model's effectiveness in managing and optimizing traffic within control applications. This transition marks a pivotal point in our research, bridging theoretical foundations with real-world applications, and aiming to narrow the gap between theory and practice in the field of transportation management and control.

Chapter 7

An MPC-Driven VSL Control of Motorway Traffic

7.1 Abstract

Proactive traffic control measure such as the Variable Speed Limit (VSL) system, driven by Model Predictive Control (MPC) is implemented for effective and safer traffic flow operations. Conventionally, the application of VSL control hinges upon discrete Second-Order macroscopic models, exemplified by METANET as a representative case. Conversely, the MPC paradigm hardly ever employs Continuum Second-Order models for traffic control. In this paper, a continuum Second-Order macroscopic model is used as a predictive model in VSL control based on MPC because of its prediction accuracy. This VSL control is based on actual motorway traffic in Dublin and is implemented in a microscopic simulation. The findings of the study are two-fold, first, the continuum Second-Order model is examined in terms of its predictive power. The effectiveness of the MPC-driven VSL control is next assessed. Within the MPC paradigm, some segments of the motorway experience no traffic congestion, while others witness a considerable decrease in the occurrence time (or frequency) of congestion.

7.2 Introduction

The economic growth of any country is closely tied to an effective transportation system. The backbone of a road transport network is the motorways, which enables fast and safe transportation of passengers and freight on a large scale. They are constantly under stress as a result of population growth, efforts are needed to keep them functional. In our days, traffic problems such as time delays, fuel consumption, and driver fatigue are increased, stemming mostly from traffic congestion on motorways [165]. Safety, convenience, and comfort while ensuring the efficient flow of vehicles should be the prime consideration in the design of the motorways [73]. Traffic congestion has turned into a phenomenon, and it is seen on motorways frequently during peak hours. To solve this problem, several effective control approaches are proposed. Nevertheless, these approaches can be further enhanced, and thus in this paper, we propose a Variable Speed Limit (VSL) system, driven by Model Predictive Control (MPC) of motorway traffic. It helps the dissolution and reduction of traffic congestion.

The detailed literature review is provided in Section 2.2.2. In this chapter, we explore the practical utility of the Second-Order model [5]. We implement this model as a prediction model in the MPC framework. The superior performance of the models in terms of the prediction capability results in a more reliable MPC-driven VSL control. The continuum models are rarely employed in MPC-driven VSL control while conversely, most of the MPC frameworks are based on the discrete models. Exercising the continuum Second-Order model in the MPC framework not only opens up new research avenues such as the incorporation of the properties of Connected and Autonomous Vehicles CAVs and traffic physics with improved prediction capability and faster computations.

The rest of this chapter is organized as: in Section II, the initials and study design are presented. Section III presents the continuum Second-Order traffic model. In Section IV, the MPC framework is briefly discussed. Performance evaluation is given in Section V. Conclusions and future directions are given in Section VI.

7.3 Study Design

In this Section, we detail the initials and study design of this study. Mainly, two distinct analyses are performed:

- First, to challenge the prediction accuracy of the continuum Second-Order model [5], we conduct a comparative analysis of this model with microscopic simulation performed in Simulation of Urban MObility (SUMO) [100, 101] using real traffic data from Dublin motorway.

- Next, we exploit the continuum Second-Order model, and employ it as a prediction model in the MPC-framework. Hereafter, two scenarios are explicitly presented. The first scenario is no control scenario in which the traffic flow is produced in SUMO to depict the real-world, it also forms the base scenario for comparative analysis. Secondly, a control scenario is considered in which important steps include optimization of the problem using the Second-Order continuum model, the definition of objective function, and constraints as shown in Fig. 7.1. Thus,

$$\begin{cases} \text{Scenario 1,} & \text{No Control,} \\ \text{Scenario 2,} & \text{MPC-driven VSL Control.} \end{cases}$$

  For simplicity, both scenarios are shown in Fig. 7.1.

The general design includes, a 7 km stretch of the Dublin motorway divided into 7 segments of non-identical lengths, thus, $N = 7$ represents the number of segments. The motorway corridor is shown in Fig. 7.2, there are two off-ramps, one in segment 2 and the other in segment 5. The corridor has 3 on-ramps in segments 3, 5 and 6, respectively. The corridor is analyzed from segment 2 to 6. The comparative analysis of both the systems and the results of the MPC framework are presented later in this paper.

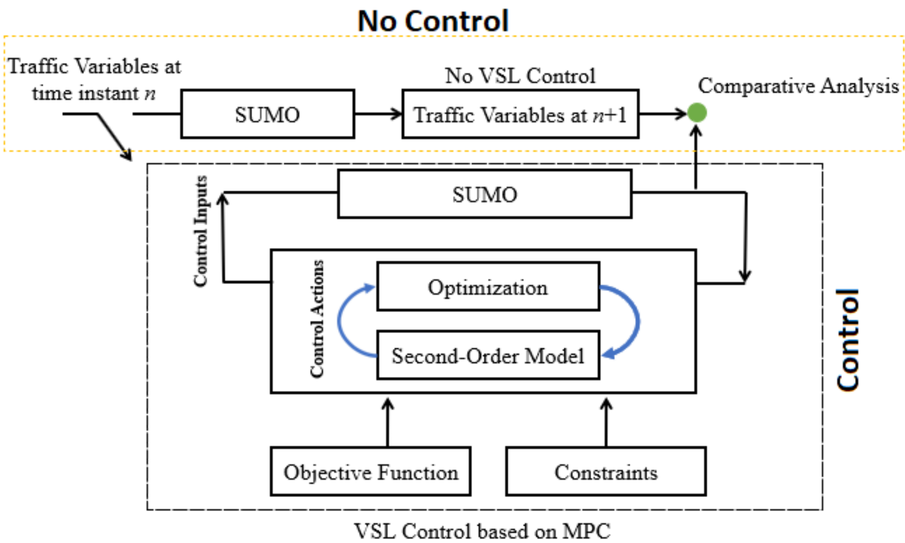

Figure 7.1. The block diagram of MPC-driven VSL control framework.

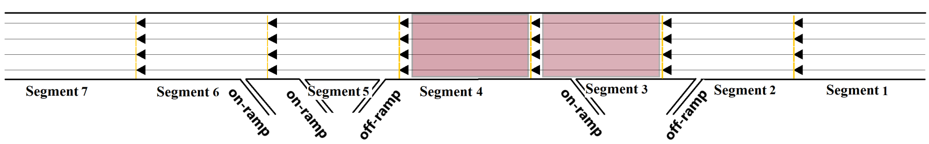

Figure 7.2. Representation of the 7 km Dublin motorway corridor.

7.4 The Continuum Second-Order Traffic Model (The Prediction Model)

The improved Second-Order traffic model [5] is an anisotropic traffic flow model. This model explicitly considers the driver reaction, sensitivity, and stimuli, and requires less calibration efforts to implement since the model parameters are based on traffic physics, and are readily available. The model is given as

$$\begin{aligned} &\frac{\partial \rho}{\partial t} + \frac{\partial \rho v}{\partial x} = if - of, \\ &\frac{\partial v}{\partial t} + \big(v - \frac{\gamma}{\delta\rho}\frac{v_m}{\rho_m}\alpha\tau\big)\frac{\partial v}{\partial x} = \frac{v(\rho) - v}{\Gamma}, \end{aligned} \tag{7.1}$$

where $\rho = \rho(x, t)$ and $v = v(x, t)$ corresponds to traffic density and velocity, respectively while γ is driver sensitivity. The density of sources and sinks is given by if and of, respectively. ρ_m and v_m are the maximum density and velocity, respectively. Transition width is given by $\delta\rho$ which represents the spatial change in density. τ is the reaction time, and α is the acceleartion. $v(\rho)$ is the velocity-density relationship, since we are dealing with a motorway traffic where the relations between traffic variables are somehow linear, we use the Greenshields model for $v(\rho)$. It is given as

$$v(\rho) = v_m\big(1 - \frac{\rho_{avg}}{\rho_m}\big), \tag{7.2}$$

where v_m is the maximum traffic velocity while ρ_{avg} and ρ_m are the average and maximum traffic density, and Γ is the relaxation time of the system. The temporal and spatial derivatives are t and x, respectively. The rearward velocity in this model is a variable, and reaction to frontal changes is non-uniform. It is given by $\frac{\gamma}{\delta\rho}\frac{v_m}{\rho_m}\alpha\tau$ in (7.1).

The two state-equations of the model describe density and velocity dynamics more realistically incorporating traffic physics. The continuous Second-Order traffic flow models represent the traffic flow in a continuous manner such as a continuous function of time and space, unlike the discrete models which consider discrete segments and cells. The continuous models are exercised for their simplicity in implementation and understanding supported by a theoretical foundation.

Continuous traffic flow models cannot be directly solved as if they were discrete models with cells or segments, primarily due to their fundamental differences in representation. Continuous models describe traffic conditions as continuous functions of space and time, using partial differential equations, whereas discrete models work with discrete segments or cells and use difference equations.

However, the continuous models can be solved numerically for simulation purposes employing numerical methods and techniques that can approximate solutions to continuous models by discretizing space and time, effectively converting them into a form that resembles discrete models. This discretization process involves breaking the continuous roadway into discrete intervals or cells and subdividing time into discrete steps. The continuous models can be solved by employing a number of numerical techniques including, but not limited to finite difference and higher resolution schemes such as Roe decomposition. Thus, improving the prediction accuracy and reliability.

Further, to implement (7.1) in this study, density dynamics are computed as

$$\begin{aligned}&\rho_i^{n+1}\\&=\rho_i^n+\frac{\Delta t}{\Delta x}(\rho_i^n(v_i^n-v_{i+1}^n))+\\&\frac{\Delta t}{\Delta x}v_i^n(\rho_{i-1}^n-\rho_i^n)+if_i^n-of_i^n,\end{aligned} \tag{7.3}$$

where the subscripts i and n are space and time indices. The velocity dynamics are computed as
if $v_i^n \leq \frac{\gamma}{\delta\rho}\frac{v_m}{\rho_m}\alpha\tau$

$$\begin{aligned}&v_i^{n+1}\\&=v_i^n+\frac{\Delta t}{\Delta x}(\frac{\gamma}{\delta\rho_i^n}\frac{v_m}{\rho_m}\alpha\tau-v_i^n)(v_{i+1}^n-v_i^n)\\&+\frac{\Delta t}{\Gamma}(v(\rho_i^n)-v_i^n),\end{aligned} \tag{7.4}$$

and otherwise

$$
\begin{aligned}
& v_i^{n+1} \\
& = v_i^n + \frac{\Delta t}{\Delta x}(\frac{\gamma}{\delta \rho_i^n}\frac{v_m}{\rho_m}\alpha\tau - v_i^n)(v_i^n - v_{i-1}^n) \\
& + \frac{\Delta t}{\Gamma}(v(\rho_i^n) - v_i^n).
\end{aligned}
\tag{7.5}
$$

7.5 Principle for the assessment of the accuracy of the continuum Second-Order Model

The comparative analysis involves both the SUMO and the macroscopic traffic model. This assessment is conducted by examining traffic data variables at a specific time step denoted as $n + 1$. In this context, n represents the current time step within the simulation, and $n + 1$ signifies the subsequent time step immediately following it. Essentially, it is the point in time at which we evaluate and compare the traffic data between the two systems to understand how they perform in predicting or representing traffic conditions as the simulation progresses.

Thus, the traffic is first generated in SUMO for 24 hours, and then the data from SUMO is used as the initial conditions for the macroscopic model, allowing the Second-Order macroscopic model to perform predictions. The block diagram explaining the procedure of the comparative analysis is given in Fig. 7.3. The accuracy of the macroscopic model to reproduce the Dublin motorway traffic is quantitatively measured by employing the RMSPE. Comprehensive results are presented in Section 7.7.

7.6 The Design of MPC-driven VSL Control

MPC is a model-based control approach, it optimizes a certain objective function subject to certain constraints by evaluating the future traffic states with a predictive model. The optimal values of control variables are computed by an iterative procedure [166]. In this regard, the MPC computes the optimal control action trajectory u^* inside the control horizon N_c in order to optimize the given objective function by solving the optimization problem in real-time. The prediction of the traffic states is

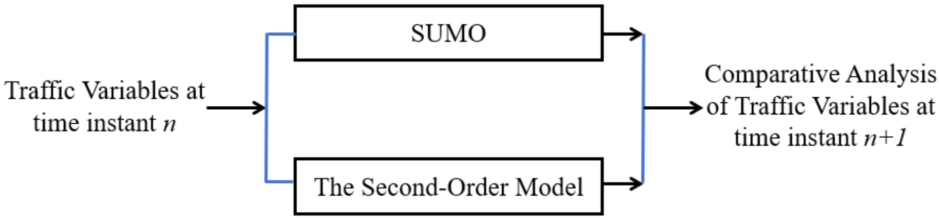

Figure 7.3. The block diagram of the systems' comparative analysis.

performed by using a mathematical model that predicts the dynamics of the system over the prediction horizon N_p. The first element of the u^* is applied to the system by the receding horizon principle [167] as shown in Fig. 7.4.

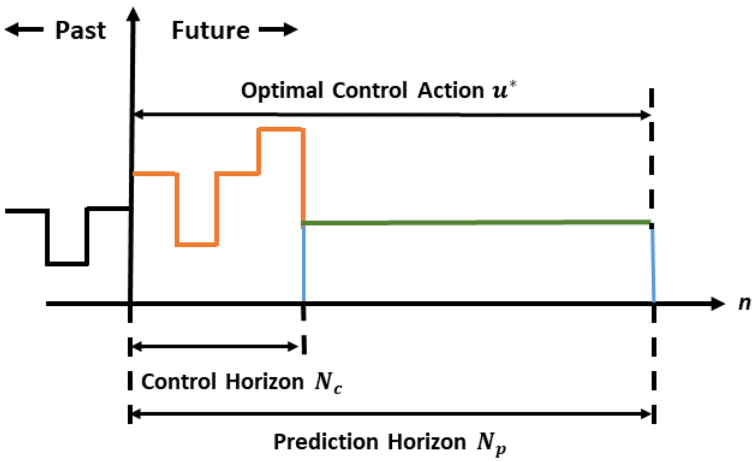

Figure 7.4. Principle of the receding horizon.

We use the objective function given by (7.12), and (7.1) has been used for the prediction of the future states of traffic. The desired speed in the Second-Order Model is given by

$$v(\rho_i^n) = v_m\big(1 - \frac{\rho_i^n}{\rho_m}\big). \tag{7.6}$$

In [78], the desired speed has been replaced with a VSL decided by the MPC

$$v(\rho_i^n) = SL_i^n, \tag{7.7}$$

where the control variable is represented by the speed limit (SL_i^n) of specific motorway segments at the time instant n. However, this implies that even at very high densities, setting a high VSL would lead to a very high flow, which is unrealistic. It is well-known that a VSL value may truncate the fundamental diagram, not replace it altogether. Thus, we modify (7.6), and replace v_m with SL_i^n. Thus, it is expressed as

$$v(\rho_i^n) = SL_i^n\big(1 - \frac{\rho_i^n}{\rho_m}\big). \tag{7.8}$$

It considers the new updated maximum speed (SL_i^n) for each segment, and the density to ensure equilibrium conditions.

In the MPC framework, during the whole observation time T (i.e simulation time), the controller at each control time step $n_{MPC} = k\Delta_{MPC}$, $k \in \mathbb{N}$, solves a constrained optimization problem by using a forecasting model given by Eqs. (7.3), (7.4) and (7.5) that predicts, within a prediction horizon window N_p, the state variable values of the plant whose behaviour it wants to optimize. The parameter Δ_{MPC} represents the controller sample time that establishes its operating frequency, while the prediction horizon window N_p is an integer number expressed as the number of time steps Δt (i.e time step of prediction model) in which the forecasting procedure is carried out using Eqs. (7.3), (7.4) and (7.5).

The N_p has been fixed to 6 sample time steps, Δ_{MPC} to 300 s and the N_c, in this case, has been chosen equal to the prediction horizon. The MPC-driven VSL control framework is shown in Fig. 7.1. The important steps of scenario 2 are the optimization of the problem using the Second-Order continuum model as a prediction model, the definition of the objective function, and constraints.

Based on the aforementioned assumptions, the optimization problem is:

$$\min_{SL_i^n}(TTT(\rho(n))),$$

subject to

$$(7.3), (7.4), (7.5),$$

$$0 \leq v_i^n \leq v_m, \tag{7.9}$$

$$0 \leq \rho_i^n \leq \rho_m, \tag{7.10}$$

$$\mathrm{SL}_l \leq \mathrm{SL}_i^n \leq \mathrm{SL}_u, \tag{7.11}$$

$$\forall i \in N, \forall n \in [n_{MPC}, n_{MPC} + np, n_{MPC} + np + 1, ..., n_{MPC} + np + N_p - 1],$$

where np is the sample time step such that $np = k \cdot \Delta t$, $k \in \mathbb{N}$, and the objective function is the Total Travel Time (Total Travel Time (TTT)), which has been computed as:

$$TTT = \Delta t \sum_{n=n_{MPC}}^{n_{MPC}+np+N_p-1} \sum_{i=1}^{N_{cs}} \Delta x_i \rho_i(n), \tag{7.12}$$

it is the sum of density over all prediction model time steps, thus, the optimizer minimizes this value subject to the SL_i^n of the controlled segments. Due to congestion in two segments, we only apply control on two segments such as segments 3 and 4, the number of controlled segments is given by N_{cs}.

The optimization of the objective function is subjected to constraints (7.3), (7.4), and (7.5), that are used to predict the density and velocity dynamics. The optimization is also subjected to physical constraints on traffic variables given by (7.9) and (7.10). The bounds on speed limits are given by (7.11).

Since the simulation time is too large (24 hours), it is not essential to run the MPC controller for all the time. Thus, the activation of the MPC controller is subject to a condition when the ρ_{avg} exceeds the ρ_{cr}. ρ_{avg} is the average traffic density of each segment, while ρ_{cr} is the crtical density of each segment as shown in Fig. 7.5. The ρ_{cr} is obtained by the calibration of the fundamental diagram for each segment. Thus, we call it a conditional MPC controller with the following conditions:

$$\begin{cases} \rho_{avg} \leq \rho_{cr}, & \text{no action needed,} \\ \rho_{cr} > \rho_{avg}, & \text{activate controller.} \end{cases}$$

So, if the traffic is in free flow conditions or in the left side of the fundamental diagram, no action is needed. But, if the flow is saturated such that the right side of the fundamental diagram, represents congestion, the controller is then activated.

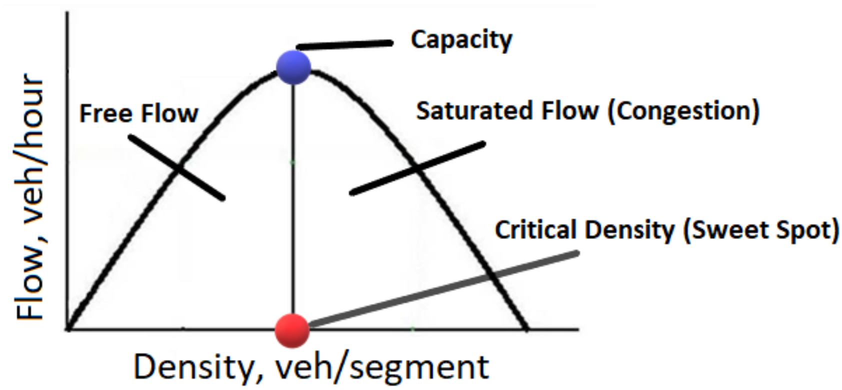

Figure 7.5. Representation of typical MFD.

7.7 Performance Evaluation

In this Section, the results of this study are detailed. As discussed in Section 7.3, the results of this study are two-fold. First, the accuracy of the Second-Order Model to reproduce the real-world traffic is analyzed. Later, the comparative analysis of the no-control scenario (Scenario 1) and the VSL control (Scenario 2) are presented in the current MPC framework. The simulation parameters for the Second-Order Model and SUMO are given in Table 7.1. The total simulation time is 24 hours, time step for both, SUMO and the Second-Order model is 20 s. The maximum speed

v_m for scenario 1 is 28 m/s, the SL_u and SL_l are 36 m/s and 22 m/s, respectively in scenario 2. The length of the motorway stretch is 7 km (7000 m), and the lengths of all segments are non-identical. The relaxation time T is 22 s, and the reaction time τ is 1.5 s. The average length of vehicles is 4 m, and the minimum gap is 1.5 m.

Table 7.1. Simulation Parameters

Description	Value
Simulation time, T	24 hours
Length of the motorway corridor	7000 m
Maximum velocity for scenario 1	28 m/s
SL_u	36 m/s
SL_l	22 m/s
Sample time, Δt for the Second-Order model	20 s
Sample time, Δ_{SUMO} for SUMO	0.5 s
Aggregation time	300 s
Relaxation time, Γ	22 s
Sample time of the controller, Δ_{MPC}	300 s
Reaction time, τ	1.5 s
Average length of a vehicle, L	4 m
Minimum gap	1.5 m

7.7.1 Prediction Accuracy of the Second-Order Continuum Model

7.7.1.1 On the Density Behavior of the Second-Order Continuum Model

The density behavior of the Second-Order model for 24 hours is shown in Fig. 7.6. As the motorway stretch is divided into different segments, the density behavior of each segment is shown. The Second-Order model reproduces the SUMO scenario, and the results are closely similar. Moreover, it results in stable outcomes during the change occurrence. In all the segments of the motorway, the density behavior of the proposed model is closely similar to that of the SUMO. The accuracy of the Second-Order model to reproduce the motorway traffic is evaluated using the RMSPE which is given in Table 7.2. The RMSPE on density in segment 2 is 3.36%, it is 5.60% in segment 3. In segment 4 and segment 5, the RMSPE is 1.41% and 1.51%, respectively. It is 1.43% in segment 6.

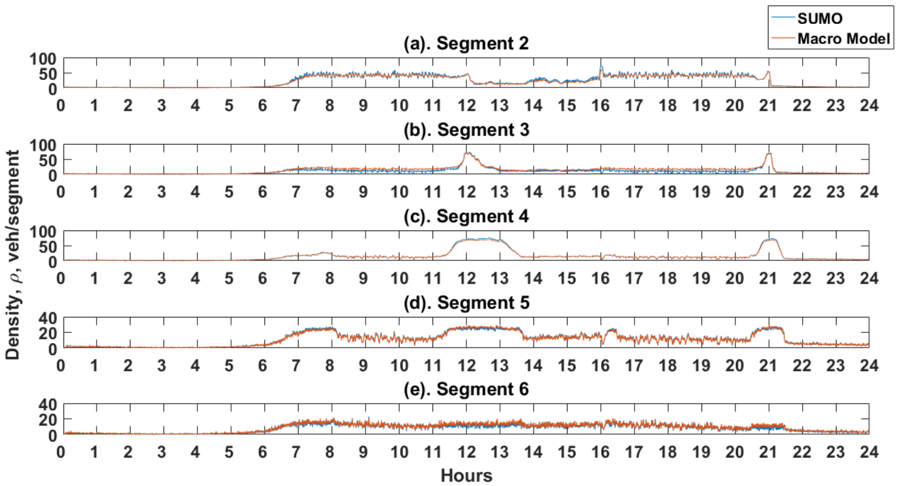

Figure 7.6. Analysis of the density behavior of the Second-Order model and SUMO for 24 hours. Each sub-figure represent the average density of each segment. From (a) to (e), it is given for segment (2) to (6).

7.7.1.2 On the Velocity Behavior of the Second-Order Continuum Model

The velocity behavior of the Second-Order model for 24 hours is shown in Fig. 7.7. It reproduces the SUMO scenario more accurately, and the results are closely similar. Moreover, it results in stable outcomes during the change occurrence which guarantees that the model can be employed in any traffic condition. The accuracy of the Second-Order model to reproduce the motorway traffic velocity is evaluated using the RMSPE which is given in Table 7.2. The RMSPE on velocity in segment 2 is 3.77%, it is 4.26% in segment 3. In segment 4 and segment 5, the RMSPE is 2.33% and 5.50%, respectively. It is 3.61% in segment 6. The results are promising, next, we extend the results to the second part in which we control the motorway traffic based on MPC-driven VSL control.

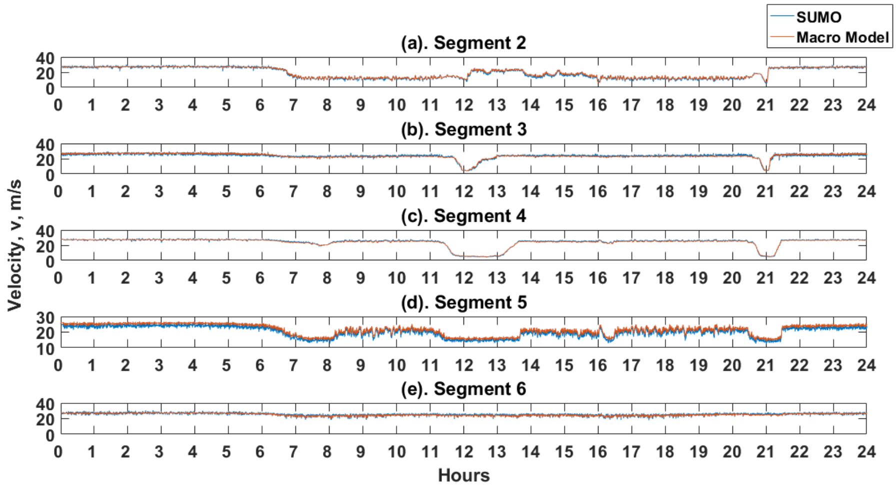

Figure 7.7. Analysis of the velocity behavior with the Second-Order model and SUMO for 24 hours. Each sub-figure represents the average velocity of each segment. From (a) to (e), it is given for segments (2) to (6).

Table 7.2. RMSPE on Density and Velocity of the Second-Order model.

Segment	RMSPE on Density (%)	RMSPE on Velocity (%)
2	3.36	3.77
3	5.60	4.26
4	1.43	2.33
5	1.51	5.50
6	1.43	3.61

7.7.2 The MPC-driven VSL control of the Dublin Motorway

7.7.2.1 Overall Dynamics of the Traffic Density over the Corridor

Previously, we discussed the ability and accuracy of the Second-Order model to reproduce motorway traffic. Onwards, we present the results of the MPC-driven VSL control. The density dynamics in no control scenario (scenario 1) are illustrated in Fig. 7.8 for the entire motorway corridor. It is observable that the ρ_{cr} exceeds ρ_{avg} in segments 3 and 4 which can be identified by following the red lines in the figure. $\rho_{cr} > \rho_{avg}$ is also the condition for the MPC controller to activate. The rest of the corridor is not congested, and the density evolution is smooth. Thus, we control only the congested segments that are 3 and 4. Next, we further elaborate on the results of scenarios 1 and 2.

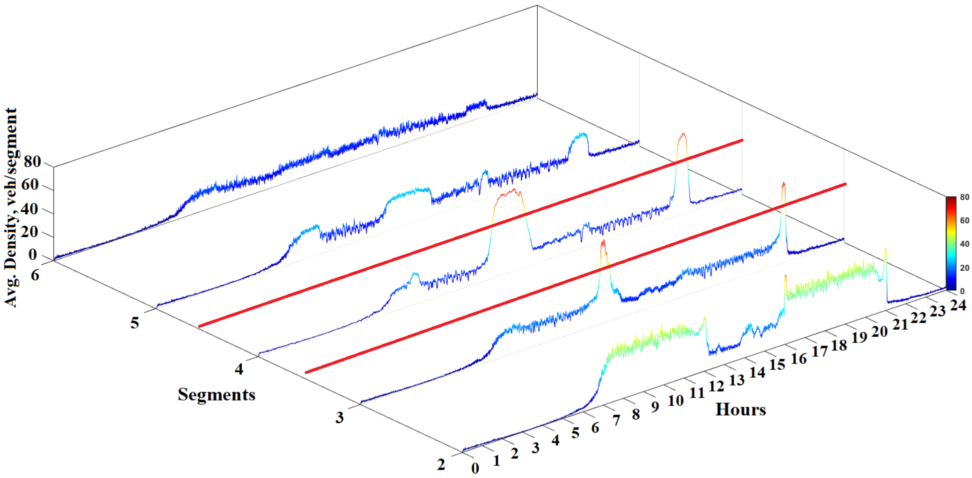

Figure 7.8. Density evolution in no control scenario on the motorway corridor for 24 hours.

7.7.2.2 Scenario 1

The results of scenario 1 are illustrated in Fig. 7.9. The congestion occurrence ($\rho_{cr} > \rho_{avg}$) over time in different segments of the motorway is observable. The traffic congestion occurs mainly between 11 : 00 to 13 : 00 of the first half of the day. In the second half, it is evident that the congestion occurrence is between 20 : 45 and 21 : 20. The congestion occurs only in two segments, 3 and 4 while the traffic operations are smooth on the rest of the corridor.

7.7.2.3 Scenario 2

The control scenario with VSL control implemented is shown in Fig. 7.10. It is evident from the results that after the implementation of VSL control, the congestion is fully dissolved in segment 3. While in segment 4 the congestion occurrence time is reduced. The density evolution as compared to scenario 1 is smoother and without any major disruption of traffic flow. In the preceding analysis, it was observed that in Segment 4, the occurrence of congestion is not fully mitigated, but significantly minimized. Additionally, it was noted that the presence of concurrent congestion in Segment 3 contributed to the inability to completely mitigate the congestion in Segment 4. Nevertheless, the MPC-driven VSL control was found effective and viable under these circumstances and has been demonstrated in the findings.

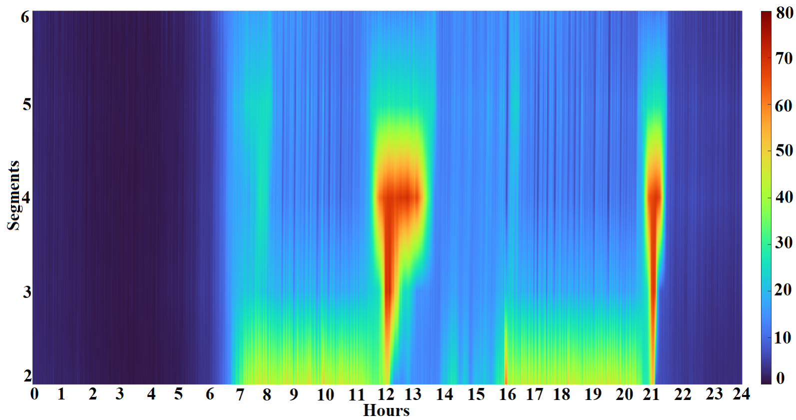

Figure 7.9. Density evolution on the motorway corridor for 24 hours in scenario 1.

7.8 Conclusion and Future Research

In this paper, we present an MPC-driven VSL control for motorway traffic. The MPC framework employs a more precise Continuum Second-Order model, enhancing the performance of MPC-driven VSL control by reducing the model's prediction error. The results are twofold: first, we

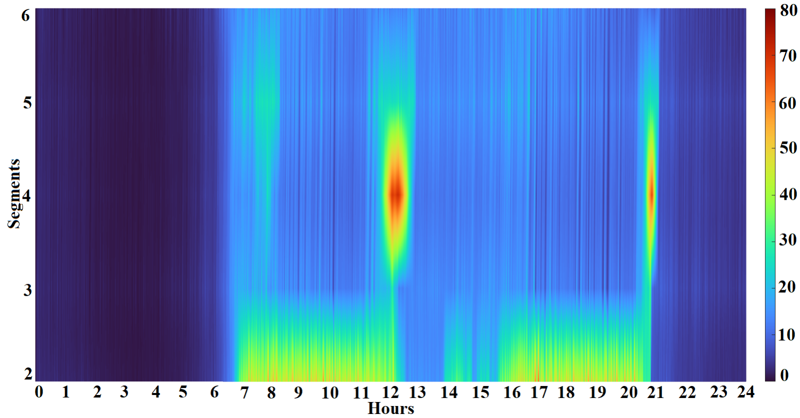

Figure 7.10. Density evolution on the motorway corridor for 24 hours in scenario 2.

assess the accuracy of the Continuum Second-Order model. The findings clearly demonstrate that this model exhibits lower prediction errors, as measured by the RMSPE. Secondly, we implement an MPC framework, utilizing the Second-Order model in the optimization process.

Primarily, we apply control exclusively to two congested segments, as evident from the results. MPC-driven VSL control proves to be effective and feasible. In Segment 3, congestion is completely mitigated after implementing VSL control, while in Segment 4, congestion occurrence time is significantly reduced.

Future research opportunities arise within the context of this study due to the effectiveness and precision of Second-Order traffic models. Currently, these models only consider Human-Driven Vehicles (HDVs) in homogeneous traffic. However, Connected and Autonomous Vehicles (CAVs) are poised to play a substantial role in the future of traffic flow on motorways. Consequently, incorporating the features of CAVs into Continuum Second-Order models for use in traffic control (in the context of the present MPC framework) is a promising research direction.

7.9 Preview of the Next Chapter

In this chapter, we have implemented an MPC-driven VSL control on the Dublin motorway. We have harnessed a continuum Second-Order traffic model in the MPC paradigm yielding sufficiently plausible results. Within the context of continuum Second-Order models, they are flexible to accommodate traffic physics and we have successfully revised them for the features of CAVs. Next, we employ the proposed continuum Second-Order model presented in chapter 4 in the MPC framework as in this chapter. We extend our study to the control of motorway traffic with CAVs and present a novel control within the context of CAVs in a mixed-traffic environment.

Chapter 8

A Novel MPC-Driven Regulation of Traffic Flow with Connected and Autonomous Vehicles

8.1 Abstract

Traffic congestion on motorways is the major problem of our days. Control approaches such as Variable Speed Limit (VSL) as introduced in the last chapter are employed to control traffic congestion on motorways. VSL is a conventional and effective traffic control approach. It has been widely investigated in the context of Human-Driven Vehicles (HDVs). With the advent of Connected and Autonomous Vehicles (CAVs), technological developments offer new possibilities to control traffic congestion. These possibilities include but are not limited to the control of intrinsic features of CAVs in mixed traffic environment. Time headway is one of the sensitive parameters that impact the traffic flow. With this in mind, CAVs offer a possibility to control the time headway instead of implementing the conventional control methods. Time headway can impact the capacity of a particular road section. Thus, to replace the conventional control methods, we in this chapter propose a novel Model Predictive Control (MPC)-Driven control of traffic with CAVs. To ensure safety, we design a multi-

objective cost function that at the same time handles the safety of the vehicles and ensures efficient flow of the vehicles. The findings demonstrate that congestion can be controlled and efficient flow can be achieved by controlling a specific Penetration Rate (PR) of CAVs.

8.2 Introduction

Traffic congestion is characterized as: when the operational capacity of any road is exceeded by vehicular demand. It impacts the operations of highways and results in an increase in travel time, environmental emissions, safety issues, and overall economic cost. Thus, the mitigation of traffic congestion is of prime importance. Several methodologies are proposed for the control of traffic congestion such as the conventional Variable Speed Limit (VSL). Most studies employed Model Predictive Control (MPC)-driven VSL control approaches for conventional traffic such as traffic in the presence of Human-Driven Vehicles (HDVs). This conventional traffic control is previously demonstrated in Chapter 7 of this dissertation. Lately, the advent of CAVs revolutionizes traffic studies as the traffic dynamics alter significantly with the features of CAVs. The advent of CAVs offers possibilities to reinvent novel control strategies due to the developing Intelligent Transportation System (ITS).

The advent of CAVs signifies the control of traffic flow with alternative control inputs such as time headway, distance headway, and reaction time of the vehicles. Thus, the conventional control VSL can be replaced with a novel control input variable provided only to CAVs. An effective Penetration Rate (PR) of CAVs can be used to control flow on any particular road segment. In the context of the MPC paradigm, one important aspect is the prediction model. It plays a vital role in the accuracy and effectiveness of MPC-driven control. In our days, the prediction models are revised for the properties of CAVs. The macroscopic Second-Order continuum model is revised for the characteristics of mixed traffic in Chapter 4 of this dissertation. However, a detailed discussion on the models and MPC is already provided in the earlier Chapters of this dissertation.

Further, to control traffic congestion and to regulate the traffic flow on motorways, in this Chapter, the characteristics of CAVs are harnessed, and a dynamic time headway control strategy based on the MPC method is proposed. Initially, the revised model for mixed traffic as in Chapter 4 is considered as a prediction model in the MPC paradigm. The MPC paradigm is prompted to regulate traffic flow on motorways to avoid traffic congestion and improve the overall efficiency of the motorway. The effectiveness of the novel control strategy with the PR of CAVs set to 40% is analyzed thoroughly.

8.3 The Macroscopic Model

The prediction model in the MPC paradigm plays a vital role. In this study, we employed a macroscopic continuum model for mixed traffic proposed in Chapter 4. This model explicitly considers the microscopic driving characteristics of HDVs and CAVs. The model is given by

$$\begin{aligned}
&\frac{\partial \rho(x,t)}{\partial t} + \frac{\partial \rho(x,t)\cdot v(x,t)}{\partial x} = i_q(x,t) - e_q(x,t),\\
&\frac{\partial v(x,t)}{\partial t} + (v(x,t) - [\zeta_* + \varphi_*]))\frac{\partial v(x,t)}{\partial x} = \frac{V(\rho(x,t)) - v(x,t)}{\Gamma}.
\end{aligned} \tag{8.1}$$

A detailed explanation of the model can be found in Chapter 4. The class-specific behavior of HDVs and CAVs is represented by ζ_* and φ_* whereas the impact of change in the time headway τ_h of CAVs in the Fundamental Diagram (FD) is captured by calibrating them for various values of τ_h. In the proposed model τ_h is equivalent to change occurrence time, which is the sum of reaction time (τ_r) and harmonization time (τ_b). Further details can be traced in Chapter 4.

8.4 Scenario Design

In this Section, the design of the traffic scenario is discussed. A mixed traffic environment is considered comprising of HDVs and CAVs. The CAVs have vehicle 2 vehicle (V2V) and Vehicle 2 Infrastructure (V2I) capabilities. The PR of CAVs is fixed to 40 % of the total demand, while the rest are HDVs. The motorway corridor is shown in Figure 7.2. Since the demand and the vehicle types are changed from that in the network in Chapter 7, thus, the dynamics of traffic flow are also changed. Moreover, we only control the CAVs in the network so that an explicit and meaningful demonstration can be achieved from this study.

The MPC-driven dynamic time headway control strategy takes the desired time headway of CAVs within different areas of the upstream parts of the motorway as the control variables. The MPC framework is employed as from Chapter 7, and is illustrated in Figure 7.4. The MPC observes traffic states and computes the optimal CAVs time headway value, and carries out real-time CAVs dynamic time headway controls. In doing so, the dynamics of CAVs impact the HDVs in the network, they work like actuators, the HDVs follow the actions of CAVs, and thus the dynamics in the corridor are altered, and traffic flow is regulated.

8.5 The MPC Design

In general, the same MPC design is followed in this Chapter as in the previous Chapter and given in Section 7.6. However, some differences are covered in this Section. The control variable is ${\tau_h}_i^n$ with upper bound 1.2 s and lower bound 0.5 s. We calibrate the FD for value between 0.5 s and 1.2 s, thus when the value of τ_h is changed their respective calibrated FD is adopted, such as

$$V(\rho_i^n) = \begin{cases} v(\rho_{0.5}\binom{n}{i}), & 0.5 < \tau_h < 0.6 \\ v(\rho_{0.6}\binom{n}{i}), & 0.6 < \tau_h < 0.7 \\ v(\rho_{0.7}\binom{n}{i}), & 0.7 < \tau_h < 0.8 \\ v(\rho_{0.8}\binom{n}{i}), & 0.8 < \tau_h < 0.9 \\ v(\rho_{0.9}\binom{n}{i}), & 0.9 < \tau_h < 1 \\ v(\rho_{1}\binom{n}{i}), & 1 < \tau_h < 1.1 \\ v(\rho_{1.1}\binom{n}{i}), & 1.1 < \tau_h < 1.2 \\ v(\rho_{1.2}\binom{n}{i}), & \tau_h = 1.2 \end{cases} \tag{8.2}$$

8.6 The Objective Function

A multi-objective function has been design in order to ensure safety and efficiency of the traffic system. To ensure safety, the standard deviation of the velocity is minimized. In doing so, any unforeseen situation can be avoided. While to ensure the efficiency of the system the mean velocity of the motorway segments is maximized. The objective function is represented by θ, the safety function is given by θ_1 and the efficiency represented as θ_2, thus

$$\theta = \theta_1 - \theta_2,$$

where

$$\theta_1 = \sum_i \frac{v_i(\tau_h) - \bar{v}_i}{N-1}, \tag{8.3}$$

and

$$\theta_2 = \sum_i \frac{v_i(\tau_h)}{N}. \tag{8.4}$$

Weight functions are assigned to θ_1 and θ_2 in order to prioritize safety and efficiency according to traffic conditions, thus,

$$\theta = \frac{\theta_1}{\theta_{i,max}} - \frac{\theta_2}{\theta_{i,max}}. \tag{8.5}$$

So,

$$\min_{\tau_{h_i}^n}(\theta),$$

is the multi-objective function accounting for the safety and efficiency of the motorway.

8.7 Dynamics of The Macroscopic Fundamental Diagram Associated with Time Headway

The microscopic spatiotemporal variables such as time headway and distance headway impact the shape of the FD. To exemplify, we demonstrate the example of τ_h, by setting the PR of CAVs to 40 % in the simulation, we capture the change in FD caused by the variation in τ_h.

The behavior of FD with varying τ_h is analyzed in this section. The results are shown in Figures 8.1-8.5 and are given in Table 8.1. It is observable that with smaller τ_h, the critical density (ρ_{cr}) changes. Segment-wise FD is analyzed, in Segment 1, the behavior of FD is analyzed in all-HDVs and a mixed traffic environment. For all-HDVs, the ρ_{cr} is 15 veh/km. While, in the mixed traffic environment with τ_h=1 s, it is 23 veh/km, which further improves to 28 veh/km with τ_h=0.5 s.

In segment 2, in an all-HDVs scenario, the ρ_{cr} is 22 veh/km. While in the mixed traffic environment, it improves to 35 veh/km with τ_h=1 s, and eventually to 40 veh/km with τ_h=0.5 s. Similarly, in segment 3, in an all-HDVs scenario, the ρ_{cr} is 29 veh/km. While in the mixed traffic environment, it improves to 36 veh/km with τ_h=1 s, and eventually to 41 veh/km with τ_h=0.5 s. In segment 4, in an all-HDVs scenario, the ρ_{cr} is 17 veh/km. While in the mixed traffic environment, it improves to 22 veh/km with τ_h=1 s, and eventually to 27 veh/km with τ_h=0.5 s. In segment 5, in an all-HDVs scenario, the ρ_{cr} is 21 veh/km. While in the mixed traffic environment, it improves to 29 veh/km with τ_h=1 s, and eventually to 35 veh/km with τ_h=0.5 s.

Observations reveal a notable correlation between alterations in the FD and changes in the parameter τ_h. Specifically, when τ_h is smaller, there is an increase in the ρ_{cr} of the motorway segments. Reducing the value of τ_h can be interpreted as a means to augment the capacity of the motorway segment in terms of its ability to accommodate vehicles within a unit length of the roadway. This, in turn, has the effect of improving the overall efficiency and operational behavior of the traffic flow. The rationale behind this phenomenon can be attributed to the reduction in the time delay associated with the headway τ_h, allowing vehicles to more seamlessly traverse the motorway segment.

Given the empirical evidence supporting this association between τ_h and the FD, it becomes obvious to consider τ_h as a potential control variable for the purpose of regulating and optimizing traffic flow dynamics. The manipulation of τ_h can be envisaged as a mechanism to finely tune the traffic system's performance characteristics, with the objective of achieving an optimal balance between traffic density and flow rate.

In practice, the implementation of such control measures involving τ_h would necessitate a systematic approach that takes into account various factors, including traffic volume, road geometry, and driver behavior. Furthermore, the integration of advanced traffic management systems and real-time data analysis could enable the dynamic adjustment of τ_h in response to changing traffic conditions, thereby enhancing the overall resilience and adaptability of the motorway.

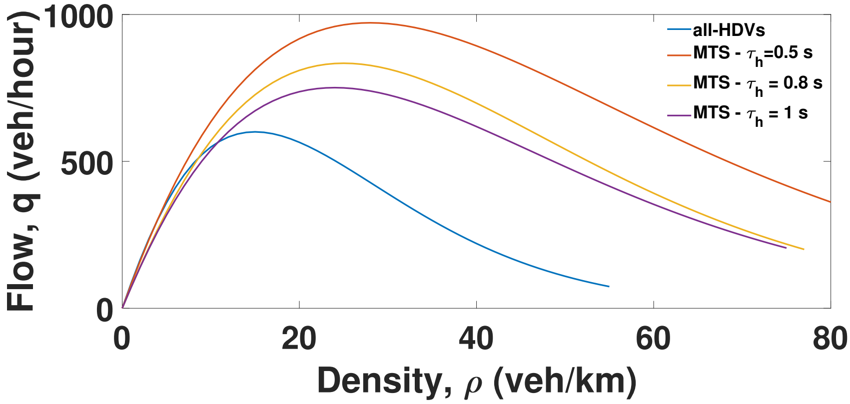

Figure 8.1. FD of segment 1, all-HDVs scenario compared with mixed traffic scenario (MTS), CAVs=40% and τ_h = 0.5 s, 0.8 s and 1 s.

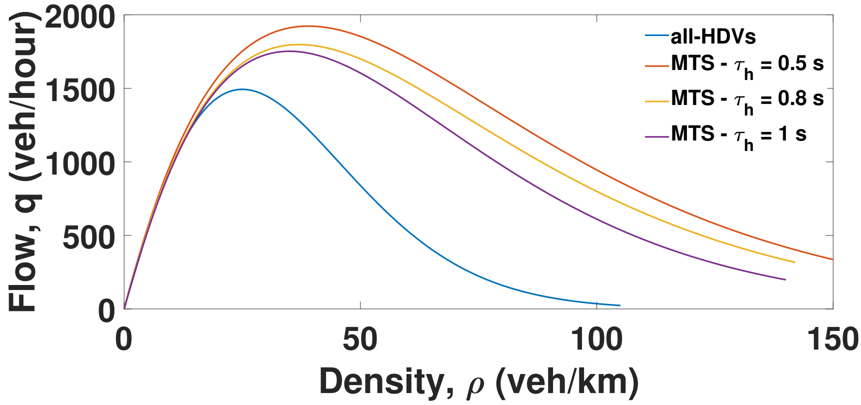

Figure 8.2. FD of segment 2, all-HDVs scenario compared with mixed traffic scenario (MTS), CAVs=40% and τ_h = 0.5 s, 0.8 s and 1 s.

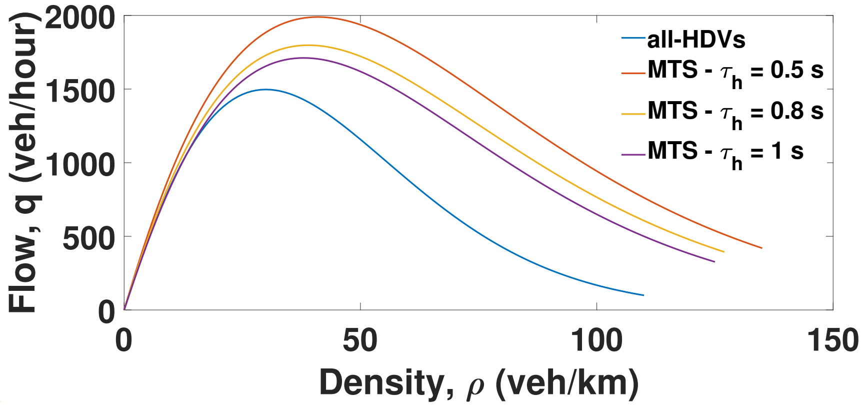

Figure 8.3. FD of segment 3, all-HDVs scenario compared with mixed traffic scenario (MTS), CAVs=40% and τ_h = 0.5 s, 0.8 s and 1 s.

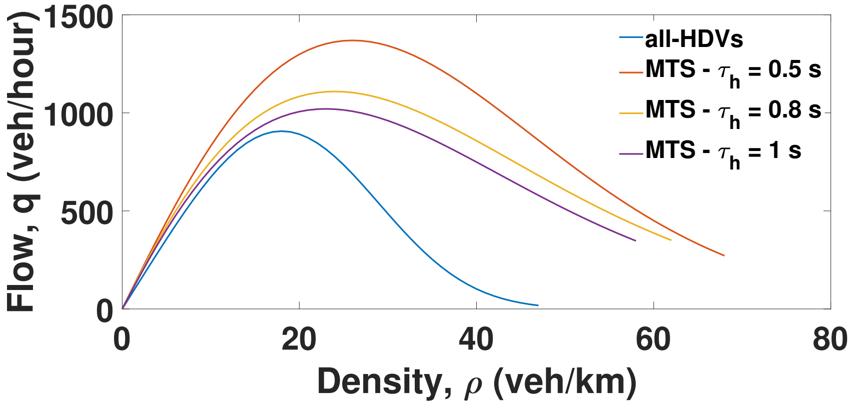

Figure 8.4. FD of segment 4, all-HDVs scenario compared with mixed traffic scenario (MTS), CAVs=40% and $\tau_h = 0.5$ s, 0.8 s and 1 s.

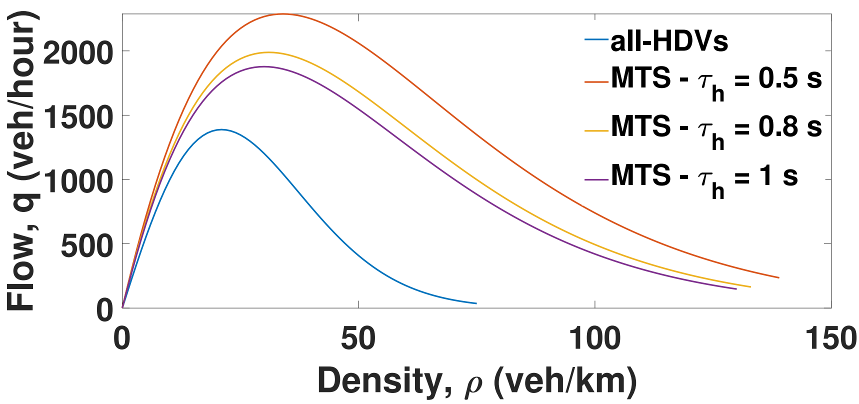

Figure 8.5. FD of segment 5, all-HDVs scenario compared with mixed traffic scenario (MTS), CAVs=40% and $\tau_h = 0.5$ s, 0.8 s and 1 s.

Table 8.1. Analysis of ρ_{cr} with assorted τ_h.

Description	Segment 1	Segment 2	Segment 3	Segment 4	Segment 5
All-HDVs with $\tau_h = 1.2$	15	22	28	17	21
40 % CAVs with $\tau_h = 1$ s	23	35	36	22	29
40 % CAVs with $\tau_h = 0.8$ s	25	37	38	24	32
40 % CAVs with $\tau_h = 0.5$ s	28	40	41	27	35

8.8 Outcomes of the proposed Novel Control of Traffic Flow with Connected and Autonomous Vehicles

In this Section, the outcomes of the proposed novel control of traffic flow are analyzed. Two scenarios are considered:

1. Scenario I: No-control scenario in which the total traffic demand comprises 40 % CAVs and 60 % HDVs. Segment-based PR of CAVs is calculated in real-time in Simulation of Urban MObility (SUMO). Typical values of the parameters of the model are considered while the τ_h is uniform throughout this scenario.

2. Scenario II: In this scenario, the MPC-driven novel control of traffic with CAVs is implemented. Only the CAVs are controlled and the control variable τ_h is optimized and the simulations are performed. The FD is subject to varying values of τ_h in each segment, thus each varying τ_h is assigned its specific FD which captures the changes in traffic flow.

8.8.1 The Macroscopic Fundamental Diagram of the Motorway Corridor

Figure 8.6 provides a graphical representation of the FD for both controlled and uncontrolled motorway scenarios. The depicted data reveal notable enhancements in traffic flow dynamics attributable to the implementation of a novel control strategy. In the uncontrolled scenario, it is evident that traffic dynamics significantly deviate from those observed in the controlled scenario. Specifically, in the absence of control measures, congestion becomes observable, manifesting at a ρ_{cr} of 19 veh/km.

In contrast, the controlled scenario presents a distinct picture, characterized by a marked reduction in congestion. This reduction is particularly evident beyond the ρ_{cr} threshold. In the controlled scenario, the ρ_{cr} has been improved, now standing at 29 veh/km. This substantial increase in ρ_{cr} translates to an increase in capacity when compared to the uncontrolled scenario.

The outcomes showcased here can be attributed to the innovative control strategy implemented in the controlled scenario. The efficacy of this strategy in enhancing traffic conditions is evident from the depicted results, highlighting its potential to address congestion-related issues and enhance overall motorway performance. These findings underscore the practicality and promise of the proposed control approach in real-world traffic management scenarios. Next, we assess the segment-based flow to capture the explicit improvement in the flow contributed by the proposed novel control.

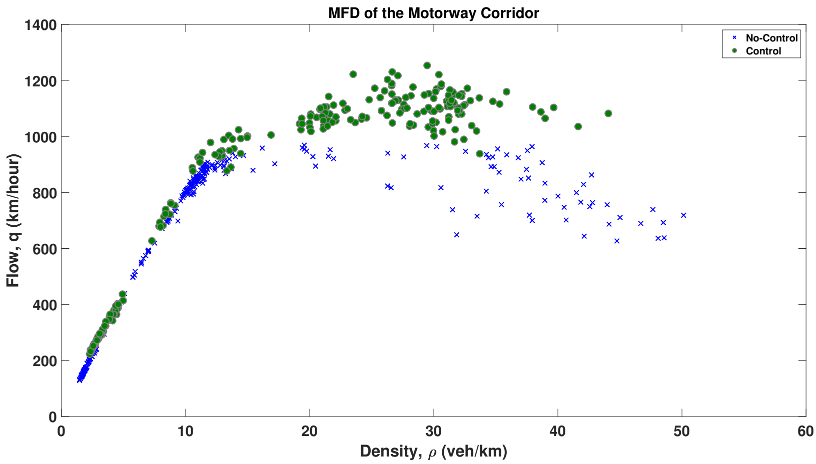

Figure 8.6. The FD of the motorway representing the no-control and control scenarios.

8.8.2 Flow Dynamics in Segment 1 of the Motorway

The flow dynamics in both the controlled and uncontrolled scenarios are presented in figure 8.7 in segment 1. Overall, there is an increase in flow uniformity in the controlled scenario compared to the uncontrolled one. In the controlled scenario, there is clear evidence of flow enhancement, indicating a substantial improvement in traffic dynamics.

Specifically, the controlled scenario exhibits an average flow rate increase of 15 %. This noteworthy improvement can be attributed to the implementation of the proposed novel control strategy. These findings support the feasibility and effectiveness of the proposed control approach in optimizing traffic flow, thereby resulting in the observed favorable outcome.

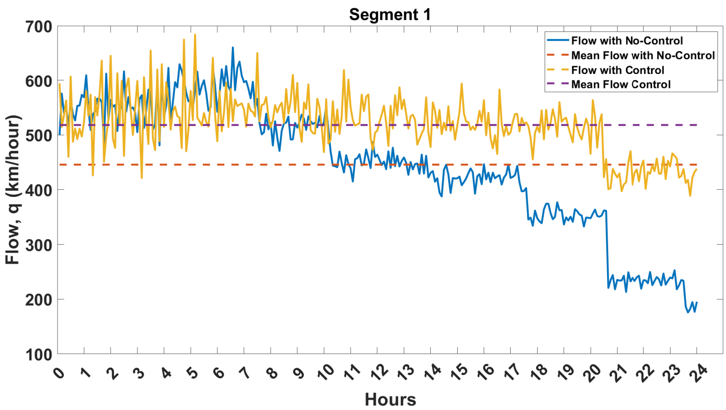

Figure 8.7. Flow dynamics of the segment 1 of the motorway in scenarios 1 and 2.

8.8.3 Flow Dynamics in Segment 2 of the Motorway

The figure presented as Figure 8.8 shows the flow dynamics observed in both the controlled and uncontrolled scenarios in segment 2. In general, the controlled scenario exhibits a more uniform flow pattern when compared to the uncontrolled scenario. This improved flow pattern in the controlled scenario is indicative of significant enhancements in traffic dynamics. Notably, the controlled scenario showcases an increased average flow rate increase of 16%.

8.8.4 Flow Dynamics in Segment 3 of the Motorway

The flow dynamics in both the controlled and uncontrolled scenarios are presented in figure 8.9 in segment 1. In this segment, there is an increase in flow in the controlled scenario compared to the uncontrolled one. In the controlled scenario, there is clear evidence of flow enhancement, indicating

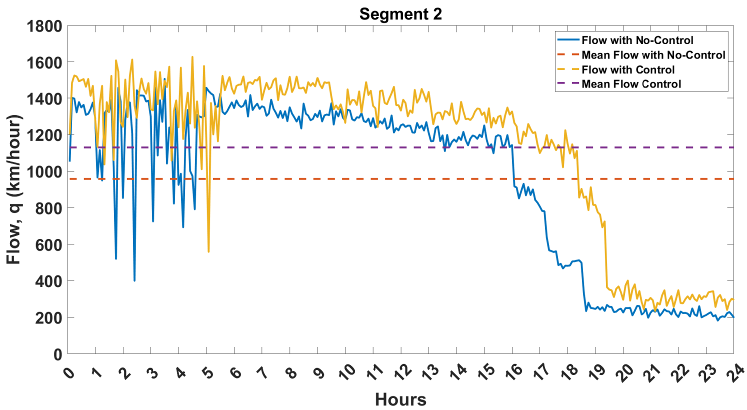

Figure 8.8. Flow dynamics of the segment 2 of the motorway in scenarios 1 and 2.

a substantial improvement in traffic dynamics. The controlled scenario exhibits an average flow rate increase of 16 %.

8.8.5 Flow Dynamics in Segment 4 of the Motorway

The figure presented as Figure 8.10 shows the flow dynamics observed in both the controlled and uncontrolled scenarios in segment 4. In general, the controlled scenario exhibits a more uniform flow pattern when compared to the uncontrolled scenario. Further, the controlled scenario showcases an increased average flow rate increase of 16%.

8.8.6 Flow Dynamics in Segment 5 of the Motorway

The figure presented as Figure 8.11 shows the flow dynamics observed in both the controlled and uncontrolled scenarios in segment 5. In general, the controlled scenario exhibits a more uniform flow pattern when compared to the uncontrolled scenario. Further, the controlled scenario showcases an increased average flow rate increase of 18%. Generally, this segment is always less congested and conditions remain free-flow, however, the efficacy of the proposed novel control is plausible in given traffic conditions as we witness improvement in all segments of the motorway. The increase in flow rate almost converges to 16%.

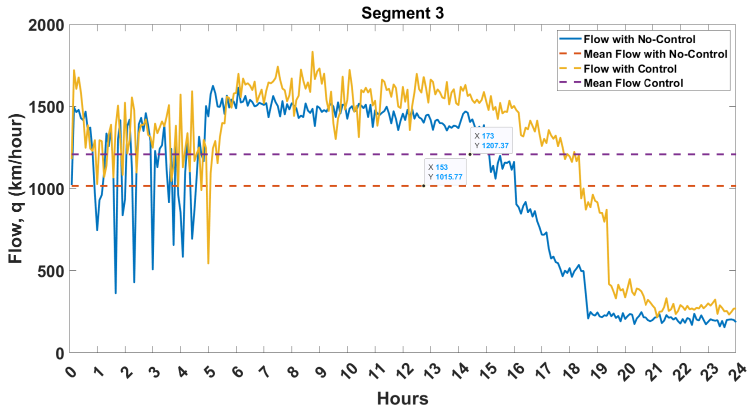

Figure 8.9. Flow dynamics of the segment 3 of the motorway in scenarios 1 and 2.

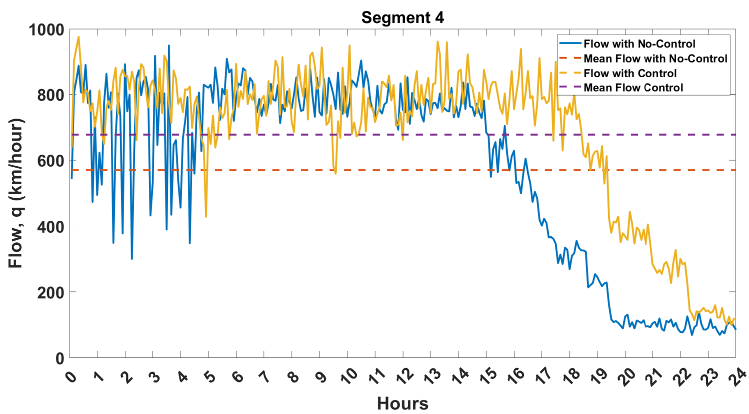

Figure 8.10. Flow dynamics of the segment 4 of the motorway in scenarios 1 and 2.

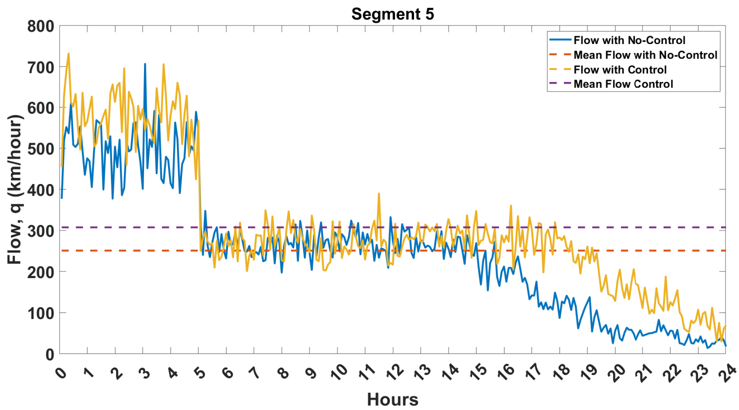

Figure 8.11. Flow dynamics of the segment 5 of the motorway in scenarios 1 and 2.

8.9 Conclusion

The emergence of Connected and Autonomous Vehicles (CAVs) is poised to result in a significant transformation in traffic dynamics, necessitating corresponding adaptations in modeling and control strategies. While recent efforts have seen revisions in modeling and control approaches tailored to conventional Human-Driven Vehicles (HDVs), there is a compelling imperative to extend these advancements involving CAVs.

Chapter 4 of this dissertation introduced a new macroscopic model for mixed traffic flow, laying the foundation for subsequent exploration. In Chapter 7, we proposed a Model Predictive Control (MPC)-driven Variable Speed Limit (VSL) control specifically designed for motorway traffic, focusing primarily on scenarios involving HDVs.

The present chapter has brought to the forefront a novel control paradigm grounded in MPC. Our study encompasses a mixed traffic environment, featuring 40 % CAVs alongside HDVs, with control measures exclusively targeting CAVs within the motorway. Departing from conventional VSL control practices, our approach centers on the regulation of time headway (τ_h) among CAVs, acknowledging the substantial impact of this parameter on Fundamental Diagrams (FD).

Our findings present compelling evidence of substantial enhancements in the FD of the motorway corridor. Most notably, the critical density (ρ_{cr}) within the FD has increased significantly, rising from 19 veh/km to 29 veh/km. This represents a noteworthy milestone in traffic management. Furthermore, our study demonstrates an approximate 16 % increase in flow rates across all segments of the motorway.

The outcomes of this study hold profound significance, particularly in the context of advancing Intelligent Transportation Systems (ITS). The pressing need to devise novel control strategies capable of alleviating congestion while enhancing traffic management techniques cannot be overstated. As a promising avenue for future research, the implications of our findings can be extended to explore scenarios involving varied CAVs Penetration Rates (PR) and comparisons with conventional VSL control strategies. Additionally, conducting safety assessments for the remarkably small values of τ_h is essential to ensure the efficient management of future traffic scenarios.

Chapter 9

Conclusions and Future Directions

In this Chapter, the main findings of this dissertation are concluded followed by recommendations for future work. The aims of this dissertation are successfully achieved. The content of this dissertation is crucial to investigate in the context of developing Intelligent Transportation Systems (ITS). Additionally, with the emergence of Connected and Autonomous Vehicles (CAVs), traffic dynamics are believed to alter significantly, thus, necessitating the revisions of the Macroscopic Continuum Traffic Flow Models (MCTFMs). The MCTFMs are revised significantly for various driving characteristics, including, but not limited to physiological responses, driver reactions, and stimuli for Human-Driven Vehicles (HDVs). However, the future traffic seems a complex mixture of more than one typical behavior as the Internet of Things (IoT) and the advent of new technologies will allow CAVs to have marginal characteristics. In light of the aforementioned assertions, current models and control approaches are questioned and thus revised in this dissertation.

9.1 Conclusions

In Chapter 2 of this dissertation, the basic definitions and theory is presented followed by the state-of-the-art literature review of the MCTFMs. The literature review is provided in the context of the context of Continuum Traffic Flow Models (CTFMs). Particularly, the Second Order Continuum Traffic Flow Models (SOTFMs) are studied in detail in the context of HDVs and the current gaps for revising these models for the characteristics of CAVs are identified. In the same Chapter, the practical utility of SOTFMs in traffic control is explored. It has been noted that the SOTFMs are rarely used in the control applications. Thus, later in the dissertation attention has been paid to the applications of SOTFMs in traffic control. Hereafter, this dissertation is carried out in two distinct directions. One focusing on the revisions of the conventional SOTFMs for CAVs, and the other focused on the application of these models in traffic control.

To start with, in Chapter 3, the conventional SOTFMs are considered for a detailed appraisal. The rationale behind presenting the appraisal of the SOTFMs is to explore the characteristics of structural terms of these models and to identify the impacts of the model parameters on the stability and overall outcome. Thus, in this Chapter, numerical simulations and sensitivity analysis are conducted of the specific set of SOTFMs. The performance of the set of SOTFMs is compared with the microscopic simulation performed in Simulation of Urban Mobility (SUMO) that is a high-fidelity traffic simulation software. It has been demonstrated that the SOTFMs are promising models in context to reproduce real-world traffic patterns. The prediction capability of the set of SOTFMs is explored, and the most sensitive parameters of the models are identified.

In Chapter 4, the well-known JQZ model is revised for mixed traffic following a pragmatic approach. In this Chapter, the driving characteristics of HDVs and CAVs are distinctly characterized. Specifically, the headway characteristics of HDVs and CAVs are modeled. A new SOTFM has been proposed, and validated on microscopic data obtained from Dublin motorway in Ireland. The proposed model is capable of reproducing traffic patterns and phenomena. The proposed model and the results from microscopic simulations are thoroughly compared in the presence of different Penetration Rates (PRs) of CAVs. The practical significance of the proposed model is showcased by conducting the Level of Service (LOS) analysis of the Dublin motorway. It has been demonstrated that the LOS significantly improves with the increase in the PR of CAVs. Additionally, the traffic shockwave formation and dissipation is studied in the presence of CAVs. It has been observed that with higher PR of CAVs, the traffic shockwave dissipates rapidly as compared to that in the presence of HDVs. However, a pragmatic approach is followed in this Chapter which can be questioned as the Fundamental Diagram (FD) of traffic is calibrated for each scenario which captures the dynamics of the traffic, and the microscopic dynamics impacting the FD of traffic are not modeled. However, this approach relies on real-time traffic data.

In order to respond to the aforementioned gap, a continuum approach instead of a pragmatic approach is followed and a new SOTFM is proposed for traffic mixture in Chapter 5. In this Chapter, the SOTFM is revised for traffic mixture comprising CAVs, HDVs, Heavy Vehicles (HVs), and Connected Heavy Vehicles (CHVs). In this part of the dissertation, a unique approach has been followed. The microscopic characteristics of the traffic impacting FD are explicitly model for FD. Thus, two developments are considered, one the revisions of the anticipation term of the well-known JQZ model for mixed traffic, and the other, to explicitly model the FD of traffic for traffic mixture. Additionally, this new macroscopic model is contemplated with an emissions model and the study is further extended to the investigations of fuel consumption and greenhouse gas (GHG) emissions. The findings of the study demonstrate that HVs in the traffic mixture can cause a friction effect on the traffic flow and even a small PR of HVs can decrease the traffic flow rate, while the CHVs in the mixture yield positive impacts. Further, the substantial reduction in fuel consumption and GHG emissions reduction been demonstrated with the increase in the PR of CAVs, while the HVs negatively impact the fuel consumption and GHG emissions.

In Chapter 6, the modeling perspective of CAVs is considered, but study is more focused on the regulations of the characteristics of CAVs on the macroscopic level. In this research, we investigate the dynamics of traffic flow in the presence of CAVs considering the anticipation behavior of CAVs. The criticality associated with the smaller reaction times of CAVs is the prime concern. This Chapter explores the impacts of density-dependent reaction times of CAVs. The aim of this chapter is to propose a methodology for the adjustment of reaction times of CAVs given any particular traffic conditions. In this approach modeling of the characteristics of CAVs is performed to regulate the driving characteristics of CAVs according to the density conditions. This approach ensures the safety of the traffic flow. This model can be practically employed in product developments for CAVs to predict future traffic situations based on the current traffic conditions and alter their driving characteristics accordingly. Results demonstrate that the traffic dynamics significantly improve by improving the driving characteristics of CAVs. Significant development in the critical density of traffic is observed associated with smaller reaction times and lengthways gap.

With Chapter 6, the facet of this dissertation is comes to an end. Next, the role of SOTFMs in practical applications particularly in traffic control is explored. To do so, first, a Model Predictive Control (MPC)-driven Variable Speed Limit (VSL) control is implemented on the Dublin motorway in the context of all-HDVs. In doing so, we first validate the role of SOTFM in the MPC paradigm as the SOTFM is employed as a prediction model in the optimization process. After doing so, the same MPC framework is extended for control of mixed traffic employing the SOTFM proposed for mixed traffic in Chapter 4.

In Chapter 7, the MPC-driven VSL control of motorway traffic is implemented for conventional traffic. The prediction model in the optimization process in the MPC framework is a SOTFM proposed by [5]. The control input is the speed limit implemented in the segments of the motorway. Within the MPC paradigm, congestion in one segment of the motorway is mitigated with in the other its occurrence time is significantly reduced. After, the successful implementation of VSL control driven on MPC, next, the same methodology is extended for the regulation of traffic flow in mixed traffic by proposing a novel control approach.

In Chapter 8, a novel strategy for the regulation of traffic flow with CAVs is proposed. At present, one mixed traffic scenario such that 40 percent CAVs and 60 percent HDVs are considered. Within this approach, the same MPC framework of Chapter 7 is followed. Instead of the conventional VSL control, the flow is regulated with CAVs by regulating their time headway. Time headway is crucial for the changes in traffic. The FD of traffic alters significantly with any variation in the time headway of CAVs. It has been demonstrated in this Chapter in detail. With smaller time headway, the critical density can be enhanced and this allows smooth transition of the capacity of the road segment from congested to uncongested. The FD of traffic is practically calibrated, each FD associated with the time headway is employed in the optimization process to decide the optimal value of time headway, and the CAVs are regulated accordingly. The FD of traffic improves significantly within the context of the proposed novel control with CAVs, and the traffic flow is smoother after the implementation of control, approximately 16 percent of improvement is witnessed by all segments of the motorway.

This dissertation concludes here, the modeling and control perspectives associated with CAVs in mixed traffic environments are extensively examined. Far-reaching analysis and different modeling approach with a novel control approach with CAVs is successfully presented. Next, the future directions are presented.

9.2 Future Directions

In the final Section of this dissertation, some suggestions are suggested as a direction for future research.

- We explore and revise the SOTFMs for CAVs in a specific model tree of the MCTFMs, further gaps can be identified in the other conventional developments and extensions of MCTFMs.

- We explore the driving characteristics of CAVs, sometimes, they are associated with critically small values of the parameters of the models taken from the literature. Safety analysis can be performed on the parameters of the models to identify the optimal range of the parameters of the models.

- In this dissertation, we propose a novel regulation of traffic flow with CAVs, we consider only one scenario of mixed traffic, this particular part of the dissertation can be extended to consider more complex scenarios. Further, a comparative analysis of the conventional control approaches and the proposed control approach can be performed.

- The proposed SOTFMs in this dissertation can be employed in real-time management such as flow predictions in adverse weather and road conditions. Prevailing traffic conditions can be investigated in mixed traffic environments for an effective management strategies.

- Investigating the issues with calibration and validation of the proposed SOTFMs to extract the best model performances in mixed traffic environments.

Bibliography

[1] Maxime Guériau and Ivana Dusparic. Quantifying the impact of connected and autonomous vehicles on traffic efficiency and safety in mixed traffic. In *2020 IEEE 23rd International Conference on Intelligent Transportation Systems (ITSC)*, pages 1–8. IEEE, 2020.

[2] Govinda R Timilsina and Hari B Dulal. Urban road transportation externalities: Costs and choice of policy instruments. *The World Bank Research Observer*, 26(1):162–191, 2011.

[3] Koohong Chung, Jittichai Rudjanakanoknad, and Michael J Cassidy. Relation between traffic density and capacity drop at three freeway bottlenecks. *Transportation Research Part B: Methodological*, 41(1):82–95, 2007.

[4] Amudapuram Mohan Rao and Kalaga Ramachandra Rao. Measuring urban traffic congestion-a review. *International Journal for Traffic & Transport Engineering*, 2(4), 2012.

[5] Zawar H Khan, Waheed Imran, Thomas Aaron Gulliver, Khurram S Khattak, Zahid Wadud, and Akhtar Nawaz Khan. An anisotropic traffic model based on driver interaction. *IEEE Access*, 8:66799–66812, 2020.

[6] Agachai Sumalee and Hung Wai Ho. Smarter and more connected: Future intelligent transportation system. *IATSS Research*, 42(2):67–71, 2018.

[7] I Spyropoulou and MG Karlaftis. Incorporating intelligent speed adaptation systems into microscopic traffic models. *IET Intelligent Transport Systems*, 2(4):331–339, 2008.

[8] Hamid Khayyam, Bahman Javadi, Mahdi Jalili, and Reza N Jazar. Artificial intelligence and internet of things for autonomous vehicles. *Nonlinear Approaches in Engineering Applications: Automotive Applications of Engineering Problems*, pages 39–68, 2020.

[9] Soumya Kanti Datta, Rui Pedro Ferreira Da Costa, Jérôme Härri, and Christian Bonnet. Integrating connected vehicles in internet of things ecosystems: Challenges and solutions. In *2016 IEEE 17th International Symposium on a World of Wireless, Mobile and Multimedia Networks (WoWMoM)*, pages 1–6. IEEE, 2016.

[10] Waheed Imran, Zawar H Khan, T Aaron Gulliver, Khurram S Khattak, and Hassan Nasir. A macroscopic traffic model for heterogeneous flow. *Chinese Journal of Physics*, 63:419–435, 2020.

[11] Waheed Imran and Luigi Pariota. Macroscopic evaluation of traffic flow in view of connected and autonomous vehicles: A simulation-based approach. *Alexandria Engineering Journal*, 79:581–590, 2023.

[12] Zawar H. Khan, Waheed Imran, Sajid Azeem, Khurram S. Khattak, T Aaron Gulliver, and Muhammad Sagheer Aslam. A macroscopic traffic model based on driver reaction and traffic stimuli. *Applied Sciences*, 9(14):2848, 2019.

[13] Waheed Imran, Zawar H Khan, Thomas Aaron Gulliver, Khurram S Khattak, Salman Saeed, and M Sagheer Aslam. Macroscopic traffic flow characterization for stimuli based on driver reaction. *Civil Engineering Journal*, 7(1):1–13, 2021.

[14] Zawar Hussain Khan, Thomas Aaron Gulliver, Waheed Imran, Khurram Shehzad Khattak, Ahmed B Altamimi, and Azhar Qazi. A macroscopic traffic model based on relaxation time. *Alexandria Engineering Journal*, 61(1):585–596, 2022.

[15] Dong Ngoduy and R Eddie Wilson. Multianticipative nonlocal macroscopic traffic model. *Computer-Aided Civil and Infrastructure Engineering*, 29(4):248–263, 2014.

[16] Amir Hossein Karbasi, Behzad Bamdad Mehrabani, Mario Cools, Luca Sgambi, and Mahmoud Saffarzadeh. Comparison of speed-density models in the age of connected and automated vehicles. *Transportation Research Record*, 2677(3):849–865, 2023.

[17] Waheed Imran, Zawar H Khan, T Aaron Gulliver, Muhammad Alam, and Khurram S Khattak. Non-homogeneous traffic characterization based on driver reaction and stimuli. *Transportation Research Interdisciplinary Perspectives*, 21:100858, 2023.

[18] BD Greenshields. A study of traffic capacity. in proceedings of the 14th annual meeting of the highway research board. 1935.

[19] Markos Papageorgiou, Jean-Marc Blosseville, and Habib Hadj-Salem. Macroscopic modelling of traffic flow on the boulevard périphérique in paris. *Transportation Research Part B: Methodological*, 23(1):29–47, 1989.

[20] Hiroshi Makino, Shunsuke Kamijo, C Shin, and E Chung. Intelligent transport systems (its) introduction guide. *Japan Society of Civil Engineers (JSCE)*, 2016.

[21] Muhammad Alam, Joaquim Ferreira, and José Fonseca. Introduction to intelligent transportation systems. *Intelligent Transportation Systems: Dependable Vehicular Communications for Improved Road Safety*, pages 1–17, 2016.

[22] Markos Papageorgiou, Moshe Ben-Akiva, Jon Bottom, Piet HL Bovy, Serge P Hoogendoorn, Nicholas Brian Hounsell, Apostolos Kotsialos, and Mike McDonald. ITS and traffic management. *Handbooks in Operations Research and Management Science*, 14:715–774, 2007.

[23] Aidil Redza Khan, Mohd Faizal Jamlos, Nurmadiha Osman, Muhammad Izhar Ishak, Fatimah Dzaharudin, You Kok Yeow, and Khairil Anuar Khairi. DSRC technology in Vehicle-to-Vehicle (V2V) and Vehicle-to-Infrastructure (V2I) IoT system for Intelligent Transportation System (ITS): A review. *Recent Trends in Mechatronics Towards Industry 4.0: Selected Articles from iM3F 2020, Malaysia*, pages 97–106, 2022.

[24] Phil Blythe. Rfid for road tolling, road-use pricing and vehicle access control. In *IEE colloquium on RFID technology (Ref. No. 1999/123)*, pages 8–1. IET, 1999.

[25] MY Idna Idris, YY Leng, EM Tamil, NM Noor, Zaidi Razak, et al. Car park system: A review of smart parking system and ITS technology. *Information Technology Journal*, 8(2):101–113, 2009.

[26] Kashif Naseer Qureshi and Abdul Hanan Abdullah. A survey on intelligent transportation systems. *Middle-East Journal of Scientific Research*, 15(5):629–642, 2013.

[27] Carlos E Garcia and Manfred Morari. Internal model control. a unifying review and some new results. *Industrial & Engineering Chemistry Process Design and Development*, 21(2):308–323, 1982.

[28] James B Rawlings. Tutorial overview of model predictive control. *IEEE Control Systems Magazine*, 20(3):38–52, 2000.

[29] Max Schwenzer, Muzaffer Ay, Thomas Bergs, and Dirk Abel. Review on model predictive control: An engineering perspective. *The International Journal of Advanced Manufacturing Technology*, 117(5-6):1327–1349, 2021.

[30] David Q Mayne, James B Rawlings, Christopher V Rao, and Pierre OM Scokaert. Constrained model predictive control: Stability and optimality. *Automatica*, 36(6):789–814, 2000.

[31] Benedetto Piccoli, Andrea Tosin, et al. Vehicular traffic: A review of continuum mathematical models. *Encyclopedia of Complexity and Systems Science*, 22:9727–9749, 2009.

[32] Carlo Caligaris, Simona Sacone, and Silvia Siri. On an implicit and stable resolution scheme for the Payne–Whitham model. *Mathematical and Computer Modelling*, 54(1-2):378–387, 2011.

[33] Maya Briani, Emiliano Cristiani, and Paolo Ranut. Macroscopic and multi-scale models for multi-class vehicular dynamics with uneven space occupancy: a case study. *Axioms*, 10(2):102, 2021.

[34] Michael James Lighthill and Gerald Beresford Whitham. On kinematic waves II. a theory of traffic flow on long crowded roads. *Proceedings of the Royal Society of London. Series A. Mathematical and Physical Sciences*, 229(1178):317–345, 1955.

[35] PI Richards. Shock waves on the highway. *Operations Research. pp. 42_51*, 1956.

[36] Daud Khan, Zawar Hussain Khan, Waheed Imran, Khurram Shehzad Khattak, and Thomas Aaron Gulliver. Macroscopic flow characterization at t-junctions. *Transportation Research Interdisciplinary Perspectives*, 14:100591, 2022.

[37] Waheed Imran, Zawar H Khan, Thomas Aaron Gulliver, Khurram S Khattak, Salman Saeed, and M Sagheer Aslam. Macroscopic traffic flow characterization for stimuli based on driver reaction. *Civil Engineering Journal*, 7(1):1–13, 2021.

[38] Guoqing Liu, Anastasios S Lyrintzis, and Panos G Michalopoulos. Improved high-order model for freeway traffic flow. *Transportation Research Record*, 1644(1):37–46, 1998.

[39] Carlos F Daganzo. Requiem for second-order fluid approximations of traffic flow. *Transportation Research Part B: Methodological*, 29(4):277–286, 1995.

[40] Zawar H Khan and T Aaron Gulliver. A macroscopic traffic model for traffic flow harmonization. *European Transport Research Review*, 10(2):1–12, 2018.

[41] Ismael M Pour and Habibollah Nassiri. A macroscopic traffic flow model that includes driver sensitivity to the number of free spaces ahead. *Transportmetrica B: Transport Dynamics*, 8(1):290–306, 2020.

[42] Shi-Teng Zheng, Rui Jiang, Bin Jia, Junfang Tian, and Ziyou Gao. Impact of stochasticity on traffic flow dynamics in macroscopic continuum models. *Transportation Research Record*, 2674(10):690–704, 2020.

[43] Zawar H Khan, Syed Abid Ali Shah, and T Aaron Gulliver. A macroscopic traffic model based on weather conditions. *Chinese Physics B*, 27(7):070202, 2018.

[44] Sven Maerivoet and Bart De Moor. Transportation planning and traffic flow models. Technical Report 05–155, Katholieke Universiteit Leuven, July 2005.

[45] Harold J Payne. Model of freeway traffic and control. *Mathematical Model of Public System*, pages 51–61, 1971.

[46] Gerald Beresford Whitham. *Linear and nonlinear waves*. John Wiley & Sons, 1971.

[47] Markos Papageorgiou. Some remarks on macroscopic traffic flow modelling. *Transportation Research Part A: Policy and Practice*, 32(5):323–329, 1998.

[48] A. Aw and Michel Rascle. Resurrection of “second order" models of traffic flow. *SIAM Journal of Applied Mathematics*, 60(3):916–938, 2000.

[49] Zawar H. Khan, Waheed Imran, Sajid Azeem, Khurram S. Khattak, T Aaron Gulliver, and Muhammad Sagheer Aslam. A macroscopic traffic model based on driver reaction and traffic stimuli. *Applied Sciences*, 9(14):2848, 2019.

[50] Dirk Helbing and AF Johansson. On the controversy around Daganzo's requiem for and aw-rascle's resurrection of second-order traffic flow models. *The European Physical Journal B*, 69(4):549–562, 2009.

[51] HM Zhang. Comment on “on the controversy around Daganzo's requiem for and aw-rascle's resurrection of second-order traffic flow models" by D. Helbing and AF Johansson. *The European Physical Journal B*, 69(4):563–568, 2009.

[52] Rui Jiang, Qing-Song Wu, and Zuo-Jin Zhu. A new continuum model for traffic flow and numerical tests. *Transportation Research Part B: Methodological*, 36(5):405–419, 2002.

[53] Saeed Mohammadian, Zuduo Zheng, Md Mazharul Haque, and Ashish Bhaskar. Performance of continuum models for realworld traffic flows: Comprehensive benchmarking. *Transportation Research Part B: Methodological*, 147:132–167, 2021.

[54] Antonella Ferrara, Simona Sacone, Silvia Siri, Antonella Ferrara, Simona Sacone, and Silvia Siri. Fundamentals of traffic dynamics. *Freeway Traffic Modelling and Control*, pages 25–44, 2018.

[55] Yuwei Bie, Tony Z Qiu, Can Zhang, Cunbao Zhang, et al. Introducing weather factor modelling into macro traffic state prediction. *Journal of Advanced Transportation*, 2017, 2017.

[56] Cong Zhai and Weitiao Wu. A continuum model considering the uncertain velocity of preceding vehicles on gradient highways. *Physica A: Statistical Mechanics and its Applications*, 588:126561, 2022.

[57] Lu Sun, Ammar Jafaripournimchahi, Alain Kornhauser, and Wusheng Hu. A new higher-order viscous continuum traffic flow model considering driver memory in the era of autonomous and connected vehicles. *Physica A: Statistical Mechanics and Its Applications*, 547:123829, 2020.

[58] Tie-Qiao Tang, Yan-Feng Shi, Hai-Jun Huang, and Hua-Yan Shang. A new macro model for traffic flow on a highway with bus stop. *Communications in Theoretical Physics*, 55(6):1113, 2011.

[59] Cong Zhai and Weitiao Wu. A continuous traffic flow model considering predictive headway variation and preceding vehicle's taillight effect. *Physica A: Statistical Mechanics and its Applications*, 584:126364, 2021.

[60] LC Davis. Nonlinear dynamics of autonomous vehicles with limits on acceleration. *Physica A: Statistical Mechanics and its Applications*, 405:128–139, 2014.

[61] Zhihong Yao, Rong Hu, Yangsheng Jiang, and Taorang Xu. Stability and safety evaluation of mixed traffic flow with connected automated vehicles on expressways. *Journal of Safety Research*, 75:262–274, 2020.

[62] Liang Zheng, Peter J Jin, and Helai Huang. An anisotropic continuum model considering bi-directional information impact. *Transportation Research Part B: Methodological*, 75:36–57, 2015.

[63] Dong Ngoduy and D Jia. Multi anticipative bidirectional macroscopic traffic model considering cooperative driving strategy. *Transportmetrica B: Transport Dynamics*, 5(1):96–110, 2017.

[64] D Ngoduy, SP Hoogendoorn, and R Liu. Continuum modeling of cooperative traffic flow dynamics. *Physica A: Statistical Mechanics and its Applications*, 388(13):2705–2716, 2009.

[65] D Ngoduy. Application of gas-kinetic theory to modelling mixed traffic of manual and acc vehicles. *Transportmetrica*, 8(1):43–60, 2012.

[66] Anargiros I Delis, Ioannis K Nikolos, and Markos Papageorgiou. Simulation of the penetration rate effects of ACC and CACC on macroscopic traffic dynamics. In *2016 IEEE 19th International Conference on Intelligent Transportation Systems (ITSC)*, pages 336–341. IEEE, 2016.

[67] Argiris I Delis, Ioannis K Nikolos, and Markos Papageorgiou. Macroscopic traffic flow modeling with adaptive cruise control: Development and numerical solution. *Computers & Mathematics with Applications*, 70(8):1921–1947, 2015.

[68] KT Waldeer. Kinetic theory in vehicular traffic flow modeling. In *25th International Symposium on Rarefied Gas Dynamics, Saint-Petersburg, Russia*, 2006.

[69] Hari Hara Sharan Nagalur Subraveti, Victor L Knoop, and Bart van Arem. First order multi-lane traffic flow model–an incentive based macroscopic model to represent lane change dynamics. *Transportmetrica B: Transport Dynamics*, 7(1):1758–1779, 2019.

[70] Yuting Jin, Zhihong Yao, Jiazhe Han, Lu Hu, and Yangsheng Jiang. Variable cell transmission model for mixed traffic flow with connected automated vehicles and human-driven vehicles. *Journal of Advanced Transportation*, 2022:1–15, 2022.

[71] Reza Mohajerpoor and Mohsen Ramezani. Mixed flow of autonomous and human-driven vehicles: Analytical headway modeling and optimal lane management. *Transportation Research Part C: Emerging Technologies*, 109:194–210, 2019.

[72] Abebe Dress Beza, Mohammad Maghrour Zefreh, and Adam Torok. Impacts of different types of automated vehicles on traffic flow characteristics and emissions: a microscopic traffic simulation of different freeway segments. *Energies*, 15(18):6669, 2022.

[73] Silvia Siri, Cecilia Pasquale, Simona Sacone, and Antonella Ferrara. Freeway traffic control: A survey. *Automatica*, 130:109655, 2021.

[74] José Ramón Domínguez Frejo and Eduardo Fernández Camacho. Global versus local mpc algorithms in freeway traffic control with ramp metering and variable speed limits. *IEEE Transactions on Intelligent Transportation Systems*, 13(4):1556–1565, 2012.

[75] Bao-Lin Ye, Weimin Wu, Keyu Ruan, Lingxi Li, Tehuan Chen, Huimin Gao, and Yaobin Chen. A survey of model predictive control methods for traffic signal control. *IEEE/CAA Journal of Automatica Sinica*, 6(3):623–640, 2019.

[76] Lakshmi Dhevi Baskar, Bart De Schutter, J Hellendoorn, and Zoltan Papp. Traffic control and intelligent vehicle highway systems: a survey. *IET Intelligent Transport Systems*, 5(1):38–52, 2011.

[77] Danjue Chen, Soyoung Ahn, and Andreas Hegyi. Variable speed limit control for steady and oscillatory queues at fixed freeway bottlenecks. *Transportation Research Part B: Methodological*, 70:340–358, 2014.

[78] Yuwei Bie, Mudasser Seraj, Can Zhang, and Tony Z Qiu. Improving traffic state prediction model for variable speed limit control by introducing stochastic supply and demand. *Journal of Advanced Transportation*, 2018, 2018.

[79] Yu Han, Meng Wang, Ziang He, Zhibin Li, Hao Wang, and Pan Liu. A linear lagrangian model predictive controller of macro-and micro-variable speed limits to eliminate freeway jam waves. *Transportation Research part C: Emerging Technologies*, 128:103121, 2021.

[80] Andreas Hegyi, Bart De Schutter, and Johannes Hellendoorn. Optimal coordination of variable speed limits to suppress shock waves. *IEEE Transactions on Intelligent Transportation Systems*, 6(1):102–112, 2005.

[81] Shubin Li, Tao Wang, Hualing Ren, Baiying Shi, Xiangke Kong, Jianyong Chai, and Xuejuan Wang. Variable speed limit strategies based on the macro hierarchical control traffic flow model. *Journal of Advanced Transportation*, 2021:1–10, 2021.

[82] Danjue Chen, Soyoung Ahn, and Andreas Hegyi. Variable speed limit control for steady and oscillatory queues at fixed freeway bottlenecks. *Transportation Research Part B: Methodological*, 70:340–358, 2014.

[83] Danjue Chen and Soyoung Ahn. Variable speed limit control for severe non-recurrent freeway bottlenecks. *Transportation Research Part C: Emerging Technologies*, 51:210–230, 2015.

[84] Jose Ramon D Frejo, Ioannis Papamichail, Markos Papageorgiou, and Bart De Schutter. A new macroscopic model for variable speed limits. *IFAC-PapersOnLine*, 51(9):343–348, 2018.

[85] José Ramón D Frejo, Ioannis Papamichail, Markos Papageorgiou, and Bart De Schutter. Macroscopic modeling of variable speed limits on freeways. *Transportation Research Part C: Emerging Technologies*, 100:15–33, 2019.

[86] Shuai Liu, Bart De Schutter, and Hans Hellendoorn. Model predictive traffic control based on a new multi-class metanet model. *IFAC Proceedings Volumes*, 47(3):8781–8786, 2014.

[87] Monique Van den Berg, Andreas Hegyi, Bart De Schutter, and Hans Hellendoorn. Integrated traffic control for mixed urban and freeway networks: A model predictive control approach. *European Journal of Transport and Infrastructure Research*, 7(3), 2007.

[88] Nikolas Geroliminis, Jack Haddad, and Mohsen Ramezani. Optimal perimeter control for two urban regions with macroscopic fundamental diagrams: A model predictive approach. *IEEE Transactions on Intelligent Transportation Systems*, 14(1):348–359, 2012.

[89] José Ramón Domínguez Frejo. Model predictive control for freeway traffic networks. 2015.

[90] Femke. Kessels. *Traffic Flow Modelling: Introduction to Traffic Flow Theory Through a Genealogy of Models*. Springer, 2018.

[91] Paola Goatin. Macroscopic traffic flow modelling: from kinematic waves to autonomous vehicles. *Communications in Applied and Industrial Mathematics*, 14(1):1–16, 2023.

[92] Apostolos Kotsialos, Markos Papageorgiou, Christina Diakaki, Yannis Pavlis, and Frans Middelham. Traffic flow modeling of large-scale motorway networks using the macroscopic modeling tool metanet. *IEEE Transactions on Intelligent Transportation Systems*, 3(4):282–292, 2002.

[93] Jiah Song and Smadar Karni. A second order traffic flow model with lane changing. *Journal of Scientific Computing*, 81(3):1429–1445, 2019.

[94] Jorge A Laval. Self-organized criticality of traffic flow: Implications for congestion management technologies. *Transportation Research Part C: Emerging Technologies*, 149:104056, 2023.

[95] Daiheng Ni. Limitations of current traffic models and strategies to address them. *Simulation Modelling Practice and Theory*, 104:102137, 2020.

[96] Elvira Thonhofer, Toni Palau, Andreas Kuhn, Stefan Jakubek, and Martin Kozek. Macroscopic traffic model for large scale urban traffic network design. *Simulation Modelling Practice and Theory*, 80:32–49, 2018.

[97] Ludovica Adacher and Marco Tiriolo. A macroscopic model with the advantages of microscopic model: A review of cell transmission model's extensions for urban traffic networks. *Simulation Modelling Practice and Theory*, 86:102–119, 2018.

[98] Waheed Imran, Zawar H Khan, T Aaron Gulliver, Khurram S Khattak, and Hassan Nasir. A macroscopic traffic model for heterogeneous flow. *Chinese Journal of Physics*, 63:419–435, 2020.

[99] Zawar H Khan and T Aaron Gulliver. A macroscopic traffic model based on transition velocities. *Journal of computational science*, 43:101131, 2020.

[100] Daniel Krajzewicz. Traffic simulation with SUMO–Simulation of Urban Mobility. In *Fundamentals of Traffic Simulation*, pages 269–293. Springer, 2010.

[101] Mega Ayu Dian Khumara, Lubna Fauziyyah, and Prima Kristalina. Estimation of urban traffic state using Simulation of Urban Mobility (SUMO) to optimize intelligent transport system in smart city. In *2018 International Electronics Symposium on Engineering Technology and Applications (IES-ETA)*, pages 163–169. IEEE, 2018.

[102] Joanne V Morgan. *Numerical methods for macroscopic traffic models*. PhD thesis, Citeseer, 2002.

[103] Hari Krishna Gaddam, Anjaneyulu Chinthireddy, and K Ramachandra Rao. Comparison of numerical schemes for LWR model under heterogeneous traffic conditions. *Periodica Polytechnica Transportation Engineering*, 44(3):132–140, 2016.

[104] Jingang Yi, Hao Lin, Luis Alvarez, and Roberto Horowitz. Stability of macroscopic traffic flow modeling through wavefront expansion. *Transportation Research Part B: Methodological*, 37(7):661–679, 2003.

[105] Liang Zheng, Zhengbing He, and Tian He. An anisotropic continuum model and its calibration with an improved monkey algorithm. *Transportmetrica A: Transport Science*, 13(6):519–543, 2017.

[106] TQ Tang, Yong Hong Wu, Louis Caccetta, and HJ Huang. A new car-following model with consideration of roadside memorial. *Physics Letters A*, 375(44):3845–3850, 2011.

[107] Jean-Patrick Lebacque, Salim Mammar, and Habib Haj-Salem. The aw–rascle and zhang's model: Vacuum problems, existence and regularity of the solutions of the riemann problem. *Transportation Research Part B: Methodological*, 41(7):710–721, 2007.

[108] Femke van Wageningen-Kessels, Bas van't Hof, Serge P Hoogendoorn, Hans Van Lint, and Kees Vuik. Anisotropy in generic multi-class traffic flow models. *Transportmetrica A: Transport Science*, 9(5):451–472, 2013.

[109] MN Smirnova, A Bogdanova, Zuojin Zhu, and NN Smirnov. Traffic flow sensitivity to parameters in viscoelastic modelling. *Transportmetrica B: transport dynamics*, 5(1):111–127, 2017.

[110] Angelo Coppola, Luca Di Costanzo, Luigi Pariota, Stefania Santini, and Gennaro Nicola Bifulco. An integrated simulation environment to test the effectiveness of glosa services under different working conditions. *Transportation Research Part C: Emerging Technologies*, 134:103455, 2022.

[111] Palak Maheshwary, Kinjal Bhattacharyya, Bhargab Maitra, and Manfred Boltze. A methodology for calibration of traffic micro-simulator for urban heterogeneous traffic operations. *Journal of Traffic and Transportation Engineering (English Edition)*, 7(4):507–519, 2020.

[112] Maurice George Kendall et al. The advanced theory of statistics. *The advanced theory of statistics.*, (2nd Ed), 1946.

[113] Andrea Saltelli, Marco Ratto, Terry Andres, Francesca Campolongo, Jessica Cariboni, Debora Gatelli, Michaela Saisana, and Stefano Tarantola. *Global Sensitivity Analysis: The primer*. John Wiley & Sons, 2008.

[114] Saman Razavi, Anthony Jakeman, Andrea Saltelli, Clémentine Prieur, Bertrand Iooss, Emanuele Borgonovo, Elmar Plischke, Samuele Lo Piano, Takuya Iwanaga, William Becker, et al. The future of sensitivity analysis: An essential discipline for systems modeling and policy support. *Environmental Modelling & Software*, 137:104954, 2021.

[115] Francesca Pianosi and Thorsten Wagener. A simple and efficient method for global sensitivity analysis based on cumulative distribution functions. *Environmental Modelling & Software*, 67:1–11, 2015.

[116] Jian Yang, Yinjie Ma, Jianqin Fu, Jun Shu, and Jingping Liu. Parametric study of gasoline properties on combustion characteristics of gasoline compression engines using reaction kinetics simulation and density-based global sensitivity analysis. *Applied Energy*, 255:113858, 2019.

[117] Shobhit Chaturvedi and Elangovan Rajasekar. Application of a probabilistic lhs-pawn approach to assess building cooling energy demand uncertainties. In *Building Simulation*, volume 15, pages 373–387. Springer, 2022.

[118] Angelo Coppola, Claudio D'Aniello, Luigi Pariota, and Gennaro Nicola Bifulco. Assessing safety functionalities in the design and validation of driving automation. *Transportation Research Part C: Emerging Technologies*, 154:104243, 2023.

[119] Francesca Pianosi and Thorsten Wagener. Distribution-based sensitivity analysis from a generic input-output sample. *Environmental Modelling & Software*, 108:197–207, 2018.

[120] Valentina Noacco, Fanny Sarrazin, Francesca Pianosi, and Thorsten Wagener. Matlab/r workflows to assess critical choices in global sensitivity analysis using the safe toolbox. *MethodsX*, 6:2258–2280, 2019.

[121] Christina Diakaki, Markos Papageorgiou, Ioannis Papamichail, and Ioannis Nikolos. Overview and analysis of vehicle automation and communication systems from a motorway traffic management perspective. *Transportation Research Part A: Policy and Practice*, 75:147–165, 2015.

[122] Adeel Lari, Frank Douma, and Ify Onyiah. Self-driving vehicles: current status of autonomous vehicle development and minnesota policy implications. *The Minnesota Journal of Law, Science and Technology*, 22:000–000, 2015.

[123] Kun Li and Petros Ioannou. Modeling of traffic flow of automated vehicles. *IEEE Transactions on Intelligent Transportation Systems*, 5(2):99–113, 2004.

[124] Lili Du, Lanshan Han, and Shuwei Chen. Coordinated online in-vehicle routing balancing user optimality and system optimality through information perturbation. *Transportation Research Part B: Methodological*, 79:121–133, 2015.

[125] Xiaobo Qu, Shuaian Wang, and Jin Zhang. On the fundamental diagram for freeway traffic: A novel calibration approach for single-regime models. *Transportation Research Part B: Methodological*, 73:91–102, 2015.

[126] Lishan Sun, Zeyu Cheng, Dewen Kong, Yan Xu, Shangwu Wen, and Kangyu Zhang. Modeling and analysis of human-machine mixed traffic flow considering the influence of the trust level toward autonomous vehicles. *Simulation Modelling Practice and Theory*, In Press, Journal Pre-proof(1):102741, 2023.

[127] Xiaobo Qu, Jin Zhang, and Shuaian Wang. On the stochastic fundamental diagram for freeway traffic: model development, analytical properties, validation, and extensive applications. *Transportation Research Part B: Methodological*, 104:256–271, 2017.

[128] Giulia Piacentini, Paola Goatin, and Antonella Ferrara. Traffic control via platoons of intelligent vehicles for saving fuel consumption in freeway systems. *IEEE Control Systems Letters*, 5(2):593–598, 2020.

[129] Yongfu Li, Qingxiu Lv, Hao Zhu, Haiqing Li, Huaqing Li, Simon Hu, Shuyou Yu, and Yibing Wang. Variable time headway policy based platoon control for heterogeneous connected vehicles with external disturbances. *IEEE Transactions on Intelligent Transportation Systems*, 23(11):21190–21200, 2022.

[130] Fang Zhou, Xiaopeng Li, and Jiaqi Ma. Parsimonious shooting heuristic for trajectory design of connected automated traffic part i: Theoretical analysis with generalized time geography. *Transportation Research Part B: Methodological*, 95:394–420, 2017.

[131] Jiaqi Ma, Xiaopeng Li, Fang Zhou, Jia Hu, and B Brian Park. Parsimonious shooting heuristic for trajectory design of connected automated traffic part ii: Computational issues and optimization. *Transportation Research Part B: Methodological*, 95:421–441, 2017.

[132] Michael W Levin and Stephen D Boyles. A multiclass cell transmission model for shared human and autonomous vehicle roads. *Transportation Research Part C: Emerging Technologies*, 62:103–116, 2016.

[133] Zawar Hussain Khan, Thomas Aaron Gulliver, H Nasir, A Rehman, and K Shahzada. A macroscopic traffic model based on driver physiological response. *Journal of Engineering Mathematics*, 115(1):21–41, 2019.

[134] Zawar H Khan, T Aaron Gulliver, Khurram S Khattak, and Azhar Qazi. A macroscopic traffic model based on reaction velocity. *Iranian Journal of Science and Technology, Transactions of Civil Engineering*, 44(1):139–150, 2020.

[135] Michael Burger, Simone Göttlich, and Thomas Jung. Derivation of second order traffic flow models with time delays. *Networks & Heterogeneous Media*, 14(2):265, 2019.

[136] WenHuan Ai, JiuNiu Zhu, WenShan Duan, and DaWei Liu. A new heterogeneous traffic flow model based on lateral distance headway. *International Journal of Modern Physics B*, 35(23):2150237, 2021.

[137] Zawar Hussain Khan, Thomas Aaron Gulliver, Waheed Imran, Khurram Shehzad Khattak, Ahmed B Altamimi, and Azhar Qazi. A macroscopic traffic model based on relaxation time. *Alexandria Engineering Journal*, 61(1):585–596, 2022.

[138] Gabriel Obed Fosu, Francis Tabi Oduro, and Carlo Caligaris. Multilane analysis of a viscous second-order macroscopic traffic flow model. *SN Partial Differential Equations and Applications*, 2(1):1–17, 2021.

[139] Andreas Schadschneider, Debashish Chowdhury, and Katsuhiro Nishinari. *Stochastic Transport in Complex Systems: from Molecules to Vehicles*. Elsevier, 2010.

[140] Nicolas Louveton, Gilles Montagne, Catherine Berthelon, and Reinoud J Bootsma. Intercepting a moving traffic gap while avoiding collision with

lead and trail vehicles: Gap-related and boundary-related influences on drivers' speed regulations during approach to an intersection. *Human Movement Science*, 31(6):1500–1516, 2012.

[141] Paweł Droździel, Sławomir Tarkowski, Iwona Rybicka, and Rafał Wrona. Drivers' reaction time research in the conditions in the real traffic. *Open Engineering*, 10(1):35–47, 2020.

[142] Michail Makridis, Konstantinos Mattas, Daniele Borio, Raimondo Giuliani, and Biagio Ciuffo. Estimating reaction time in adaptive cruise control system. In *2018 IEEE Intelligent Vehicles Symposium (IV)*, pages 1312–1317. IEEE, 2018.

[143] Dayi Qu, Xiufeng Chen, Wansan Yang, and Xiaohua Bian. Modeling of car-following required safe distance based on molecular dynamics. *Mathematical Problems in Engineering*, 2014:000–0000, 2014.

[144] Yan Kuang, Xiaobo Qu, Jinxian Weng, and Amir Etemad-Shahidi. How does the driver's perception reaction time affect the performances of crash surrogate measures? *PLOS One*, 10(9):e0138617, 2015.

[145] Carlos Flores, Vicente Milanés, and Fawzi Nashashibi. A time gap-based spacing policy for full-range car-following. In *2017 IEEE 20th International Conference on Intelligent Transportation Systems (ITSC)*, pages 1–6. IEEE, 2017.

[146] Haiyang Yu, Rui Jiang, Zhengbing He, Zuduo Zheng, Li Li, Runkun Liu, and Xiqun Chen. Automated vehicle-involved traffic flow studies: A survey of assumptions, models, speculations, and perspectives. *Transportation Research Part C: Emerging Technologies*, 127:103101, 2021.

[147] Yangzexi Liu, Jingqiu Guo, John Taplin, and Yibing Wang. Characteristic analysis of mixed traffic flow of regular and autonomous vehicles using cellular automata. *Journal of Advanced Transportation*, 2017:1–10, 2017.

[148] David Elliott, Walter Keen, and Lei Miao. Recent advances in connected and automated vehicles. *Journal of Traffic and Transportation Engineering (English edition)*, 6(2):109–131, 2019.

[149] Zhihong Yao, Yunxia Wu, Yangsheng Jiang, and Bin Ran. Modeling the fundamental diagram of mixed traffic flow with dedicated lanes for connected automated vehicles. *IEEE Transactions on Intelligent Transportation Systems*, 2022.

[150] Jianzhong Chen, Huan Liang, Jing Li, and Zhaoxin Xu. A novel distributed cooperative approach for mixed platoon consisting of connected and automated vehicles and human-driven vehicles. *Physica A: Statistical Mechanics and its Applications*, 573:125939, 2021.

[151] Dong-Fan Xie, David ZW Wang, and Zi-You Gao. Macroscopic analysis of the fundamental diagram with inhomogeneous network and instable traffic. *Transportmetrica A: Transport Science*, 12(1):20–42, 2016.

[152] Jonghae Suh and Hwasoo Yeo. An empirical study on the traffic state evolution and stop-and-go traffic development on freeways. *Transportmetrica A: Transport Science*, 12(1):80–97, 2016.

[153] Toshiyuki Inagaki and Thomas B Sheridan. A critique of the sae conditional driving automation definition, and analyses of options for improvement. *Cognition, Technology & Work*, 21(4):569–578, 2019.

[154] Martin Treiber and Arne Kesting. *Traffic Flow Dynamics*. Springer, 2013.

[155] Vicente Milanés and Steven E Shladover. Modeling cooperative and autonomous adaptive cruise control dynamic responses using experimental data. *Transportation Research Part C: Emerging Technologies*, 48:285–300, 2014.

[156] Carlos A de Moura and Carlos S Kubrusly. *The Courant-Friedrichs-Lewy (CFL) condition: 80 years after its discovery*. Birkhäuser Basel, 2012.

[157] Trans. Research Board. 2010. *Transportation Research Board, National Research Council, Washington, DC*, 1207:000, 2010.

[158] Xue Chen, Linhui Jiang, Yan Xia, Lu Wang, Jianjie Ye, Tangyan Hou, Yibo Zhang, Mengying Li, Zhen Li, Zhe Song, et al. Quantifying on-road vehicle emissions during traffic congestion using updated emission factors of light-duty gasoline vehicles and real-world traffic monitoring big data. *Science of The Total Environment*, 847:157581, 2022.

[159] Shashank Bharadwaj, Sudheer Ballare, Munish K Chandel, et al. Impact of congestion on greenhouse gas emissions for road transport in mumbai metropolitan region. *Transportation Research Procedia*, 25:3538–3551, 2017.

[160] Kyoungho Ahn, Hesham Rakha, Antonio Trani, and Michel Van Aerde. Estimating vehicle fuel consumption and emissions based on instantaneous speed and acceleration levels. *Journal of Transportation Engineering*, 128(2):182–190, 2002.

[161] Tie-Qiao Tang, Hai-Jun Huang, and Hua-Yan Shang. An extended macro traffic flow model accounting for the driver's bounded rationality and numerical tests. *Physica A: Statistical Mechanics and its Applications*, 468:322–333, 2017.

[162] Benedetto Piccoli and Andrea Tosin. Vehicular traffic: A review of continuum mathematical models. *Encyclopedia of Complexity and Systems Science*, 22:9727–9749, 2009.

[163] Zawar H Khan and T Aaron Gulliver. A macroscopic traffic model based on anticipation. *Arabian Journal for Science and Engineering*, 44:5151–5163, 2019.

[164] Zawar H Khan, T Aaron Gulliver, Khurram S Khattak, and Azhar Qazi. A macroscopic traffic model based on reaction velocity. *Iranian Journal of Science and Technology, Transactions of Civil Engineering*, 44:139–150, 2020.

[165] Markos Papageorgiou, Christina Diakaki, Vaya Dinopoulou, Apostolos Kotsialos, and Yibing Wang. Review of road traffic control strategies. *Proceedings of the IEEE*, 91(12):2043–2067, 2003.

[166] Shuai Liu, Hans Hellendoorn, and Bart De Schutter. Model predictive control for freeway networks based on multi-class traffic flow and emission models. *IEEE Transactions on Intelligent Transportation Systems*, 18(2):306–320, 2016.

[167] David Q Mayne, James B Rawlings, Christopher V Rao, and Pierre OM Scokaert. Constrained model predictive control: Stability and optimality. *Automatica*, 36(6):789–814, 2000.

About the Author

I was born in Swat, Pakistan, and commenced my educational journey at Excelsior College Swat. Subsequently, I continued my academic pursuits at Swat Public School in my hometown. Upon the successful completion of my secondary education, I embarked on a path leading to a Bachelor of Science degree in Civil Engineering at Wah Engineering College in Wah Cantt, Pakistan, ultimately graduating in 2015. Following my graduation, I gained practical experience as a Junior Site Engineer in Islamabad, Pakistan, and later transitioned into a role as a Lab Engineer at a university.

In 2018, I furthered my academic journey by achieving a Master of Science degree in Urban Infrastructure Engineering from the University of Engineering and Technology in Peshawar, Pakistan. During this period, I made contributions to the field by publishing my research work in esteemed journals. In the same year, I assumed the role of a Lecturer in the Department of Civil Engineering. From 2018 to 2020, I served as a Research Associate at the National Center in Big Data and Cloud Computing at the University of Engineering and Technology in Peshawar, Pakistan.

Towards the end of 2020, I embarked on a new chapter in my academic career by relocating to Naples, Italy, to pursue a Ph.D. in Civil Systems Engineering. My dedication to the field of transportation engineering has persisted since my undergraduate studies, extending into the domain of my Ph.D. studies. I have made substantial contributions to my field, evidenced by the authorship of over 10 journal papers. My research endeavors have encompassed areas such as Macroscopic Traffic Flow Modeling, Macroscopic Traffic Control, Macroscopic Fundamental Diagrams, Intelligent Transportation Systems, Connected and Autonomous Vehicles, and Pedestrian Flow Modeling.

Author's Publications

- Imran, Waheed, and Luigi Pariota. "Macroscopic evaluation of traffic flow in view of connected and autonomous vehicles: A simulation-based approach." *Alexandria Engineering Journal* 79 (2023): 581-590.
- Imran, Waheed, Zawar H. Khan, T. Aaron Gulliver, Muhammad Alam, and Khurram S. Khattak. "Non-homogeneous traffic characterization based on driver reaction and stimuli." *Transportation Research Interdisciplinary Perspectives* 21 (2023): 100858.
- Islam, Shamsul, Zawar H. Khan, T. Aaron Gulliver, Khurram S. Khattak, and Waheed Imran. "Pedestrian Traffic Characterization Based on Pedestrian Response." *IEEE Access* 10 (2022): 118397-118408.
- Khan, Daud, Zawar Hussain Khan, Waheed Imran, Khurram Shehzad Khattak, and Thomas Aaron Gulliver. "Macroscopic flow characterization at T-junctions." *Transportation Research Interdisciplinary Perspectives* 14 (2022): 100591.
- Sarir, Muhammad, Rawid Khan, Muhammad Alam, Muhammad Tariq Khan, and Waheed Imran. "Performance evaluation of asphalt concrete mixtures using bagasse ash as filler." *Iranian Journal of Science and Technology, Transactions of Civil Engineering* (2022): 1-18.
- Khan, Ali, Khurram Khattak, Zawar Khan, T. Gulliver, Waheed Imran, and Nasru Minallah. "Internet-of-video things based real-time traffic flow characterization." *EAI Endorsed Transactions on Scalable Information Systems* 8, no. 33 (2021).
- Khan, Zawar Hussain, Thomas Aaron Gulliver, and Waheed Imran. "A macroscopic traffic model based on the safe velocity at transitions." *Civil Engineering Journal* 7, no. 06 (2021).
- Khan, Zawar Hussain, Thomas Aaron Gulliver, Waheed Imran, Khurram Shehzad Khattak, Ahmed B. Altamimi, and Azhar Qazi. "A macroscopic

traffic model based on relaxation time." *Alexandria Engineering Journal* 61, no. 1 (2022): 585-596.

- Imran, Waheed, Zawar H. Khan, Thomas Aaron Gulliver, Khurram S. Khattak, Salman Saeed, and M. Sagheer Aslam. "Macroscopic traffic flow characterization for stimuli based on driver reaction." *Civil Engineering Journal* 7, no. 1 (2021): 1-13.
- Khan, Zawar H., Waheed Imran, Thomas Aaron Gulliver, Khurram S. Khattak, Zahid Wadud, and Akhtar Nawaz Khan. "An anisotropic traffic model based on driver interaction." *IEEE Access* 8 (2020): 66799-66812.
- Imran, Waheed, Zawar H. Khan, T. Aaron Gulliver, Khurram S. Khattak, and Hassan Nasir. "A macroscopic traffic model for heterogeneous flow." *Chinese Journal of Physics* 63 (2020): 419-435.
- Umer, M., Z. H. Khan, W. Imran, S. Saeed, K. S. Khattak, K. Azam, and M. A. Khan. "Behavioral analysis of LWR model under different equilibrium velocity distributions." *Pakistan Journal of Science* 71, no. 4 (2019): 194.
- H. Khan, Zawar, Waheed Imran, Sajid Azeem, Khurram S. Khattak, T. Aaron Gulliver, and Muhammad Sagheer Aslam. "A macroscopic traffic model based on driver reaction and traffic stimuli." *Applied Sciences* 9, no. 14 (2019): 2848.